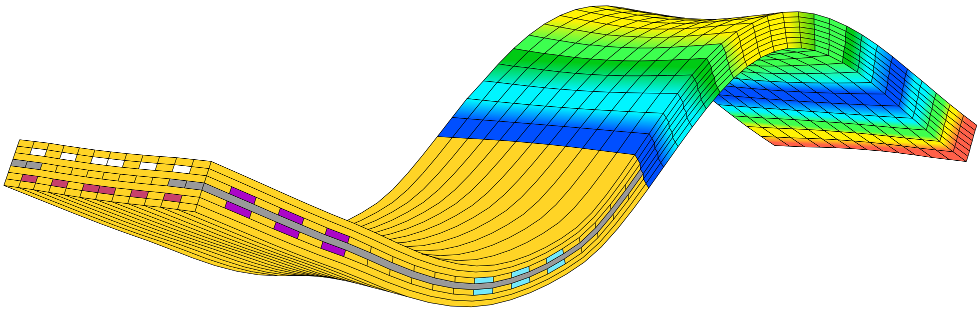

IMPACT OF DIFFERENT LAMELLAE MATERIALS ON VIBRATIONS IN CLT PANELS

A numerical study of concrete, air or elastomer materials

SAM JOHANSSON and KHUONG AN UNG

Structural Mechanics

Master's Dissertation

DEPARTMENT OF CONSTRUCTION SCIENCES
DIVISION OF STRUCTURAL MECHANICS

ISRN LUTVDG/TVSM--24/5270--SE (1-178) | ISSN 0281-6679
MASTER'S DISSERTATION

IMPACT OF DIFFERENT LAMELLAE MATERIALS ON VIBRATIONS IN CLT PANELS

A numerical study of concrete, air or elastomer materials

SAM JOHANSSON and KHUONG AN UNG

Supervisor: PETER PERSSON, Associate Professor, Division of Structural Mechanics, LTH.
Assistant Supervisor: ANNIE BOHMAN, MSc, Division of Structural Mechanics, LTH.
Examiner: Professor KENT PERSSON, Division of Structural Mechanics, LTH.

Printed by V-husets tryckeri LTH, Lund, Sweden, June 2024 *(Pl).*

For information, address:
Division of Structural Mechanics,
Faculty of Engineering LTH, Lund University, Box 118, SE-221 00 Lund, Sweden.
Homepage: www.byggmek.lth.se

Abstract

Timber structures are increasingly growing in importance and utilization. A contributing factor to this trend is the introduction of cross-laminated timber (CLT). CLT is an engineered wood product comprising layers of wood made up of multiple boards, alternately referred to as "lamellae". Each layer is positioned perpendicular to the next and bonded together with adhesives. CLT is mostly utilized in floor or wall panels.

Timber structures offer more advantages in terms of sustainability and climate change compared to conventional concrete buildings. However, they are more sensitive to dynamic loading, necessitating the need to improve the design of multi-story wood buildings to reduce vibration levels and low-frequency structure-borne sound levels. Previous studies show potential to integrate viscoelastic materials in CLT panels to achieve this. This dissertation further explores this potential by examining the effects of exchanging lamellae with alternative materials other than conventional spruce. These alternative materials include concrete and two types of elastomer. Additionally, the possibility to remove certain lamellae without significantly impacting the dynamic behavior of the panel was evaluated.

The predictions of vibrations were accomplished through the utilization of the commercial FE software Abaqus. In Abaqus, two finite element models were constructed, named "Layered model" and "Lamellae model". The Layered model compromised of layers excluding the individual lamellae, used for obtaining spruce material parameters that accurately represent reality. The Lamellae model consisted of layers including the individual lamellae, used to determine the impact of different lamellae material.

The material parameters for spruce were calibrated using Newton optimization on the most influential parameters. Several calibrations were performed, with the most accurate calibration displaying a normalized relative frequency difference (NRFD) of less than 1%.

When studying the impact of different lamellae material two CLT panels were used, consisting of different dimensions and lay-ups. The results were evaluated mainly in root mean square (RMS) and 1/3 octave bands.

Significant reductions in the level of vibration can be achieved by replacing spruce lamellae with concrete, particularly when the concrete lamellae are located close to the outermost parts of the panels. Replacing 2% of the spruce lamellae with concrete indicated approximately 60% reduction in the vibration levels.

Furthermore, air cavities in CLT panels can be modeled as an empty space because modeling air as an acoustic medium in comparison to as an empty space indicated no significant difference in vibration level.

Moreover, a potential was found to remove spruce lamellae in CLT panels giving up

to 20% material reduction without significantly amplifying the vibration levels.

Additionally, exchanging spruce lamellae to elastomer demonstrated reductions in vibration level at certain frequency intervals and amplifications in others. However, there were certain configurations, which showed significant reduction in vibration level over continuous frequency intervals. It demonstrates potential to place elastomer lamellae in a way that is favorable for specific frequency intervals. For example, replacing 14% of the spruce lamellae with elastomer showed approximately 50% reduction in the vibration levels.

Acknowledgments

The dissertation marks the end of our five-year academic journey at Lund University. We are deeply grateful to the amazing people who supported and guided us along the way.

Our sincerest gratitude extends to our dissertation supervisor, Peter Persson and Annie Bohman, our assistant supervisor, for their invaluable guidance and support. Kent Persson, our examiner, we deeply appreciate both your examination and the invaluable insights you provided throughout the process.

Special thanks to Per Jørstad, and the entire team at Sweco for providing a welcoming and collaborative working environment.

Thanks to Södra as well, for the discussions in the study visit.

Thanks to Johannes Jonasson for providing us with the newton optimization code.

We would also like to extend our gratitude to the Division of Structural Mechanics, where we primarily conducted our master's dissertation. We appreciate their provision of essential tools and the nurturing work environment. We are especially thankful for the coffee – it kept us fueled and somewhat sane throughout those long research sessions.

And to our friends, relatives and family: you've been our rocks throughout these five years. Your support means the world to us!

Thanks, everyone, for making this journey unforgettable!

Sam Johansson & Khuong An Ung
Lund, 2024

Contents

1 Introduction

In this chapter, the background and aim of the project are given, followed by presentation of the methodology and limitations.

1.1 Background

Timber structures are increasingly growing in importance and utilization, driven by an increased focus on environmentally friendly materials, sustainability, and climate change [1]. A contributing factor to this trend is the introduction of cross–laminated timber (CLT), which was introduced in the 1990s. The notable structural advantage of CLT is its considerable bending stiffness in two directions, proving particularly beneficial when facing out–of–plane loading [2]. This is especially applicable in floor elements.

Despite timber structures offering environmental benefits and being more advantageous in terms of sustainability and climate change compared to conventional concrete buildings. However, they are more sensitive to dynamic loading, particularly regarding vibroacoustic comfort. Dynamic loading, such as footfall, vibrating machinery, loudspeakers, and rail/road traffic, causes vibrations and structure borne sound in residential buildings [3]. This may result in excessive vibration and noise levels, which can cause annoyance and discomfort for inhabitants, and malfunction of sensitive equipment. The frequency content of structure borne noise below 100 Hz has been proven to significantly impact how individuals subjectively perceive and evaluate the noise [3].

Residents and people working in multistory timber buildings can perceive vibrations and structure borne noise bothersome despite the structures meeting building regulations. This shows the necessity to improve the design of multi–story wood buildings so that vibration levels and low–frequency structure borne sound levels are reduced. Previous studies show that the utilization of viscoelastic material as an intermediate layer in CLT panels could achieve this [4]. Therefore, the possibility to use boards of viscoelastic material to achieve the same was introduced. The investigation into the optimal orientation, quantity, and placement of these boards is an essential area requiring further exploration, forming the foundational context for the master's dissertation. Furthermore, the possibility to use concrete as well will be investigated. Additionally, the possibility to remove certain boards without significantly impacting the dynamic behavior of the panel will be evaluated.

Moreover, the variation in mechanical behavior of complex structures involving many connections complicates the prediction of the structure's response due to dynamic loading. The material variability in timber further complicates this, even within the same species.

1.2 Aim

The aim of this master's dissertation is to improve the dynamic performance of CLT panels. The objective is to investigate how the vibration level of CLT panels are affected by exchanging some boards with material other than the conventional timber. This objective will be achieved by addressing the following questions:

- How does the dynamic behavior of CLT panels change when some of the boards of conventional timber are exchanged with other materials?
- Is there a favorable placement of these alternative materials?
- Is there a potential to exclude boards from CLT panels without significantly increasing the vibration response?

1.3 Methodology

The prediction of vibrations will be accomplished through the utilization of numerical solid Finite Element (FE) models developed using the commercial FE software Abaqus. The main research methodology will be numerical, complemented with literature review.

1.4 Limitations

The focus of this dissertation is confined to an investigation of the dynamic behavior of CLT panels. It is important to note that certain crucial aspects, for example, structural strength, moisture content, and fire resistance, are not within the scope of this dissertation.

2 Cross–laminated timber

In this chapter, an overview of cross–laminated timber is presented, including general information and the manufacturing process.

2.1 Wood material structure

Wood, as a natural material, stands as a versatile material with applications spanning diverse industries. Functioning as a suitable construction material, timber has had a major impact on human development with evidence of utilization in structural construction extending back 476 000 years [5].

Wood is acknowledged as an anisotropic material, meaning it has inherent variations in properties along various directions. Specifically, wood has variable properties along three perpendicular axes, categorizing it as an orthotropic material. These axes are denoted as longitudinal (L) – trunk's longitudinal direction, tangential (T) – perpendicular with the grains and parallel with annual rings, and radial (R) – perpendicular with the grains and annual rings (see Figure 2.1). Notably, wood exhibits its highest stiffness and strength in the fiber direction, i.e., the longitudinal direction, while displaying its lowest stiffness and strength perpendicular to the grain.

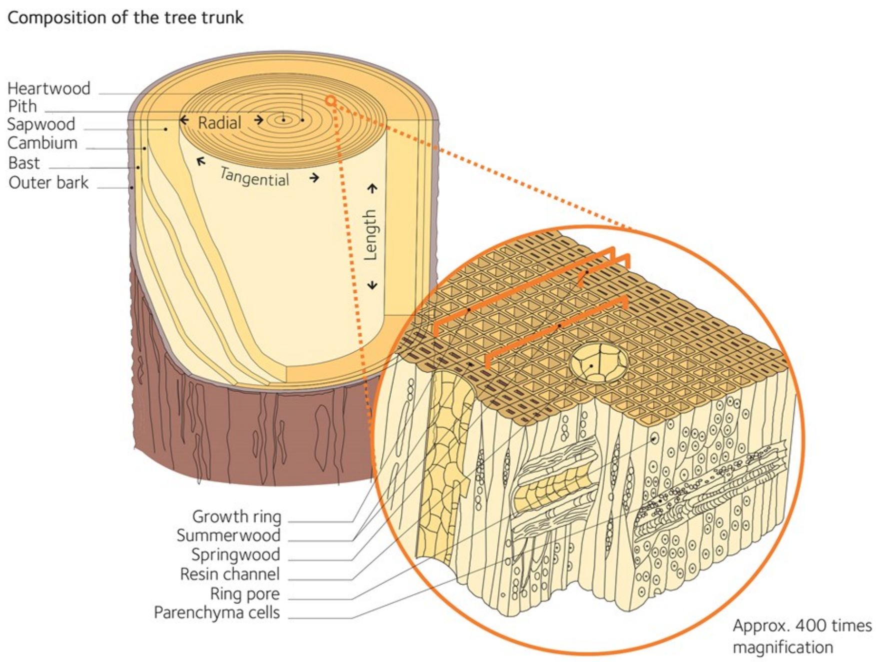

Figure 2.1: Composition of the tree trunk. [6]

2.2 Wood quality variation and strength classes

Due to wood being a natural material, its properties exhibit significant variability influenced by factors such as wood species and growth conditions. In construction, terms like "clear wood" and "timber" are commonly used. Clear wood denotes wood specimens consisting of only straight wood fibers without anomalies. Timber implies processed wood characterized by natural imperfections like knots, juvenile wood, reaction wood, and spiral grain [7]. These natural factors negatively affect wood strength and stiffness. When dealing with larger wood specimens, there is a higher likelihood of encountering these imperfections, necessitating their consideration in estimating timber strength.

To facilitate the use of timber in load–bearing applications, having a standardized grading system for timber is advantageous. Various methods exist for grading timber, depending on the aspect under consideration. However, in the construction context, grading systems based on timber strength are essential. The European standard SS–EN 338:2016 outlines structural timber grading based on strength [8]. Softwood strength classes are ranged from C14 to C50, where the number indicates bending strength in megapascals (MPa) [8]. It's important to note that besides wood species and natural imperfections, moisture is a significant factor that impacts timber strength [7].

2.3 General information

Cross–laminated timber (CLT) is an engineered wood material utilized primarily for walls and floor structures. Recognized for its eco–friendly and recyclable nature, CLT offers a long service life when employed appropriately [9].

CLT consist of minimum three layers of glued boards or planks, typically crafted from coniferous or deciduous wood, each layer positioned perpendicular to the next, see Figure 2.2. These panels consist of boards or planks, alternatively referred to as laminates or lamellae. While the standard method involves gluing the layers together, alternative bonding systems such as nails or dowels may also be used, though such products do not qualify as cross–laminated timber [9]. Henceforth, the term "lamella" (plural: "lamellae") will be consistently utilized throughout the report to refer to the individual planks or boards used in the construction of cross–laminated timber panels.

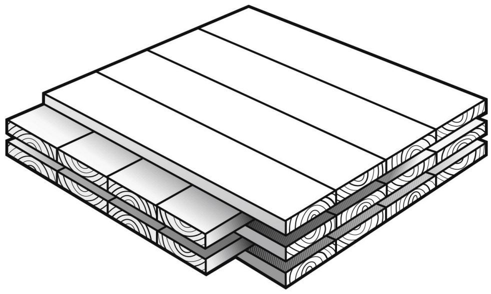

Figure 2.2: Example configuration of a 5–layer CLT panel, the orthogonal orientation of adjacent layers can be seen [2].

Through the utilization of lamellae and layers oriented orthogonally, the inherent anisotropic properties and imperfections of wood, such as knots, can be minimized, resulting in a more homogenized material.

In scenarios requiring longer spans, it might prove advantageous to orientate the two outermost layers in the same direction. This alignment enhances load–carrying capacity and stiffness in that particular direction.

One of CLT's defining features is its allowance for large–format wooden panels, reaching widths of up to 4.80 meters and lengths of 30 meters, with thicknesses ranging from approximately 60 to 500 millimeters [9]. Individual lamellae within CLT panels can range from 20 to 60 millimeters in thickness and 40 to 300 millimeters in width. However, it should be noted that these values are not typically applied. More commonly, plates range from 80 to 300 mm in thickness, 1.2 to 3 meters in width, and 16 meters in length (as manufactured), while lamellae typically measure 20 to 45 mm in thickness and 80 to 200 mm in width [9].

The length of an individual lamella is naturally limited, necessitating joint connections in the longitudinal direction [10]. Such connections can be constructed by the use of "finger joints", see Figure 2.3. These joints feature machined "fingers" along the edges of the lamellae, which interlock together with adhesives when assembled. Compared to a standard edge–to–edge connection of the lamellae, finger joints increase the glued surface, resulting in a stronger connection [10].

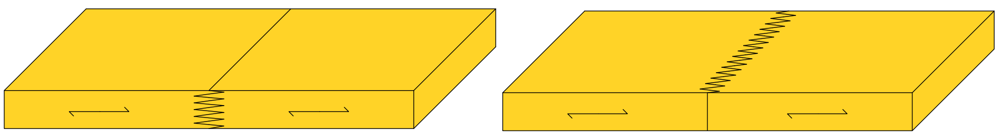

Figure 2.3: Example of finger joints.

Cross–laminated timber is commonly constructed with softwoods such as pine and spruce. Its composition and method of manufacture offer huge opportunities, since the panel can be glued and worked into almost any shape and size [9].

Rolling shear is a phenomenon that significantly reduces shear strength in cross–laminated timber plates, especially in out–of–plane loading. Shear stresses in the fiber direction causes the wood fibers to roll or slide between each other, resulting in larger shear deformations and reduced shear force capacity, see Figure 2.4.

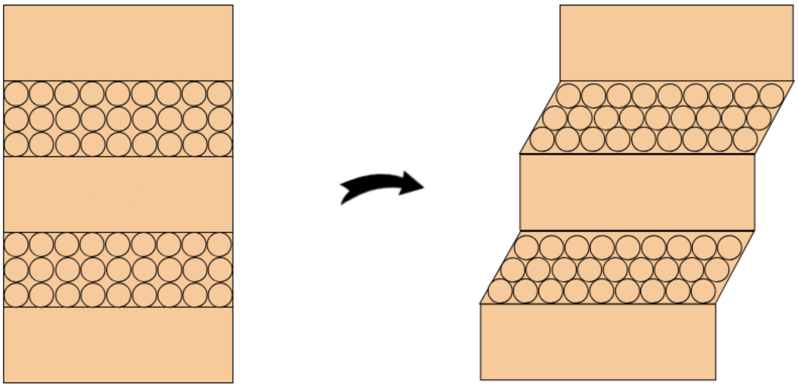

Figure 2.4: Effect of rolling shear in CLT plates.

2.4 Manufacturing process

Every manufacturer of CLT establishes its own set of standard thicknesses and strength classifications. Additionally, variations exist in the cross–section and layer orientation across different manufacturers. However, the manufacturing process for CLT remains largely consistent regardless of the manufacturer or location [9].

The manufacturing process of CLT involves a series of sequential steps, see Figure 2.5. Initially, lamellae are created by processing and cutting tree logs. Then, the lamellae undergo a drying process to reduce the moisture content to between 8% and 15% to ensure that the strength of the bond is sufficient [9]. Following this, strength grading is conducted to ensure that the lamellae meet the required standards. Then, the lamellae are connected to increase length by aforementioned finger jointing. Once hardened, the lamellae are planed before sent for gluing into sheets. Here, the batches of lamellae are glued and assembled into sheets. These sheets are then pressed together under the necessary force, using either vacuum or hydraulic pressure. Following the curing of the glue, final finishing is conducted in a CNC (Computer Numerical Control) machine. This may involve drilling holes, milling channels for installations, sawing edges and preparing for joints and fixings. Lastly, the visible surfaces of each panel undergo polishing, followed by visual inspection and labeling of the components before being packaged and loaded for transport to either a warehouse or a construction site [9].

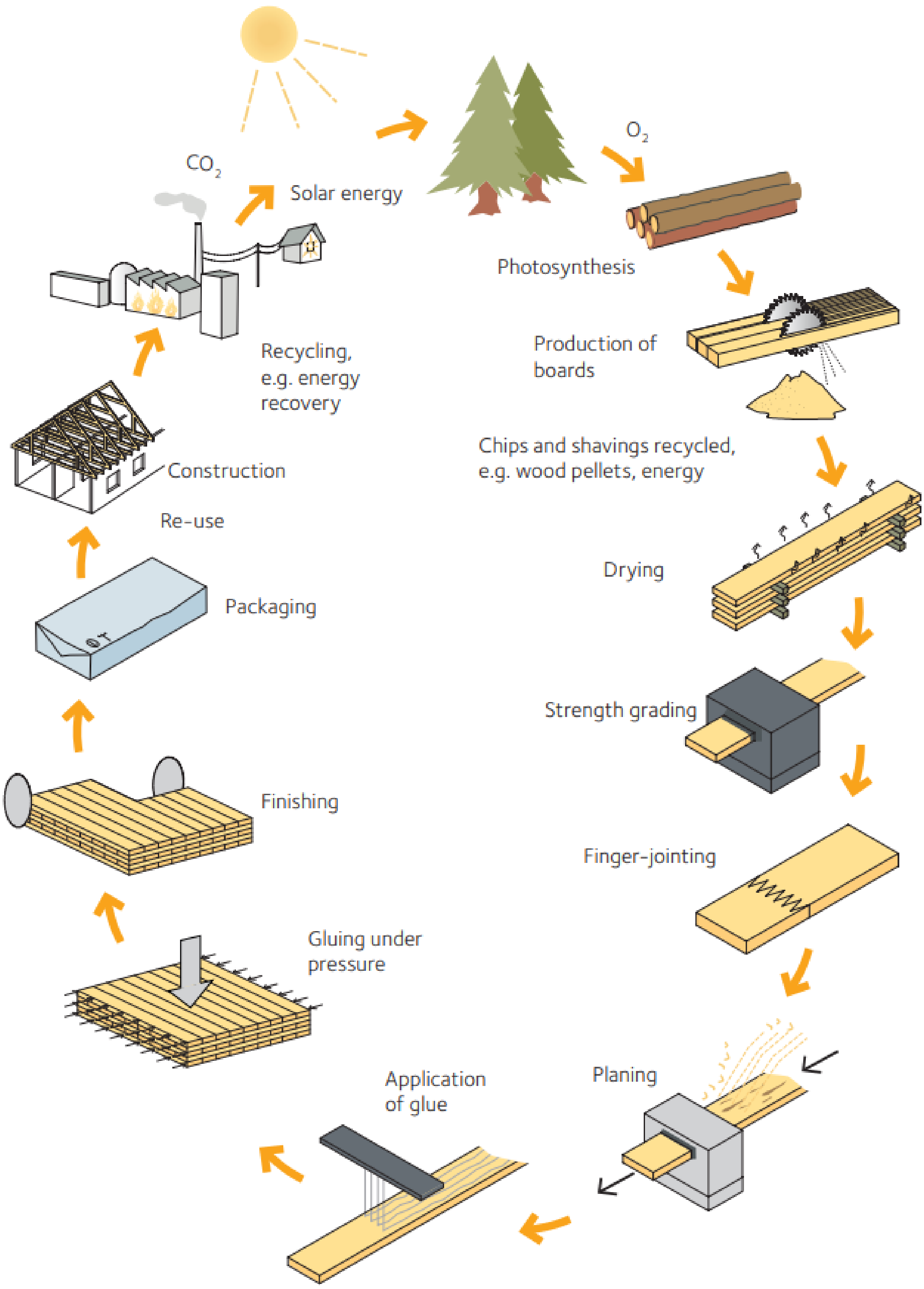

Figure 2.5: Illustration of the production process of CLT panels [9].

3 Fundamental theory

In this chapter, the fundamental theory regarded as necessary for the understanding of this dissertation is presented.

3.1 Equation of motion

A Multi Degrees Of Freedom (MDOF) system can be used for describing the dynamic behavior of large dynamic systems. The equation of motion for a MDOF system is described below:

$$\mathbf{m}\ddot{\mathbf{u}}(t) + \mathbf{c}\dot{\mathbf{u}}(t) + \mathbf{k}\mathbf{u}(t) = \mathbf{p}(t) \tag{3.1}$$

In this equation, $\mathbf{m}$ represents the mass matrix, $\mathbf{c}$ is the damping matrix, and $\mathbf{k}$ denotes the stiffness matrix. Additionally, $\mathbf{p}(t)$ signifies the external force vector, while $\mathbf{u}(t)$ represents the displacement vector. The variables $\dot{\mathbf{u}}(t)$ and $\ddot{\mathbf{u}}(t)$ denote the first and second derivatives of the displacement vector with respect to time, representing the velocity and acceleration vectors, respectively.

3.2 Damping

Damping in structural dynamics refers to the loss of energy within a system, resulting in a decay of vibration amplitude over time [11]. Damping parameters are complex and not well–defined, which presents challenges when constructing the damping matrix.

However, there are various approaches to apply damping. One such approach is modal damping, where damping ratios are assigned to specific natural modes. In modal damping, if damping ratios are known for a certain number of natural modes, these ratios can be applied individually to each corresponding mode. This means that each mode has a unique damping.

3.3 Natural Frequencies analysis

In a Single Degree Of Freedom (SDOF) system, natural frequency refers to the frequency at which a system oscillates freely when disturbed from its equilibrium position. This natural frequency can be determined by:

$$\omega_n = \sqrt{\frac{k}{m}} \tag{3.2}$$

Damping does have impact on these natural frequencies and this impact could be taken in to account as below:

$$\omega_{nD} = \omega_n \sqrt{1 - \zeta_n^2} \tag{3.3}$$

where ω_{nD} is the angular natural frequency with respect to damping, ω_n is the angular natural frequency without damping and ζ_n is the damping ratio. However, the effect of damping is neglectable for damping ratio $\zeta_n < 20\%$, which applies to most structures.

In a MDOF system, there are several natural frequencies. With no external forces and neglected damping, Equation 3.1 can be rewritten as:

$$\mathbf{m}\ddot{\mathbf{u}}(t) + \mathbf{k}\mathbf{u}(t) = 0 \tag{3.4}$$

The displacement vector $\mathbf{u}(t)$ can be expressed by Equation 3.5, where N is the number of degrees of freedom, ϕ_r is the time independent deflected mode shape vector at mode number r and $q_r(t)$ is the time dependent modal coordinates (scalar multipliers).

$$\mathbf{u}(t) = \sum_{r=1}^{N} \phi_r q_r(t) = \mathbf{\Phi}\mathbf{q}(t) \tag{3.5}$$

where $q_r(t)$ can be expressed with constant A_r and B_r:

$$q_r(t) = A_r \cos\omega_r t + B_r \sin\omega_r t \tag{3.6}$$

and the second derivatives of the time dependent modal coordinates becomes:

$$\ddot{q}_r(t) = -\omega_r^2 (A_r \cos\omega_r t + B_r \sin\omega_r t) \tag{3.7}$$

Then, the acceleration vector can be described as:

$$\ddot{\mathbf{u}}(t) = -\omega_r^2 \mathbf{u}(t) \tag{3.8}$$

Substitution of Equation 3.5 and Equation 3.8 in Equation 3.4 gives a matrix eigenvalue problem for free vibration as:

$$[\mathbf{k} - \omega_r^2 \mathbf{m}]\mathbf{\Phi}\mathbf{q}(t) = 0 \tag{3.9}$$

Equation 3.9 should be applicable at all times regardless modal coordinates. The trivial solution for this equation is $\mathbf{\Phi} = \mathbf{0}$ but it also means there is no motion in the system and it can therefore be omitted. A non–trivial solution can be acquired using the determinant, see Equation 3.10

$$det[\mathbf{k} - \omega_r^2 \mathbf{m}] = 0 \tag{3.10}$$

By solving Equation 3.10, N natural angular frequencies can be determined. Insert these natural frequencies back in Equation 3.9 to obtain the eigenvectors (mode shapes) at each resonance frequency.

3.4 Steady–state dynamic

When a system is subjected to a harmonic load, its response comprises both a steady–state and a transient response. At the moment when the load is applied the transient vibration is also triggered. However, in a damped system, the transient vibration dissipates due to damping, leaving only the steady–state response.

The steady–state response of a structure to harmonic excitation can be characterized by displacements, velocities, and accelerations.

3.4.1 Direct analysis

With a harmonic load, Equation 3.1 can be described as:

$$\mathbf{m}\ddot{\mathbf{u}}(t) + \mathbf{c}\dot{\mathbf{u}}(t) + \mathbf{k}\mathbf{u}(t) = \mathbf{p}_0 e^{i\omega t} \tag{3.11}$$

where $\mathbf{p}_0$ is the load amplitude vector which is considered to be real.

The steady–state solution is periodic with a phase lag due to damping. According to Euler's formula:

$$\mathbf{u}(t) = \mathbf{u}^* e^{i\omega t} \tag{3.12}$$

where $\mathbf{u}^*$ is a vector containing the complex amplitude and phase lag of displacements

The first time derivative gives:

$$\dot{\mathbf{u}}(t) = i\omega\mathbf{u}(t) \tag{3.13}$$

and the second time derivative gives:

$$\ddot{\mathbf{u}}(t) = -\omega^2\mathbf{u}^* e^{i\omega t} \tag{3.14}$$

Substitution of Equations 3.12, 3.13 and 3.14 in Equation 3.11 gives

$$(-\omega^2\mathbf{m} + i\omega\mathbf{c} + k)\mathbf{u}^* = \mathbf{p}_0 \tag{3.15}$$

Solving Equation 3.15 gives

$$\mathbf{u}^* = (-\omega^2\mathbf{m} + i\omega\mathbf{c} + k)^{-1}\mathbf{p}_0 \tag{3.16}$$

The phase lag (θ) between the displacement at a certain degrees of freedom u_j^* and its corresponding force component p_{0j} can be found as:

$$\theta = arg(u_j^*) \tag{3.17}$$

The steady–state solution can be found inserting 3.17 in Equation 3.12

$$\mathbf{u}(t) = (-\omega^2\mathbf{m} + i\omega\mathbf{c} + k)^{-1}\mathbf{p}_0 e^{i\omega t} \tag{3.18}$$

3.4.2 Modal analysis

Inserting Equation 3.5 in Equation 3.1 and pre–multiplying with ϕ_n^T gives:

$$\sum_{r=1}^{N} \phi_n^T \mathbf{m} \phi_r \ddot{q}_r(t) + \sum_{r=1}^{N} \phi_n^T \mathbf{c} \phi_r \dot{q}_r(t) + \sum_{r=1}^{N} \phi_n^T \mathbf{k} \phi_r q_r(t) = \phi_n^T \mathbf{p}(t) \tag{3.19}$$

However, the modes are orthogonal with respect to the mass matrix $\mathbf{m}$ and the stiffness matrix $\mathbf{k}$, i.e. $\phi_n^T \mathbf{m} \phi_r = 0$ and $\phi_n^T \mathbf{k} \phi_r = 0$. Due to the orthogonality only the terms with $r = n$ differs from zero. This orthogonality is also valid for classical damping (i.e. the damping matrix $[\mathbf{c}]$ is diagonal), Equation 3.19 can be rewritten as:

$$\phi_n^T \mathbf{m} \phi_n \ddot{q}_n(t) + \phi_n^T \mathbf{c} \phi_n \dot{q}_n(t) + \phi_n^T \mathbf{k} \phi_n q_n(t) = \phi_n^T \mathbf{p}(t) \tag{3.20}$$

or

$$M_n \ddot{q}_n(t) + C_n \dot{q}_n(t) + K_n q_n(t) = P_n(t) \tag{3.21}$$

where the generalized mass M_n, stiffness K_n and force C_n are defined as

$$M_n = \phi_n^T \mathbf{m} \phi_n \qquad ; K_n = \phi_n^T \mathbf{k} \phi_n \qquad ; C_n = \phi_n^T c \phi_n \qquad \text{and} \quad P_n = \phi_n^T \mathbf{p}(t)$$

Rewriting Equation 3.21 on standard form by dividing this equation by M_n and using $\omega_n^2 = K_n/M_n$ gives:

$$\ddot{q}_n(t) + 2\zeta_n \omega_n \dot{q}_n(t) + \omega_n^2 q_n(t) = \frac{P_n(t)}{M_n} \tag{3.22}$$

where the modal damping ζ_n can be expressed as

$$\zeta_n = \frac{C_n}{2M_n\omega_n}$$

A trial solution to Equation 3.22 is:

$$q_n(t) = q_{0n} e^{i\omega t} \tag{3.23}$$

According to Equation 3.23, the first and second derivatives of modal coordinates can be determined as:

$$\dot{q}_n(t) = i\omega q_n(t) \tag{3.24}$$

$$\ddot{q}_n(t) = -\omega^2 q_n(t) \tag{3.25}$$

Inserting Equations 3.24 and 3.25 in Equation 3.22 together with using $M_n = K_n/\omega_n^2$ gives:

$$-\omega^2 q_n(t) + 2\zeta_n \omega_n i\omega q_n(t) + \omega_n^2 q_n(t) = \frac{P_n(t)}{M_n} \tag{3.26}$$

$$\Rightarrow q_n(t)[\omega_n^2 - \omega^2 + i2\zeta_n\omega_n\omega] = \frac{P_n(t)}{K_n/\omega_n^2} \tag{3.27}$$

Dividing by ω_n^2 gives:

$$\Rightarrow q_n(t)[1-(\omega/\omega_n)^2+i2\zeta_n(\omega/\omega_n)] = \frac{P_n(t)}{K_n} \tag{3.28}$$

$$\Rightarrow q_n(t) = \frac{P_n(t)}{K_n}\frac{1}{[1-(\omega/\omega_n)^2]+i[2\zeta_n(\omega/\omega_n)]} \tag{3.29}$$

Harmonic loading can be expressed as:

$$\mathbf{p}(t) = \mathbf{p}_0 e^{i\omega t} \tag{3.30}$$

$$\Rightarrow P_n(t) = \phi_n^T \mathbf{p}_0 e^{i\omega t} \tag{3.31}$$

Equation 3.29 can then be express as:

$$q_n(t) = \frac{\phi_n^T \mathbf{p}_0}{K_n}\frac{1}{[1-(\omega/\omega_n)^2]+i[2\zeta_n(\omega/\omega_n)]}e^{i\omega t} \tag{3.32}$$

By performing the modal transformation as in Equation 3.19 but using N different ϕ_n^T which corresponding to N natural modes (where N is the number of degrees of freedoms), N uncoupled equations are obtained.

The steady–state solution can be found by solving these equations and inserting Equation 3.32 in Equation 3.5

$$\mathbf{u}(t) = \sum_{n=1}^{N}\phi_n q_n(t) = \sum_{n=1}^{N}\frac{\phi_n\phi_n^T\mathbf{p}_0}{K_n}\frac{1}{[1-(\omega/\omega_n)^2]+i[2\zeta_n(\omega/\omega_n)]}e^{i\omega t} \tag{3.33}$$

3.4.3 Frequency Response Functions

Frequency Response Functions (FRFs) serve as a valuable tool for analyzing dynamic systems, allowing for the examination of dynamic behavior in the frequency domain. FRFs represent the relation between an output signal and the corresponding input signal. Various types of FRFs exist depending on the specific inputs and outputs of interest.

Receptance $\mathbf{H}(\omega)$ expresses relation between displacement $\mathbf{u}(\omega)$ and force $\mathbf{p}(\omega)$.

$$\mathbf{H}(\omega) = \mathbf{u}(\omega)/\mathbf{p}(\omega) \tag{3.34}$$

Mobility $\mathbf{Y}(\omega)$ expresses relation between velocity $\dot{\mathbf{u}}(\omega)$ and force $\mathbf{p}(\omega)$.

$$\mathbf{Y}(\omega) = \dot{\mathbf{u}}(\omega)/\mathbf{p}(\omega) \tag{3.35}$$

Accelerance $\mathbf{A}(\omega)$ expresses relation between acceleration $\ddot{\mathbf{u}}(\omega)$ and force $\mathbf{p}(\omega)$.

$$\mathbf{A}(\omega) = \ddot{\mathbf{u}}(\omega)/\mathbf{p}(\omega) \tag{3.36}$$

The FRF – Accelerance according to the direct analysis in Section 3.4.1, can be found by inserting Equations 3.14, 3.30 and 3.18 in Equation 3.36.

$$\mathbf{A}(\omega) = \frac{\ddot{\mathbf{u}}(t)}{\mathbf{p}(t)} = (-\omega^2\mathbf{m} + i\omega\mathbf{c} + k)^{-1} \tag{3.37}$$

The FRF – Accelerance according to the modal analysis in Section 3.4.2, can be found by inserting Equations 3.25, 3.30 and 3.33 in Equation 3.36.

$$\mathbf{A}(\omega) = \frac{\ddot{\mathbf{u}}(t)}{\mathbf{p}(t)} = \sum_{n=1}^{N} \frac{\phi_n \phi_n^T}{K_n} \frac{-\omega_n^2}{[1-(\omega/\omega_n)^2] + i[2\zeta_n(\omega/\omega_n)]} \tag{3.38}$$

FRFs provide valuable insights, allowing for the determination of natural frequencies by studying the frequencies of the peaks. Additionally, FRFs obtained from real experiments can also provide information regarding damping. However, it is important to acknowledge the potential for modal overlap, particularly at higher frequencies, where multiple natural frequencies may closely coincide within FRFs.

3.4.4 Modal truncation

The modal expansion in Equation 3.5 can be truncated by neglecting higher modes. This truncated modal expansion can be expressed as below:

$$\mathbf{u}(t) \approx \sum_{n=1}^{J} \phi_n q_n(t) = \mathbf{\Phi}_J \mathbf{q}_J(t) \tag{3.39}$$

where J is the number of natural frequencies that are considered in the modal analysis and $J < N$.

It is worth noting that modal truncation significantly reduces computational costs. However, it also introduces an error compared to the full modal expansion due to neglecting the higher modes. This error must be kept insignificant to prevent excessive alteration of the system's dynamic response.

3.5 Newton optimization

The aim of Newton optimization in this dissertation is to optimize the material parameters of spruce to reflect real–world conditions and to make the numerical analysis as realistic as possible.

The differences in natural frequencies between the experimental and numerically obtained values can be determined using the Normalized Relative Frequencies Difference (NRFD) (see Section 3.6.1). However, NRFD can yield positive or negative values. Therefore, the objective function to be minimized could be chosen as follows:

$$f = \sum_{1}^{N} \left(\frac{f_{n,num} - f_{n,exp}}{f_{n,exp}} \right)^2 \tag{3.40}$$

Where $f_{n,num}$ is the numerically obtained natural frequency, $f_{n,exp}$ is the experimental natural frequency and N is number of considered natural modes.

Newton calibration was employed to minimize the difference in natural frequencies between the experimental and numerical models, i.e. to find the minimum values to Equation 3.40.

The foundational algorithm behind this optimization method is described below:

The function f in Equation 3.40 is a twice differentiable function and according to Taylor expansion, a quadratic approximation of a function $f(\boldsymbol{x})$ around a certain point $\boldsymbol{x}^{(k)}$ could be found as:

$$f(\boldsymbol{x}) \approx f(\boldsymbol{x}^{(k)}) + (\boldsymbol{x} - \boldsymbol{x}^{(k)})\boldsymbol{\nabla} f(\boldsymbol{x}^{(k)}) + \frac{1}{2}(\boldsymbol{x} - \boldsymbol{x}^{(k)})^T \boldsymbol{\nabla}^2 f(\boldsymbol{x}^{(k)})(\boldsymbol{x} - \boldsymbol{x}^{(k)}) \triangleq q(\boldsymbol{x}) \quad (3.41)$$

Where $\boldsymbol{x}^{(k)}$ is the initial guess, $\boldsymbol{\nabla} f(\boldsymbol{x}^{(k)})$ is the gradient and $\boldsymbol{\nabla}^2 f(\boldsymbol{x}^{(k)})$ is the Hessian matrix at the point $\boldsymbol{x}^{(k)}$.

The minimum value to Equation 3.41 could be found by setting the first–order derivative of this equation equal to zero, which yields:

$$\begin{aligned}
\boldsymbol{\nabla} q(\boldsymbol{x}) &= 0 \\
\Rightarrow \boldsymbol{\nabla} f(\boldsymbol{x}^{(k)}) + \boldsymbol{\nabla}^2 f(\boldsymbol{x}^{(k)})(\boldsymbol{x} - \boldsymbol{x}^{(k)}) &= 0 \\
&\Rightarrow \boldsymbol{x} = \boldsymbol{x}^{(k)} - \frac{\boldsymbol{\nabla} f(\boldsymbol{x}^{(k)})}{\boldsymbol{\nabla}^2 f(\boldsymbol{x}^{(k)})} \\
&\Rightarrow \boldsymbol{x} = \boldsymbol{x}^{(k)} - \boldsymbol{\nabla}^2 f(\boldsymbol{x}^{(k)})^{-1} \boldsymbol{\nabla} f(\boldsymbol{x}^{(k)})
\end{aligned}$$

Newton optimization is an iterative method and a new approximation would be performed in the same way having $\boldsymbol{x}^{(k+1)} = \boldsymbol{x}$ as the guess to the next iteration, which results in:

$$\boldsymbol{x}^{(k+1)} = \boldsymbol{x}^{(k)} - \boldsymbol{\nabla}^2 f(\boldsymbol{x}^{(k)})^{-1} \boldsymbol{\nabla} f(\boldsymbol{x}^{(k)})$$

The Newton optimizations, that were performed in this dissertation, had 0.01 as the limit, i.e. while the step length between two consecutive iterations is larger than 0.01, the optimization would keep going and making new approximations. When the step length is less than 0.01 the optimization would be stopped.

However, there are challenges to find the first– and second–order derivatives of Equation 3.40 by an analytical method. Another way to decide these derivatives is utilizing the central difference method, which yields:

$$\frac{\partial f}{\partial x_1} = \frac{f(\boldsymbol{x} + \Delta \boldsymbol{x}) - f(\boldsymbol{x} - \Delta \boldsymbol{x})}{2\Delta \boldsymbol{x}} \quad (3.42)$$

$$\frac{\partial^2 f}{\partial \boldsymbol{x_1} \partial \boldsymbol{x_2}} = \frac{f(\boldsymbol{x} + \Delta \boldsymbol{x}) - 2f(\boldsymbol{x}) + f(\boldsymbol{x} - \Delta \boldsymbol{x})}{\Delta \boldsymbol{x}^2} \quad (3.43)$$

It is important to emphasize that initial guesses play a crucial role in Newton optimization. They must closely approximate the actual results; otherwise, the step length between iterations may significantly increase and the minimum values would never be found.

3.6 Evaluation metrics

In this section, the main evaluation metrics utilized in this dissertation are presented.

3.6.1 Normalized Relative Frequencies Difference

The Normalized Relative Frequency Difference (NRFD) serves as a metric to evaluate the relative difference between models and measurements. NRFD compares the natural frequencies predicted by one model to those of another, normalized by the frequencies of the latter according to:

$$\text{NRFD} = \frac{f_{ni,A} - f_{ni,B}}{f_{ni,B}} \tag{3.44}$$

where $f_{ni,A}$ represents the natural frequency of the i–th mode in model A, and $f_{ni,B}$ represents the natural frequency of the i–th mode in the reference model B.

A value of 0% indicates perfect agreement, while positive values imply that model A predicts higher natural frequencies and negative values suggests lower predictions.

3.6.2 Modal assurance criterion

The Modal Assurance Criterion (MAC) is a measure used in modal analysis to assess the similarity between two mode shapes at their respective natural frequencies.

MAC is particularly useful when comparing experimentally obtained mode shapes with numerical (finite element) mode shapes. It can also be used to compare mode shapes using different numerical models or between the same numerical models under different conditions, such as different materials, material parameters, or boundary conditions.

The Modal Assurance Criterion is defined as:

$$\text{MAC} = \frac{\left|\boldsymbol{\phi_i}^T \cdot \boldsymbol{\phi_j}\right|^2}{(\boldsymbol{\phi_i}^T \cdot \boldsymbol{\phi_i}) \cdot (\boldsymbol{\phi_j}^T \cdot \boldsymbol{\phi_j})} \tag{3.45}$$

where:

$\boldsymbol{\phi_i}$ and $\boldsymbol{\phi_j}$ are the mode shapes being compared.
$\boldsymbol{\phi_i}$ is the i–th mode shape.
$\boldsymbol{\phi_j}$ is the j–th mode shape.

The MAC–values range between 0 and 1, where a MAC–value of 1 indicates identical mode shapes, and a MAC–value of 0 indicates orthogonal mode shapes.

3.6.3 Root mean square

In structural dynamics, calculations often produce both positive and negative values, which can make a mean value less representative. However, utilizing the root mean square (RMS) allows for a more accurate assessment of the data. The RMS is calculated with the formula in Equation 3.46.

$$\mathrm{RMS} = \sqrt{\frac{1}{n}\sum_{i=1}^{n} x_i^2} \tag{3.46}$$

where x_i represents the value of the i:th data point, and n represents the number of data points.

3.6.4 Third–octave band

Third–octave band or 1/3 octave band is a method used to divide the frequency spectrum into narrow frequency intervals. It is a so–called constant relative bandwidth filter, where a bandwidth is proportional to its center frequency f_c [12]. The lower f_l and upper limit f_u of 1/3 octave band could be found as below

$$f_l = f_c/\sqrt[6]{2} \tag{3.47}$$

$$f_u = f_c\sqrt[6]{2} \tag{3.48}$$

1/3 octave band could be used to examine sound or vibration characteristics across a frequency range. The RMS–values can be calculated within each 1/3 octave band. The use of 1/3 octave band was mainly to evaluate the impact of different lamellae material in Chapters 7–11.

4 Numerical modeling

In this chapter, an introduction to the finite element method (FEM) and its application using the commercial FE software Abaqus, central to this dissertation, are presented. Additionally, the two types of modeling approaches utilized will be contrasted.

4.1 Finite element method

The finite element method (FEM) is a numerical technique for approximating solutions to general differential equations. It solves partial differential equations across one–dimensional, two–dimensional, or three–dimensional regions.

The problem–solving process involves dividing the entire region into smaller parts called "finite elements". Within these elements, variables are approximated using, e.g., linear or quadratic polynomials to describe the element behavior. These variables are determined at specific nodal points, often located along the element boundaries which can be then interpolated. Unlike these approximations, real–world problems have an infinite number of unknowns between known nodal points, i.e. it is continuous. The collection of all these finite elements forms what is called the "finite element mesh".

4.2 Abaqus software

The CLT panels were modeled in the commercial FE software Abaqus. In Abaqus, commands are automatically executed by Abaqus/CAE following each operation performed in the graphical user interface. The commands can be recorded using the Abaqus function *Macro Manager* and saved as a python file using the Abaqus python development environment (PDE) interface. The saved python files can be run in said interface which streamlines iterative works. The process utilized in this dissertation.

The majority of the analyses performed required iterative work. The Abaqus PDE interface made it possible to easily modify input parameters, perform successive analyses, and extract results in a much more efficient manner.

4.3 Finite element models

In this section, description of the two types of modeling approaches used to simulate realistic CLT panels are presented.

The study conducted by Johannes et al. [13] demonstrated that a model, where one solid part was horizontally partitioned to simulate layers, yielded similar modal behavior to another model where these layers were further partitioned into lamellae, albeit with significantly reduced computational time. Therefore, the model created to determine realistic spruce material parameters in Chapter 5, comprised of solely layers. This model was named “Layered model”.

However, when studying the impact of different lamellae material in Chapters 8–11, the necessity of alternating the material in various lamellae meant that the Layered model was not sufficient. Therefore, models where the layers are further partitioned into lamellae were modeled and named “Lamellae model”.

4.3.1 Layered model

In the so–called Layered model, one solid part was partitioned horizontally to simulate layers, see Figure 4.1. The partitions simulate tie–constraints between adjacent layers to mimic the behavior of manufactured CLT panels, as described in Section 2.5. Material orientation was utilized to arrange the layers in an orthogonal manner, representing a CLT panel.

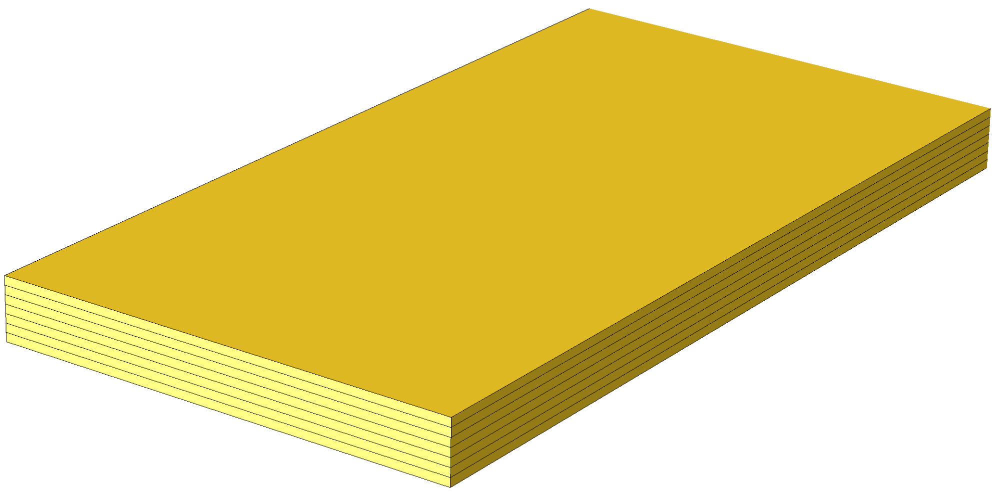

Figure 4.1: Illustration of the Layered model.

For the finite element approximations, quadratic brick 3D stress elements with full integration were employed, i.e. C3D20 elements according to the Abaqus naming convention. These elements use $3 \times 3 \times 3$ integration points, see Figure 4.2.

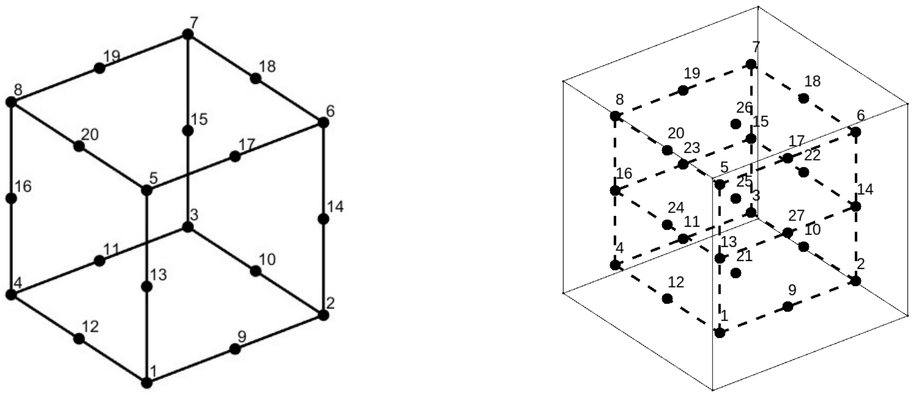

(a) Nodal points for C3D20 elements

(b) Integration points for C3D20 elements

Figure 4.2: C3D20 elements

4.3.2 Lamellae model

The Lamellae model closely resembles the Layered model, where a solid part is partitioned to create distinct layers. However, the Lamellae model further partitions each layer to simulate individual lamellae, see Figure 4.3. This mean that tie–constraints are applied horizontally between adjacent lamellae, in contrast to only gluing layer–to–layer. Because glue slips between the lamellae in the gluing process the Lamellae model is appropriate. The calibrations performed in Section 5.3 do, to some extent, account for this, as further described in the discussion.

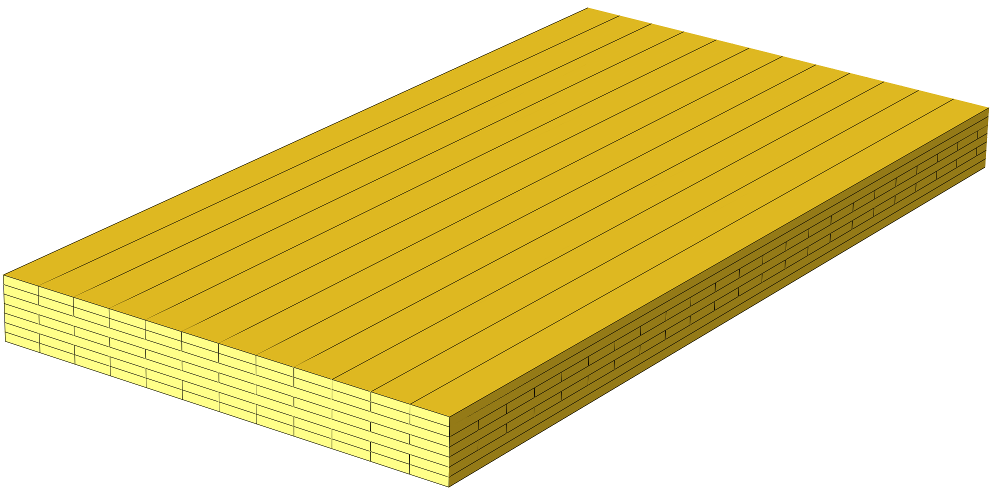

Figure 4.3: Illustration of the Lamellae model.

For the finite element approximations, linear brick continuum solid shell elements with full integration were employed, i.e. CSS8 elements according to the Abaqus naming convention. These elements use $2 \times 2 \times 2$ integration points, see Figure 4.4. Comparing natural frequencies computed using the linear element, CSS8, with the quadratic element, C3D20, revealed minimal deviation, despite the significantly faster computational time for the model with linear element, CSS8.

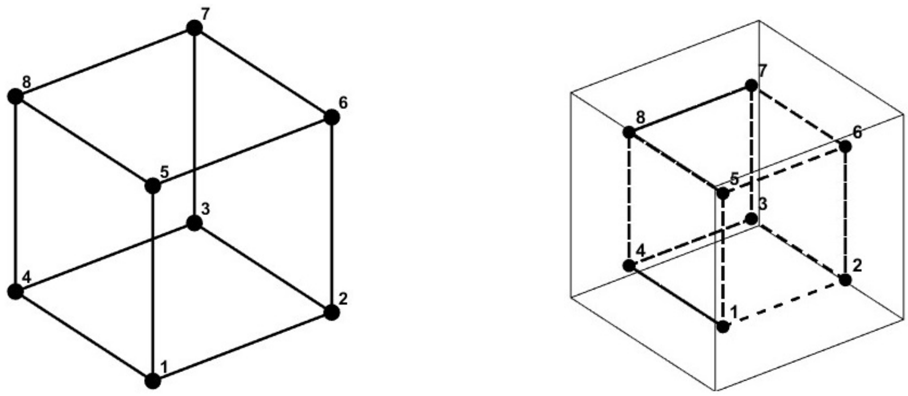

(a) Nodal points for CSS8 elements

(b) Integration points for CSS8 elements

Figure 4.4: CSS8 elements

5 Mechanical properties of spruce

In this chapter, the process of determining realistic spruce properties that accurately represent reality is presented.

The process involves replicating an appropriate experimental setup in Abaqus for the mechanical properties of spruce calibrations. Subsequently, to ensure model accuracy, mesh convergence was performed. Following this, a sensitivity analysis was conducted to identify mechanical properties influencing the dynamic behavior. Finally, calibrations of these properties were conducted.

5.1 Overview of experiment

This section describes the experiment and experimental data selected to obtain the most appropriate modeling approach. It includes details of the experimental configuration, dimensions of the test specimen, and key results.

For comprehensive details regarding the testing, readers are referred to the original article by Ljunggren [4].

5.1.1 Experimental configuration

The experimental configuration involved 16 CLT panels measuring 60 mm in thickness (three layers), 0.5 m in width, and 4 m in length. The tests were conducted in laboratory conditions using modal analysis up to 5 modes and the timber strength class was C24.

For boundary conditions (BC), elastic ropes were utilized to suspend the CLT panels, simulating a free–free boundary condition. An electromagnetic shaker served as the excitation source during testing, see Figure 5.1.

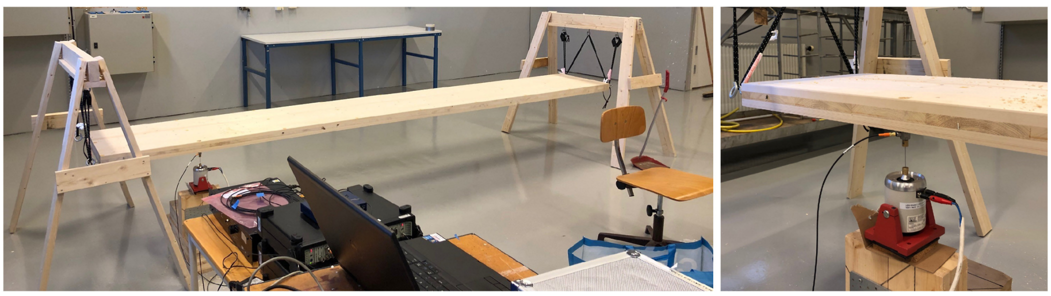

Figure 5.1: Experiment configuration [4].

Accelerometers were utilized to measure the response of the CLT panel, positioned in an approximate 25 × 50 cm grid over the surface, see Figure 5.2.

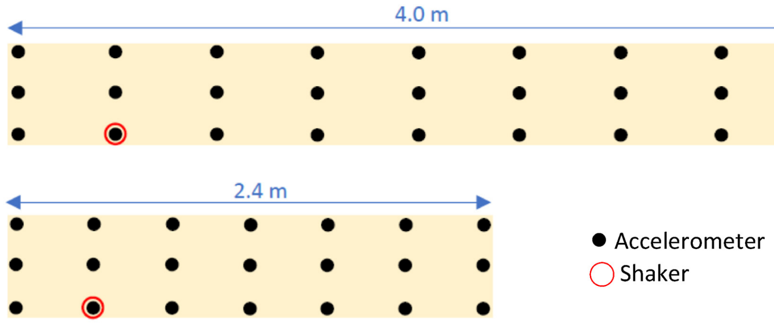

Figure 5.2: Accelerometers and shaker positions [4]. Note that the panel with 4 m in length is the one described in this section.

5.1.2 Results from experiment

Key results from the 16 conducted experiments are presented in this section. Table 5.1 shows the mean natural frequencies values for each mode.

Table 5.1: Mean values of natural frequencies from experiment.

Mode	1	2	3	4	5
Mean natural frequency [Hz]	19.69	32.36	52.05	66.98	98.67

Figure 5.3 illustrates the corresponding mode shapes. The first, third, and fifth modes corresponded to the first, second, and third bending modes, while the second and fourth modes represented the first and second torsional modes, respectively.

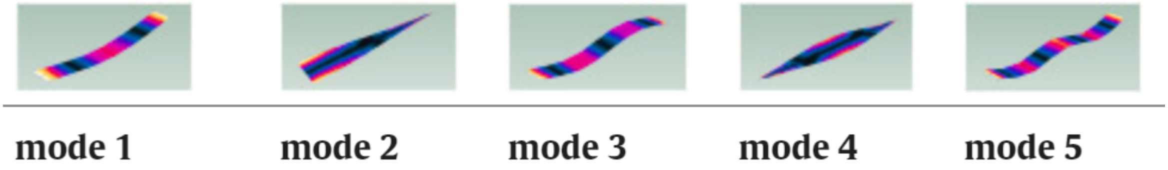

Figure 5.3: Mode shapes from experiment [4].

The damping ratios obtained from the 16 experiments, are plotted in Figure 5.4. A constant damping ratio of 0.7% was deemed representative of the experimental data.

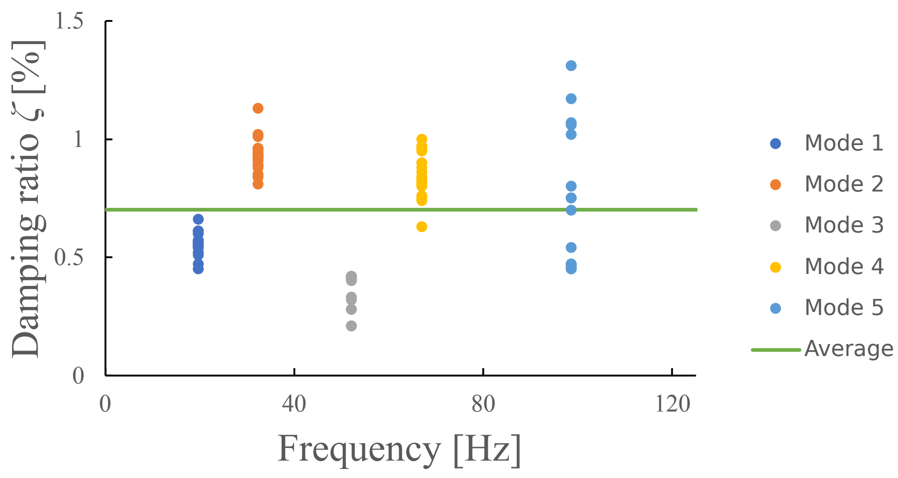

Figure 5.4: Damping ratios obtained from [4].

5.2 Sensitivity analysis

In this section, the conducted sensitivity analysis is presented, which identifies the mechanical properties that have significant effect on the natural frequencies. The sensitivity analysis was performed using the Layered model, described in Section 4.1.

5.2.1 Model development

To identify the mesh size that yields accurate and converged results, a mesh convergence study was conducted on a CLT panel with dimensions equivalent to those used in the experiment in Section 5.1 ($0.5 \times 4 \times 0.06$ m^3) [4] using the Layered model, described in Section 4.1.

This analysis involved comparing the natural frequencies obtained from the current mesh size to those from the finest mesh size. This was achieved by assessing the relative differences in natural frequencies. Once these differences were deemed insignificant, the corresponding mesh size was considered acceptable for the sensitivity analysis in Section 5.2 and calibrations in Section 5.3.

5.2.1.1 Elements per layer

The mesh convergence study in thickness direction was performed using 100 mm mesh size in longitudinal and 50 mm in transverse direction. In this study, the mesh size was categorized by the number of elements per layer. Meaning 1 element per layer would be the same mesh size as the layer thickness (0.02 m), and 2 elements per layer would be half of this (0.01 m). The tested number of elements per layer ranged from 1 to 20. The results are shown in Figure 5.5, where the relative difference maintained low values under 0.03% for all number of elements per layer. Therefore, 1 element per layer was deemed necessary moving forward.

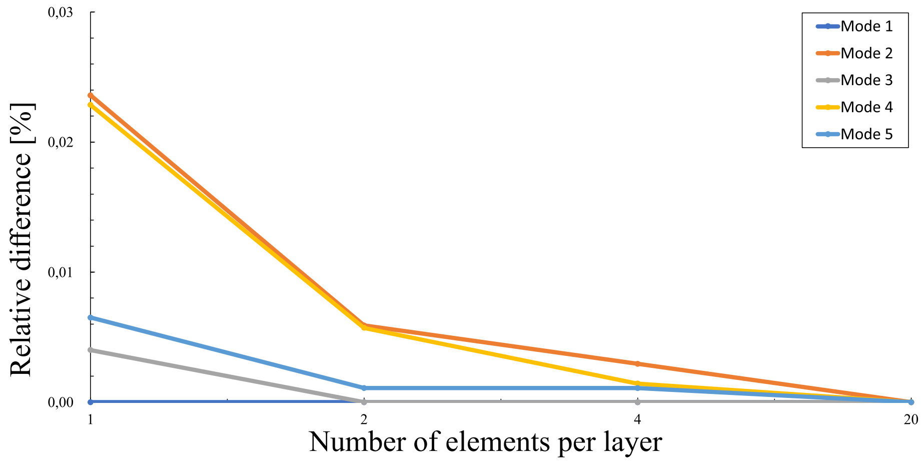

Figure 5.5: Results of convergence study in thickness direction

5.2.1.2 Mesh size in longitudinal direction

Utilizing one element per layer and maintaining the mesh size in the transverse direction at 125 mm, the mesh size in the longitudinal direction was varied from 5 to 300 mm. The results are shown in Figure 5.6, where the relative difference maintained low values under 0.1% for all mesh sizes. However, the computational time was low for the mesh size of 100 mm, thus chosen to retain the most accurate model possible.

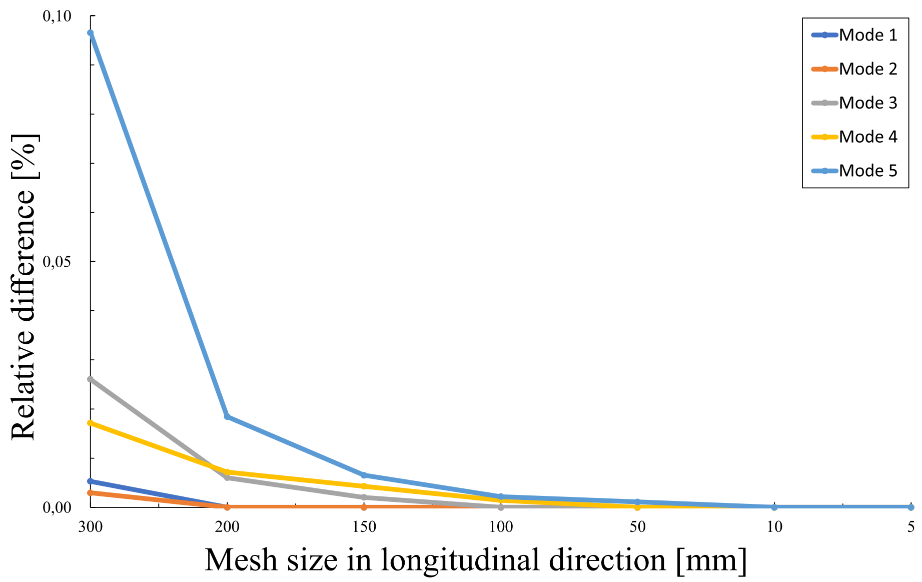

Figure 5.6: Results of convergence study in longitudinal direction

5.2.1.3 Mesh size in transverse direction

Again, employing one element per layer height and ensuring a constant mesh size of 50 mm in the longitudinal direction, the mesh size in the transverse direction was ranged from 5 to 300 mm. The results are shown in Figure 5.7, where the relative difference maintained low values under 0.4% for all mesh sizes. However, the computational time was low for the mesh size of 50 mm, thus chosen to retain the most accurate model possible.

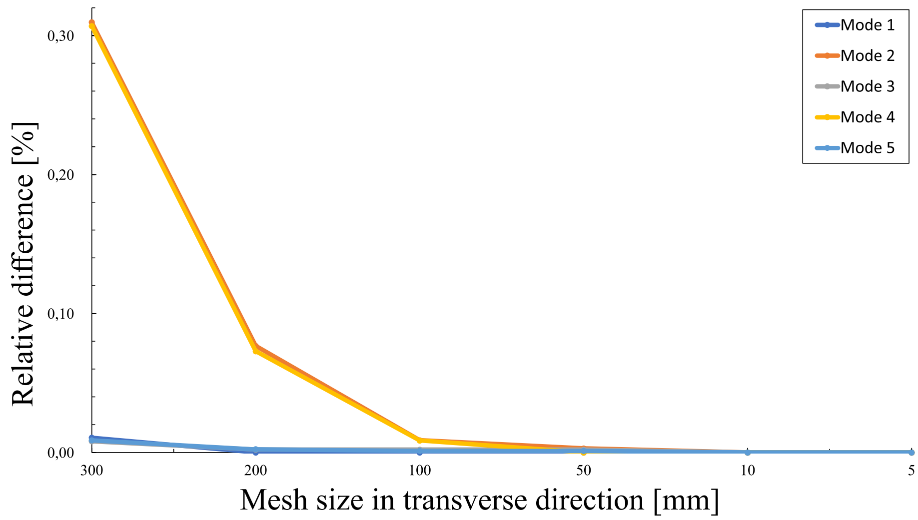

Figure 5.7: Results of convergence study in transverse direction

5.2.1.4 Mesh size – summery

Based on the results of the mesh convergence study, the mesh sizes utilized for the sensitivity analysis in Section 5.2 and calibrations in Section 5.3 are:

- 20 mm in thickness direction (1 element per layer)
- 100 mm in longitudinal direction
- 50 mm in transverse direction

5.2.2 Mechanical properties from literature study

The most common timber strength class for CLT is C24 – grading according to SS–EN 338:2016 [8]. This timber strength class was used in the experiment by Ljunggren [4], described in Section 5.1. In SS–EN 338:2016, timber strength classes ranges from C14, the lowest grade, to C50, the highest. However, for the sensitivity analysis, an upper limit of C40 was chosen as it was considered more reasonable, while the lower limit remained at C14.

The SS–EN 338:2016 gives values of E_L, E_L, E_T , G_{LT} and G_{LR} for strength classes C14 – C40 [8]. However, information about the Poisson's ratios and rolling shear modulus are not given. Therefore, these were obtained in other ways described below.

In [14], the Poisson's ratios used for C24 were $\upsilon_{LT} = 0.48$, $\upsilon_{LR} = 0.42$ and $\upsilon_{RT} = 0.28$, which was also used for the entirety of this dissertation. Moreover, they do not affect the vibration response to any applicable extent. In previous studies [13, 14, 15], Poisson's ratio has shown to have minimal effect on the natural frequencies and mode order. Therefore, Poisson's ratio was not included in the sensitivity analysis.

In [16], several tests were conducted to obtain mechanical properties of European softwoods. From these, average values for spruce are presented, where a ratio between G_{LT}/G_{RT} and G_{LR}/G_{RT} have been found to approximately 14. This ratio was used to estimate the rolling shear modulus for timber strength classes ranging from C14 to C40.

The density information was obtained through personal contact with Ljunggren [4], who informed that the mean density of the measured spruce panels was 428 kg/m^3.

The sensitivity analysis was performed by studying five values of each mechanical properties between the values of C14 and C40, while having C24 values as reference. See Table 5.2 for these intervals.

Table 5.2: Interval for sensitivity analysis. Moduli in MPa. Value 1,3 and 5 are obtained from SS–EN 338:2016 [8], while 2 and 4 are not physical parameters.

Value	E_L	E_T	E_R	G_{LT}	G_{LR}	G_{RT}
1 – C14 (lower limit)	7 000	230	230	440	440	31.11
2	9 000	300	300	565	565	39.95
3 – C24 (reference)	11 000	370	370	690	690	48.79
4	12 500	420	420	785	785	55.51
5 – C40 (upper limit)	14 000	470	470	880	880	62.22

5.2.3 Sensitivity analysis – results

Results from the sensitivity analysis showed that the elastic modulus in longitudinal direction E_L had significant impact on natural frequencies for the bending modes. The shear modulus G_{LT} had significant effect on torsional modes and the rolling shear modulus G_{RT} had impact on both bending– and torsional modes. The remaining properties E_T, E_R and G_{LR} showed negligible impact on the natural frequencies thus not presented. No variation in the mode order was observed. For the NRFDs of each value, see Figure 5.8.

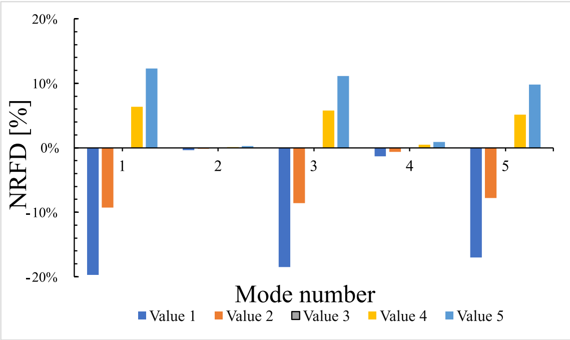

(a) E_L

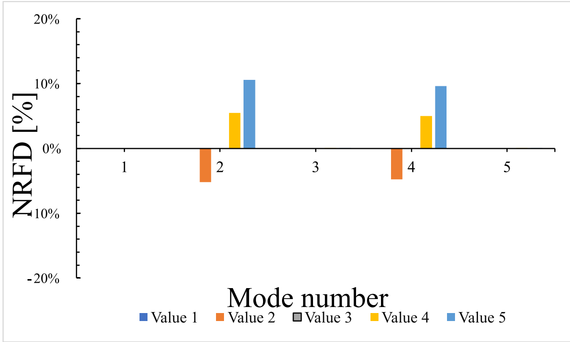

(b) G_{LT}

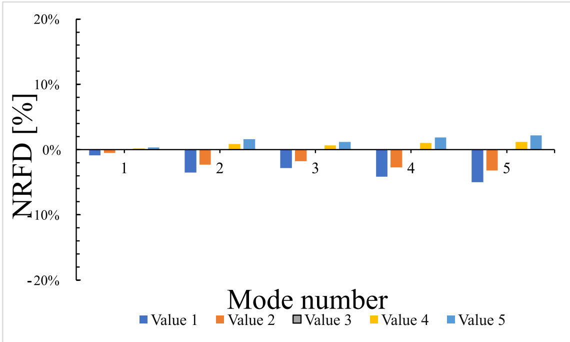

(c) G_{RT}

Figure 5.8: NRFDs of the three mechanical properties which had significant impact on the natural frequencies in the sensitivity study. Testing on five values for each mechanical property, having C24 (value 3) as references.

5.3 Calibrations of spruce properties

This section outlines the calibration process for calibrating realistic spruce mechanical properties, conducted using the Layered model, detailed in Section 4.1.

The calibrations were conducted through iterative procedures. Each calibration involved a significant number of iterations, during which mode shapes obtained from the numerical Layered model were compared to experimental ones using MAC values. For the experimental values used, see Table 5.1. A high degree of similarity between numerical and experimental modes was considered achieved when the diagonal MAC values were equal or exceed 0.95. Additionally, NRFDs was computed for each iteration, together with an averaged absolute value in NRFD over the five modes.

Density was excluded from sensitivity analysis and calibrations, as it is known. The properties subjected to calibrations were those with significant impact on natural frequencies, namely E_L, G_{LT} and G_{RT}. Two properties were calibrated simultaneously, and considering that three properties influence natural frequencies and mode shapes, a total of six combinations could be performed. It's noteworthy that for each of these six calibrations, all five modes were considered. Additionally, two further calibrations were performed by solely considering either bending modes or rotational modes. Further details for each calibration can be found below.

Calibration 1

In Calibration 1, all three properties were calibrated: E_L, G_{LT} and G_{RT}. This calibration process consisted of three runs and incorporating all five modes. During the first round, E_L and G_{LT} were calibrated. In the second round, the calibrated G_{LT} was set as fixed, and the calibrated E_L from the first run served as the initial guess. During this second round, both E_L and G_{RT} were calibrated. Finally, in the third round of calibration, the calibrated E_L was held fixed, and both G_{LT} and G_{RT} were calibrated.

Calibration 2

In Calibration 2, all three properties were calibrated: E_L, G_{LT}, and G_{RT}. Similar to Calibration 1, this process also consisted of three runs, each incorporating all five modes. During the first round, E_L and G_{LT} were calibrated, mirroring the first round of Calibration 1. In the second round, the calibrated E_L was held fixed, G_{LT} and G_{RT} were calibrated. Lastly, the last round of calibration, the calibrated G_{LT} was held fixed, and both E_L and G_{RT} were calibrated.

Calibration 3

In Calibration 3, all three properties E_L, G_{LT}, and G_{RT} were calibrated. Once again, this process comprised three runs, encompassing all five modes. This time, during the initial round, the properties calibrated were E_L and G_{RT}. In the subsequent round, E_L remained fixed while G_{LT} and G_{RT} were calibrated. Finally, in the last round of calibration, G_{RT} was held constant, and both E_L and G_{LT} were calibrated.

Calibration 4

In Calibration 4, all three properties E_L, G_{LT}, and G_{RT} were calibrated also with three runs and all five modes. The first round is exactly the same as the first round of Calibration 3. In the second round, G_{RT} remained fixed while E_L and G_{LT} were calibrated. Eventually, in the third round of calibration, the calibrated E_L was held fixed, and both G_{LT} and G_{RT} were calibrated.

Calibration 5

Calibration 5 consisted of three rounds and incorporating all five modes, where E_L, G_{LT}, and G_{RT} were calibrated. During the first round, calibration on G_{LT} and G_{RT} was done. In the second round, E_L and G_{LT} were calibrated. Finally, in the last round, both E_L and G_{RT} underwent calibration.

Calibration 6

Calibration 6 consisted also of three rounds and incorporating all five modes, where E_L, G_{LT}, and G_{RT} were calibrated. During the first round was the performed as the first round in calibration 5. In the second round, E_L and G_{RT} was optimized. Lately, in the last round, E_L and G_{LT} were calibrated.

Calibration 7

Calibration 7 was done with two runs. In the first round, when calibrating E_L and G_{RT}, only bending modes were compared (as E_L mostly impacts the bending modes). In the second round G_{LT} and G_{RT} was optimized by only comparing torsional modes (as G_{LT} mostly impacts the torsional modes). G_{RT} impacts all modes and therefore used for both rounds.

Calibration 8

Calibration 8 was performed in about same way as calibration 7, although with opposite order, i.e. G_{LT} and G_{RT} were calibrated in the first round comparing only torsional modes and calibrating E_L and G_{RT} in the second round comparing only bending modes.

Calibration results

Calibrations 5 and 6 gave invalid results, negative values, therefore they will not be presented. This is due to the relative small impact for the properties, G_{LT} and G_{RT}, compared to E_L on the bending modes.

Based on the calculated averaged absolute NRFD results, it was observed that calibration 2 yielded the lowest value, see Figure 5.9. Therefore, the properties obtained from the final results of this calibration were selected as the mechanical properties of interest.

The properties from calibration 2 were then adjusted to engineering–oriented values to account for the fact that the calibrated values, derived from experimental data, represent approximations of reality. This adjustment helps mitigate the potential false sense of “exactness” associated with the calibrated values, as they remain approximations. Another adjustment was made to the G_{LR} property, aligning its value with G_{LT} due to the difficulty in determining tangential and radial orientation in practical applications. These adjusted values are presented in Table 5.3.

For the calibrated values from all calibrations, see Table 5.4.

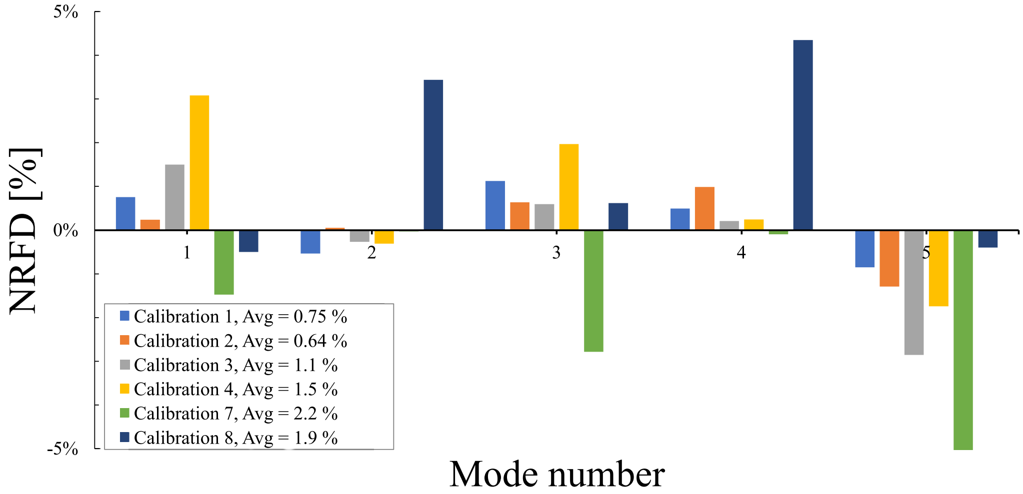

Figure 5.9: NRFD for all calibrations, including an absolute averaged value.

Table 5.3: The adjusted values of calibrations 2. Moduli in MPa.

E_L	E_T	E_R	G_{LT}	G_{LR}	G_{RT}
12 000	370	370	600	600	62

Table 5.4: Initial guess and results for each round of calibration, excluding calibrations 5 & 6. Calibrated properties are in bold and final results for each calibration are highlighted with gray background. Mduli in MPa.

	E_L	E_T	E_R	G_{LT}	G_{LR}	G_{RT}
Calibration 1 – round 1, initial guess	**11 000**	370	370	**690**	690	49
Calibration 1 – round 1, results	**12 275**	370	370	**610**	690	49
Calibration 1 – round 2, initial guess	**12 275**	370	370	610	690	**49**
Calibration 1 – round 2, results	**12 074**	370	370	610	690	**56**
Calibration 1 – round 3, initial guess	12 074	370	370	**610**	690	**56**
Calibration 1 – round 3, final results	12 074	370	370	**588**	690	**62**
Calibration 2 – round 1, initial guess	**11 000**	370	370	**690**	690	49
Calibration 2 – round 1, results	**12 275**	370	370	**610**	690	49
Calibration 2 – round 2, initial guess	12 275	370	370	**610**	690	**49**
Calibration 2 – round 2, results	12 275	370	370	**597**	690	**56**
Calibration 2 – round 3, initial guess	**12 275**	370	370	597	690	**56**
Calibration 2 – round 3, final results	**11 946**	370	370	597	690	**62**
Calibration 3 – round 1, initial guess	**11 000**	370	370	690	690	**49**
Calibration 3 – round 1, results	**12 770**	370	370	690	690	**36**
Calibration 3 – round 2, initial guess	12 770	370	370	**690**	690	**36**
Calibration 3 – round 2, results	12 770	370	370	**617**	690	**46**
Calibration 3 – round 3, initial guess	**12 770**	370	370	**617**	690	46
Calibration 3 – round 3, final results	**12 385**	370	370	**618**	690	46
Calibration 4 – round 1, initial guess	**11 000**	370	370	690	690	**49**
Calibration 4 – round 1, results	**12 770**	370	370	690	690	**36**
Calibration 4 – round 2, initial guess	**12 770**	370	370	**690**	690	36
Calibration 4 – round 2, results	**12 796**	370	370	**647**	690	36
Calibration 4 – round 3, initial guess	12 796	370	370	**647**	690	**36**
Calibration 4 – round 3, final results	12 796	370	370	**618**	690	**45**
Calibration 7 – round 1, initial guess	**11 000**	370	370	690	690	**49**
Calibration 7 – round 1, results	**11 713**	370	370	690	690	**78**
Calibration 7 – round 2, initial guess	11 713	370	370	**690**	690	**78**
Calibration 7 – round 2, final results	11 713	370	370	**640**	690	**39**
Calibration 8 – round 1, initial guess	11 000	370	370	**690**	690	**49**
Calibration 8 – round 1, results	11 000	370	370	**628**	690	**44**
Calibration 8 – round 2, initial guess	**11 000**	370	370	627	690	**44**
Calibration 8 – round 2, final results	**11 702**	370	370	628	690	**78**

5.4 Mechanical properties of spruce – summary

The final mechanical properties of spruce chosen when studying the impact of different lamellae material in Chapters 7–11, are presented in Table 5.5.

Table 5.5: The mechanical properties chosen when studying the impact of different lamellae material. Moduli in MPa, density (ρ) in kg/m^3 and the damping ratio (ζ) in%.

E_L	E_T	E_R	G_{LT}	G_{LR}	G_{RT}	ρ	ζ
12 000	370	370	600	600	62	428	0.7

In line with the calibration process, NRFDs was computed for the values in Table 5.5. This gave an average absolute NRFD of less than 1%, maintaining a low relative error.

6 Concrete, Air cavities & Elastomer properties

Analyzing the effect of using lamellae of other materials than spruce on the vibration response is the central part of this dissertation. This chapter describes the materials that were used to analyze the impact of different lamellae materials and their properties. These materials are concrete, air and elastomer.

6.1 Concrete

The conventional concrete strength class C25/30 is utilized when studying the impact of concrete lamellae material in Chapter 8. A concrete lamellae is meshed using continuum solid shell element, denoted by CSS8 according to the Abaqus naming convention.

Table 6.1: Concrete properties – The characteristic cylinder compressive strength (f_{ck}), modulus of elasticity (E_{cm}), and Poisson's ratio (υ), were obtained from Eurocode 2 [17], while the density (ρ) was obtained from Eurocode 1 [18].

Concrete type	ρ [kg/m^3]	f_{ck} [MPa]	E_{cm} [MPa]	υ
C25/30	2400	25	31	0.2

6.2 Air cavity

The material air was modeled with two different methods. First, modeling air as an acoustic medium with density of $\rho_0 = 1.21$ kg/m^3 and the speed of sound in air, $c = 343$ m/s (at 20°C and 1 atm)[12]. The bulk modulus, which is used as input parameter in Abaqus, can be calculated according to [19] as:

$$K = \rho_0 c^2 = 1.21 \cdot 343^2 = 142.4 \text{ MPa} \tag{6.1}$$

The flow resistance of an acoustic medium indicates the dissipation of energy [20]. This flow resistivity can be assumed to zero for air [19]. In Abaqus, the resistivity of a material could be express by a parameter called volumetric drag. This parameter was set to zero. A lamellae with air as acoustic medium is meshed using acoustic element, denoted by AC3D8 according to the Abaqus naming convention.

The second method of modeling air was to model it as “Empty space”, a static “solid” homogeneous material. The air’s density was set to $\rho_0 = 1.21$ kg/m^3 and the Young’s modulus together with the Poisson’s ratio were set to a value close to zero, in this case $1 \cdot 10^{--9}$. In this dissertation, this material is referred to as “Empty space”. An empty space lamellae is meshed using continuum solid shell element, denoted by CSS8 according to the Abaqus naming convention.

6.3 Elastomer

In this dissertation, two types of elastomer material were analyzed in CLT panels, one soft and one stiff type. Their properties were based on Sylodyn material. Sylodyn is a viscoelastic material made of closed–cell PU elastomer (Polyurethane), produced by a German company called Getzner Werkstoffe [21]. Getzners assortment includes different qualities of Sylodyn depending on its static range of use, the softest and lightest one is Sylodyn NB and the stiffest and heaviest one is Sylodyn NF.

It is of importance to note that properties of Sylodyn NF and NB were calibrated in this section using linear hybrid elements (denoted with C3D8RH according to Abaqus naming convention). However, when studying the impact of elastomer lamellae in Chapters 10 and 11, the elastomer lamellae are meshed using continuum solid shell elements, denoted by CSS8 according to the Abaqus naming convention.

To be clear, it is not precisely Sylodyn NF and Sylodyn NB that have been modeled, but rather close replicas of these materials. Nevertheless, the primary focus of this dissertation is to analyze the dynamic behavior of CLT panels with elastic lamellae material, rather than modeling precisely Sylodyn NF and NB. Therefore, for ease of communication, these types will continue to be referred to as Sylodyn NF and Sylodyn NB. These two types were tested in CLT panels when studying the impact of stiff and soft elastomer lamellae material in Chapters 10–11, with the stiff elastomer referred to as “Sylodyn NF” and the soft elastomer referred to as “Sylodyn NB”.

6.3.1 Modeling methodology

The methodology of modeling Sylodyn as a viscoelastic material has been presented in a previous study [22]. An overview of the modeling methodology of Sylodyn is presented. For more comprehensive details regarding said modeling methodology, readers are referred to the original article by Negreira [22].

Static behavior
As mentioned before, Sylodyn is a viscoelastic material, i.e. its properties are frequency dependent. The static behavior of Sylodyn can be defined by the static Young’s modulus E^{∞} and the static Poisson’s ratio v^{∞}.

The static Young’s modulus E^{∞} is the long–term modulus due to low loading rates [22]. The static shear modulus G^{∞} and static bulk modulus K^{∞} are connected to the static Young’s modulus as:

$$G^{\infty} = \frac{E^{\infty}}{2(1+v^{\infty})} \tag{6.2}$$

and

$$K^{\infty} = \frac{E^{\infty}}{3(1--2v^{\infty})} \tag{6.3}$$

Dynamic behavior
The complex Young's modulus of Sylodyn can be described as:

$$E^{*} = E^{dyn}\mathrm{cos}\delta + iE^{dyn}\mathrm{sin}\delta = E^{dyn}\mathrm{cos}\delta(1 + i\mathrm{tan}\delta) \tag{6.4}$$

Where E^{dyn} is the dynamic modulus and $\mathrm{tan}\delta$ represents the loss factor which indicates energy dissipation.

In the same manner as the complex Young's modulus E^{*}, the complex shear modulus G^{*} and complex bulk modulus K^{*} can be described as:

$$G^{*} = G^{dyn}\mathrm{cos}\delta + iG^{dyn}\mathrm{sin}\delta \tag{6.5}$$

$$K^{*} = K^{dyn}\mathrm{cos}\delta + iK^{dyn}\mathrm{sin}\delta \tag{6.6}$$

Dynamic shear modulus G^{dyn} and dynamic bulk modulus K^{dyn} are connected to the dynamic Young's modulus as equations below in the same way as the static ones however with the complex Poisson's ratio. The complex Poisson's ratio is assumed to be real and constant, i.e. $v^{*} = v^{\infty}$, the relation can be expressed as:

$$G^{dyn} = \frac{E^{dyn}}{2(1+v^{\infty})} \tag{6.7}$$

and

$$K^{dyn} = \frac{E^{dyn}}{3(1--2v^{\infty})} \tag{6.8}$$

The ratio between the dynamic and static Young's modulus is defined with scale factor $\alpha(f)$ as:

$$\alpha(f) = \frac{E^{dyn}(f)}{E^{\infty}} \tag{6.9}$$

The ratio between the dynamic and static shear moduli, as well as bulk modulus gives:

$$\frac{G^{dyn}(f)}{G^{\infty}} = \frac{\frac{E^{dyn}(f)}{2(1+v^{\infty})}}{\frac{E^{\infty}}{2(1+v^{\infty})}} = \frac{E^{dyn}(f)}{E^{\infty}} = \alpha(f) \tag{6.10}$$

and:

$$\frac{K^{dyn}(f)}{K^{\infty}} = \frac{\frac{E^{dyn}(f)}{3(1--2v^{\infty})}}{\frac{E^{\infty}}{3(1--2v^{\infty})}} = \frac{E^{dyn}(f)}{E^{\infty}} = \alpha(f) \tag{6.11}$$

It is importance to note that when a load is applied in certain boundary conditions, that allowing the Sylodyn to bulge, it would create structural effects (detonated with subindex c), i.e,the structural–dependent static Young's modulus is detonated with E_c^∞ and the structural–dependent dynamic Young's modulus with E_c^{dyn} (see Figure 6.1a and 6.1c). These structural effects happens in most cases due to friction. However, when eliminating these structural effects, the material is able to deform freely and resulting in lower values for the static as well as the dynamic Young's modulus (see Figure 6.1b and 6.1d). Additionally, the structural–dependent moduli are proportional to the non–structural–dependent ones with the same constant k_c as:

$$E_c^\infty = k_c E^\infty \tag{6.12}$$

and

$$E_c^{dyn} = k_c E^{dyn} \tag{6.13}$$

Therefore, the scale factor can also be expressed by the ratio between the structural–dependent dynamic and static Young's modulus.

$$\frac{E_c^{dyn}(f)}{E_c^\infty} = \frac{E^{dyn}(f)}{E^\infty} = \alpha(f) \tag{6.14}$$

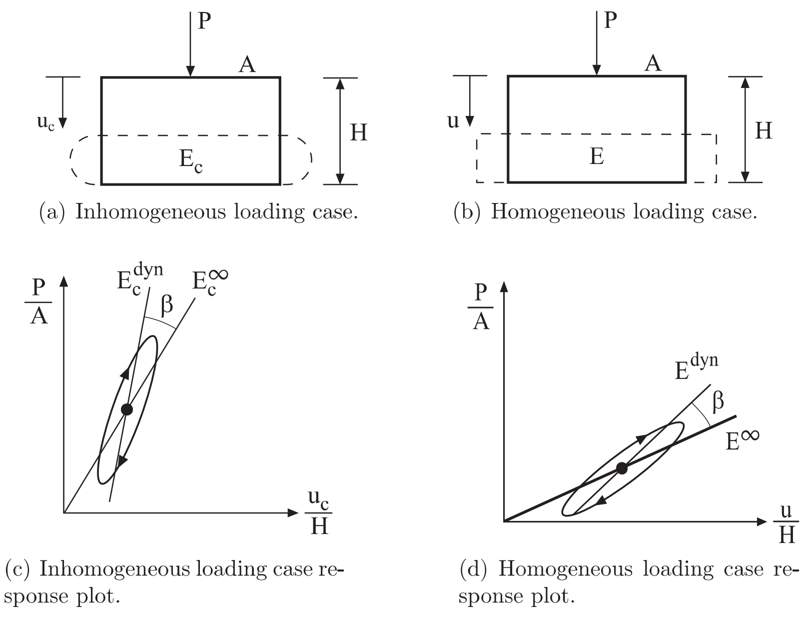

(a) Inhomogeneous loading case.

(b) Homogeneous loading case.

(c) Inhomogeneous loading case response plot.

(d) Homogeneous loading case response plot.

Figure 6.1: Structural effects on Young's moduli. Compression test that is not allowing Sylodyn to bulge (a and c) and allowing bulging (b and d) [22]

.

In Abaqus, a frequency dependence viscoelastic material can be created by these following steps: **Mechanical** → **Elasticity** → **Viscoelastic: Domain: Frequency** and **Frequency: Tabular**

In Abaqus, the dynamic behavior of a viscoelastic material can be expressed by the real and imaginary parts of the non–dimensional (structural–independent) shear and bulk relaxation functions $g(t)$ and $k(t)$, see Abaqus's manual for more details [20]. These parts are defined as:

$$\omega\Re(g^*) = \frac{G^{dyn}\cos\delta}{G^\infty} = \alpha(f)\cos\delta \tag{6.15}$$

$$\omega\Im(g^*) = 1 - \frac{G^{dyn}\sin\delta}{G^\infty} = 1 - \alpha(f)\sin\delta \tag{6.16}$$

$$\omega\Re(k^*) = \frac{K^{dyn}\cos\delta}{K^\infty} = \alpha(f)\cos\delta \tag{6.17}$$

$$\omega\Im(k^*) = 1 - \frac{K^{dyn}\sin\delta}{K^\infty} = 1 - \alpha(f)\sin\delta \tag{6.18}$$

6.3.2 Sylodyn – static material properties

In [22], an experiment was performed with the aim of finding out the structural–independent static Young's modulus of Sylodyn NE which resulted in $E^\infty = 3.2$ MPa.

The densities of Sylodyn are not given in the data sheets [21], however the density of Sylodyn NE was measured to 750 kg/m^3 and presented in [22]. The densities of type NB and NF were obtained through personal contact with Sylodyn–responsible product manager of the company Christian Berner – a technology intermediary supplier [23]. See Table 6.2 for these densities.

Table 6.2: Density for various Sylodyn types

Type	Density kg/m^3
Sylodyn NB	380 [23]
Sylodyn NE	750 [22]
Sylodyn NF	840 [23]

In general, the data sheets of Sylodyn provide material parameters at a specific load (the maximal limit in static range of use of a certain Sylodyn type) and at a so–called shape factor q = 3 (See Figure 6.2 for definition of shape factor). Both the Young's modulus and displacement are dependent on this shape factor for all types of Sylodyn.

The dimensions of the lamellae results in a shape factor between 4–5 (see Chapter 7 for dimensions of lamellae). Having two lamellae or more next to each other makes the shape factor larger than 6. Moreover, the change in Young's modulus and displacement both approach zero for shape factor larger than 6. Comparing Young's modulus and displacement of shape factor 4–5 with shape factor 6, the changes are smaller than 5% for Sylodyn NE, smaller than 8% for Sylodyn NF and almost 0 for Sylodyn NB. Taking these factors into account, the application of the Sylodyn material parameter

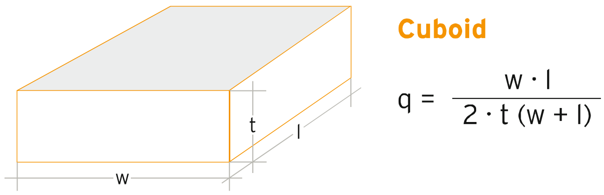

Figure 6.2: Definition of shape factor [24].

to different lamellae is facilitated by assuming that the material parameters for form factor 6 are valid for all lamellae.

The process of extracting static material parameters is summarized below:

1. Sylodyn NE – Note that Sylodyn NE was not tested when studying the impact of different lamellae material in Chapters 8–11. This step must be performed for obtaining the static material parameters of Sylodyn NF and NB.

   (a) A quadratic block of Sylodyn NE was created (as a static material) with shape factor 6 and thickness 12.5 mm in Abaqus using experimental static Young's modulus of $E^{\infty} = 3.2$ MPa and density. The mesh approximation used for this block was linear hybrid elements (denoted with C3D8RH according to Abaqus naming convention).

   (b) The displacements at the bottom of the block were set to zero in all directions.

   (c) A displacement–load with loading rate 0.125 mm/s (other load rates have been tested and provided the same results) was applied and the stress in the middle of the block's surface was measured.

   (d) The Poisson's ratio was calibrated by comparing the load–displacement curve from the FE–model with the corresponding one from in the data sheet (corresponded for form factor 6) [24]. The calibrated Poisson's ratio was obtained to $v^{\infty} = 0.41$ see Figure 6.3a.

   (e) The process above was repeated for other FE–models with the same factor q = 6, but with thicknesses 25 mm, 37.5 mm and 50 mm. The calibrated Poisson's ratio $v^{\infty} = 0.41$ was valid also for these thicknesses. The Poisson's ratio was assumed to be constant and would be used for obtaining the static Young's modulus (E^{∞}) for other types of Sylodyn, see Figure 6.3b.

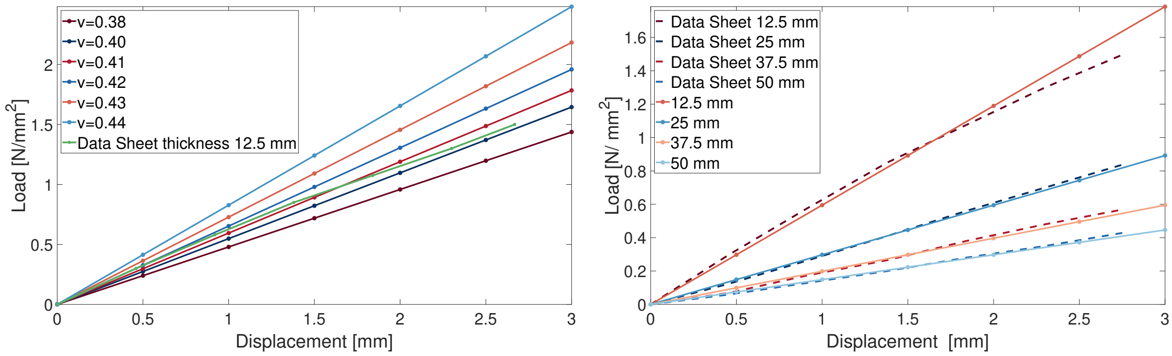

(a) Thickness 12.5 mm **(b)** Different thicknesses

Figure 6.3: Sylodyn NE. Load – Displacement Curves. $E^{\infty} = 3.2.$ MPa. Calibration of v^{∞}. See [24] for the data sheet of Sylodyn NE.

2. Sylodyn NF

   (a) The same FE models in the steps in Sylodyn NE was created with the same load and boundary conditions.

   (b) However, the calibrated Poisson's ratio $v^{\infty} = 0.41$ was used here. The structural–independent static Young's modulus of Sylodyn NF was calibrated by comparing the load–displacement curve from the FE–model with the corresponding one from in the data sheet (corresponded for form factor 6). The calibrated static Young's modulus was obtained to $E^{\infty} = 7$ MPa and this value was valid for all last–mentioned thicknesses, see Figure 6.4.

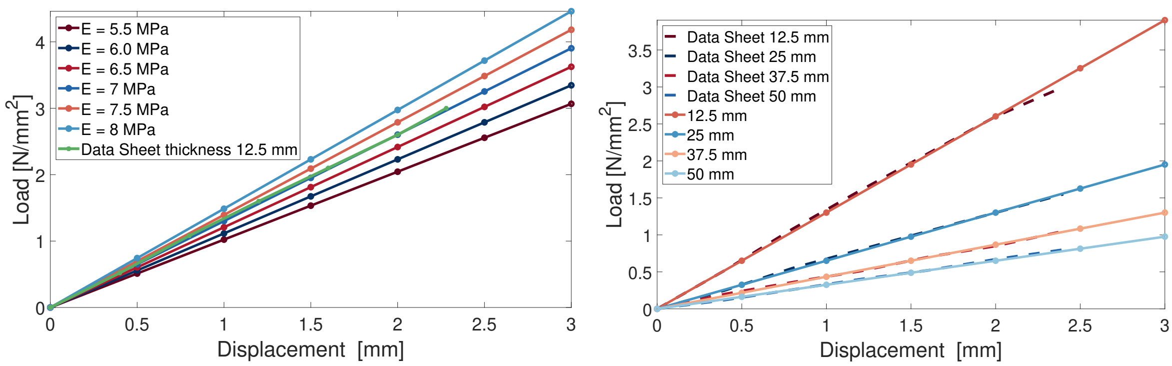

(a) Sylodyn NF. Load – Displacement Curve. Thickness 12.5 mm **(b)** Sylodyn NF. Load – Displacement Curve. Different thicknesses

Figure 6.4: Sylodyn NF. Load – Displacement Curves. $v^{\infty} = 0.41$. Calibration of E^{∞}. See [25] for the data sheet of Sylodyn NF.

3. Sylodyn NB

   (a) The same steps in Sylodyn NF were repeated. The calibration of static Young's modulus of Sylodyn NB was performed for the FE model with different thicknesses, and this was obtained to $E^{\infty} = 0.5$ MPa, see Figure 6.5.

   (b) It is notable that the relationship between displacement and load of different thicknesses was non–linear. However, the static Young's modulus

($E^{\infty} = 0.5$ MPa) appeared to be valid for small displacements. Due to the load magnitude when studying the impact of different lamellae material in Chapters 7–11, the static Young's modulus (E^{∞}) was deemed to be 0.5 MPa. Therefore, this value was assumed to be sufficient when studying the impact of lamellae material Sylodyn NB in Chapter 11.

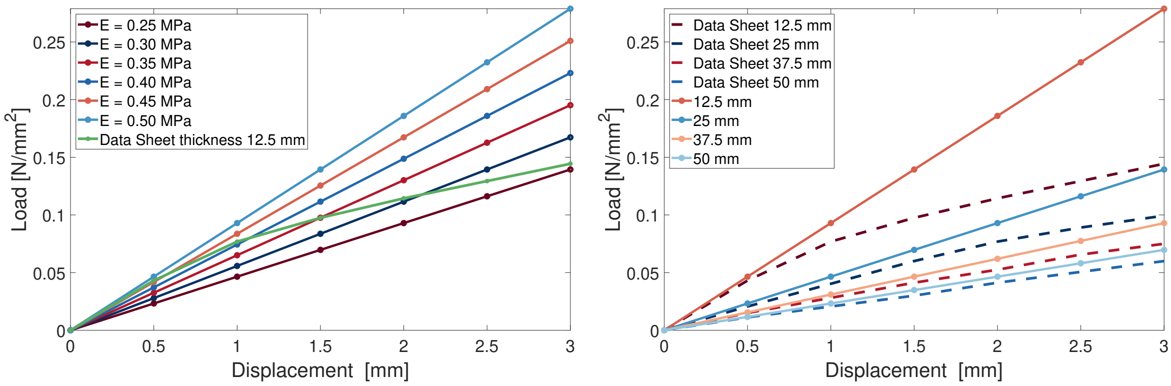

(a) Sylodyn NB. Load – Displacement Curve. Thickness 12.5 mm

(b) Sylodyn NB. Load – Displacement Curve. Different thicknesses

Figure 6.5: Sylodyn NB. Load – Displacement Curves. $v^{\infty} = 0.41$. Calibration of E^{∞}. See [26] for the data sheet of Sylodyn NB.

6.3.3 Sylodyn – dynamic material properties

The scale factor $\alpha(f)$ can be calculated by Equation 6.14 and the dimensional (structural–dependent) dynamic and static Young's modulus can be read in data sheet [27], see Figure 6.6 (assuming that values for 1 Hz applicable for the static ones).

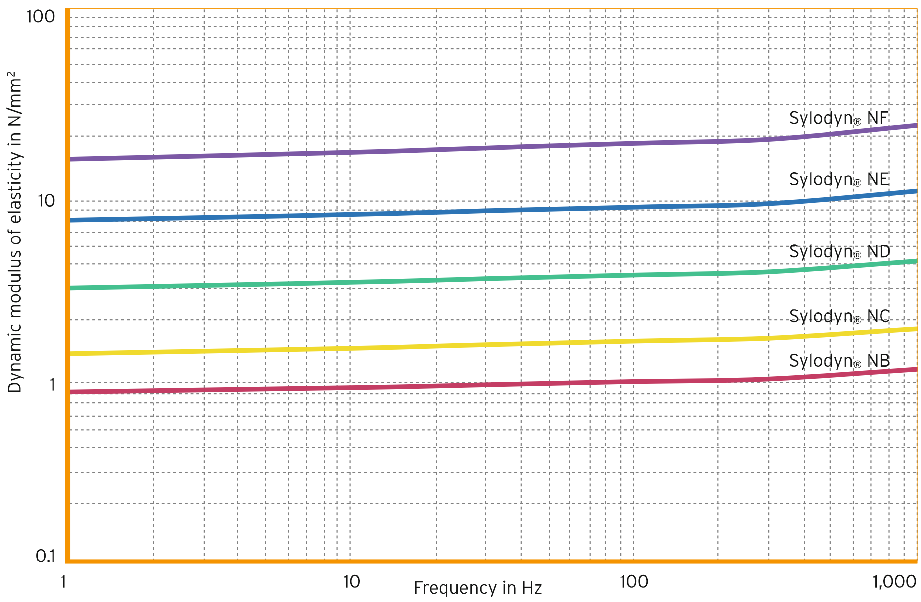

Figure 6.6: Dynamic modulus of elasticity depending on the frequency [27].

The loss factors can also be found in product data sheets [27]. However, these were given only for a couple of frequencies (1, 50 100 and 100 Hz) which required interpolation for the other frequencies than the given ones (see Figure 6.7 for interpolation of loss factors). For small phase angle, the following approximation is valid tan$\delta \approx \delta$.

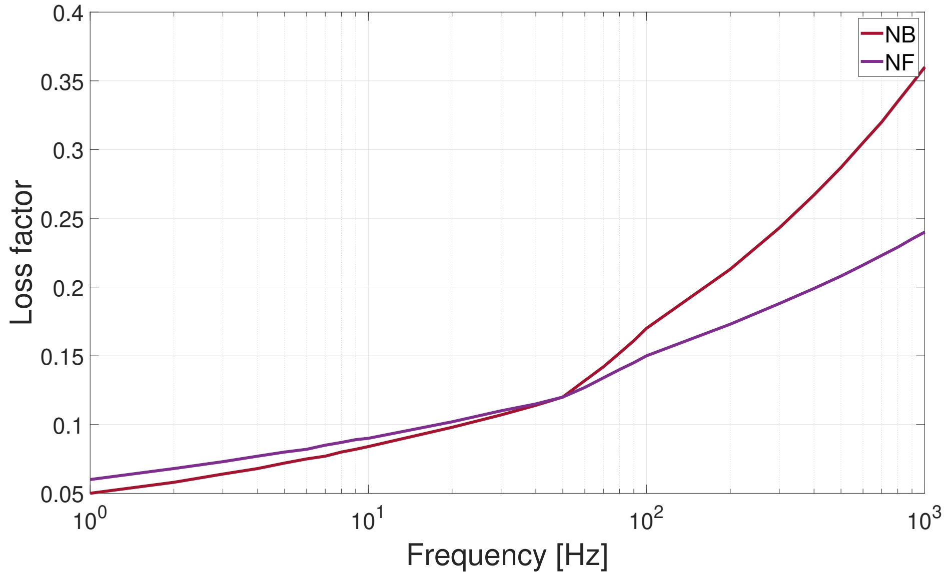

Figure 6.7: Dependency of the two Sylodyn type NB and NF frequency on the loss factor.

The inputs to Abaqus for modeling Sylodyn, with tabular values according to Section 6.3.1, were presented in Tables 6.3 and 6.4. It is noteworthy that the color marked values in Tables 6.3 and 6.4 are the given loss factor in the detailed data sheet of Sylodyn [27].

Table 6.3: Sylodyn NF – Inputs to Abaqus. The loss factors obtained from the data sheet are highlighted with a colored background.

	Data Sheet			Scale factor	Abaqus input	
f [Hz]	E_c^{dyn} [MPa]	E_c^{∞} [MPa]	$\tan\delta \approx \delta$	$\alpha(f)$	$\omega\Re(g^*)$ $\omega\Re(k^*)$	$\omega\Im(g^*)$ $\omega\Im(k^*)$
1	11.99	11.99	0.06000	1.000	0.06000	0.001800
2	12.81	11.99	0.06784	1.068	0.07243	–0.06600
3	13.32	11.99	0.07289	1.111	0.08089	–0.10771
4	13.69	11.99	0.07671	1.142	0.08748	–0.1382
5	13.98	11.99	0.07980	1.166	0.09296	–0.1625
6	14.23	11.99	0.08242	1.187	0.09770	–0.1827
7	14.44	11.99	0.08470	1.204	0.10188	–0.2000
8	14.62	11.99	0.08673	1.220	0.1057	–0.2152
9	14.79	11.99	0.08856	1.234	0.1091	–0.2287
10	14.94	11.99	0.09023	1.246	0.1123	–0.2410
20	15.69	11.99	0.10202	1.309	0.1333	–0.3018
30	16.15	11.99	0.1096	1.347	0.1473	–0.3386
40	16.48	11.99	0.1153	1.374	0.1582	–0.3652
50	16.74	11.99	0.1200	1.396	0.1671	–0.3861
60	16.96	11.99	0.1273	1.414	0.1795	–0.4028
70	17.14	11.99	0.1337	1.430	0.1906	–0.4170
80	17.31	11.99	0.1396	1.443	0.2008	–0.4293
90	17.45	11.99	0.1450	1.455	0.2103	–0.4401
100	17.58	11.99	0.1500	1.466	0.2191	–0.4498
200	18.46	11.99	0.1728	1.540	0.2648	–0.5170
300	19.00	11.99	0.1877	1.585	0.2957	–0.5568
400	20.09	11.99	0.1991	1.676	0.3314	–0.6425
500	20.98	11.99	0.2083	1.750	0.3619	–0.7119
600	21.74	11.99	0.2162	1.813	0.3889	–0.7706
700	22.40	11.99	0.2231	1.868	0.4133	–0.8215
800	22.98	11.99	0.2293	1.917	0.4357	–0.8667
900	23.51	11.99	0.2349	1.961	0.4564	–0.9073
1000	24.00	11.99	0.2400	2.002	0.4758	–0.9443

Table 6.4: Sylodyn NB – Inputs to Abaqus. The loss factors obtained from the data sheet are highlighted with a colored background

	Data Sheet			Scale factor	Abaqus input	
f [Hz]	E_c^{dyn} [MPa]	E_c^{∞} [MPa]	$\tan\delta \approx \delta$	$\alpha(f)$	$\omega\Re(g^*)$ $\omega\Re(k^*)$	$\omega\Im(g^*)$ $\omega\Im(k^*)$
1	0.7500	0.7500	0.05000	1.000	0.04998	0.001250
2	0.7788	0.7500	0.05839	1.038	0.06060	−0.03663
3	0.7962	0.7500	0.06394	1.062	0.06782	−0.05937
4	0.8087	0.7500	0.06819	1.078	0.07347	−0.07576
5	0.8186	0.7500	0.07168	1.091	0.07817	−0.08862
6	0.8267	0.7500	0.07466	1.102	0.08223	−0.09923
7	0.8337	0.7500	0.07728	1.112	0.08582	−0.1083
8	0.8398	0.7500	0.07963	1.120	0.08906	−0.1161
9	0.8451	0.7500	0.08176	1.127	0.09202	−0.1231
10	0.8500	0.7500	0.08371	1.133	0.09476	−0.1294
20	0.8619	0.7500	0.09775	1.149	0.1122	−0.1437
30	0.8689	0.7500	0.1070	1.159	0.1238	−0.1519
40	0.8740	0.7500	0.1142	1.165	0.1327	−0.1577
50	0.8779	0.7500	0.1200	1.171	0.1401	−0.1621
60	0.8811	0.7500	0.1315	1.175	0.1541	−0.1647
70	0.8838	0.7500	0.1421	1.178	0.1669	−0.1666
80	0.8862	0.7500	0.1520	1.182	0.1789	−0.1680
90	0.8883	0.7500	0.1612	1.184	0.1901	−0.1690
100	0.8902	0.7500	0.1700	1.187	0.2008	−0.1698
200	0.9026	0.7500	0.2131	1.204	0.2545	−0.1763
300	0.9100	0.7500	0.2432	1.213	0.2922	−0.1776
400	0.9522	0.7500	0.2671	1.270	0.3351	−0.2246
500	0.9862	0.7500	0.2872	1.315	0.3725	−0.2611
600	1.015	0.7500	0.3048	1.353	0.4061	−0.2909
700	1.040	0.7500	0.3205	1.387	0.4368	−0.3159
800	1.062	0.7500	0.3348	1.416	0.4652	−0.3374
900	1.082	0.7500	0.3479	1.443	0.4917	−0.3561
1000	1.100	0.7500	0.3600	1.467	0.5167	−0.3726

7 Impact of different lamellae material – model development

In this chapter, an overview of the model development for when studying the impact of different lamellae material is presented. This includes introducing the dimensions and lay–ups of the panels analyzed, the convergence analysis to validate the model and description of the chapter structure and terminology used.

When studying the impact of different lamella material, two panels were tested on, each with the same width of 2.4 m but varying lengths of 5 and 9 m as well as different lay–ups and heights. These panels were labeled as medium sized panel (M–sized panel) and large sized panel (L–sized panel), corresponding to lengths of 5 m and 9 m, respectively, see Figure 7.1. The width of each lamella was 200 mm in the L–sized panel and 120 mm in the M–sized panel, except for the two outer lamellae in the length direction of the M–sized panel, which had a width of 160 mm (in each layer). The study was primarily conducted on the L-sized panel, with additional analyses performed on the M-sized panel to determine if dimensions and/or lay-ups influence the changes in dynamic behavior.

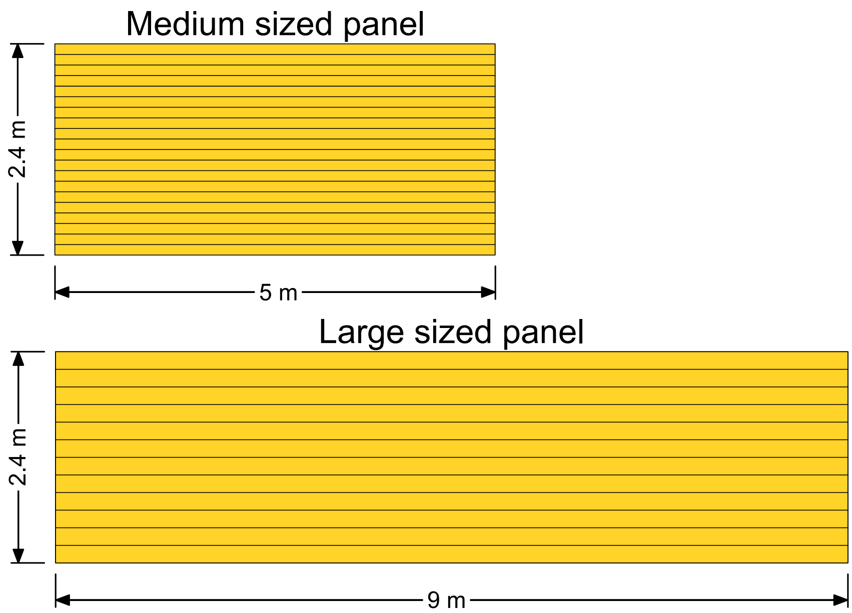

Figure 7.1: Illustrations of the two different panel sizes labeled medium sized panel and large sized panel respectively.

The M–sized panel consists of 5 layers of 30 mm thick lamellae and the L–sized panel of 7 layers of 45 mm thick lamellae. For the L–sized panel, the two outermost layers are oriented along the length of the panel, see Figure 7.2.

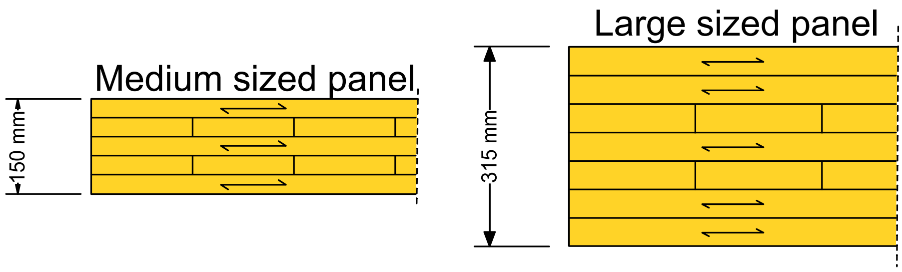

Figure 7.2: Illustrations of the two different panel lay–ups labeled medium sized panel and large sized panel respectively.

These panels were obtained from [13], were verifications following the European design codes described in [9], based on [28, 29], were performed to ensure practical relevance. These verifications were conducted in the ultimate limit state and in the serviceability limit state with assumed strength class of timber C24. For more comprehensive details regarding the verifications, readers are referred to the original article [13].

The frequency range of interest was chosen so the results would be relevant for both structural vibrations and radiated sound. Frequencies up to 100 Hz can be of interest for human comfort in structural vibrations caused by, for example, footfall or train–traffic nearby the buildings. Frequencies up to 20 000 Hz are relevant for radiated sound, as this is the upper limit of human hearing. In this dissertation, the frequency range of interest was chosen to be up to 562 Hz. Frequency 562 Hz is the upper limit for the 1/3 octave band of the center frequency 500 Hz. This is due to disturbances above this threshold are normally resolved by, for example, coverings that are used regardless of whether there are disturbances or not, such as gypsum boards. This would ensure relevance for both structural vibrations and radiated sound, and also provide the opportunity to illustrate the results in 1/3 octave band.

In this dissertation, free–free boundary conditions was utilized. This ensured that any interference on the vibration response from the boundary conditions was eliminated.

The main focus are the effects on accelerance when utilizing different materials in CLT panels. Note that accelerance connects to mobility, as described in Chapter 3.

7.1 Model development - large sized panel

To validate the model, a convergence analysis was performed on solely the L–sized panel, with the resulting mesh size and frequency step size utilized for the M–sized panel. The decision to focus on the L–sized panel for this analysis was driven by the larger dimensions and consequently greater mass. This results in a greater number of natural frequencies occurring within the same frequency range compared to the M–sized panel. Consequently, more information needs to be captured. If captured for the L–sized panel, it should also be captured for the other panel. Verifications were performed on the M–sized panel to confirm this.

The convergence studies were conducted by evaluating the steady–state dynamic response of the panel in Abaqus using the step *steady–state, Direct*, with a unit force of 1 N applied at the excitation point. For the chosen boundary condition, a standard practice placement of this excitation point would be in one of the corners, with the measurement point in the opposite corner. The same placement strategy was employed here, as depicted in Figure 7.3. This ensured the excitation of all modes within the frequency range.

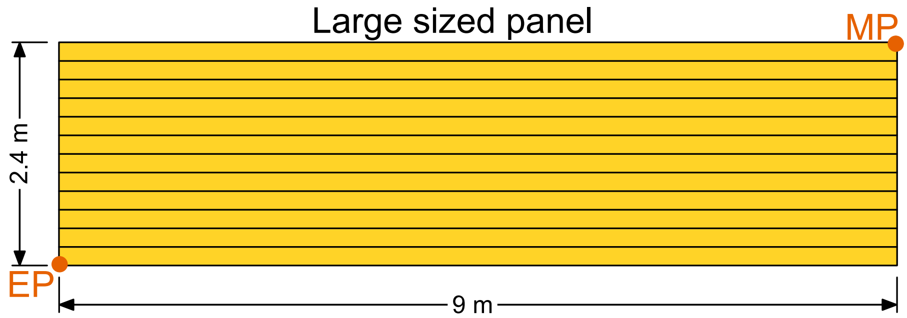

Figure 7.3: Excitation point (EP) and measure point (MP) for the L–sized panel.

7.1.1 Frequency step

To optimize computational time, a frequency step convergence analysis was conducted to determine the minimum frequency step required to achieve accurate results. It was done by comparing the steady–state dynamic responses of the panel for different frequency steps. The frequency steps tested was 0.1 Hz, 0.3 Hz 0.5 Hz and the mesh size was set to 50 mm in horizontal plane with one element per layer. In addition to directly comparing the response of the panel, the RMS–values and relative differences of said responses were also addressed.

The steady–state dynamic response for the finest tested frequency step of 0.1 Hz can be seen in Figure 7.4.

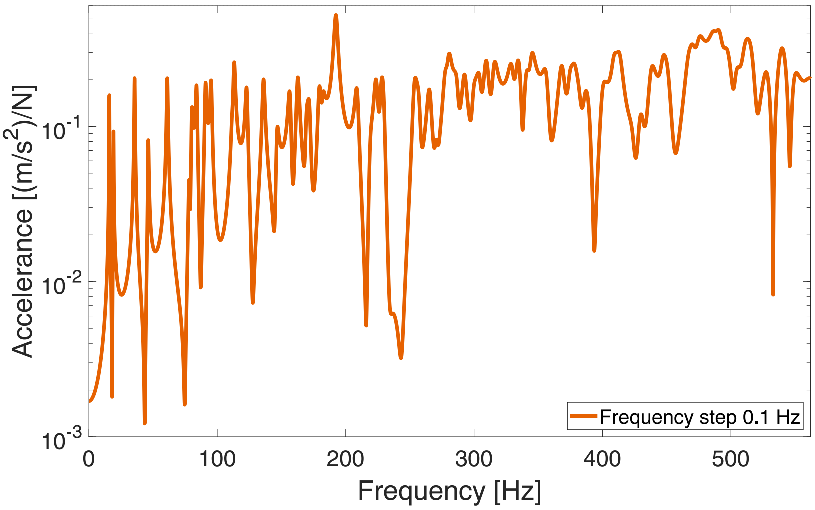

Figure 7.4: Steady–state dynamic response for the finest frequency step 0.1 Hz. The accelerance is shown in complex magnitude.

The frequency steps of 0.5 Hz and 0.3 Hz were analyzed in relative difference to the reference frequency step of 0.1 Hz, see Figure 7.5. It is important to recognize that a small deviation in frequency for the same peaks between responses could mean unreasonably high relative differences for a specific frequency. This is further explained following Figure 7.5.

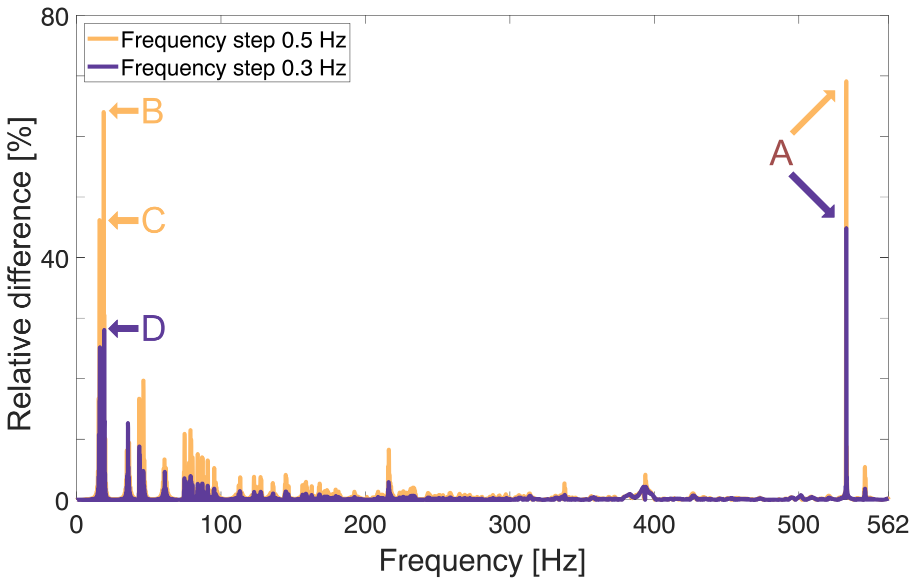

Figure 7.5: Absolute relative difference for frequency step 0.5 Hz and 0.3 Hz, with 0.1 Hz as reference.

The high value in relative differences at marker A in Figure 7.5 are troughs in the responses. A trough isn't of interest for the overall response for these types of analyses, as its holds relative small values compared to the peaks. The value in relative difference at marker B is due to almost vertical responses between the three different frequency steps, resulting in unreasonably high values in relative difference. However, the values in relative difference at marker C and marker D is in fact peaks in the responses. By closer studying these, a greater understanding of how the relative difference is calculated was obtained. The peak in response corresponding to marker C can be seen in Figure 7.6, with the relative difference illustrated for frequency 15.9 Hz.

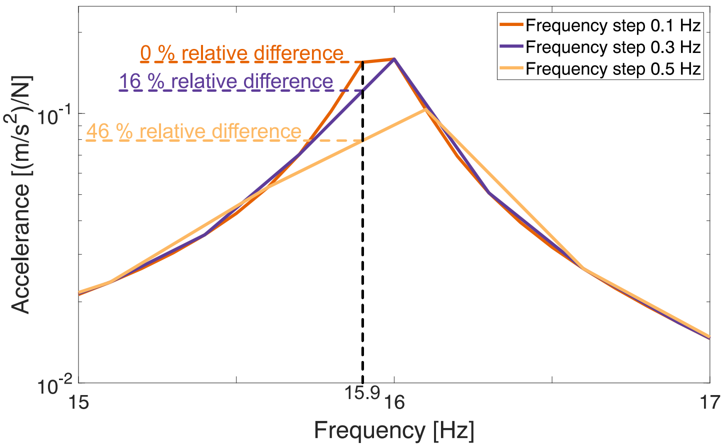

Figure 7.6: Absolute relative difference for different frequency steps at frequency 15.9 Hz.

This shows the aforementioned phenomenon of a small deviation in frequency for the same peaks causing unreasonably high relative differences. Instead, a clearer understanding of the actual deviation can be obtained by directly comparing the peaks values between the frequency steps. This resulted in a relative difference of 35% in accelerance, and 0.6% in frequency for frequency step 0.5 Hz, and 0% in both accelerance and frequency for frequency step 0.3 Hz, see Figure 7.7. Meaning a reduction from 46% to 35% in relative difference for frequency step 0.5 Hz, which still wasn't considered sufficient enough. The relative difference in frequency was almost insignificant.

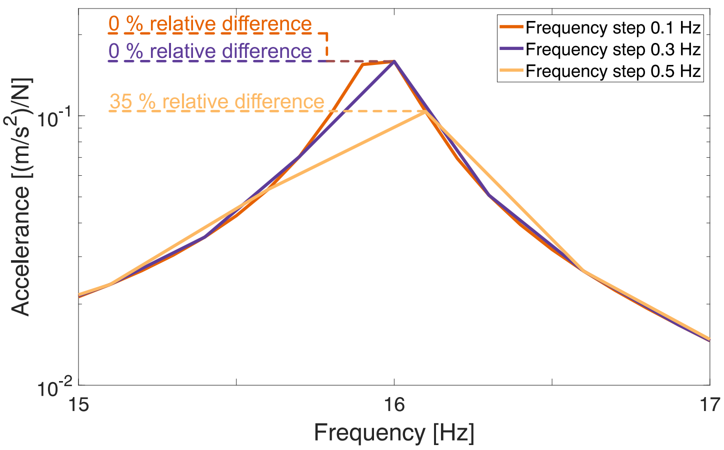

Figure 7.7: Absolute relative difference for different frequency steps comparing peak to peak at maximum absolute relative difference of interest for frequency step 0.5 Hz.

However, this was the maximum value of interest in relative difference, which corresponded to a peak in response, for the frequency step 0.5 Hz. Therefore, an additional study was conducted in the same manner, but for the frequency step 0.3 Hz. The peak in response corresponding to marker D can be seen in Figure 7.8, with the relative difference illustrated for frequency 19.2 Hz.

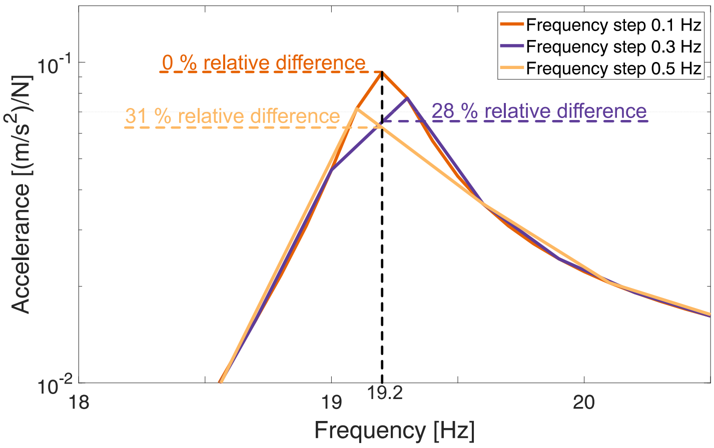

Figure 7.8: Absolute relative difference for different frequency steps at frequency 19.2 Hz.

By instead comparing the peaks, a relative difference of 17% in accelerance, and 0.5% in frequency was obtained for frequency step 0.3 Hz, see Figure 7.9. This is considerably less than frequency step 0.5 Hz but required further analysis to conclude if it is sufficient enough.

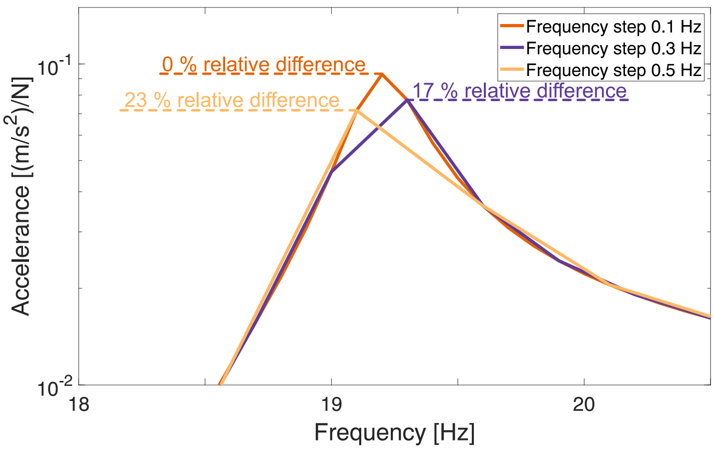

Figure 7.9: Absolute relative difference for different frequency steps comparing peak to peak at maximum absolute relative difference of interest for frequency step 0.3 Hz.

This shows the imperfections of calculating relative difference at the same frequency for different responses. Nonetheless, this method provides additional information about the convergence of the frequency steps, if studied adequately.

To further study the convergence of the frequency steps, the responses was compared directly together with the corresponding RMS–values, see Figure 7.10. Little to none deviation was observed between the responses, as well as a low relative difference of under 0.1% in RMS–value for all frequency steps.

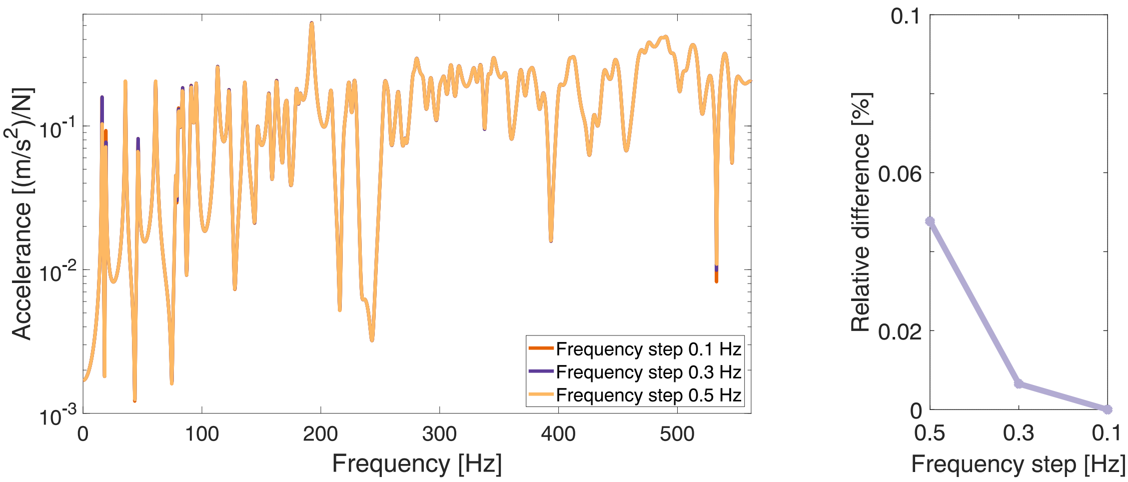

(a) Steady–state dynamic response for different frequency steps. The acceleration is shown in complex magnitude.

(b) Absolute relative difference of RMS–values for responses in Figure 7.10a.

Figure 7.10: Steady–state dynamic responses and corresponding RMS–values for different frequency steps.

Taking into account the results from the frequency step convergence analysis, the frequency step chosen moving forward was 0.3 Hz. Although the highest relative difference obtained was 17%, the majority of the response maintained low relative differences. Coupled with little to none observed deviation and low relative difference in RMS–values between the responses, the results was deemed sufficient. Furthermore, as this is a comparative study, differences of these types would to a degree cancel out each other.

7.1.2 Mesh size

In line with Section 5.2.1, a mesh size convergence analysis was conducted to determine the optimal mesh size that yields accurate and converged results with minimum computational time. However, in this section natural frequencies won't be compared directly. Instead, the steady–state dynamic response of the panel will be compared between the mesh sizes, in the same manner as the frequency step convergence analysis in Section 7.1.1.

The mesh size was limited by the partitions forming the individual lamellae in the lamellae model, described in Section 4.3. Therefore, the largest quadratic mesh size in horizontal plane tested was the same as the width of one lamella, i.e. 0.2 m, providing 1 finite element per lamella width. The mesh sizes were then categorized based on the number of elements per lamella width. For instance, 2 elements per lamella width would correspond to a mesh size of 0.1 m, while 3 elements per lamella width would result in a mesh size of approximately 0.067 m, and so forth. Likewise to Section 5.2.1, 1 element per layer was utilized here.

The steady–state dynamic response for the finest tested mesh size of 5 elements per lamella width (0.04 m) can be seen in Figure 7.11.

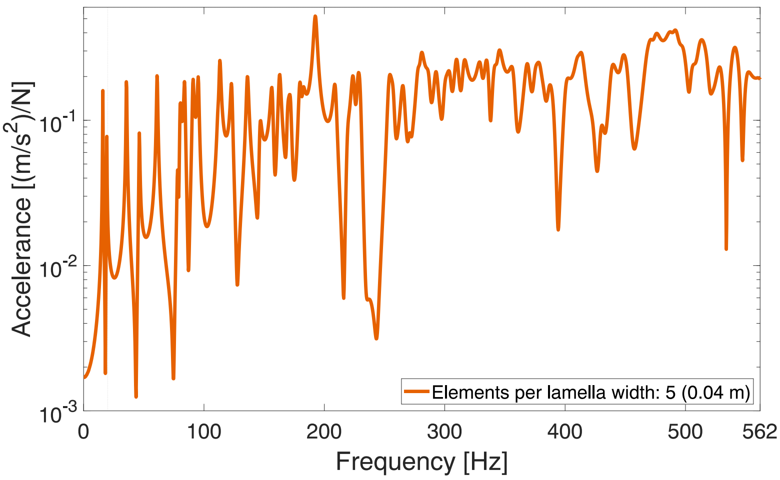

Figure 7.11: Steady–state dynamic response for the finest mesh size 5 elements per lamella width (0.04 m). The accelerance is shown in complex magnitude.

The mesh sizes were analyzed in relative difference to the reference mesh size of 5 elements per lamella width, see Figure 7.12. The mesh sizes of 1 and 2 elements per lamella width deviated heavily and are therefore not presented.

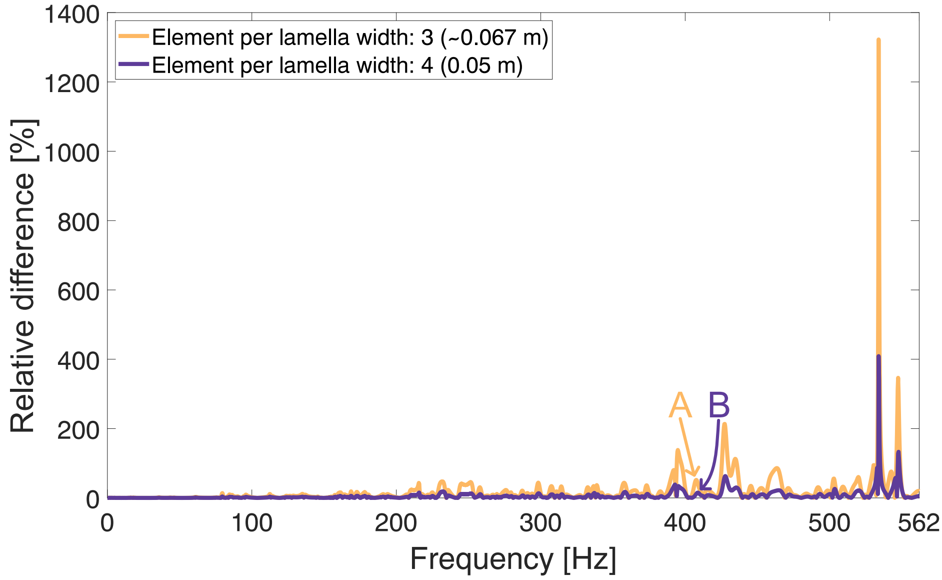

Figure 7.12: Absolute relative difference for mesh sizes 3 and 4 elements per lamella width, with 5 elements per lamella width as reference

As previously explained in Section 7.1.1, a small deviation in frequency for the same peaks between responses could mean unreasonably high relative differences for a specific frequency. Figure 7.12 further illustrates this, but on a larger scale.

These high values in relative differences were closer studied in the same manner as for the frequency step convergence analysis in Section 7.1.1. The results showed that the majority of these high values are troughs or almost vertical responses, which is neither of interest nor reasonable values. In fact, the maximum relative difference, corresponding to a peak in the response, was 52% for the mesh size of 3 elements per lamella width, and 15% for the mesh size of 4 elements per lamella width, marked with A respectively B in Figure 7.12. These values coincide at the same peak in response, at 407.7 Hz and 408.8 Hz, respectively. These peaks can be seen in Figure 7.13.

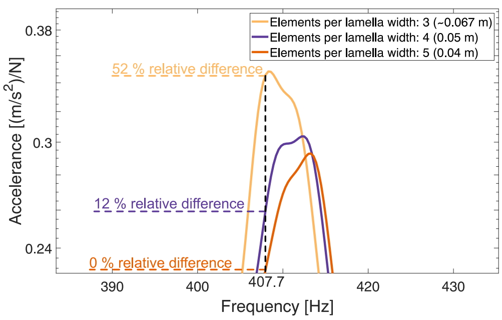

(a) Absolute relative difference for different mesh sizes at frequency 407.7 Hz. The maximum relative difference of interest for mesh size 3 elements per lamella width.

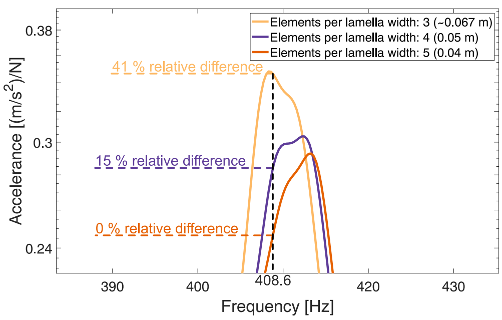

(b) Absolute relative difference for different mesh sizes at frequency 408.6 Hz. The maximum relative difference of interest for mesh size 4 elements per lamella width.

Figure 7.13: Absolute relative difference for different mesh sizes at different frequencies.

By instead comparing the peaks, a relative difference in accelerance was calculated to 19% in accelerance, and 1% in frequency for mesh size 3 elements per lamella width. For mesh size 4 elements per lamella width, only 4% in accelerance and 0.3% in frequency was obtained, see Figure 7.14. This is considerably less than mesh size 3 elements per lamella width but required further analysis to conclude if it is sufficient enough.

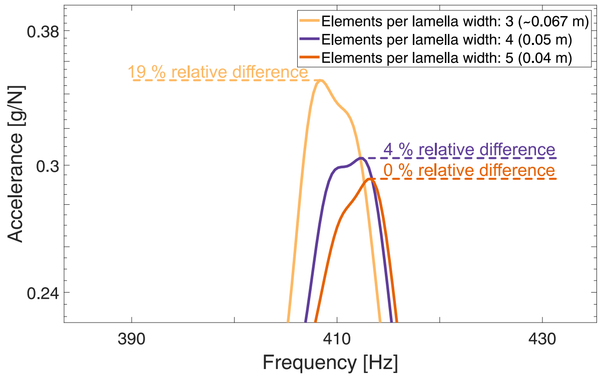

Figure 7.14: Absolute relative difference for different mesh sizes comparing peak to peak at maximum absolute relative difference of interest.

To further study the convergence of the mesh sizes, the responses was compared directly together with the corresponding RMS–values, see Figure 7.15. The relative difference in RMS–values maintained low values, below 2%, for mesh sizes 3 and 4 elements per lamella width. However, mesh size 4 elements per lamella width captured the reference response better than mesh size 3 elements per lamella width.

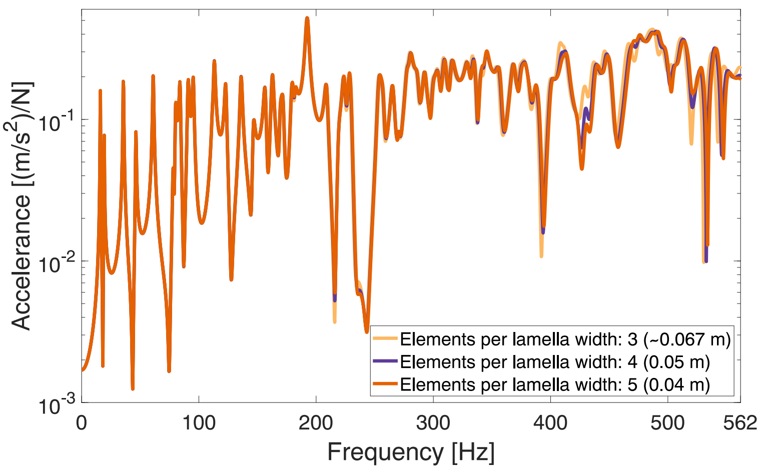

(a) Steady–state dynamic response for different mesh sizes. The accelerance is shown in complex magnitude.

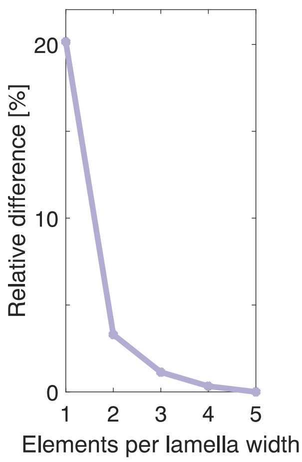

(b) Absolute relative difference of RMS–values for responses in Figure 7.15a.

Figure 7.15: Steady–state dynamic responses and corresponding RMS–values for different frequency steps.

Taking into account the results from the mesh size convergence analysis, the mesh size chosen moving forward was 4 elements per lamella width (0.05 m). Although high values in relative difference could be observed, the maximum relative difference of interest reached only 4%. Additionally, the majority of the response maintained low relative difference, and coupled with little to none observed deviation and low relative difference in RMS–values between the responses, the results were deemed sufficient. Furthermore, as this is a comparative study, differences of these types would to a degree cancel out each other.

7.1.3 Modal truncation

To further optimize computational time, a convergence analysis was performed regarding the number of modes necessary to accurately capture the steady–state dynamic response. It is standard practice to represent the number of modes for a specific response as a factor of the upper limit of the frequency range of interest. For instance, including all modes up to 562 Hz would be represented by the factor 1, while including all modes up to twice the upper limit (1124 Hz) would be represented by the factor 2, and so forth. The same representation strategy was employed here. The modal damping was set to 0.7%, according to Section 5.1.2.

The steady–state dynamic response used as reference for the modal truncation can be seen in Figure 7.16.

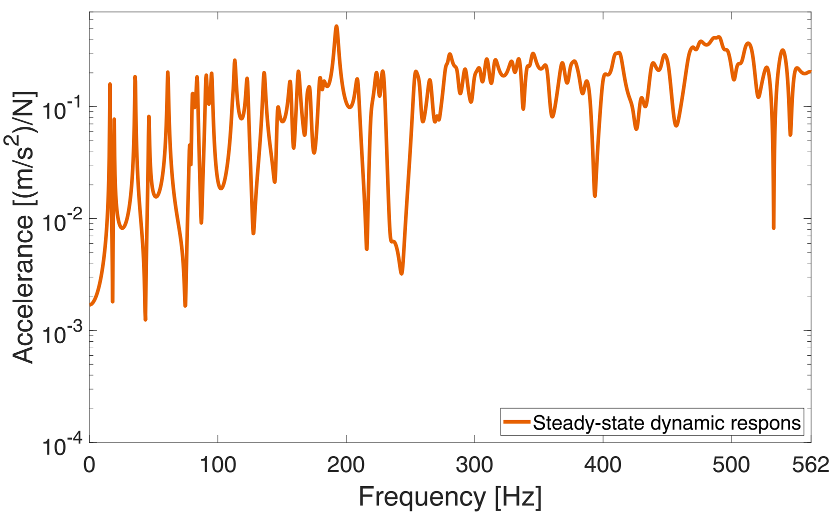

Figure 7.16: The steady–state dynamic response used as reference for the modal truncation.

The results showed large deviation for factor 0.5. Factor 1 did not deviate significantly apart from the end of the frequency range. Factor 1.5 did capture the response well, without any significant deviation. Factor 2 also captured the response well, with slightly less deviation than factor 1.5, see Figure 7.17a. The relative difference in RMS–values maintained low values, below 0.5% for Factor 1, 1.5 and 2, see Figure 7.17b.

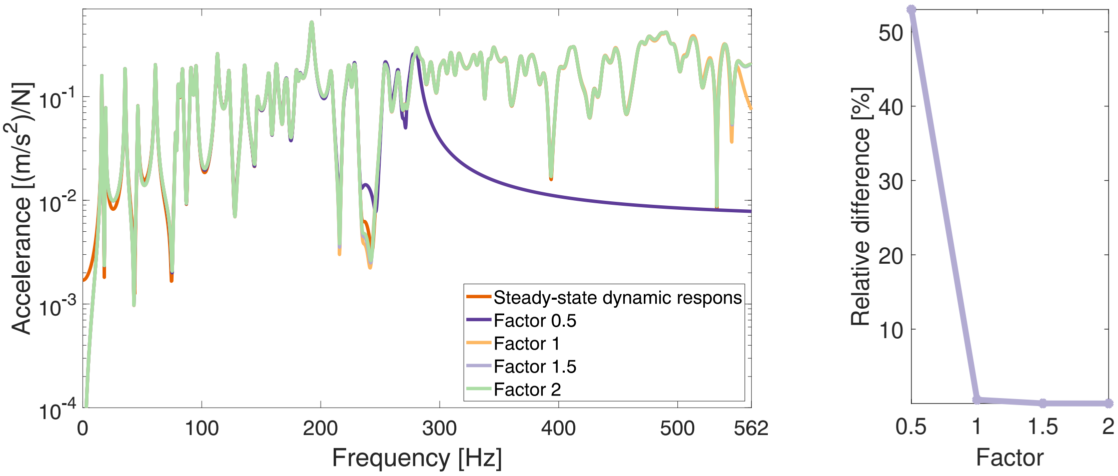

(a) Convergence of factors in the modal truncation.

(b) Absolute relative difference of RMS–values for factors in 7.17a.

Figure 7.17: Steady–state dynamic responses and corresponding RMS–values for different factors.

However, this might only be valid for spruce as integrating different materials could mean the modal truncation not capturing the behavior of those materials. Therefore, the factor 2 was chosen moving forward, as a safety precaution.

Modal truncation was opted for when studying the impact of lamellae material concrete and empty space/air. However, the modal truncation did not capture the response of Sylodyn NF/NB. Therefore, these will be evaluated in steady–state dynamic response instead.

7.1.4 Model development – large sized panel – summary

To summarize the results from the convergence analysis, a list of the values decided on moving forward are presented below:

- Frequency step size: 0.3 Hz.
- Mesh size: 4 elements per lamella width and 1 element per layer.
- Factor 2, which corresponds to including modes up to 1124 Hz in the modal truncation.

This mesh size and frequency step size will be opted for when studying the impact of different lamellae material in Chapters 8–11. The factor 2 will be utilized in the chapters were modal truncation was opted for, which is in Chapters 8-9.

7.2 Model development – Medium sized panel

The verification of the mesh size utilized on the M–sized panel, obtained in Section 7.1.4, is presented here. The responses for mesh with 4 and 5 elements per lamella width for the M–sized panel can be seen in Figure 7.18.

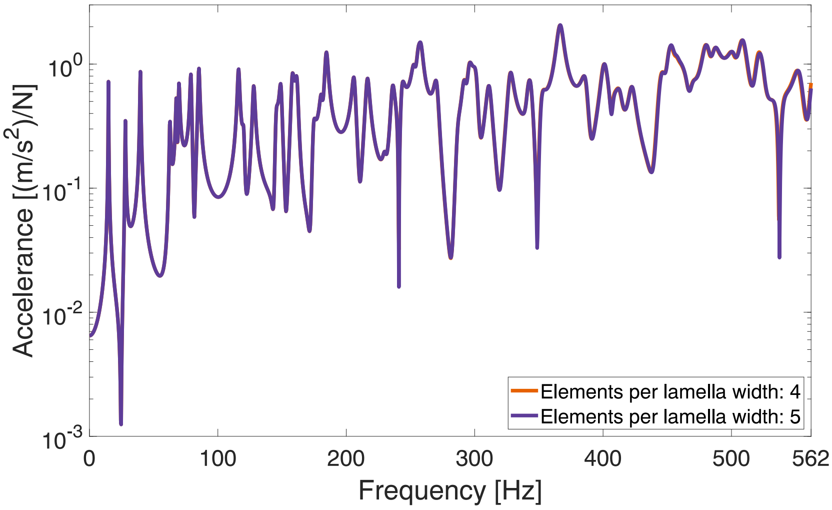

Figure 7.18: Steady–state dynamic response for different mesh sizes. The accelerance is shown in complex magnitude.

The responses showed little to none deviation between the mesh size 4 and 5 elements per lamella width, with a difference in RMS–value below 0.1%. This was considered sufficient.

Moreover, modes up to 1124 Hz was included for the modal truncation of the M–sized panel, with the same motivation as in Section 7.1.3.

7.3 Structure and terminology in the following chapters

The chapters presenting the impact of different lamellae material, Chapters 8–11, are structured according to Figure 7.19. These results are organized into four chapters, each addressing the different materials: “Concrete”, “Air”, and “Elastomer”. Each chapter is then divided into two sections: “L–sized panel” and “M–sized panel.”

The “L–sized panel” section contains three subsections: “1 layer, 2 layers, 3 layers”, where the configurations deemed necessary to illustrate the results are presented. In contrast, the “M–sized panel” section contains a single subsection named “1 layer”. These subsections are further divided into “Full layers” and “Partial layers”, presenting the results accordingly. This includes evaluating the results using RMS–values and 1/3 octave bands. The responses showcased no significant deviation below 8 Hz, which is well below the first natural frequency, giving a quasi–static response which is not of interest. Therefore, the responses will be shown starting from 8 Hz.

Additionally, summaries of section results, which are not presented here, will be included continuously.

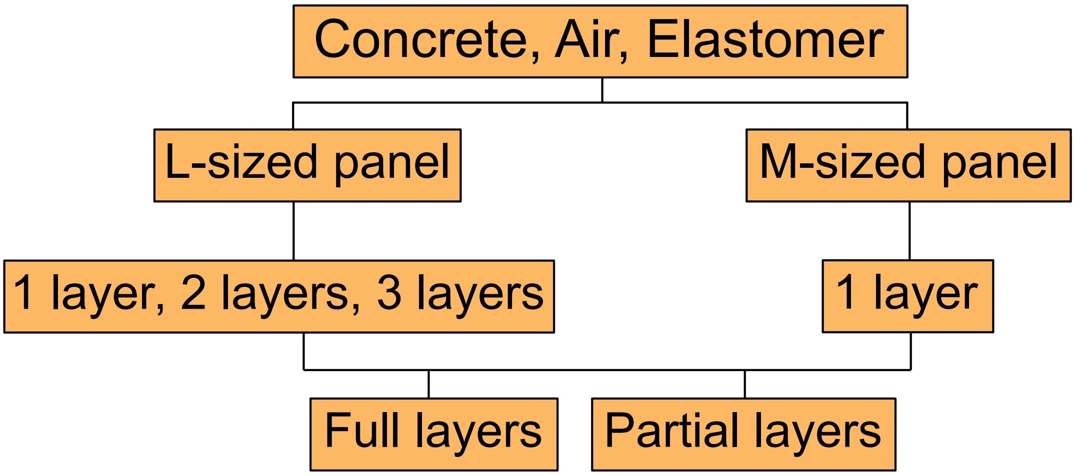

Figure 7.19: Illustration of the chapters' structure.

The terminology used when studying the impact of different lamellae material are refereed to Figure 7.20. When referring to longitudinal and transverse direction, the intended directions are thus in the length and width direction of the panel, respectively. Surface refers to the flat outer layer of the CLT panel. When referring to edge, the intended area is the side of the CLT panel.

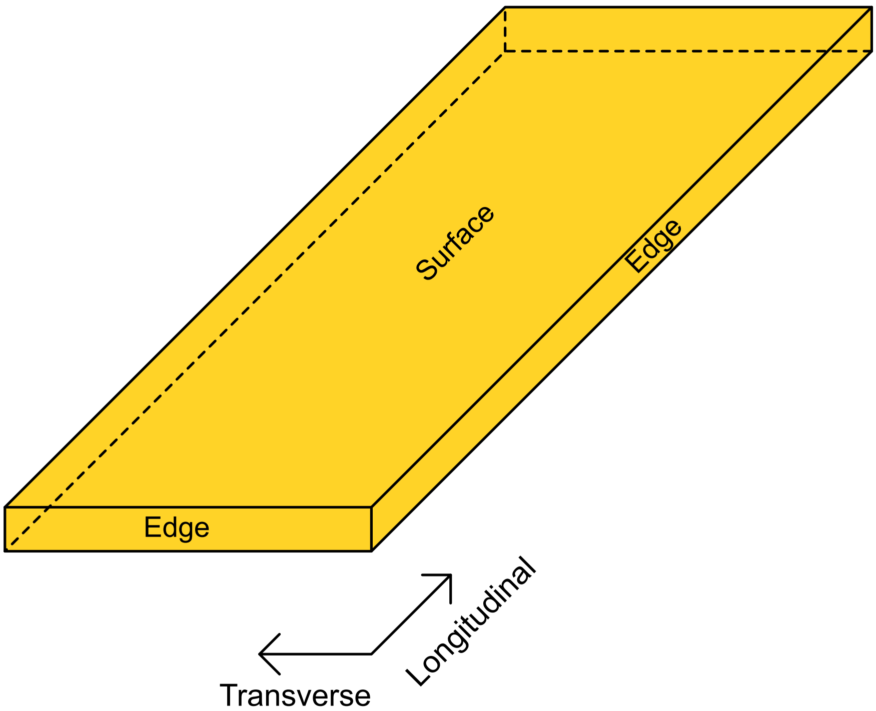

Figure 7.20: Illustration of the terminology used when studying the impact of different lamellae material.

8 Impact of concrete lamellae

In this chapter, the impact of exchanging lamellae from spruce to concrete are presented.

8.1 Large sized panel

8.1.1 1 layer

The 1 layer configurations deemed necessary to illustrate the results can be viewed in Figure 8.1, with corresponding ID:s. For the full list of 1 layer concrete configurations, see Appendix A.

The partial 1 layer configurations deemed necessary to illustrate the results can be seen in Figure 8.2.

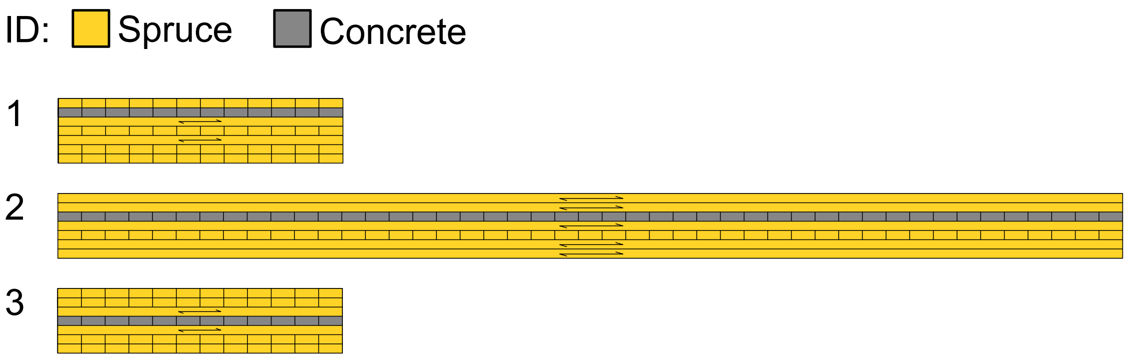

Figure 8.1: The full layers configurations for the 1 layer analyses, with corresponding ID:s. In ID1,3 lamellae in longitudinal direction are exchanged, while in ID2 lamellae in transverse direction are exchanged.

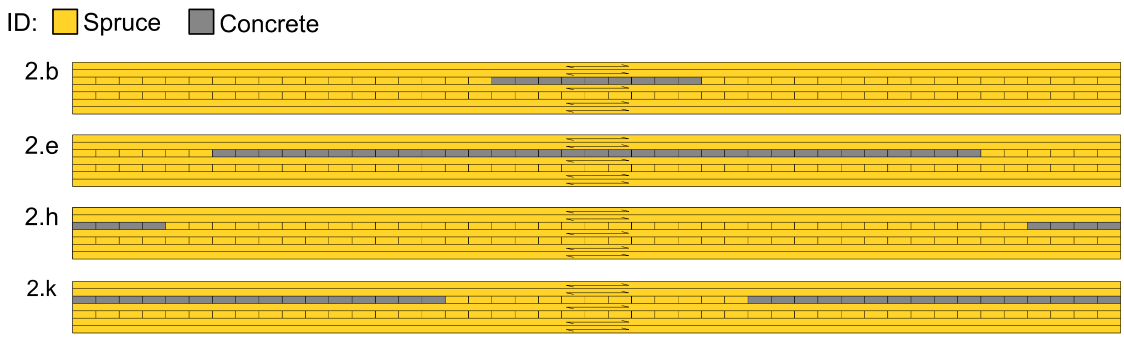

(a) Concrete partial layers of ID2, with lamellae in transverse direction.

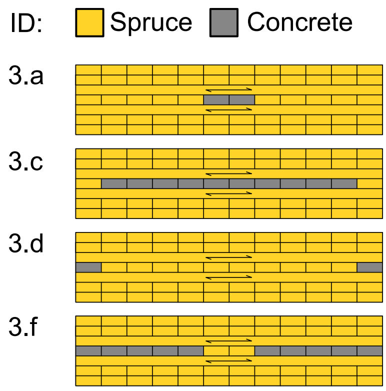

(b) Concrete partial layers of ID3, with lamellae in longitudinal direction.

Figure 8.2: The partial layers configurations for the 1 layer analyses, with corresponding ID:s.

8.1.1.1 Full layers

RMS–value

The effect on accelerance evaluated as RMS–values for ID1–3 can be seen in Table 8.1, where a negative change denotes a reduction in the level of vibration as compared to the reference level obtained by a panel comprised entirety of spruce.

Table 8.1: The change in RMS–value, compared to the reference level, and the volume ratio for configurations with ID1–3. Volume ratio indicates the percentage of concrete in the panel.

ID	RMS [%]	Volume ratio [%]
1	–29	14
2	–40	14
3	–40	14

The RMS–values for ID1–3 indicated a greater reduction in accelerance for ID2–3 compared to ID1. Additionally, ID2 exhibited the same RMS–value as ID3.

1/3 octave band

The effect on accelerance evaluated in 1/3 octave bands for ID1–3 can be seen in Figure 8.3.

ID1–3 indicated continuous reductions in accelerance from the 1/3 octave band of 63 Hz up to the band 500 Hz, apart from at 160 Hz up to the band 500 Hz, apart from at 160 Hz, where ID2 showcased no significant difference in accelerance, and at 250 Hz where ID1,3 showcased no significant difference in accelerance.

Below the 1/3 octave band of 63 Hz, ID3 indicated intervals where the accelerance was amplified, more specifically at 8, 10, 12.5 and 25 Hz, while the remaining 1/3 octave bands showcased reductions in accelerance. However, ID1 did not exhibit any amplifications in accelerance below the 1/3 octave band of 63 Hz. ID2 showcased amplification in accelerance at 12.5 Hz and no significant difference in accelerance at 8 and 10 Hz, below the 1/3 octave band of 63 Hz.

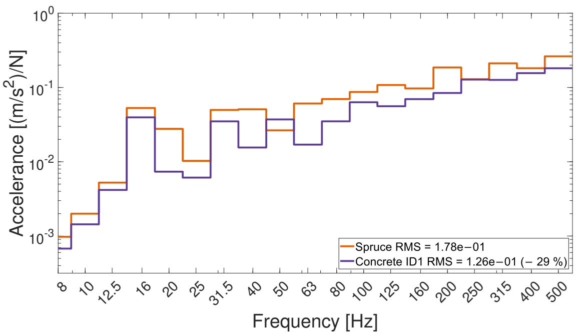

(a) Concrete ID1

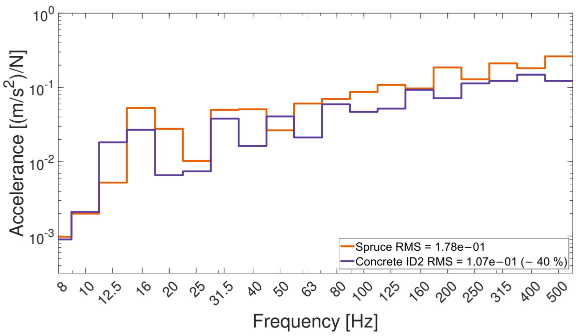

(b) Concrete ID2

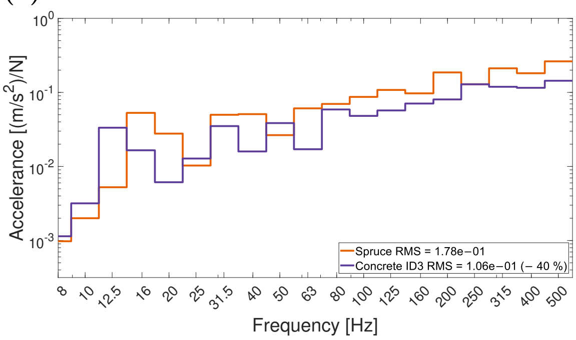

(c) Concrete ID3

Figure 8.3: Concrete – the steady–state dynamic response of configurations ID1–3, in 1/3 octave bands. The value in legend within parentheses indicates the change in RMS–value compared to the reference level. The center frequency of 1/3 octave bands are shown in the horizontal axis.

8.1.1.2 Partial layers

RMS–value

The effect on accelerance evaluated as RMS–values for the partial layer configurations of ID2,3 can be seen in Table 8.2, where a negative change denotes a reduction in the level of vibration as compared to the reference level obtained by a panel comprised entirety of spruce.

Table 8.2: The change in RMS–value, compared to the reference level, and the volume ratio for the partial layer configurations of ID2–3. Volume ratio indicates the percentage of concrete in the panel.

ID	RMS [%]	Volume ratio [%]
2b	+6	3
2e	+27	10
2h	–45	3
2k	–45	10
3a	+11	3
3c	–4	12
3d	–64	2
3f	–43	12

The RMS–values for the partial layer configurations of ID2,3 indicated significant reductions in accelerance for ID2h,k and ID3d,f, while ID2b,e and ID3a,c showcased either amplifications in accelerance or insignificant change. Additionally, ID3d showed a greater reduction in accelerance than ID2h, with approximately the same volume ratio. The RMS–value and volume ratio did not differ significantly between ID2k and ID3f.

1/3 octave band

The effect on accelerance evaluated in 1/3 octave bands for the partial layer configurations of ID2,3 can be seen in Figure 8.4.

ID2b,e and ID3a,c indicated amplifications or reductions in accelerance in different 1/3 octave bands, albeit not as significant as ID2h,k and ID3d,f. Moreover, significant reductions in accelerance were observed continuously at higher 1/3 octave bands in ID2h,k and ID3d,f compared to ID2b,e and ID3a,c. For example, ID3d showcased continuous reductions in accelerance from the 1/3 octave band of 125 Hz, and ID3a only at the smaller intervals of 20 and 25 Hz.

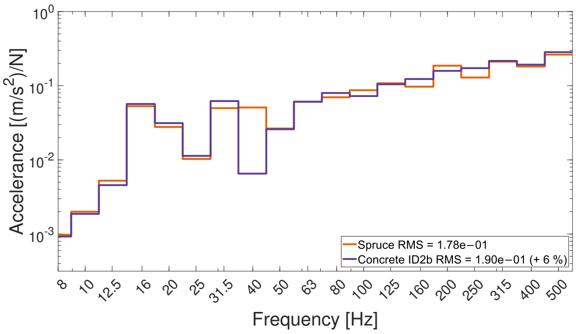

(a) Concrete ID2b

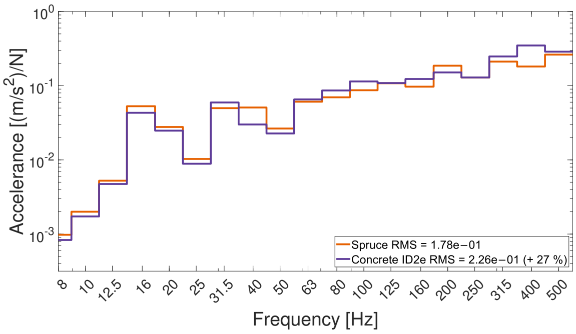

(b) Concrete ID2e

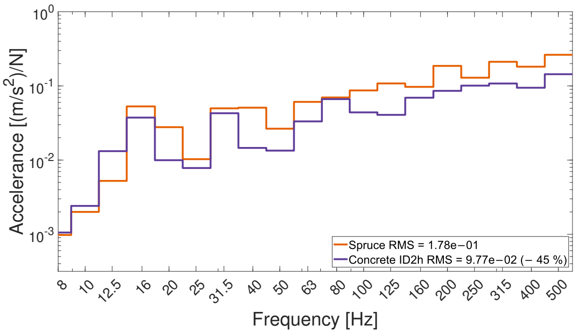

(c) Concrete ID2h

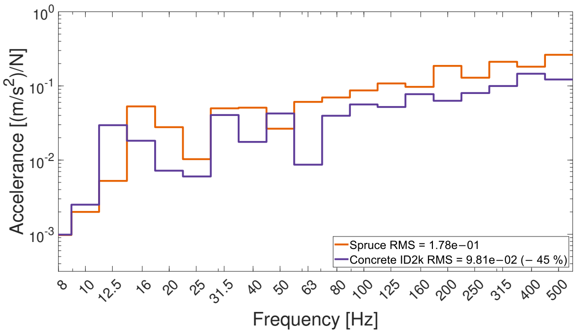

(d) Concrete ID2k

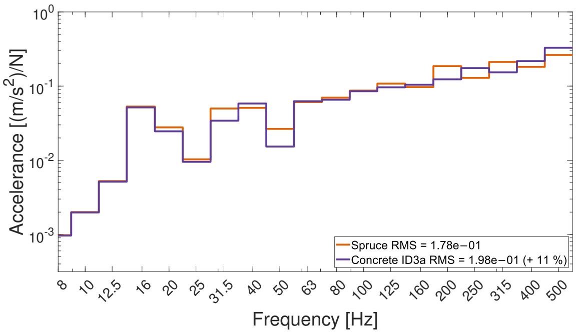

(e) Concrete ID3a

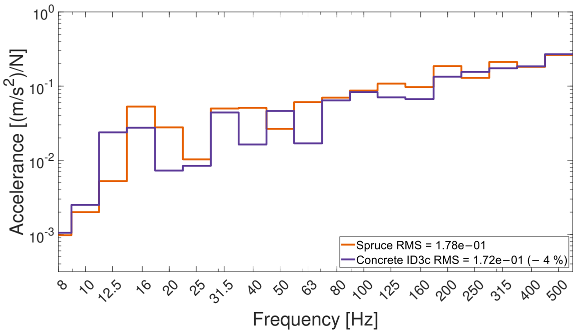

(f) Concrete ID3c

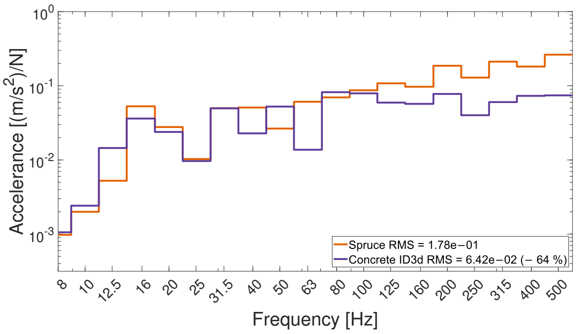

(g) Concrete ID3d

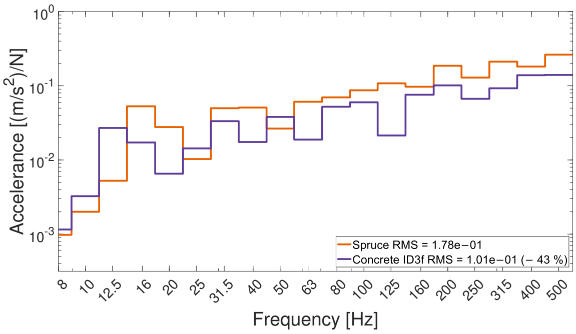

(h) Concrete ID3f

Figure 8.4: Concrete – the steady–state dynamic response for partial configurations of ID2,3, in 1/3 octave bands. The value in legend within parentheses indicates the change in RMS–value compared to the reference level. The center frequency of 1/3 octave bands are shown in the horizontal axis.

8.1.1.3 1 layer summary

For the 1 full layer results, configuration towards the center (ID3) exhibited a larger reduction in accelerance compared to the configuration towards the surface (ID1). Additionally, the difference in exchanging full layers of lamellae in longitudinal direction (ID1,3) and in transverse direction (ID2) was insignificant in accelerance towards the center of the panel (ID2 compared to ID3).

For the 1 partial layer results, configurations exchanging lamellae from the edges inwards indicated a significant reduction in accelerance (ID2h,k and ID3d,f) compared to the configurations exchanging lamellae from the center outwards (ID2b,e and ID3a,c) and their corresponding full layer configurations (ID1,2). However, a continuous reduction in accelerance was only observed from certain center frequencies, ranging from 60 to 125 Hz up to 562 Hz (ID2h,k and ID3d,f).

Even though the predicted accelerance was shown to be, for example, reduced by using an RMS–value, which is a single–value metric, the accelerance in specific 1/3 octave bands could be either amplified or reduced, respectively, in relation to the equivalent 1/3 octave bands for the reference panel.

Noteworthy is the center frequency of 12.5 Hz, where the majority of the configurations showed significant increase in response, and 63 Hz from where the majority of the configurations displayed continuous reductions in accelerance up to 562 Hz.

8.1.2 2 layers

The 2 layers configurations deemed necessary to illustrate the results can be viewed in Figure 8.5, with corresponding ID:s. For the full list of 2 layers concrete configurations, see Appendix A.

The partial 2 layers configurations deemed necessary to illustrate the results can be seen in Figure 8.6.

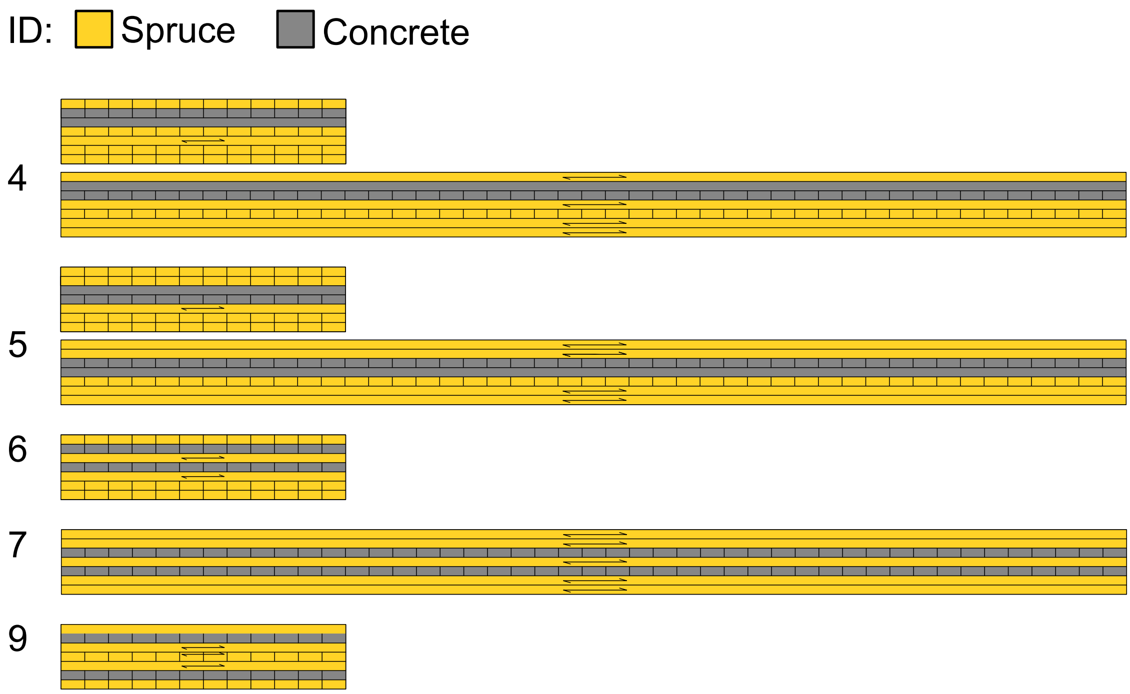

Figure 8.5: The full layers configurations for the 2 layers analyses, with corresponding ID:s. In ID4–5 lamellae in both transverse and longitudinal direction are exchanged, while in ID6,9 lamellae in longitudinal direction are exchanged. In ID7 lamellae in transverse direction are exchanged.

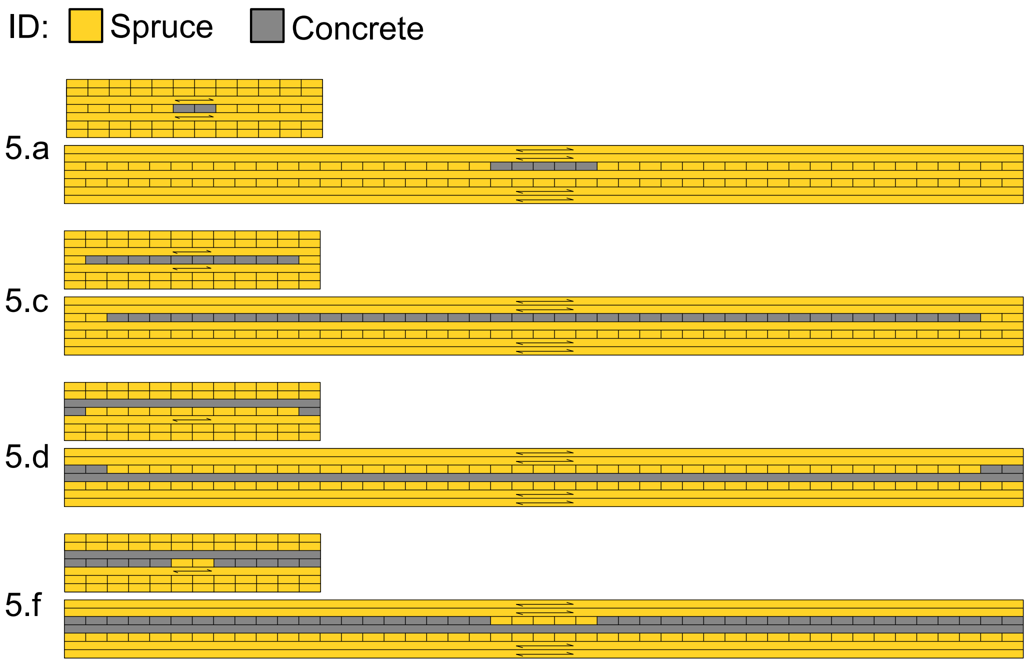

Figure 8.6: The partial layers configurations for the 2 layers analyses, with corresponding ID:s. In the upper image of each ID lamellae in longitudinal direction are exchanged, while in the lower image lamellae in transverse direction are exchanged.

8.1.2.1 Full layers

RMS–value

The effect on accelerance evaluated as RMS–values for ID4–7 and ID9 can be seen in Table 8.3, where a negative change denotes a reduction in the level of vibration as compared to the reference level obtained by a panel comprised entirety of spruce.

Table 8.3: The change in RMS–value, compared to the reference level, and the volume ratio for configurations with ID4–7,9. Volume ratio indicates the percentage of concrete in the panel.

ID	RMS [%]	Volume ratio [%]
4	–57	29
5	–61	29
6	–56	29
7	–55	29
9	–48	29

The RMS–values for ID4–7,9 indicated a greater reduction in accelerance for ID6 compared to ID9. Additionally, ID4 showed approximately the same RMS–value compared to ID5, and ID6 to ID7.

1/3 octave band

The effect on accelerance evaluated in 1/3 octave bands for ID4–7,9 can be seen in Figure 8.7.

All configurations indicated significant reductions in accelerance at every 1/3 octave band, apart from at 12.5 and 50 Hz where ID4–6 indicated amplifications in accelerance, and at 10 Hz where ID5 showcased amplification in accelerance.

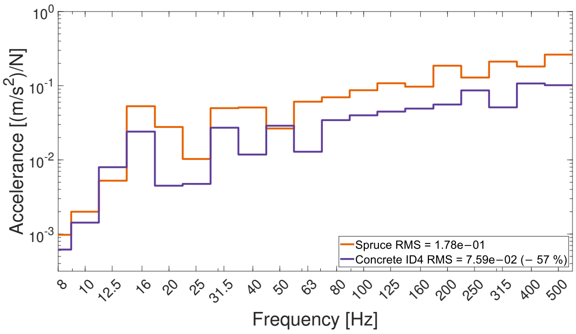

(a) Concrete ID4

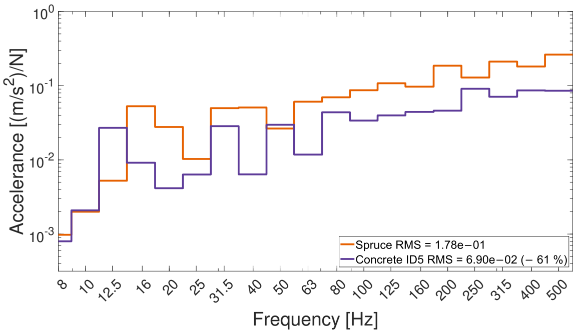

(b) Concrete ID5

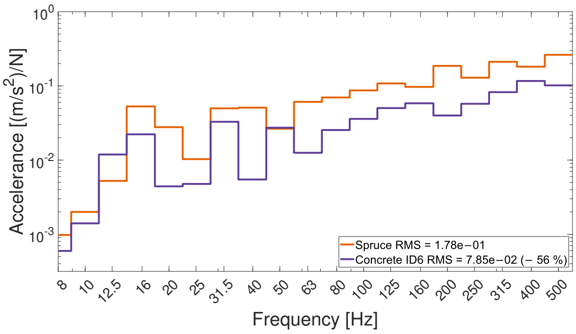

(c) Concrete ID6

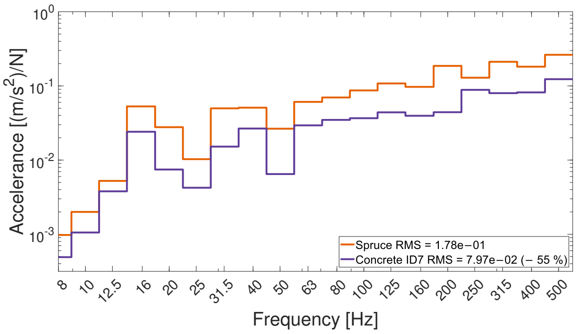

(d) Concrete ID7

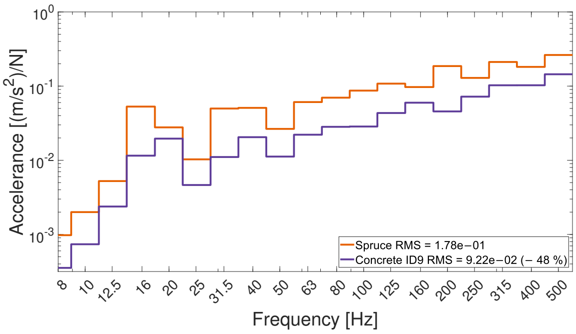

(e) Concrete ID9

Figure 8.7: Concrete – the steady–state dynamic response of configurations ID4–7,9, in 1/3 octave bands. The value in legend within parentheses indicates the change in RMS–value compared to the reference level. The center frequency of 1/3 octave bands are shown in the horizontal axis.

8.1.2.2 Partial layers

RMS–value

The effect on accelerance evaluated as RMS–values for the partial layers configurations of ID5 can be seen in Table 8.4, where a negative change denotes a reduction in the level of vibration as compared to the reference level obtained by a panel comprised entirety of spruce.

The RMS–values for the partial layers configurations of ID5 indicated significant reductions in accelerance for ID5d,f, while ID5a,c showcased amplifications in accelerance. Moreover, the reduction in accelerance was greater for ID5d compared to ID5f, despite the significantly lower volume ratio.

Table 8.4: The change in RMS–value, compared to the reference level, and the volume ratio for the partial layers configurations of ID5. Volume ratio indicates the percentage of concrete in the panel.

ID	RMS [%]	Volume ratio [%]
5a	+9	4
5c	+27	25
5d	–75	4
5f	–63	25

1/3 octave band

The effect on accelerance evaluated in 1/3 octave bands for the partial layers configurations of ID5 can be seen in Figure 8.8.

ID5a,c indicated amplifications or reductions in accelerance in different 1/3 octave bands, albeit not as significant as ID5d,f. Moreover, significant reductions in accelerance were observed continuously at higher 1/3 octave bands in ID5d,f compared to ID5a,c. For example, ID5d showcased continuous reductions in accelerance from the 1/3 octave band of 63 Hz up to the band 500 Hz, apart from at 160 Hz AND , and ID3a only at the smaller intervals of 8–25 Hz, 40–50 Hz and 80–100 Hz.

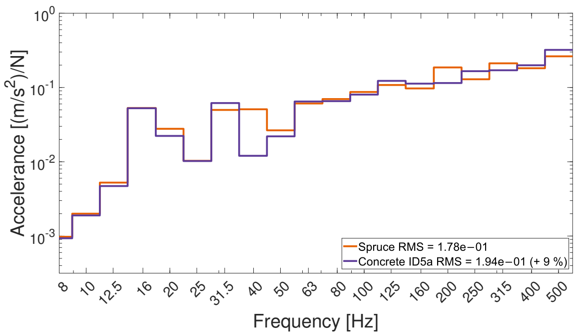

(a) Concrete ID5a

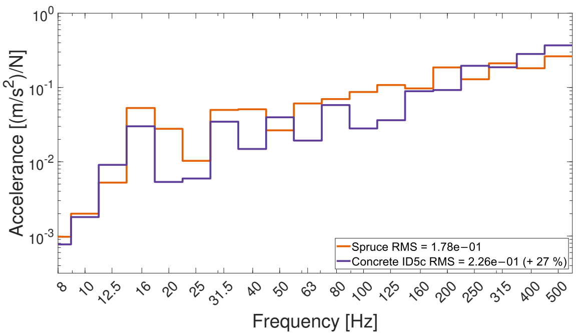

(b) Concrete ID5c

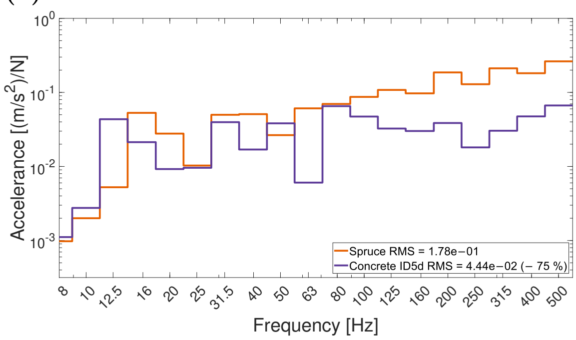

(c) Concrete ID5d

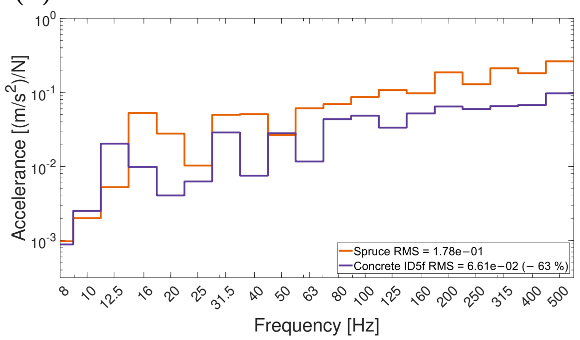

(d) Concrete ID5f

Figure 8.8: Concrete – the steady–state dynamic response for partial configurations of ID5, in 1/3 octave bands. The value in legend within parentheses indicates the change in RMS–value compared to the reference level. The center frequency of 1/3 octave bands are shown in the horizontal axis.

8.1.2.3 2 layers summary

For the 2 full layers results, configurations towards the center (ID6) exhibited a larger reduction in accelerance compared to the configurations towards the surface (ID9). Additionally, the difference in exchanging full layers of lamellae in longitudinal direction (ID6,9) and in transverse direction (ID7) was insignificant towards the center of the panel (ID6 compared to ID7).

For the 2 partial layers results, configurations exchanging lamellae from the edges inwards indicated a significant reduction in accelerance (ID5d,f) compared to the configurations exchanging lamellae from the center outwards (ID5a,c) and its corresponding full layer configuration (ID5). However, a continuous reduction in accelerance was only observed from a certain center frequency of 63 Hz up to 562 Hz (ID5d,f).

Even though the predicted accelerance was shown to be, for example, reduced by using an RMS–value, which is a single–value metric, the accelerance in specific 1/3 octave bands could be either amplified or reduced, respectively, in relation to the equivalent 1/3 octave bands for the reference panel.

Noteworthy is the center frequency of 12.5 Hz, where the majority of the configurations showed significant increase in response, and 63 Hz from where the majority of the configurations displayed continuous reductions in accelerance up to 562 Hz.

8.1.3 3 layers

The 3 layers configurations deemed necessary to illustrate the results can be viewed in Figure 8.9, with corresponding ID:s. For the full list of 3 layers concrete configurations, see Appendix A.

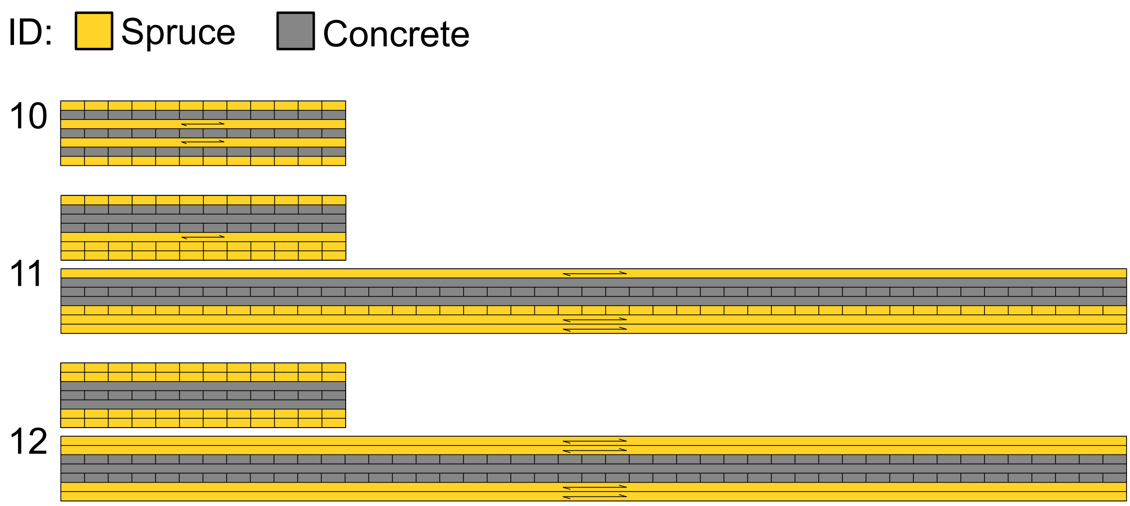

Figure 8.9: The full layers configurations for the 3 layers analyses, with corresponding ID:s. ID10 exchanges lamellae in longitudinal direction and ID11–12 in both transverse and longitudinal direction.

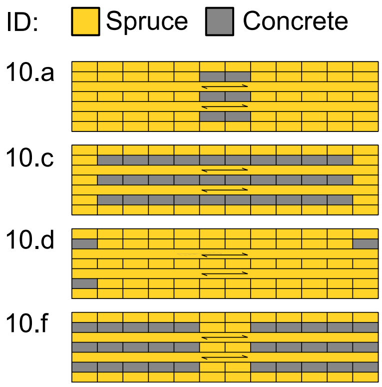

(a) Concrete partial layers of ID10, with lamellae in longitudinal direction.

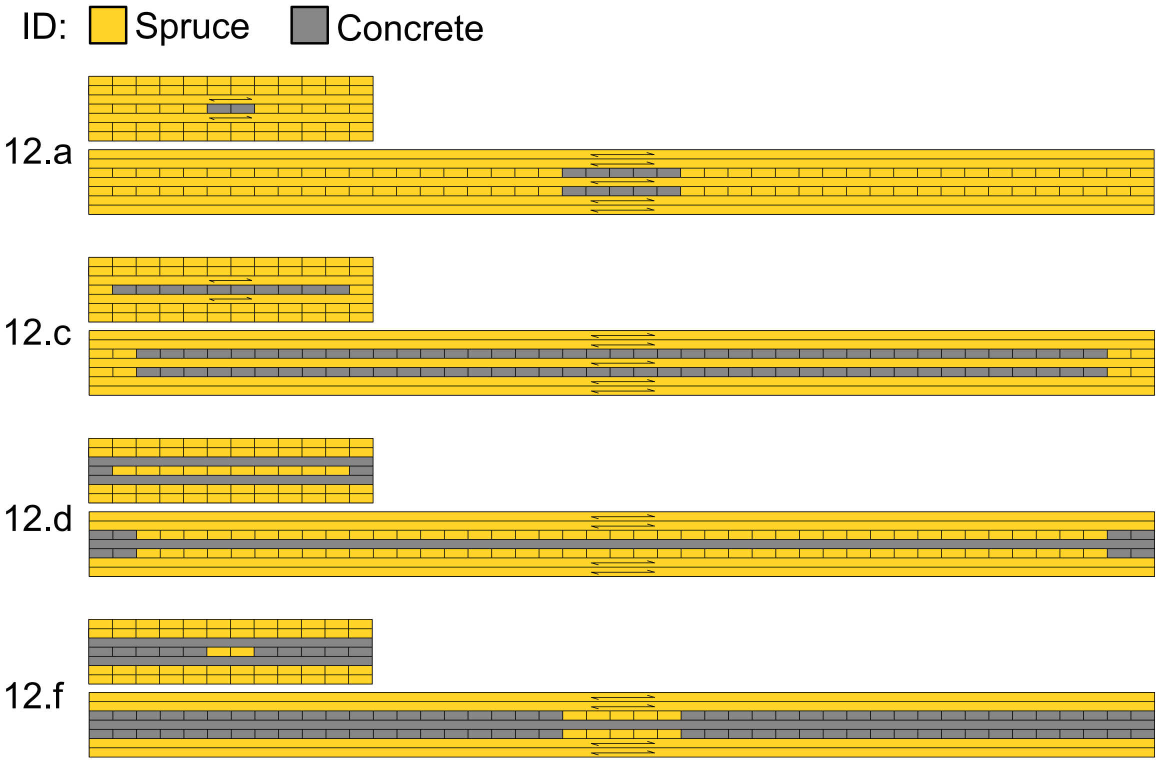

(b) Concrete partial layers of ID12, with lamellae in longitudinal– (upper image of each ID:s) and transverse (lower image of each ID:s) direction.

Figure 8.10: The partial layers configurations for the 3 layers analyses, with corresponding ID:s.

The partial 3 layers configurations deemed necessary to illustrate the results can be seen in Figure 8.10.

It is important to note that these configurations are not directly comparable for the purpose of finding potential trends in the dynamic behavior of the panel. This is due to the fact that they do not have the same number of layers in each direction. However, configurations ID10–12 were still considered as they could provide further insights into the structural behavior of the panel.

8.1.3.1 Full layers

RMS–value

The effect on accelerance evaluated as RMS–values for ID10–12 can be seen in Table 8.5, where a negative change denotes a reduction in the level of vibration as compared to the reference level obtained by a panel comprised entirety of spruce.

Table 8.5: The change in RMS–value, compared to the reference level, and the volume ratio for configurations with ID10–12. Volume ratio indicates the percentage of concrete in the panel.

ID	RMS [%]	Volume ratio [%]
10	–68	43
11	–69	43
12	–75	43

The RMS–values for ID10–12 indicated a greater reduction in accelerance for ID12 compared to ID10–11. Additionally, ID10 showed approximately the same RMS–value compared to ID11.

1/3 octave band

The effect on accelerance evaluated in 1/3 octave bands for ID10–12 can be seen in Figure 8.11.

All configurations indicated a significant reduction in accelerance at every 1/3 octave band, apart from at 12.5 Hz where all indicated amplifications in accelerance.

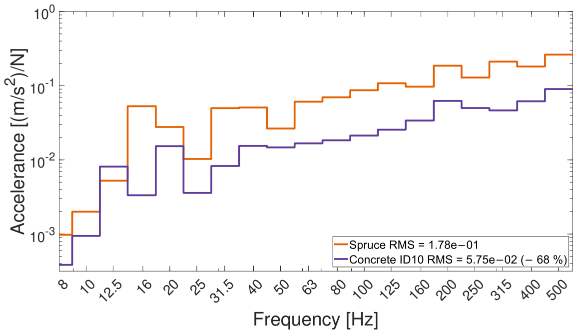

(a) Concrete ID10

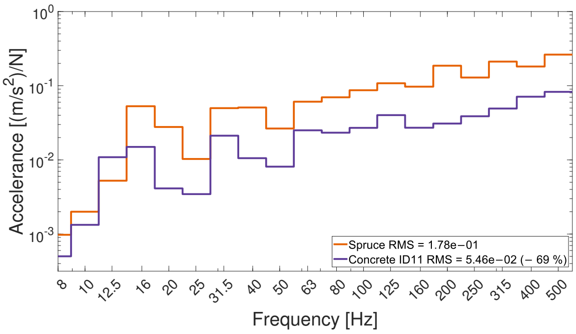

(b) Concrete ID11

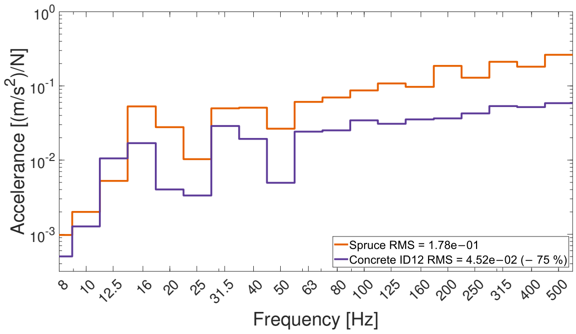

(c) Concrete ID12

Figure 8.11: Concrete – the steady–state dynamic response of configuration ID10–12, in 1/3 octave bands. The value in legend within parentheses indicates the change in RMS–value compared to the reference level. The center frequency of 1/3 octave bands are shown in the horizontal axis.

8.1.3.2 Partial layers

RMS–value

The effect on accelerance evaluated as RMS–values for the partial layers configurations of ID10–12 can be seen in Table 8.6, where a negative change denotes a reduction in the level of vibration as compared to the reference level obtained by a panel comprised entirety of spruce.

Table 8.6: The change in RMS–value, compared to the reference level, and the volume ratio for the partial layers configurations of ID10,12. Volume ratio indicates the percentage of concrete in the panel.

ID	RMS [%]	Volume ratio [%]
10a	+6	7
10c	–33	36
10d	–78	7
10f	–72	36
12a	+4	6
12c	+48	38
12d	–79	5
12f	–74	37

The RMS–values for the partial layers configurations of ID10,12 indicated significant reductions in accelerance for ID10c,d,f and ID12d,f, while ID10a and ID12a,c showcased either amplifications in accelerance or insignificant change. Additionally, ID10d showed a greater reduction in accelerance than ID10c,f despite the significantly lower volume ratio. Moreover, ID12d showed approximately the same reduction in accelerance compared to ID12f despite the significantly lower volume ratio.

1/3 octave band

The effect on accelerance evaluated in 1/3 octave bands for the partial layers configurations of ID10,12 can be seen in Figure 8.12.

ID10a and ID12a,c indicated amplifications or reductions in accelerance in different 1/3 octave bands, albeit not as significant as ID10c,d,f and ID12d,f. Moreover, significant reductions in accelerance were observed continuously at higher 1/3 octave bands in ID10c,d,f and ID12d,f compared to ID10a and ID12a,c. For example, ID12d showcased continuous reductions in accelerance from the 1/3 octave band of 63 Hz up to the band 500 Hz, apart from at 160 Hz, and ID12a only at the smaller intervals of 8–12.5 Hz and 40–50 Hz.

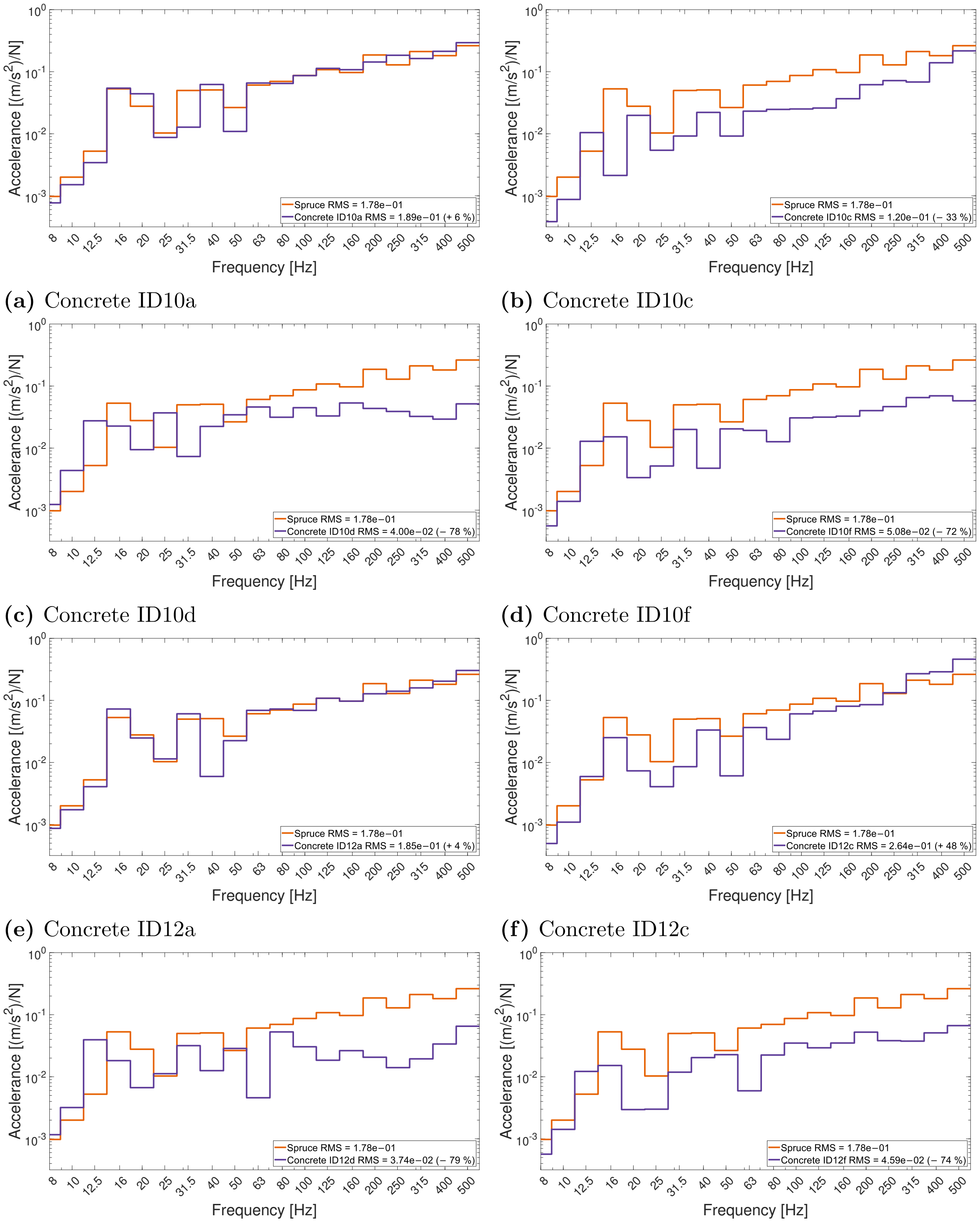

(a) Concrete ID10a **(b)** Concrete ID10c

(c) Concrete ID10d **(d)** Concrete ID10f

(e) Concrete ID12a **(f)** Concrete ID12c

(g) Concrete ID12d **(h)** Concrete ID12f

Figure 8.12: Concrete – the steady–state dynamic response for partial configurations of ID10,12, in 1/3 octave bands. The value in legend within parentheses indicates the change in RMS–value compared to the reference level. The center frequency of 1/3 octave bands are shown in the horizontal axis.

8.1.3.3 3 layers summary

For the 3 full layers results, configuration towards the center (ID12) exhibited a larger reduction in accelerance compared to the configuration towards the surface (ID10). Again, it should be noted that the 3 layers configurations are not directly comparable.

For the 3 partial layers results, configurations exchanging lamellae from the edges and inwards indicated a significant reduction in accelerance (ID10d,f and ID12d,f) compared to the configurations exchanging lamellae from the center outwards (ID10a,c and 12a,c) and their corresponding full layer configurations (ID11,12). However, continuous reductions in accelerance was only observed from certain center frequencies, ranging from 12.5 Hz to 63 Hz up to 562 Hz (ID10c,d,f and ID12d,f).

Even though the predicted accelerance was shown to be, for example, reduced by using an RMS–value, which is a single–value metric, the accelerance in specific 1/3 octave bands could be either amplified or reduced, respectively, in relation to the equivalent 1/3 octave bands for the reference panel.

Noteworthy is the center frequency of 12.5 Hz, where the majority of the configurations showed significant increase in response, and 63 Hz from where the majority of the configurations displayed continuous reductions in accelerance up to 562 Hz.

8.1.4 Large sized panel summary

The impact of exchanging lamellae from spruce to concrete in the L–sized panel are consolidated in this section.

- In full layers, a greater reduction in accelerance appeared to be achieved by placing concrete towards the center of the panel (ID3,6 and 12), rather than towards the surface (ID1,9 and 10).
- The difference in exchanging layer/layers of concrete in longitudinal and transverse direction, appeared to be insignificant towards the center of the panel (ID2 compared to ID3, and ID6 to ID7).
- In partial layers, a greater reduction in accelerance appeared to be achieved by exchanging lamellae from the edges inwards (ID2h,k, ID3d,f, ID5d,f, ID10d,f and ID12d,f), compared to exchanging full layers. This was especially applicable from certain frequencies, ranging from 12.5 Hz to 125 Hz up to 562 Hz.
- In partial layers, configurations exchanging lamellae from the edges inwards indicated a significant reduction in accelerance (ID2h,k, ID3d,f, ID5d,f, ID10d,f and ID12d,f) compared to the configurations exchanging lamellae from the center outwards (ID2b,e, ID3a,c, ID5a,c, ID10a and 12a,c).
- Even though the predicted accelerance was shown to be, for example, reduced by using an RMS–value, which is a single–value metric, the accelerance in specific 1/3 octave bands could be either amplified or reduced, respectively, in relation to the equivalent 1/3 octave bands for the reference panel.

- Noteworthy is the center frequency of 12.5 Hz, where the majority of the configurations showed significant increase in response, and 63 Hz from where the majority of the configurations displayed continuous reductions in accelerance up to 562 Hz.

8.2 Medium sized panel

1 layer

The investigation whether the dimensions and/or lay–ups of the panels influence the results are presented here.

The configurations analyzed can be viewed in Figure 8.13.

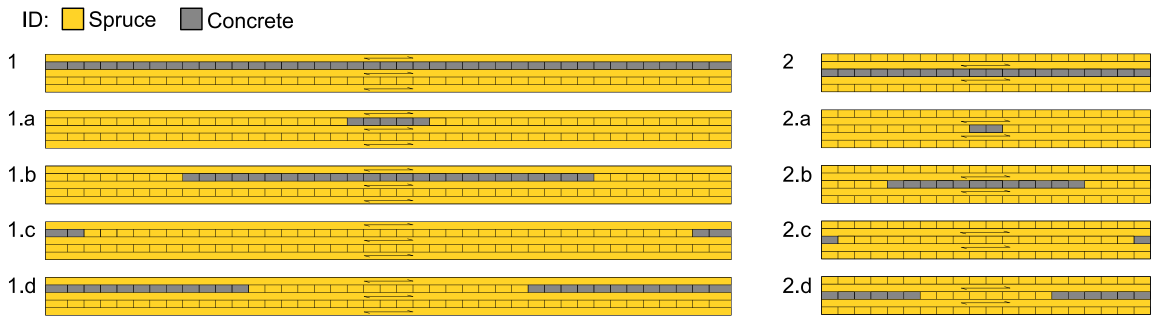

Figure 8.13: Illustration of the analyzed configuration, performed on the M–sized panel. The full layer configuration and partial layer configurations of ID1 exchanges lamellae in transverse direction. The full layer configuration and partial layer configurations of ID2 exchanges lamellae in longitudinal direction.

The effect on accelerance evaluated as RMS–value for these configurations can be seen in Table 8.7, where a negative change denotes a reduction in the level of vibration as compared to the reference level obtained by a panel comprised entirety of spruce.

The effect on accelerance evaluated in 1/3 octave bands for these configurations can be seen in Figure 8.14.

The RMS–values for the M–sized panel indicated no significant difference in accelerance by exchanging layers of concrete in longitudinal and transverse direction.

The RMS–values for the M–sized panel indicated a greater reduction in accelerance exchanging lamellae from the edges inwards (ID1c,d and ID2c,d), compared to exchanging full layers (ID1,2).

The RMS–values for the M–sized panel indicated a reduction in accelerance by exchanging lamellae from the center outwards (ID1a,b and ID2a), albeit not as much as exchanging lamellae from the edges inwards. With even one configuration showing a increase in accelerance (ID2b).

The partial layers exchanging lamellae from the center outwards indicated amplifications or reductions in accelerance in different 1/3 octave bands (ID1a,b and ID2a,b), albeit not as significant as the partial layers exchanging lamellae from the edges inwards (ID1c,d and ID2c,d). Moreover, significant reductions in accelerance were observed continuously at higher 1/3 octave bands in the partial layers exchanging lamellae from the edges inwards (ID1c,d and ID2c,d) compared to the partial layers exchanging lamellae from the center outwards (ID1a,b and ID2a,b). For example, ID1c showcased continuous reductions in accelerance from the octave band of 125 Hz, and ID1a from 250 Hz, albeit not as significant as ID1c.

Noteworthy is the center frequency of 12.5 Hz, where the majority of the configurations showed a significant increase in response.

Table 8.7: The change in RMS–value, compared to the reference level, and the volume ratio for configurations visualized in Figure 8.13. Volume ratio indicates the percentage of concrete in the panel.

ID	RMS [%]	Volume ratio [%]
1	–45	20
2	–48	20
1a	–12	2
1b	–6	12
1c	–64	2
1d	–59	12
2a	–13	2
2b	+19	12
2c	–69	2
2d	–63	12

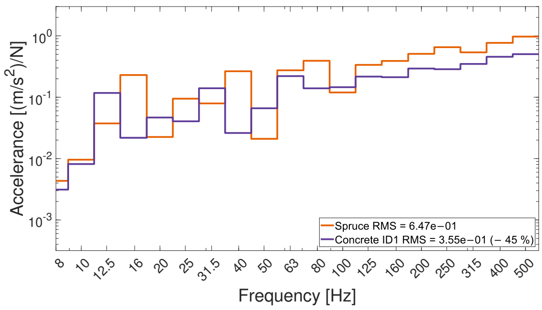

(a) Concrete M–sized panel ID1

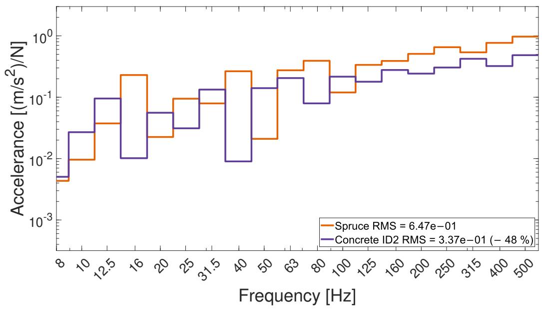

(b) Concrete M–sized panel ID2

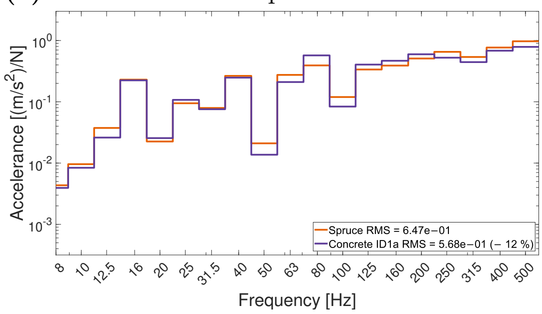

(c) Concrete M–sized panel ID1a

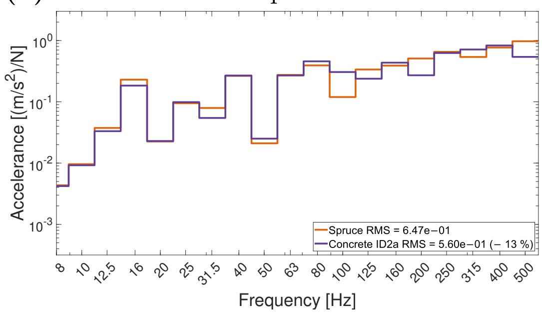

(d) Concrete M–sized panel ID2a

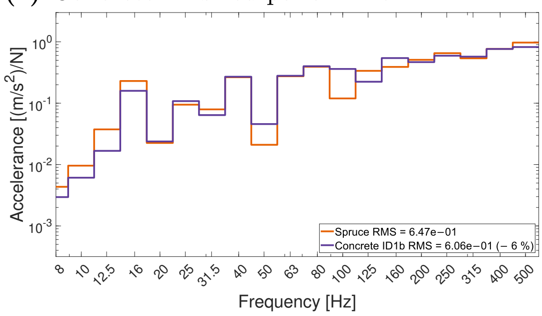

(e) Concrete M–sized panel ID1b

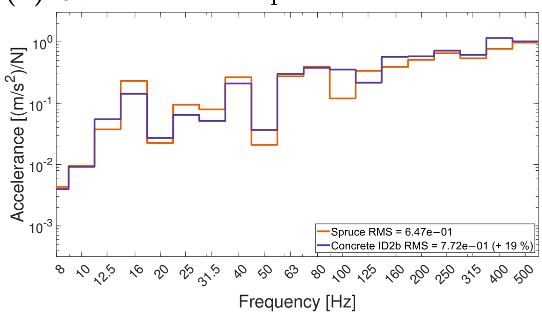

(f) Concrete M–sized panel ID2b

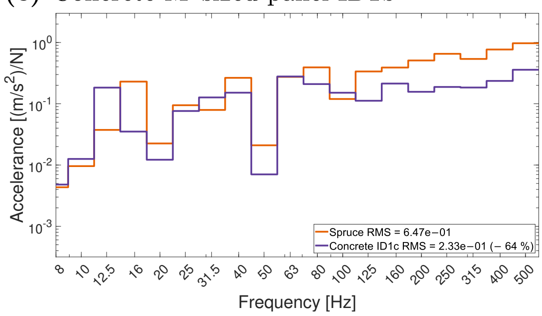

(g) Concrete M–sized panel ID1c

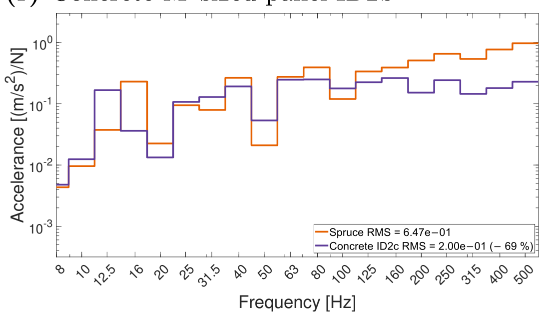

(h) Concrete M–sized panel ID2c

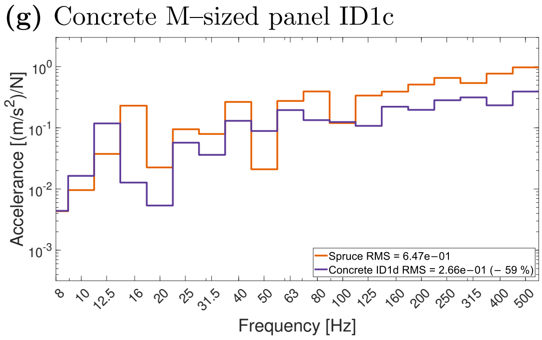

(i) Concrete M–sized panel ID1d

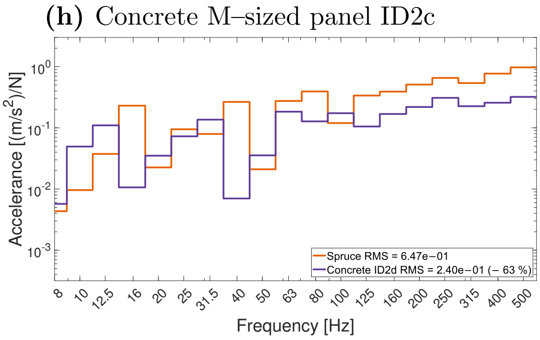

(j) Concrete M–sized panel ID2d

Figure 8.14: Concrete – the steady–state dynamic response in 1/3 octave bands for configurations illustrated in Figure 8.13. The value in legend within parentheses indicates the change in RMS–value compared to the reference level. The center frequency of 1/3 octave bands are shown in the horizontal axis.

9 Impact of air cavities

In this chapter, the impact of exchanging lamellae from spruce to air cavities is presented.

The terms "full layer/full layers" will be used in this chapter. However, the terms will not refer to exchanging the actual full layers/layers, but instead every other lamellae. This approach ensured practical relevance.

Moreover, some of the configurations tested may not be practically possible to produce or utilize in practice (configurations towards the surface). However, they are still employed to gain further insight into the structural behavior of the panel.

9.1 Large sized panel

Results have been shown that there were no significant differences in accelerance between the two studied modeling methods of air cavities, see Figure 9.1. These two modeling methods of air are described in Section 6. The relative difference in RMS–values was insignificant. The method of modeling air as empty space could save computational costs and streamline the analyses. Therefore, this method was used in analyses with air cavities and only results from empty space will be presented in this section.

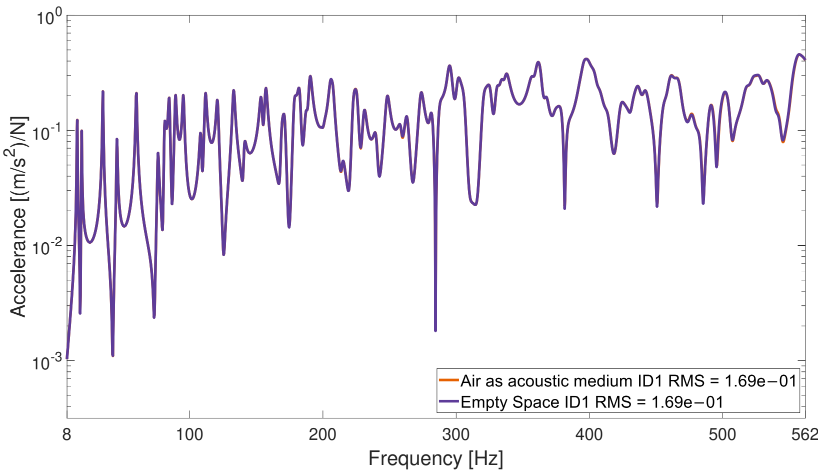

Figure 9.1: The steady–state dynamic response of configuration ID1 with air respectively empty space as lamellae. See Figure 9.2 for the configuration of ID1.

9.1.1 1 layer

The 1 layer configurations deemed necessary to illustrate the results can be viewed in Figure 9.2, with corresponding ID:s. For the full list of 1 layer empty space configurations, see Appendix B.

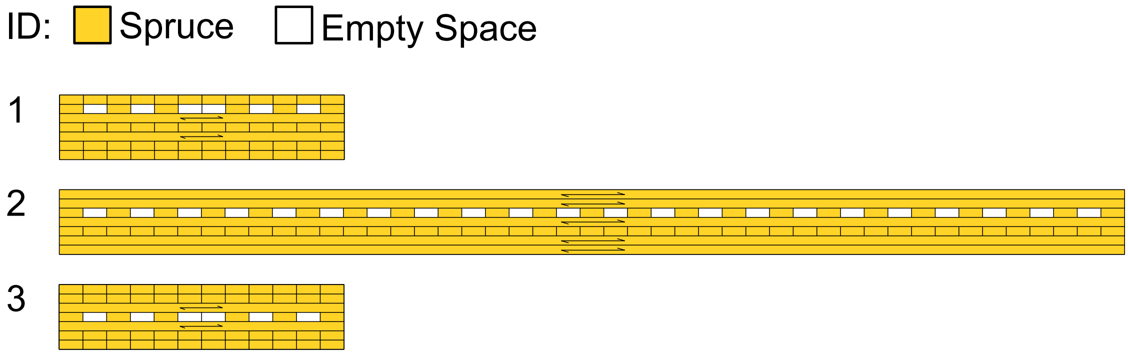

Figure 9.2: The full layers configurations for the 1 layer analyses, with corresponding ID:s. ID1,3 exchanges lamellae in longitudinal direction, while ID2 exchanges lamellae in transverse direction.

The partial 1 layer configurations deemed necessary to illustrate the results can be seen in Figure 9.3.

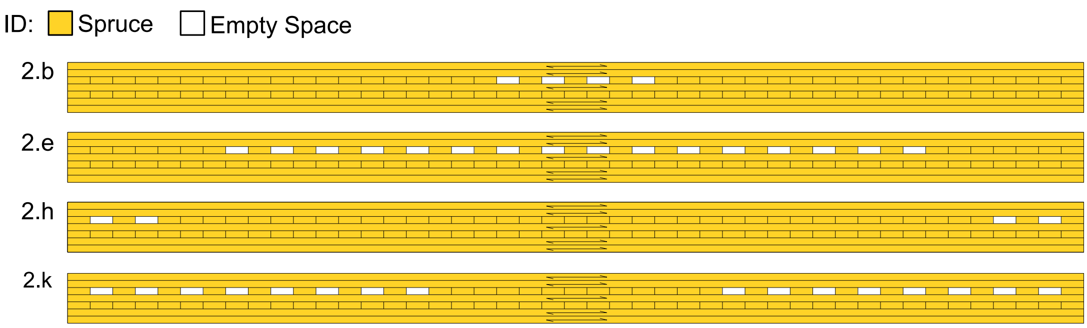

(a) Empty space partial layers of ID2, with lamellae in transverse direction.

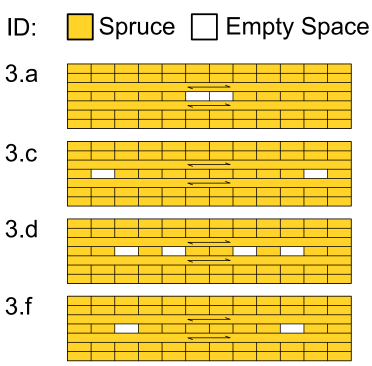

(b) Empty space partial layers of ID3, with lamellae in longitudinal direction.

Figure 9.3: The partial layers configurations for the 1 layer analyses of empty space, with corresponding ID:s.

9.1.1.1 Full layers

RMS–value
The effect on accelerance evaluated as RMS–values for ID1–3 can be seen in Table 9.1, where a negative change denotes a reduction in the level of vibration as compared to the reference level obtained by a panel comprised entirety of spruce.

Table 9.1: Empty space – the change in RMS–value, compared to the reference level, and the volume ratio for configurations with ID1–3. Volume ratio indicates the percentage of empty space in the panel.

ID	RMS [%]	Volume ratio [%]
1	–5	7
2	+14	7
3	+2	7

The RMS–values of both ID1 and ID3 did not indicate any significant change in accelerance compared to the reference level. However, the RMS–value of ID1 showed a lower RMS–value than ID3. Again, it is notable that configuration ID1 is not practical. In contrast, configuration ID2 which had empty space lamellae orientated in the transverse direction, showcased a significant amplification in accelerance.

1/3 octave band
The effect on accelerance evaluated in 1/3 octave bands for ID1–3 can be seen in Figure 9.4.

The responses of ID1,3 showcased no significant reductions or amplifications in accelerance at the majority of 1/3 octave bands over the studied frequency interval, i.e., up to 562 Hz. However, there were 1/3 octave bands where significant amplifications or reductions in accelerance occurred. For example, ID1 showcased significant amplification in accelerance at 1/3 octave band 31.5 Hz, and a significant reduction in accelerance at 1/3 octave band 40 Hz, while ID3 indicated significant amplification in accelerance at 160 Hz and 400 Hz and a significant reduction in accelerance at 200 Hz.

The response of ID2 showcased no significant reductions or amplifications in accelerance up to the 1/3 octave band of 25 Hz. However, from the 1/3 octave band of 25 Hz and upwards several bands with significant amplifications were observed. For example at 80, 160 and 400 Hz. Moreover, a significant reduction in accelerance were only indicated in a few smaller intervals, for example at 40 Hz.

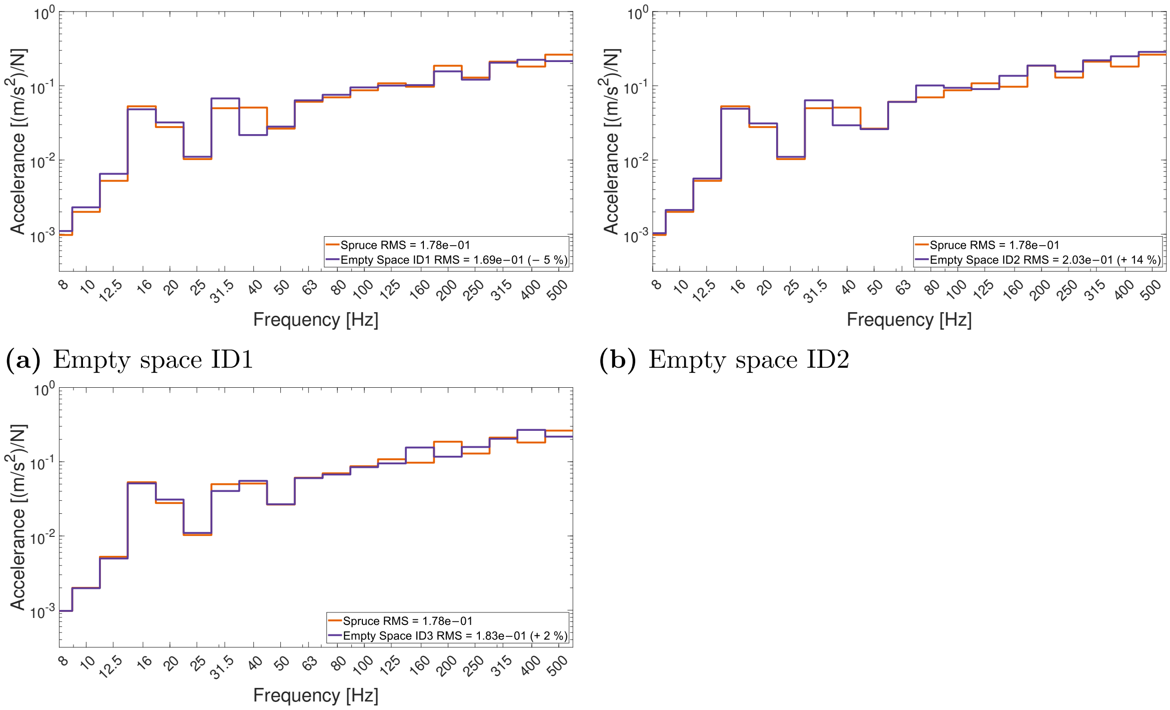

(a) Empty space ID1

(b) Empty space ID2

(c) Empty space ID3

Figure 9.4: Empty space – the steady–state dynamic responses of configurations ID1–3, in 1/3 octave bands. The values in legend withing parentheses indicates the change in RMS–value compared to the reference level. The center frequency of 1/3 octave bands are shown in the horizontal axis.

9.1.1.2 Partial layers

RMS–value

The effect on accelerance evaluated as RMS–values for the partial layer configurations of ID2–3 can be seen in Table 9.2, where a negative change denotes a reduction in the level of vibration as compared to the reference level obtained by a panel comprised entirety of spruce.

Table 9.2: Empty space – the change in RMS–value, compared to the reference level, and the volume ratio for the partial layers configurations of ID2–3. Volume ratio indicates the percentage of empty space in the panel.

ID	RMS [%]	Volume ratio [%]
2b	0	1
2e	+15	5
2h	+1	1
2k	+6	5
3a	+4	2
3c	0	2
3d	+5	5
3e	0	2

In Section 9.1.1.1, full layer of empty space lamellae in transverse direction, corresponding to ID2, showcased a significant amplification in accelerance. However, in some configurations of ID2 partial layers, the RMS–values did not show any significant amplifications compared to the reference level (ID2b,h). In contrast, remaining partial configurations of ID2 did show a significant increase in RMS–values (ID2e,k).

RMS–values for partial layers of ID3 exhibited no significant changes in accelerance compared to exchanging full layers. Considering the higher volume ratio of ID3 compared to its partial layers, it appears more favorable to exchange full layers of lamellae empty space.

1/3 octave band

The effect on accelerance evaluated as RMS–values for the partial layer configurations of ID2–3 can be seen in Figure 9.5.

The response of the partial layer configurations of ID3 showcased no significant reductions or amplifications in accelerance at the majority of 1/3 octave bands over the studied frequency interval, i.e., up to 562 Hz. However, there were 1/3 octave bands where significant amplifications or reductions in accelerance occurred. For example, ID3c showcased significant amplification in accelerance at 1/3 octave band 100 Hz, and a significant reduction in accelerance at 1/3 octave band 31.5 Hz, while ID3f indicated significant amplification in accelerance at 400 Hz and a significant reduction in accelerance at 31.5 Hz and 250 Hz.

The response of the partial layer configurations of ID2 showcased no significant reductions or amplifications in accelerance at the majority of 1/3 octave bands over the studied frequency interval, i.e., up to 562 Hz. However, there were 1/3 octave bands where significant amplifications or reductions in accelerance occurred. For example, ID2e showcased a significant amplification in accelerance at 1/3 octave band of 31.5 Hz and 400 Hz and a significant reduction in accelerance at 1/3 octave band 40 Hz, while ID2k indicated a significant amplification in accelerance at 100 Hz and a significant reduction in accelerance at 40 Hz.

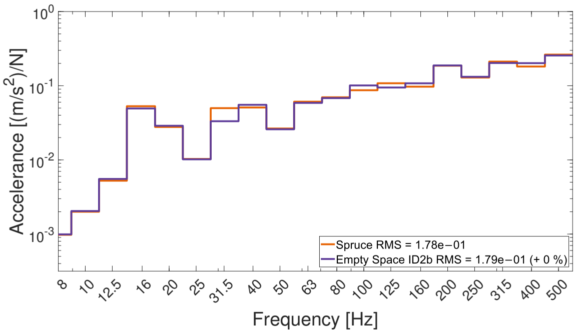

(a) Empty space ID2b

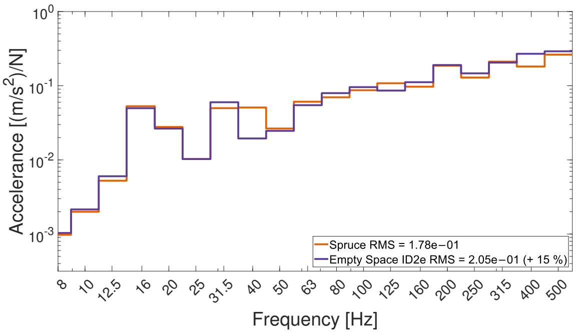

(b) Empty space ID2e

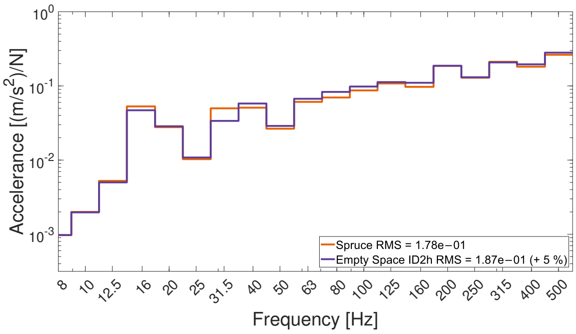

(c) Empty space ID2h

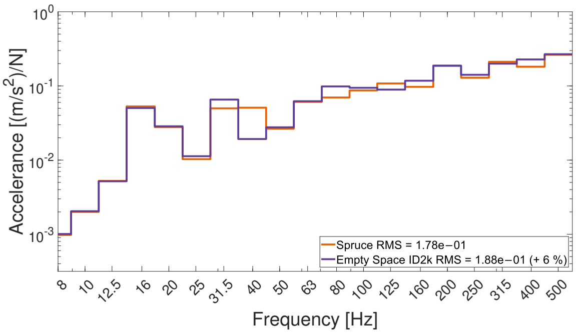

(d) Empty space ID2k

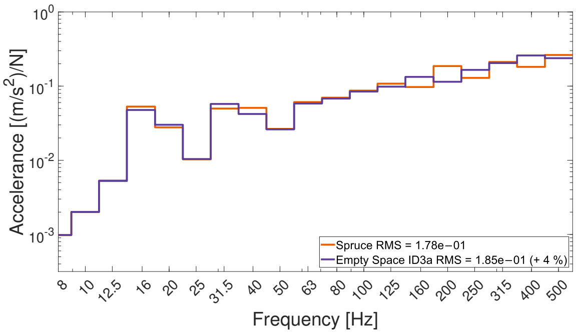

(e) Empty space ID3a

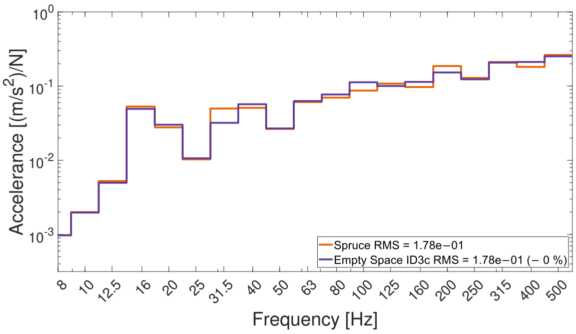

(f) Empty space ID3c

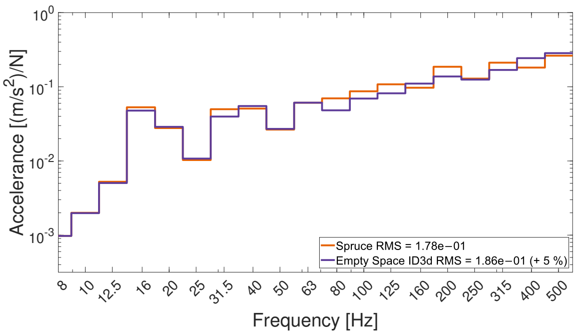

(g) Empty space ID3d

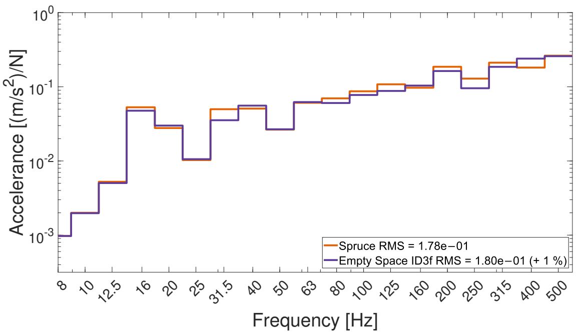

(h) Empty space ID3f

Figure 9.5: Empty space – the steady–state dynamic response for partial configurations of ID2–3, in 1/3 octave bands. The value in legend within parentheses indicates the change in RMS–value compared to the reference level. The center frequency of 1/3 octave bands are shown in the horizontal axis.

9.1.1.3 1 layer summary

In full layer configurations, exchanging spruce lamellae to empty space towards the surface (ID1) exhibited lower value in accelerance compared to the configuration towards the center (ID3), both showcasing no significant amplification. Again, it should be noted that configurations towards the surface might not be practical.

In full layer configurations, no significant change in accelerance was observed when exchanging lamellae in the longitudinal direction (ID1,3), while a significant amplification in accelerance was observed when exchanging lamellae in the transverse direction (ID2). However, some partial configurations exchanging lamellae in transverse direction exhibited no significant differences in accelerance (ID2b,h,k).

Partial layers exchanging lamellae in longitudinal direction exhibited no significant changes in accelerance compared to exchanging full layers. Considering the higher volume ratio of exchanging full layers compared to partial layers, it appears more favorable to exchange full layers of lamellae in longitudinal direction.

Configurations involving 1 layer showed that there is potential to remove up to 7% of spruce lamellae without significantly affecting the accelerance.

Even though the predicted accelerance was shown to be, for example, reduced by using an RMS–value, which is a single–value metric, the accelerance in specific 1/3 octave bands could be either amplified or reduced, respectively, in relation to the equivalent 1/3 octave bands for the reference panel.

9.1.2 2 layers

The 2 layers configurations deemed necessary to illustrate the results can be viewed in Figure 9.6, with corresponding ID:s. For the full list of 2 layers empty space configurations, see Appendix B.

The partial 2 layers configurations deemed necessary to illustrate the results can be seen in Figure 9.7.

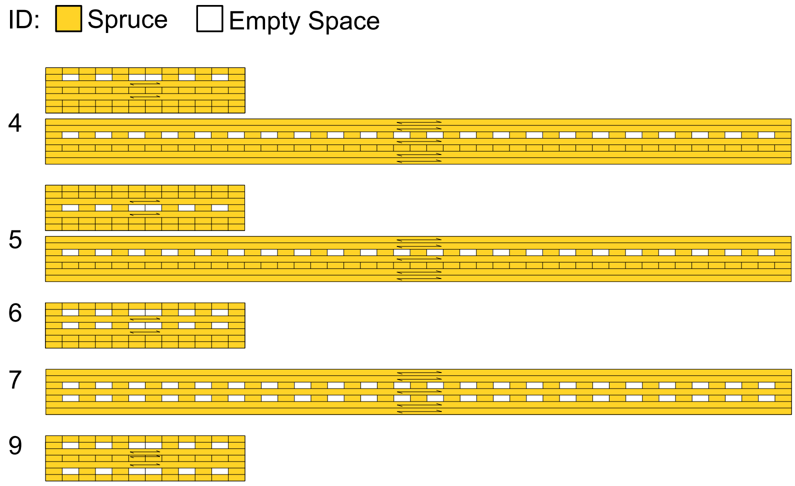

Figure 9.6: The full layers configurations for the 2 layers analyses, with corresponding ID:s. In ID4–5 lamellae in both transverse (upper image of ID4–5) and longitudinal direction (lower image of ID4–5) are exchanged, while in ID6,9 lamellae in longitudinal direction are exchanged. In ID7 lamellae in transverse direction are exchanged.

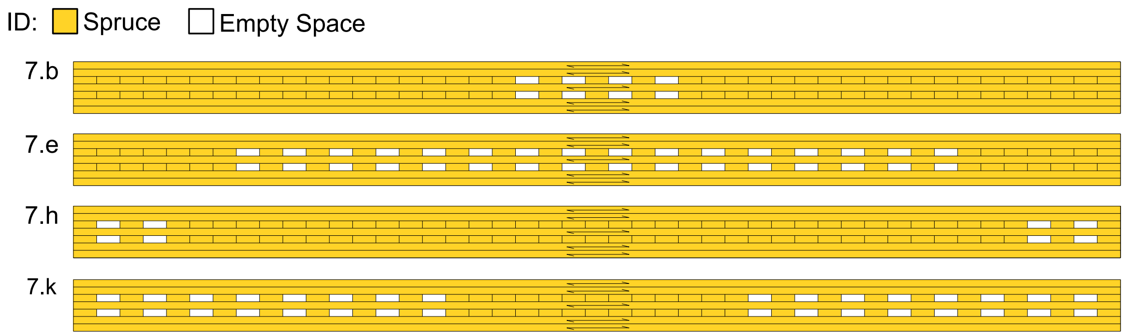

Figure 9.7: Empty space partial layers of ID7, with lamellae in transverse direction.

9.1.2.1 Full layers

RMS–value

The effect on accelerance evaluated as RMS–values for ID4–7,9 can be seen in Table 9.3, where a negative change denotes a reduction in the level of vibration as compared to the reference level obtained by a panel comprised entirety of spruce.

The RMS–values for ID4,6,9 did not indicate any significant change in accelerance. Conversely, the configurations ID5 and ID7 showcased significant amplifications in accelerance. The configuration ID4, which had more empty space lamellae towards the surface than ID5, indicated a lower RMS–values than ID5. However, the RMS–values of ID6 and ID9 did not display any significant differences in accelerance.

Table 9.3: Empty space – the change in RMS–value, compared to the reference level, and the volume ratio for configurations with ID4–7,9. Volume ratio indicates the percentage of empty space in the panel.

ID	RMS [%]	Volume ratio [%]
4	+4	14
5	+12	14
6	–5	14
7	+18	14
9	–3	14

1/3 octave band

The effect on accelerance evaluated in 1/3 octave bands for ID4–7,9 can be seen in Figure 9.8.

The responses of ID4–7,9 showcased significant reductions or amplifications in accelerance at different 1/3 octave bands over the studied frequency interval, i.e., up to 562 Hz. For example, ID4 showcased significant amplification in accelerance at 1/3 octave bands 31.5, 80 and 160 Hz, and a significant reduction in accelerance at 1/3 octave band 40 Hz, while ID7 indicated significant amplification in accelerance at 160, 250 and 400 Hz and a significant reduction in accelerance at 200 Hz. However, there were 1/3 octave bands where no significant amplifications or reductions in accelerance occurred. For example at the 1/3 octave band of 63 Hz for ID4–7.

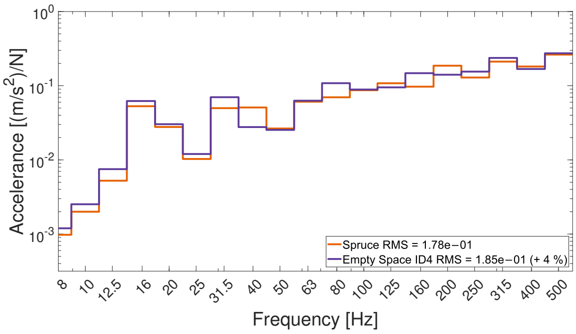

(a) Empty space ID4

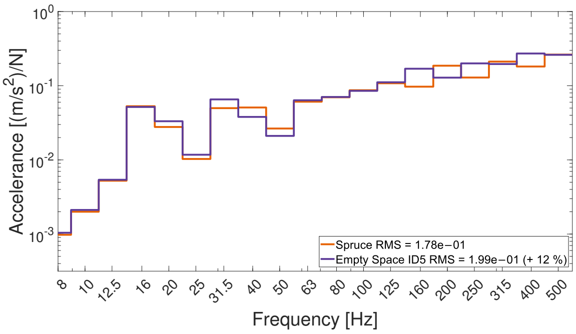

(b) Empty space ID5

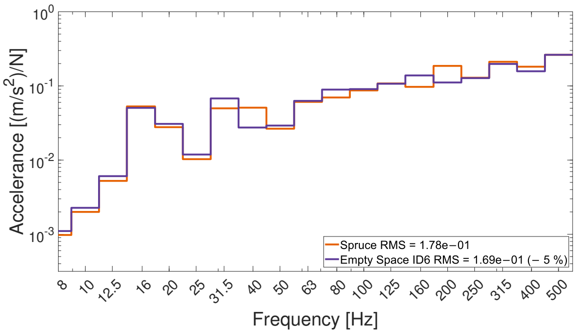

(c) Empty space ID6

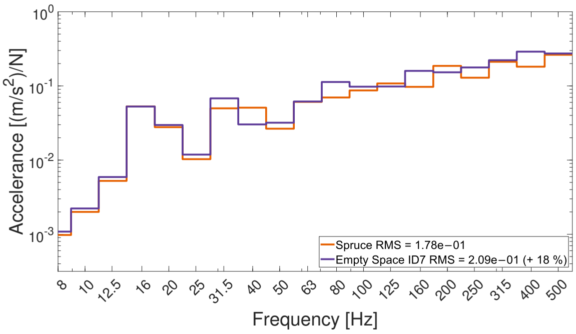

(d) Empty space ID7

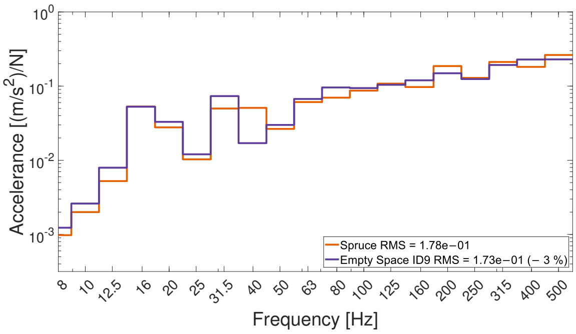

(e) Empty space ID9

Figure 9.8: Empty space – the steady–state dynamic responses of configurations ID4–7,9, in 1/3 octave bands. The value in legend within parentheses indicates the change in RMS–value compared to the reference level. The center frequency of 1/3 octave bands are shown in the horizontal axis.

9.1.2.2 Partial layers

RMS–value

The effect on accelerance evaluated as RMS–values for the partial layers configurations of ID7 can be seen in Table 9.4, where a negative change denotes a reduction in the level of vibration as compared to the reference level obtained by a panel comprised entirety of spruce.

In Section 9.1.2.1, full layers of empty space lamellae in transverse direction, corresponding to ID7, showcased significant amplification in accelerance. However, in one configuration of ID7 partial layers, the RMS–values did not show any significant amplification compared to the reference level (ID7c). In contrast, remaining partial configurations of ID7 did show significant increase in RMS–values (ID7e,i,k).

Table 9.4: The change in RMS–value, compared to the reference level, and the volume ratio for the partial layers configurations of ID7. Volume ratio indicates the percentage of empty space in the panel.

ID	RMS [%]	Volume ratio [%]
7c	+2	5
7e	+17	10
7i	+6	5
7k	+8	10

1/3 octave band

The effect on accelerance evaluated as RMS–values for the partial layer configurations of ID7 can be seen in Figure 9.9.

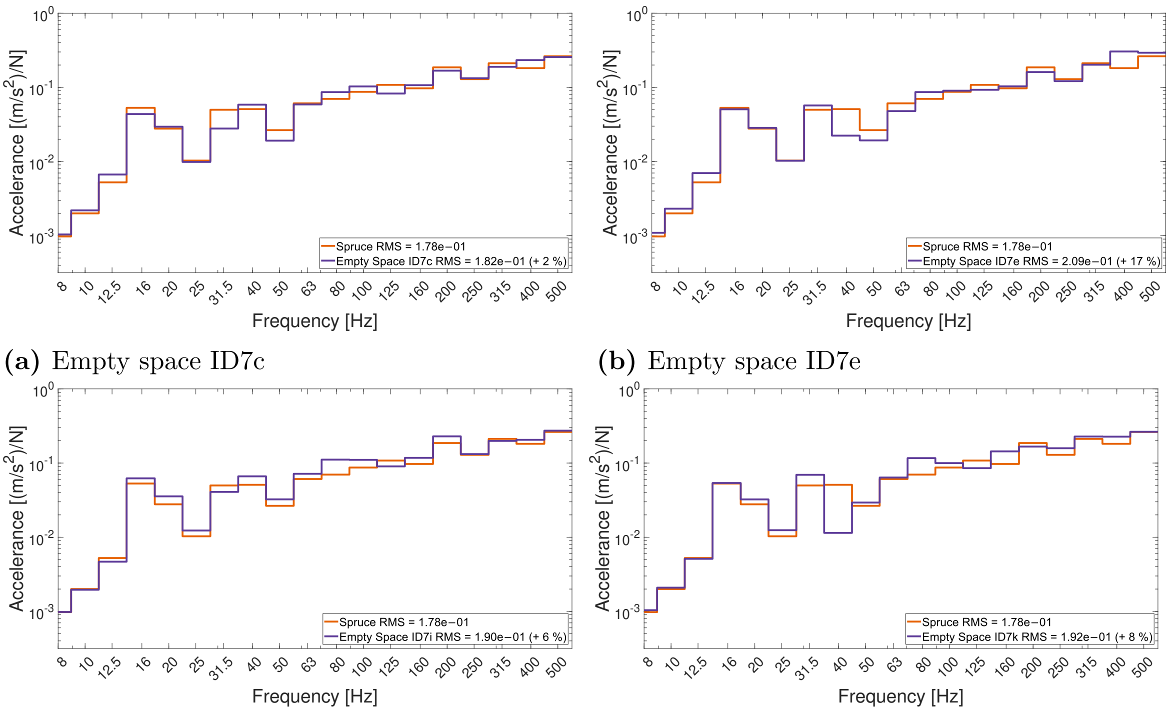

(a) Empty space ID7c

(b) Empty space ID7e

(c) Empty space ID7i

(d) Empty space ID7k

Figure 9.9: Empty space – the steady–state dynamic response for partial configurations of ID7, in 1/3 octave bands. The value in legend within parentheses indicates the change in RMS–value compared to the reference level. The center frequency of 1/3 octave bands are shown in the horizontal axis.

The response of the partial layer configurations of ID7 showcased a significant reductions or amplifications in accelerance at different 1/3 octave bands over the studied frequency interval, i.e., up to 562 Hz. For example, ID7c,e showcased a significant amplification in accelerance at 1/3 octave bands 12.5, 80 and 400 Hz, and a significant reduction in accelerance at 1/3 octave band 40–50 Hz, while ID7i,k indicated a significant amplification in accelerance at 20, 80 and 200 Hz and a significant reduction in accelerance at 125 Hz. However, there were 1/3 octave bands where no significant amplifications or reductions in accelerance occurred. For example, at the 1/3 octave band of 500 Hz for all partial configurations of ID7.

9.1.2.3 2 layers summary

In full layers configurations, exchanging spruce lamellae to empty space towards the surface exhibited larger reduction in accelerance compared to the configuration towards the center, in one comparison (ID4 compared to ID5). In another, no significant difference in accelerance were observed (ID9 compared to ID6). Again, it should be noted that configurations towards the surface might not be practical.

In full layer configurations, no significant change in accelerance was observed when exchanging lamellae in the longitudinal direction (ID6,9), while significant amplification in accelerance was observed when exchanging lamellae in the transverse direction (ID7). However, one partial configurations exchanging lamellae in transverse direction exhibited no significant differences in accelerance (ID7c).

Configurations involving 2 layers showed that there is potential to remove up to 14% of spruce lamellae without significantly affecting the accelerance.

Even though the predicted accelerance was shown to be, for example, reduced by using an RMS–value, which is a single–value metric, the accelerance in specific 1/3 octave bands could be either amplified or reduced, respectively, in relation to the equivalent 1/3 octave bands for the reference panel.

9.1.3 3 layers

The 3 layers configurations deemed necessary to illustrate the results can be viewed in Figure 9.10, with corresponding ID:s. For the full list of 3 layers empty space configurations, see Appendix B.

The partial 3 layers configurations deemed necessary to illustrate the results can be seen in Figure 9.11.

It is important to note that these configurations are not directly comparable for the purpose of finding potential trends in the dynamic behavior of the panel. This is due to the fact that they do not have the same number of layers in each direction. However, configurations ID10–12 were still considered as they could provide further insights into the structural behavior of the panel.

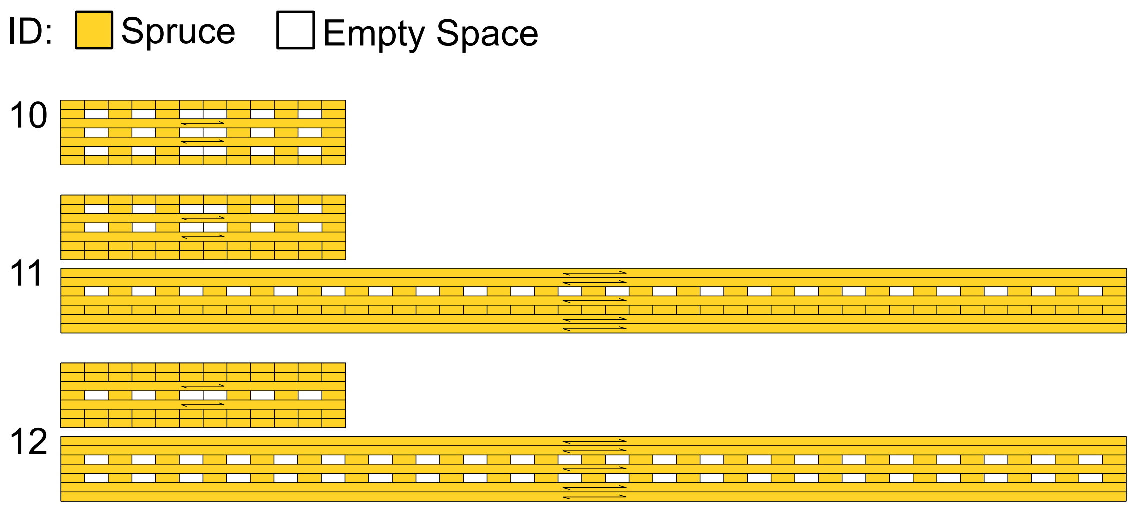

Figure 9.10: The full layers configurations for the 3 layers analyses, with corresponding ID:s. In ID11–12 lamellae in both transverse (upper image of ID11–12) and longitudinal direction (lower image of ID11–12) are exchanged, while in ID10 lamellae in longitudinal direction are exchanged.

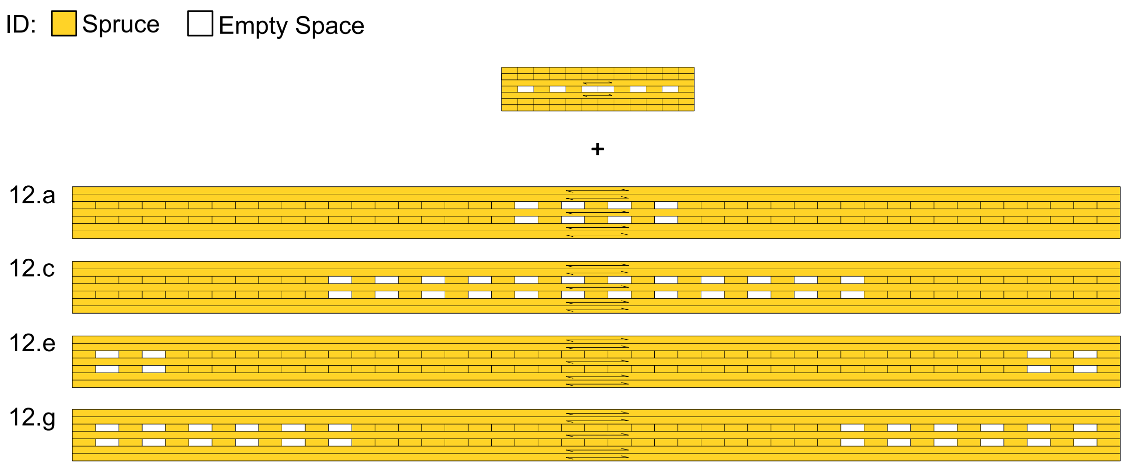

Figure 9.11: Empty space partial layers of ID12, with lamellae in both transverse and longitudinal direction.

9.1.3.1 Full layers

RMS–value

The effect on accelerance evaluated as RMS–values for ID10–12 can be seen in Table 9.5, where a negative change denotes a reduction in the level of vibration as compared to the reference level obtained by a panel comprised entirety of spruce.

The RMS–values for ID10,11 did not indicate any significant change in accelerance. Conversely, the configuration ID12 showcased a significant amplification in accelerance. The configuration ID10, which had more empty space lamellae towards the surface than ID12, indicated a lower RMS–values than ID12.

Table 9.5: Empty space – the change in RMS–value, compared to the reference level, and the volume ratio for configurations with ID10–12. Volume ratio indicates the percentage of empty space in the panel.

ID	RMS [%]	Volume ratio [%]
10	−1	21
11	+4	21
12	+20	21

1/3 octave band

The effect on accelerance evaluated in 1/3 octave bands for ID10–12 can be seen in Figure 9.12.

The responses of ID10–12 showcased significant reductions or amplifications in accelerance at different 1/3 octave bands over the studied frequency interval, i.e., up to 562 Hz. For example, ID10 showcased significant amplification in accelerance at 1/3 octave bands 31.5 and 80 Hz, and a significant reduction in accelerance at 1/3 octave band 40 Hz, while ID12 indicated significant amplification in accelerance at 160, 250 and 400 Hz and a significant reduction in accelerance at 200 Hz. However, there were 1/3 octave bands where no significant amplifications or reductions in accelerance occurred. For example at the 1/3 octave band of 100 Hz for ID10–12.

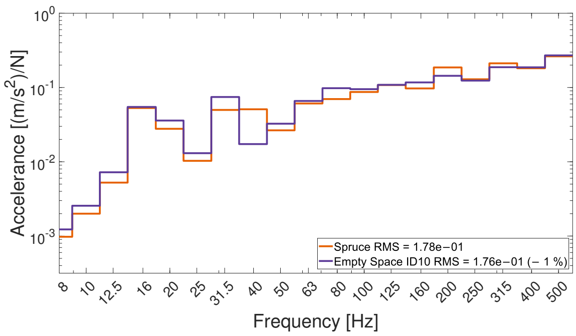

(a) Empty space ID10

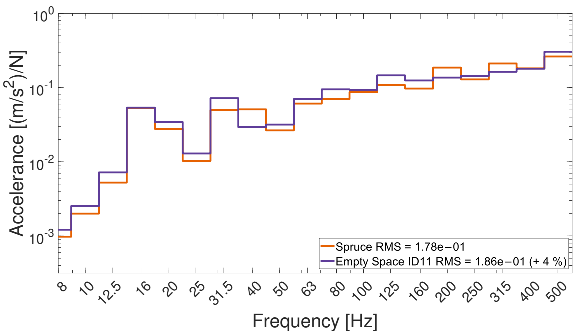

(b) Empty space ID11

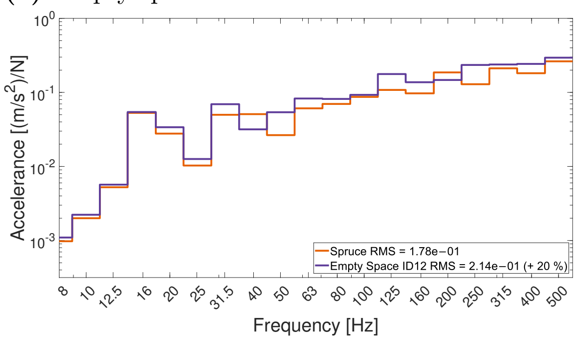

(c) Empty space ID12

Figure 9.12: Empty space – the steady–state dynamic responses of configurations ID10–12, in 1/3 octave bands. The value in legend within parentheses indicates the change in RMS–value compared to the reference level. The center frequency of 1/3 octave bands are shown in the horizontal axis.

9.1.3.2 Partial layers

RMS–value

The effect on accelerance evaluated as RMS–values for the partial layer configurations of ID12 can be seen in Table 9.6, where a negative change denotes a reduction in the level of vibration as compared to the reference level obtained by a panel comprised entirety of spruce.

Table 9.6: The change in RMS–value, compared to the reference level, and the volume ratio for the partial layers configurations of ID12. Volume ratio indicates the percentage of empty space in the panel.

ID	RMS [%]	Volume ratio [%]
12a	+7	10
12c	+7	15
12e	+17	10
12g	+15	15

In Section 9.1.3.1, ID12 showcased a significant amplification in accelerance. In the partial layers configurations of ID12, this amplification in accelerance was reduced, particularly in ID12a,c, all though still indicating significant amplifications.

1/3 octave band

The effect on accelerance evaluated as RMS–values for the partial layer configurations of ID12 can be seen in Figure 9.13.

The response of the partial layer configurations of ID12 showcased a significant reductions or amplifications in accelerance at different 1/3 octave bands over the studied frequency interval, i.e., up to 562 Hz. For example, ID12a,e showcased a significant amplification in accelerance at 1/3 octave bands 40, 160 and 400 Hz, and a significant reduction in accelerance at 1/3 octave band 31.5 and 200 Hz, while ID12c,g indicated a significant amplification in accelerance at 80, 160 and 400 Hz and a significant reduction in accelerance at 12.5 Hz. However, there were 1/3 octave bands where no significant amplifications or reductions in accelerance occurred. For example, at the 1/3 octave band of 10 Hz for all partial configurations of ID12.

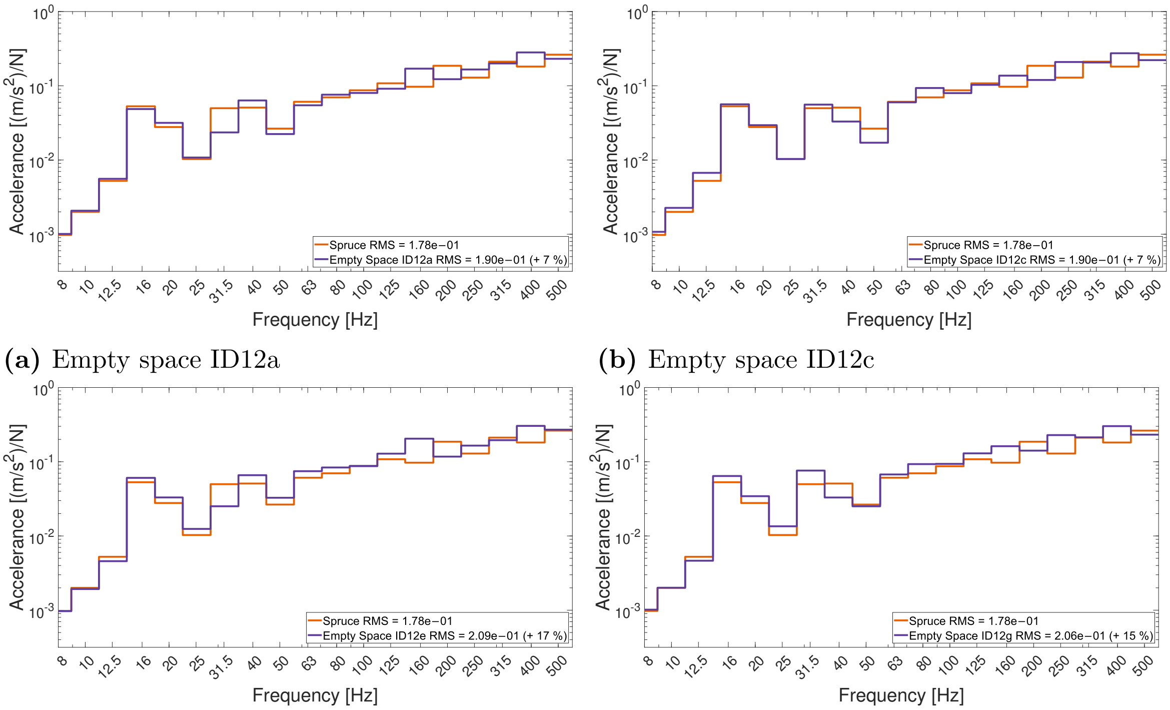

(a) Empty space ID12a

(b) Empty space ID12c

(c) Empty space ID12e

(d) Empty space ID12g

Figure 9.13: The steady–state dynamic response for partial configuration of ID12, in 1/3 octave bands. The value in legend within parentheses indicates the change in RMS–value compared to the reference level. The center frequency of 1/3 octave bands are shown in the horizontal axis.

9.1.3.3 3 layers summary

In full layers configurations, exchanging spruce lamellae to empty space towards the surface exhibited a larger reduction in accelerance compared to the configuration towards the center (ID10 compared to ID12). Again, it should be noted that configurations towards the surface might not be practical, and that the 3 layers configurations are not directly comparable.

In full layer configurations, no significant change in accelerance was observed when exchanging lamellae in the longitudinal direction (ID10), while significant amplification in accelerance was observed for the configuration exchanging two layers of lamellae in the transverse direction together with one layer of lamellae in the longitudinal direction (ID12). The partial configurations of exchanging two layers of lamellae in the transverse direction together with one layer of lamellae in the longitudinal exhibited significant amplifications in accelerance (ID12a,c,e,g).

Configurations involving 3 layers showed that there is potential to remove up to 21% of spruce lamellae without significantly affecting the accelerance.

Even though the predicted accelerance was shown to be, for example, reduced by using an RMS–value, which is a single–value metric, the accelerance in specific 1/3 octave bands could be either amplified or reduced, respectively, in relation to the equivalent 1/3 octave bands for the reference panel.

9.1.4 Large sized panel summary

The impact of exchanging lamellae from spruce to empty space in the L–sized panel are consolidated in this section.

- No significant differences in accelerance were indicated between the two studied modeling methods of air cavities. The method of modeling air cavities as empty space could save computational costs and streamline analyses.
- Exchanging spruce lamellae to empty space towards the surface (ID1,4,10) exhibited a lower amplification in accelerance compared to the configurations towards the center (ID3,5,12). With the exception of one comparison, which showed no significant difference in accelerance (ID9 compared to ID6). Again, it should be noted that configurations towards the surface might not be practical.
- No significant change in accelerance was observed when exchanging lamellae in the longitudinal direction (ID1,3,6,9,10), while a significant amplification in accelerance was observed when exchanging lamellae in the transverse direction (ID2,7). However, some partial configurations exchanging lamellae in transverse direction exhibited no significant differences in accelerance (ID2b,h,k and ID7c)
- Configurations involving 3 layers showed that there is potential to remove up to 21% of spruce lamellae without significantly affecting the accelerance (ID10).
- Even though the predicted accelerance was shown to be, for example, reduced by using an RMS–value, which is a single–value metric, the accelerance in specific 1/3 octave bands could be either amplified or reduced, respectively, in relation to the equivalent 1/3 octave bands for the reference panel.

9.2 Medium sized panel

1 layer

The investigation whether the dimensions and/or lay–ups of the panels influence the results are presented here.

The configurations analyzed can be viewed in Figure 9.14.

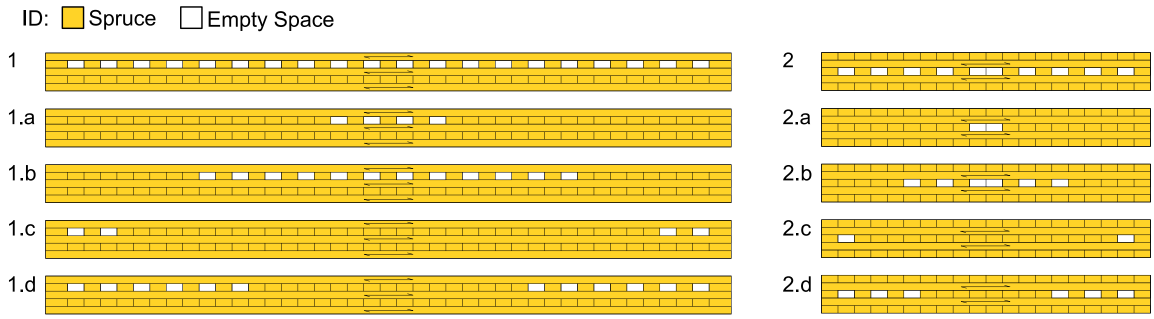

Figure 9.14: Illustration of the analyzed configuration, performed on the M–sized panel. The full layer configuration and partial layer configurations of ID1 exchanges lamellae in transverse direction. The full layer configuration and partial layer configurations of ID2 exchanges lamellae in longitudinal direction

The effect on accelerance evaluated as RMS–value for these configurations can be seen in Table 9.7, where a negative change denotes a reduction in the level of vibration as compared to the reference level obtained by a panel comprised entirety of spruce.

The effect on accelerance evaluated in 1/3 octave bands for these configurations can be seen in Figure 9.15.

Table 9.7: The change in RMS–value, compared to the reference level, and the volume ratio for configurations visualized in Figure 9.15. Volume ratio indicates the percentage of empty space in the panel.

ID	RMS [%]	Volume ratio [%]
1	–7	10
2	+1	10
1a	–2	2
1b	–4	6
1c	–4	2
1d	–7	6
2a	–7	2
2b	–14	6
2c	–1	2
2d	–4	6

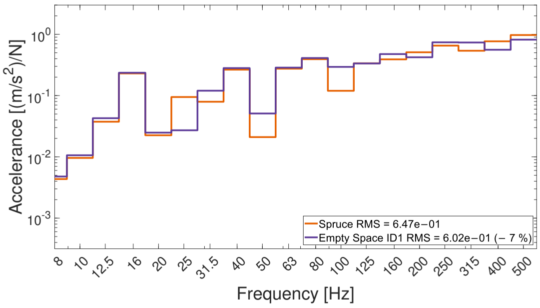

(a) Empty space M–sized panel ID1

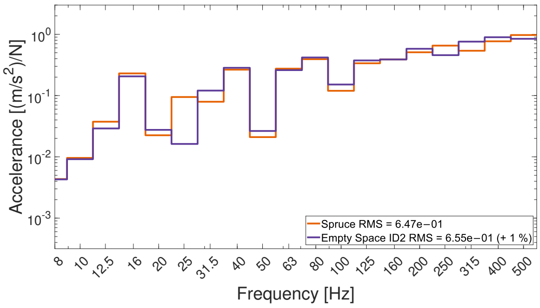

(b) Empty space M–sized panel ID2

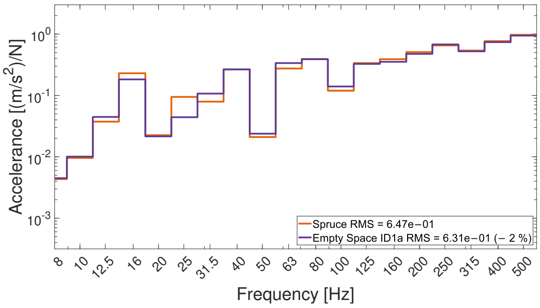

(c) Empty space M–sized panel ID1a

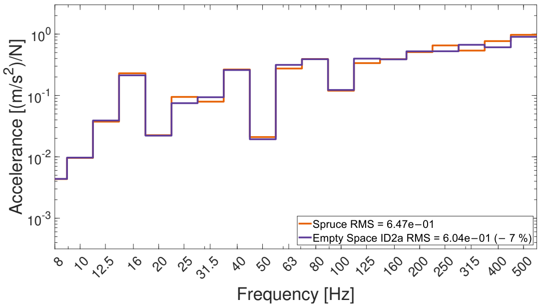

(d) Empty space M–sized panel ID2a

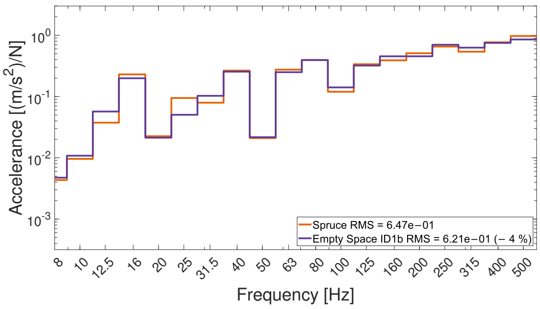

(e) Empty space M–sized panel ID1b

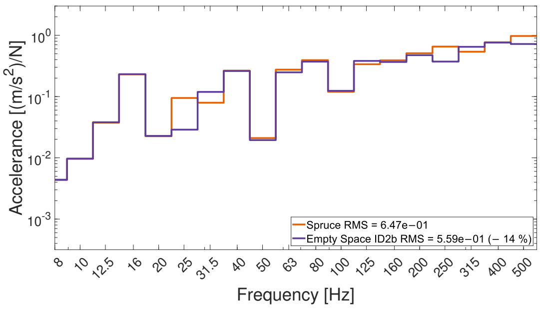

(f) Empty space M–sized panel ID2b

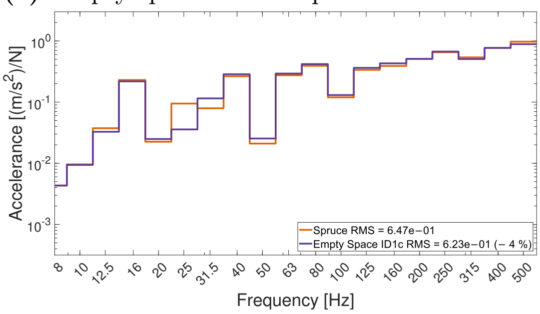

(g) Empty space M–sized panel ID1c

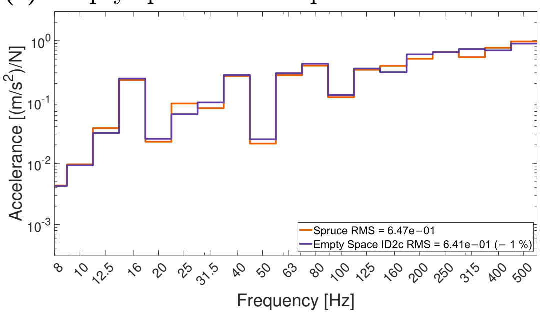

(h) Empty space M–sized panel ID2c

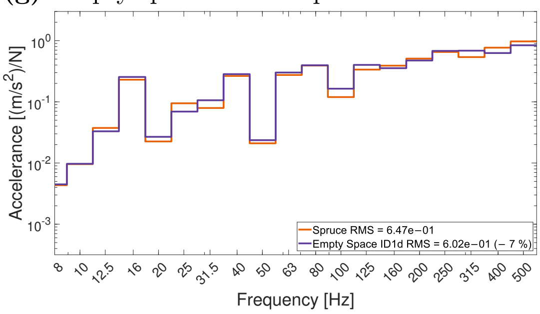

(i) Empty space M–sized panel ID1d

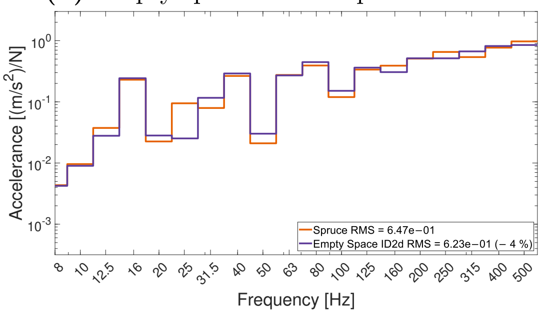

(j) Empty space M–sized panel ID2d

Figure 9.15: Empty space – the steady–state dynamic response in 1/3 octave bands for configurations illustrated in Figure 9.14. The value in legend within parentheses indicates the change in RMS–value compared to the reference level. The center frequency of 1/3 octave bands are shown in the horizontal axis.

The results for the M–sized panel indicated no significant differences in accelerance between the two studied modeling methods of air cavities, see Figure 9.16. The relative difference in RMS–values was insignificant.

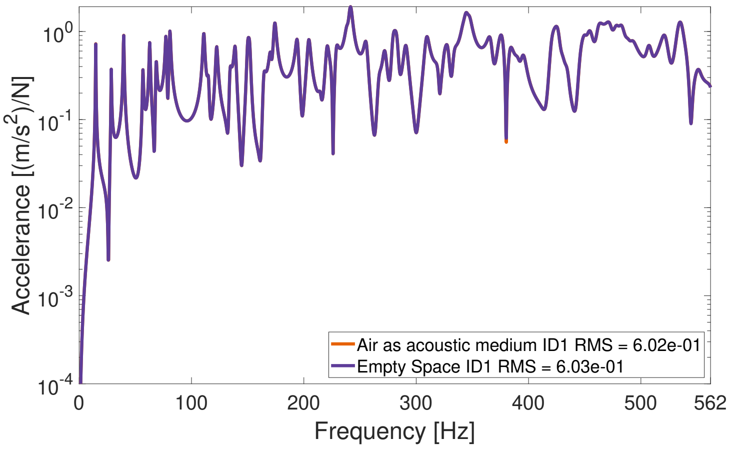

Figure 9.16: Accelerance of the configuration ID1 with air respectively empty space. See 9.14 for the configuration of ID1.

No significant amplification in accelerance was observed when exchanging spruce lamellae to empty space in either the transverse direction (ID1) or in the longitudinal direction (ID2).

Configurations involving 1 layer in the M-sized panel showed that there is potential to remove up to 10% of spruce lamellae without significantly amplifying the accelerance (ID1,2).

The responses of the configurations analyzed in the M–sized panel showcased a significant reductions or amplifications in accelerance at different 1/3 octave bands over the studied frequency interval, i.e., up to 562 Hz. For example, ID1,2 showcased a significant amplification in accelerance at 1/3 octave bands 50, 100 and 315 Hz, and a significant reduction in accelerance at 1/3 octave band 25 Hz, while ID1b and ID2b indicated a significant amplification in accelerance at 31.5 Hz and a significant reduction in accelerance at 25 Hz. However, there were 1/3 octave bands where no significant amplifications or reductions in accelerance occurred. For example at the 1/3 octave band of 125 Hz for ID1-2.

10 Impact of stiff elastomer lamellae

In this chapter, the impact of exchanging lamellae from spruce to elastomer Sylodyn NF, is presented. To be clear, it is not precisely Sylodyn NF that has been modeled, but rather a close replicate of a stiff elastomer.

The terms "full layer/full layers" will be used in this section. However, the terms will not refer to exchanging the actual full layer/layers, but instead every other lamellae. This approach ensured practical relevance.

10.1 Large sized panel

10.1.1 1 layer

The 1 layer configurations deemed necessary to illustrate the results can be viewed in Figure 10.1, with corresponding ID:s.

The partial 1 layer configurations deemed necessary to illustrate the results can be seen in Figure 10.2.

For the full list of 1 layer Sylodyn NF configurations, see Appendix C.

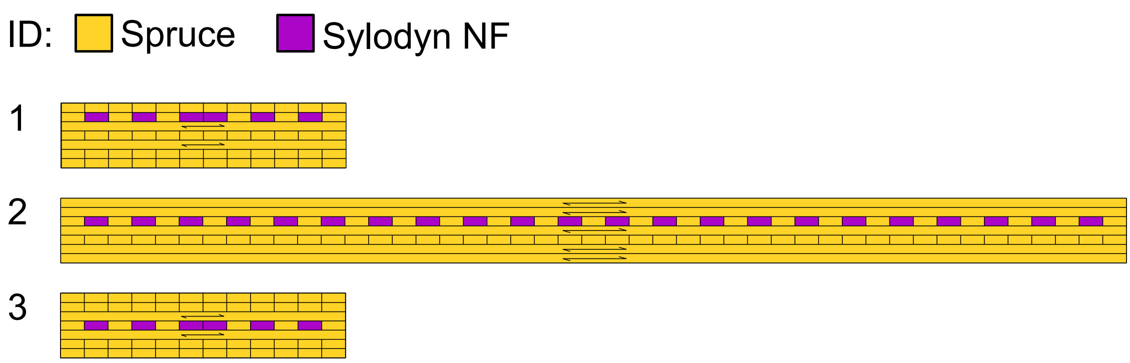

Figure 10.1: Sylodyn NF – the full layer configurations for the 1 layer analysis, with corresponding ID:s. In ID1,3 lamellae in longitudinal direction are exchanged, while in ID2 lamellae in transverse direction are exchanged.

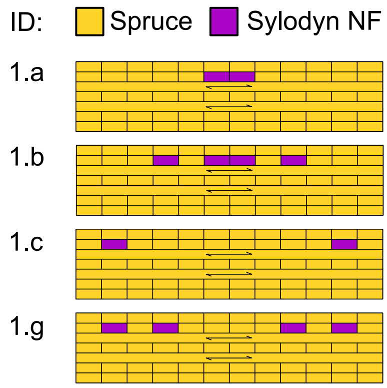

(a) Sylodyn NF – partial layer of ID1, with lamellae in longitudinal direction.

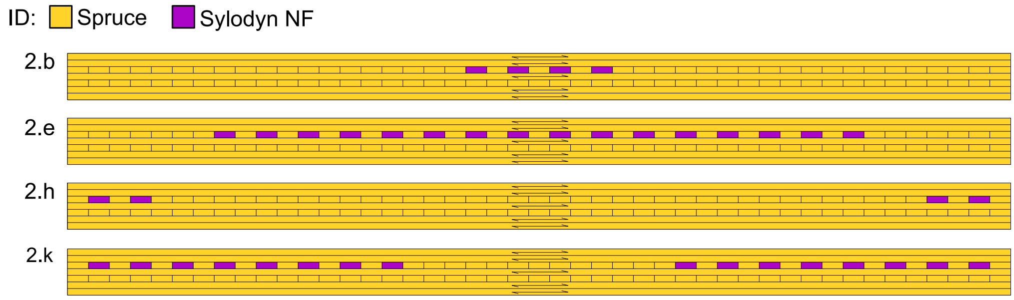

(b) Sylodyn NF – partial layer of ID2, with lamellae in transverse direction.

Figure 10.2: Sylodyn NF – the partial layer configurations for the 1 layer analysis, with corresponding ID:s.

10.1.1.1 Full layer

RMS–value

The effect on accelerance evaluated as RMS–value for ID1–3 can be seen in Table 10.1, where a negative change denotes a reduction in the level of vibration as compared to the reference level obtained by a panel composed entirely of spruce.

Table 10.1: Sylodyn NF – the change in RMS–value, compared to the reference level, and the volume ratio for configurations with ID1–3. Volume ratio indicates the percentage of Sylodyn NF in the panel.

ID	RMS [%]	Volume ratio [%]
1	–24	7
2	+0	7
3	–14	7

Configuration ID1 to ID3 had Sylodyn NF lamellae orientated in the longitudinal direction. The RMS–values of both ID1 to ID3 showed significant reductions in accelerance compared to the reference level. However, the reduction in accelerance displayed by ID1 was greater than the reduction in accelerance indicated by ID3.

In contrast, configuration ID2, which had Sylodyn NF lamellae orientated in the panel's transverse direction, showed insignificant change in RMS–values.

Comparing ID2 to ID1 and ID3, placing Sylodyn NF lamellae in longitudinal direction showed a greater reduction in accelerance than placing them in transverse direction.

Comparing ID1 to ID3, placing Sylodyn NF lamellae closer to the surface showed greater reductions in accelerance compared to placing them closer to the center.

1/3 octave band

The effect on accelerance evaluated in 1/3 octave bands for ID1–3 can be seen in Figure 10.3.

The response of ID1 showed significant reductions in accelerance between the 1/3 octave bands of 200–500 Hz. Under the 1/3 octave band of 160 Hz, ID1 showed reductions in accelerance at certain 1/3 octave bands and amplifications in others.

Configuration ID3 displayed significant reductions in accelerance between 1/3 octave bands of 40–125 Hz. Outside this interval, ID3 showed reductions in accelerance at certain 1/3 octave bands and amplifications in others.

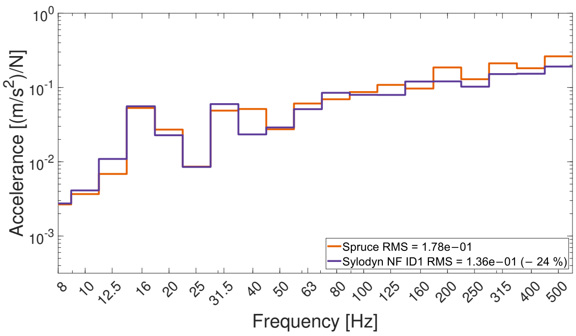

(a) Sylodyn NF ID1

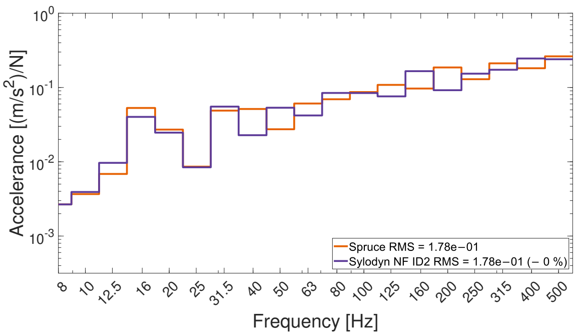

(b) Sylodyn NF ID2

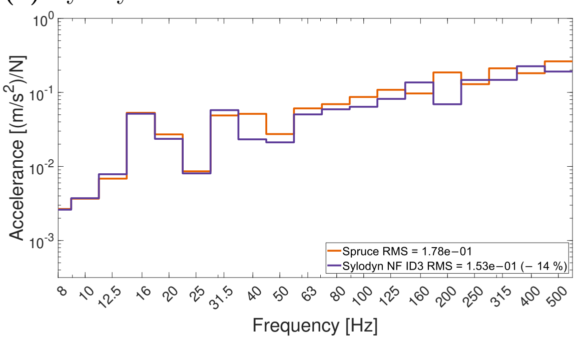

(c) Sylodyn NF ID3

Figure 10.3: Sylodyn NF – the steady–state dynamic response of configuration ID1–3, in 1/3 octave bands. The value in legend within parentheses indicates the change in RMS–value compared to the reference level. The center frequency of 1/3 octave bands are shown in the horizontal axis.

The response of ID2 showed reductions or amplifications in accelerance at different 1/3 octave bands over the entire studied frequency interval, i.e., up to 562 Hz.

It is notable that all configurations of the 1 layers configurations showed amplification in accelerance at the 1/3 octave band of 31.5 Hz and significant reductions at 40 Hz. It is due to the lowering of the peak frequency in the 40 Hz band to the 1/3 octave band just before, which is the 31.5 Hz band.

10.1.1.2 Partial layer

RMS–value

The effect on accelerance evaluated as RMS–value for the partial layer configurations of ID1–2 can be seen in Table 10.2, where a negative change denotes a reduction in the level of vibration as compared to the reference level obtained by a panel composed entirely of spruce.

Table 10.2: Sylodyn NF – the change in RMS–value, compared to the reference level, and the volume ratio for the partial layer configurations of ID1–2. Volume ratio indicates the percentage of Sylodyn NF in the panel.

ID	RMS [%]	Volume ratio [%]
1a	–11	2
1b	–5	5
1c	–19	2
1g	–22	5
2b	–0	1
2e	–1	5
2h	–7	1
2k	–13	5

The RMS–values for all partial layer configurations of ID1 exhibited a significant reductions in accelerance, except for ID1b which did not show any significant difference in accelerance.

Additionally, significant differences in accelerance were observed when comparing ID1a to ID1c, as well as ID1b to ID1g. The configurations ID1c,g provided a larger reduction in accelerance than ID1a,b. It indicated exchanging spruce lamellae with Sylodyn NF closer to the edges provided greater reductions in accelerance compared to placing Sylodyn NF closer to the center (in both directions).

The RMS–values of ID2b,e showed insignificant reductions in accelerance, while ID2h,k showed significant reductions in accelerance.

Comparing the partial configurations of ID1 and ID2, placing Sylodyn NF lamellae in longitudinal direction showed a greater reduction in accelerance than placing them in transverse direction.

1/3 octave band

The effect on accelerance evaluated in 1/3 octave bands for the partial layer configurations of ID1–2 can be seen in Figure 10.4.

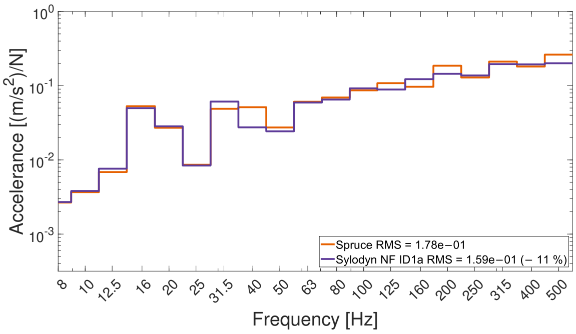

(a) Sylodyn NF ID1a

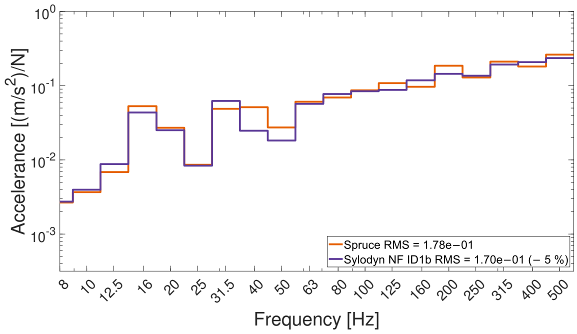

(b) Sylodyn NF ID1b

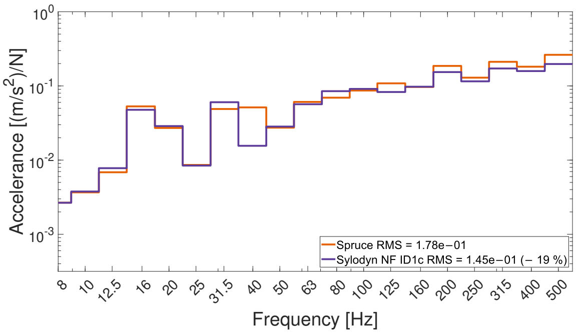

(c) Sylodyn NF ID1c

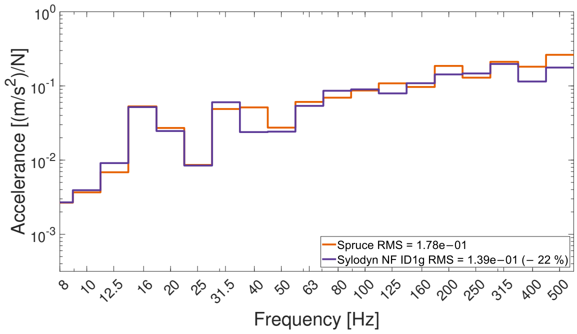

(d) Sylodyn NF ID1g

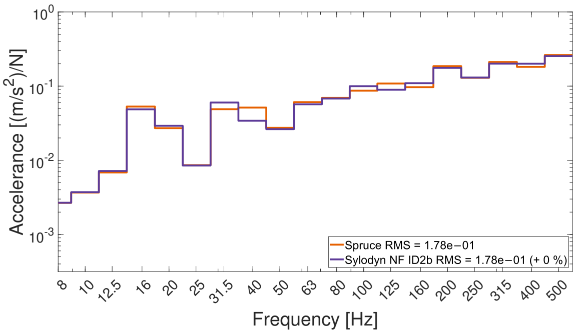

(e) Sylodyn NF ID2b

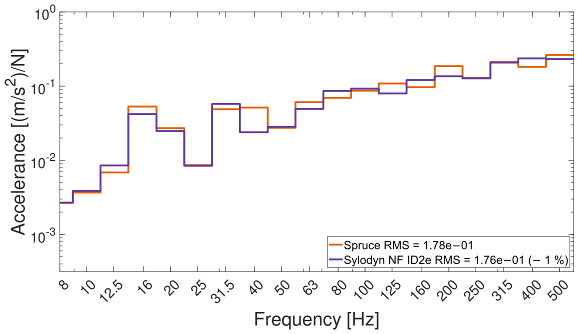

(f) Sylodyn NF ID2e

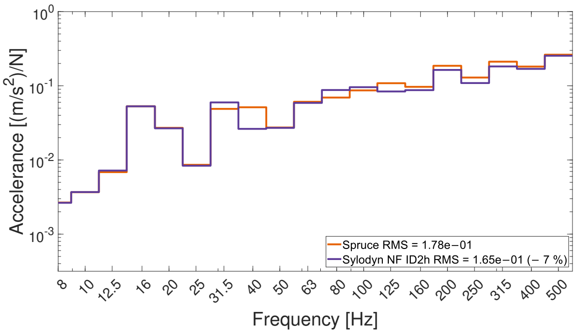

(g) Sylodyn NF ID2h

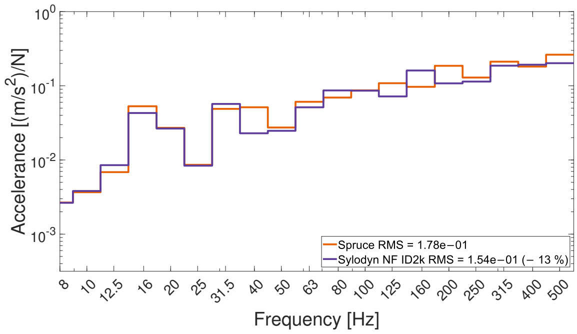

(h) Sylodyn NF ID2k

Figure 10.4: The steady–state dynamic response for partial configurations of ID1–2, in 1/3 octave bands. The value in legend within parentheses indicates the change in RMS–value compared to the reference level. The center frequency of 1/3 octave bands are shown in the horizontal axis.

The configurations ID1a,b and ID2b,e,h,k showed reductions or amplifications in accelerance at different 1/3 octave bands over the entire studied frequency interval, i.e., up to 562 Hz.

ID1c,g exhibited also reductions and amplifications in accelerance in different intervals up to the 1/3 octave band of 160 Hz. However ID1c showed reductions in accelerance continuously between the 1/3 octave band of 200–500 Hz, and ID1g between 400–500 Hz.

It is noteworthy that, in all partial 1 layer configurations, there was a typical amplification in accelerance at the 1/3 octave bands 31.5 Hz and reductions at 40 Hz. As described before, it is due to the lowering of the peak frequency in the 40 Hz band to the 1/3 octave band just before, which is the 31.5 Hz band.

10.1.1.3 1 layer summary

Considering the RMS–values, placing Sylodyn NF lamellae in longitudinal direction (ID1) showed a greater reduction in accelerance than placing them in transverse direction (ID2).

Considering the RMS–values, placing Sylodyn NF lamellae closer to the surface (ID1) showed greater reductions in accelerance compared to placing them closer to the center of the panel (ID3).

Exchanging spruce lamellae with Sylodyn NF closer to the edges (ID1c,g and ID2h,k) showed greater reductions in accelerance compared to placing Sylodyn NF closer to the center (ID1a,b and ID2b,e). This held true in both directions.

Moreover, considering RMS–values, full layer (ID1) appeared to exhibit a greater reductions in accelerance compared to its partial layers. However, the partial layers also displayed significant reductions in accelerance with lower volume ratios.

Even though the predicted accelerance was shown to be, for example, reduced by using an RMS–value, which is a single–value metric, the accelerance in specific 1/3 octave bands could be either amplified or reduced, respectively, in relation to the equivalent 1/3 octave bands for the reference panel.

10.1.2 2 layers

The 2 layer configurations deemed necessary to illustrate the results can be viewed in Figure 10.5, with corresponding ID:s.

The partial 2 layers configurations deemed necessary to illustrate the results can be seen in Figure 10.6.

For the full list of 2 layer Sylodyn NF configurations, see Appendix C.

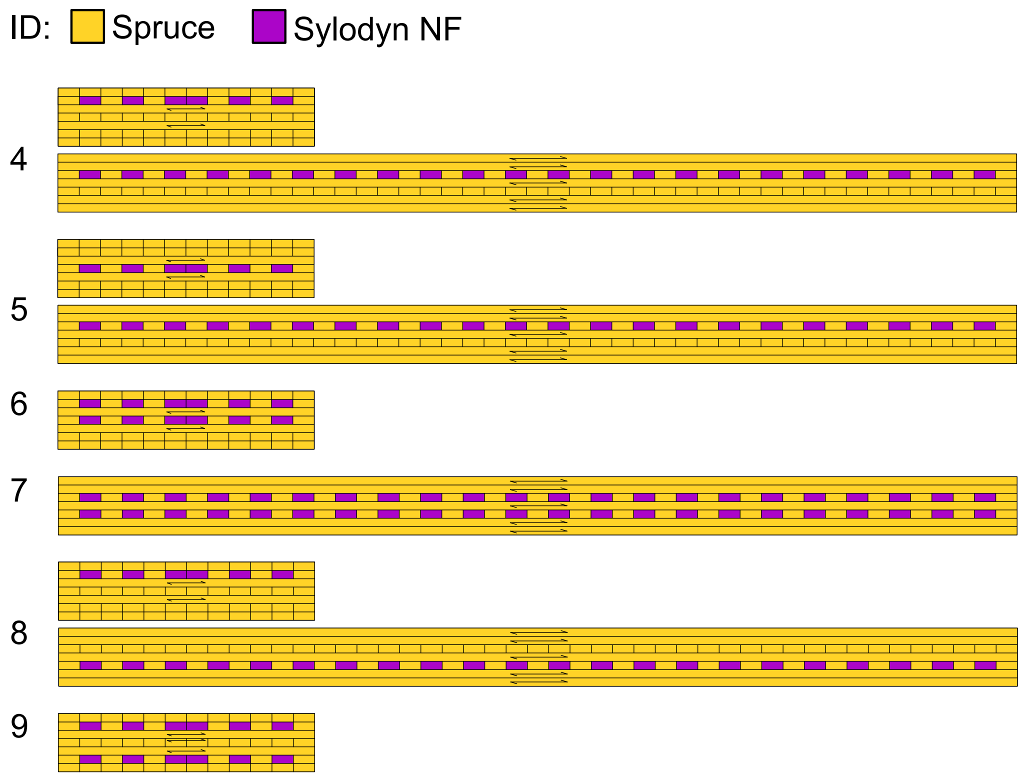

Figure 10.5: Sylodyn NF – the full layers configurations for the 2 layers analysis, with corresponding ID:s. In ID4–5,8 lamellae in both transverse and longitudinal direction are exchanged. In ID6,9 lamellae in longitudinal direction are exchanged, while in ID7 lamellae in transverse direction are exchanged.

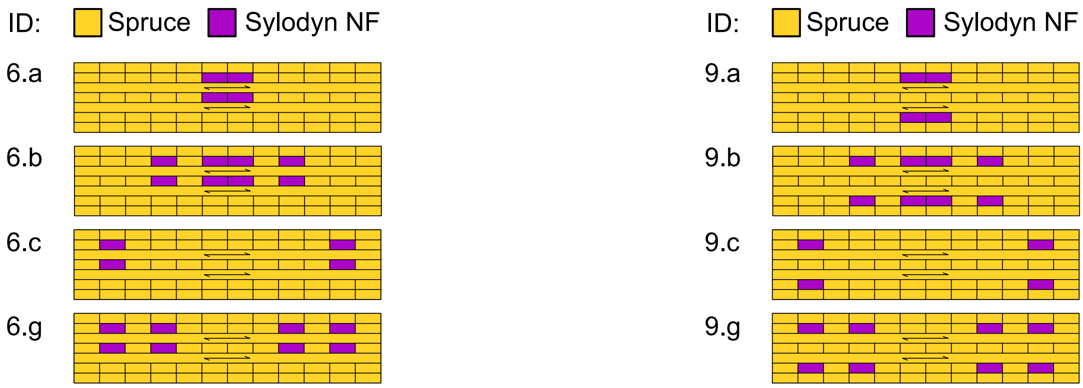

(a) Sylodyn NF – partial layer of ID6, with lamellae in longitudinal direction.

(b) Sylodyn NF – partial layer of ID9, with lamellae in longitudinal direction.

Figure 10.6: Sylodyn NF – the partial layer configurations for the 2 layer analysis, with corresponding ID:s.

10.1.2.1 Full layer

RMS–value
The effect on accelerance evaluated as RMS–value for ID4–9 can be seen in Table 10.3, where a negative change denotes a reduction in the level of vibration as compared to the reference level obtained by a panel composed entirely of spruce.

Table 10.3: Sylodyn NF – the change in RMS–value, compared to the reference level, and the volume ratio for configurations with ID4–9. Volume ratio indicates the percentage of Sylodyn NF in the panel.

ID	RMS [%]	Volume ratio [%]
4	–47	14
5	–27	14
6	–40	14
7	–7	14
8	–28	14
9	–43	14

The RMS–values for ID4–9 indicated significant reductions in accelerance. However, the reduction in accelerance of ID7 was smaller than in the other configurations.

When comparing ID7 to ID6 and ID9, placing Sylodyn NF lamellae in longitudinal direction showed a greater reduction in accelerance than placing them in transverse direction.

Comparing ID4 to ID5, placing Sylodyn NF lamellae closer to the surface (ID4) displayed a greater reduction in accelerance than placing them closer to the center of the panel (ID5). However, the difference in accelerance reduction between ID6 and 9 was not significant. Similarly, comparing RMS–values of ID8 to ID5, there also appeared to be no significant difference in accelerance between placing Sylodyn NF closer to the surfaces or closer to the center.

It appeared that the combinations of exchanging Sylodyn NF lamellae in both transverse direction and longitudinal direction provides significant reductions in accelerance (ID4,5, and 8). Moreover, ID4 showed greater reductions in accelerance than ID6 and ID9 (In ID6,9, Sylodyn NF lamellae in longitudinal direction are exchanged). Conversely, ID5 and ID8 showed less reductions in accelerance than ID6 and ID9.

1/3 octave band
The effect on accelerance evaluated in 1/3 octave bands for ID4–9 can be seen in Figure 10.7.

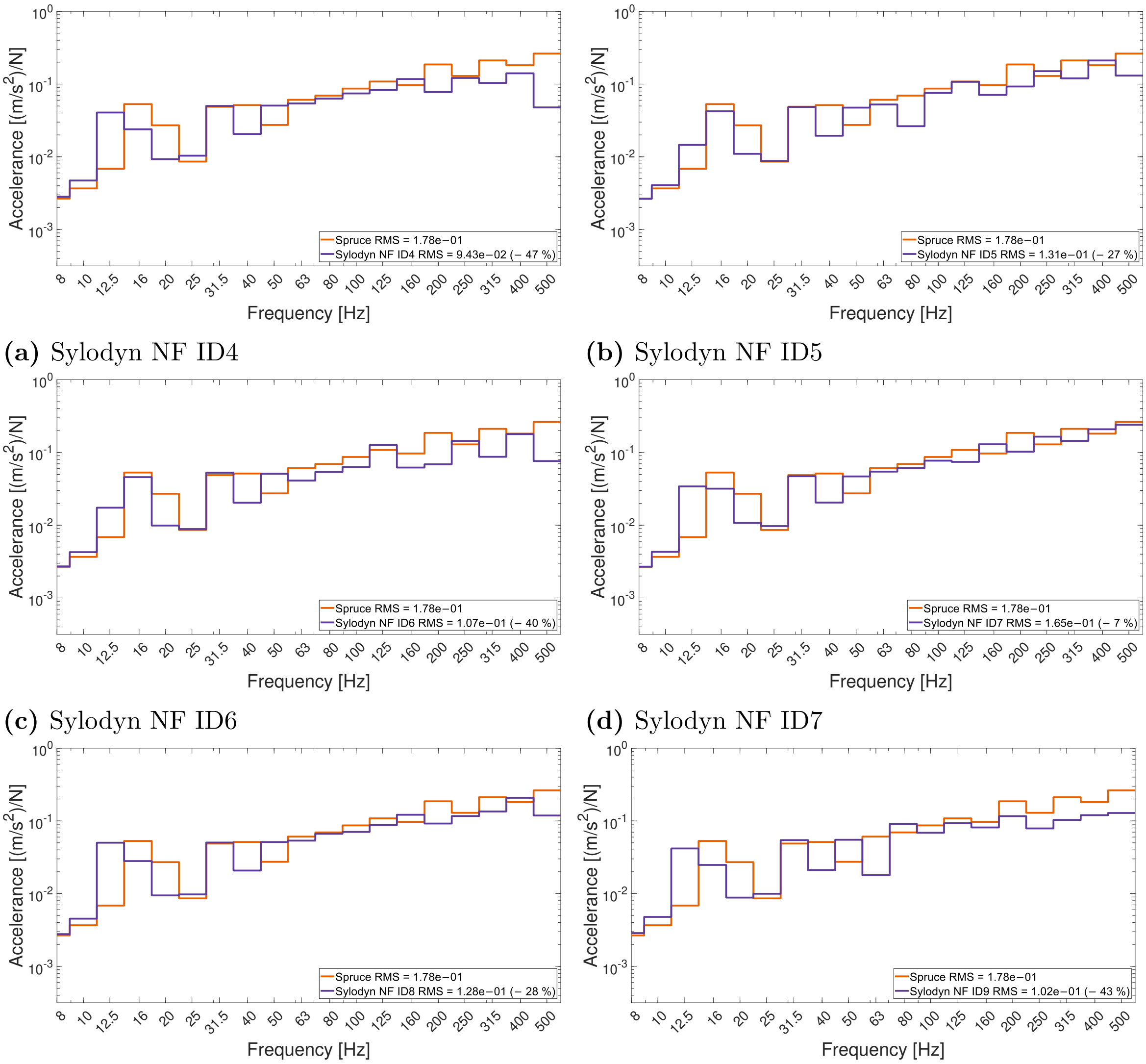

(a) Sylodyn NF ID4 **(b)** Sylodyn NF ID5

(c) Sylodyn NF ID6 **(d)** Sylodyn NF ID7

(e) Sylodyn NF ID8 **(f)** Sylodyn NF ID9

Figure 10.7: Sylodyn NF – the steady–state dynamic response of configuration ID4–9, in 1/3 octave bands. The value in legend within parentheses indicates the change in RMS–value compared to the reference level. The center frequency of 1/3 octave bands are shown in the horizontal axis.

The responses of ID4 indicated significant reductions in accelerance between the 1/3 octave bands 200 and 500 Hz, except band 250 Hz where no significant reduction in accelerance was noticed. Under 200 Hz, response of ID4 showed reductions in accelerance at certain 1/3 octave bands and amplifications in others.

The responses of ID5,7 and 8 exhibited reductions or amplifications in accelerance at different 1/3 octave bands over the entire studied frequency interval, i.e., up to 562 Hz.

The responses of ID6 provided significant reductions between the 1/3 octave bands of 63–100 Hz, and 160–200 Hz. Outside these intervals, ID6 showed reductions in accelerance at certain 1/3 octave bands and amplifications in others.

The responses of ID9 indicated significant reductions between the 1/3 octave bands of 100–500 Hz. Under the 1/3 octave band of 100 Hz, ID9 showed reductions and amplifications in vibration levels at different 1/3 octave bands.

10.1.2.2 Partial layer

RMS–value

The effect on accelerance evaluated as RMS–value for the partial layer configurations of ID6 and ID9 can be seen in Table 10.4, where a negative change denotes a reduction in the level of vibration as compared to the reference level obtained by a panel composed entirely of spruce.

Table 10.4: Sylodyn NF – the change in RMS–value, compared to the reference level, and the volume ratio for the partial layer configurations of ID6 and 9. Volume ratio indicates the percentage of Sylodyn NF in the panel.

ID	RMS [%]	Volume ratio [%]
6a	–24	5
6b	–11	10
6c	–26	5
6g	–40	10
9a	–18	5
9b	–14	10
9c	–21	5
9g	–36	10

The RMS–values of all the partial layer configurations of ID6 and ID9 exhibited significant reductions in accelerance.

Comparing ID6b to ID6g as well as ID9b to ID9g, exchanging spruce lamellae with Sylodyn NF closer to the edges showed greater reductions in accelerance than placing Sylodyn NF lamellae closer to the center of the panel.

However, comparing ID6a to ID6c as well as ID9a to ID9c, the RMS–values showed no significant different in accelerance reductions. It indicated exchanging spruce lamellae with Sylodyn NF lamellae closer to the edges do not show difference in accelerance than placing Sylodyn NF lamellae closer to the center of the panel.

1/3 octave band

The effect on accelerance evaluated in 1/3 octave bands for the partial layer configurations of ID6 and ID9 can be seen in Figure 10.8.

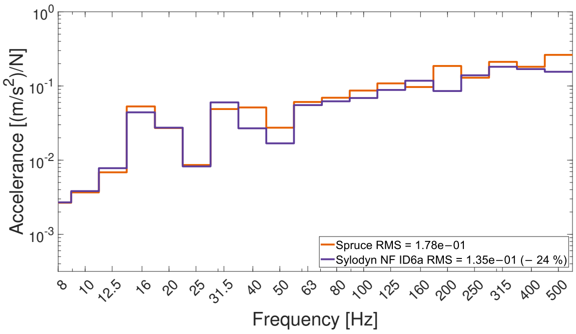

(a) Sylodyn NF ID6a

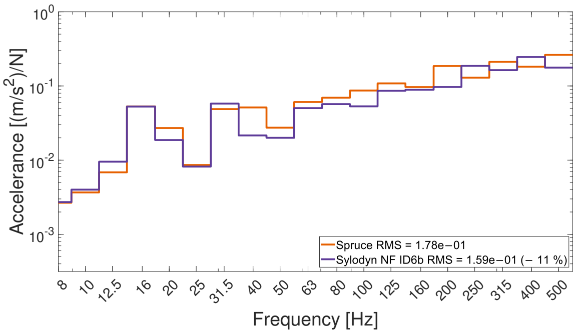

(b) Sylodyn NF ID6b

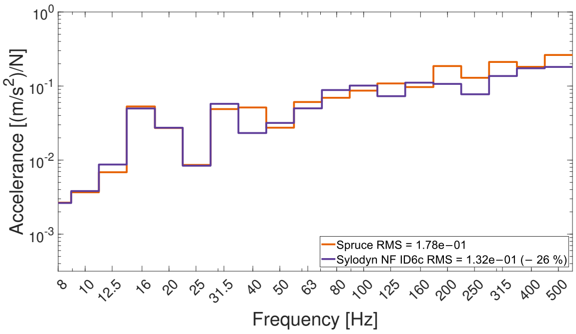

(c) Sylodyn NF ID6c

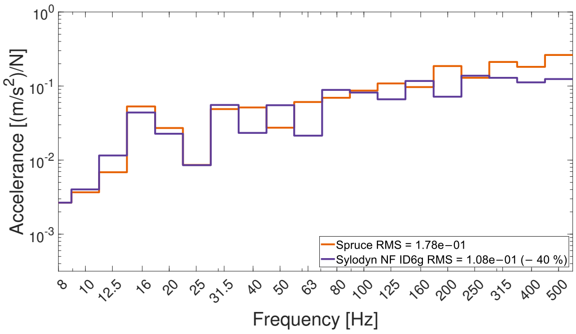

(d) Sylodyn NF ID6g

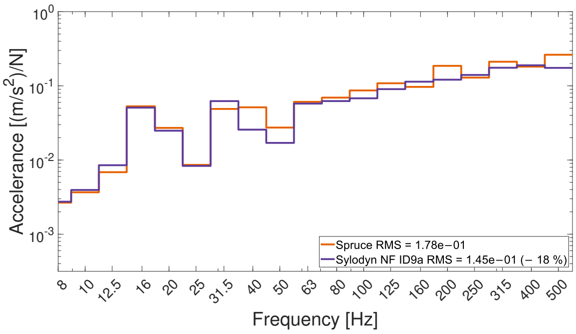

(e) Sylodyn NF ID9a

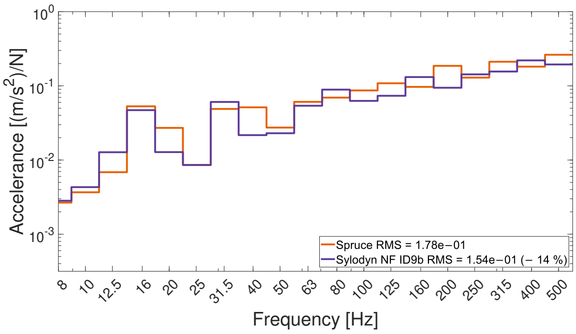

(f) Sylodyn NF ID9b

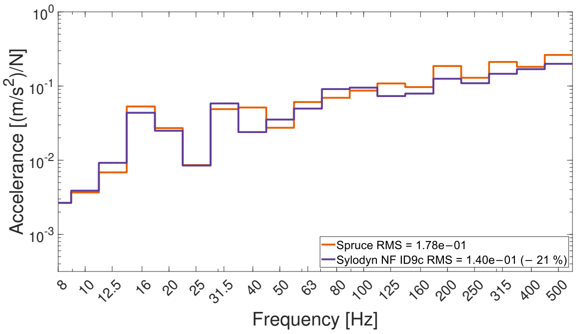

(g) Sylodyn NF ID9c

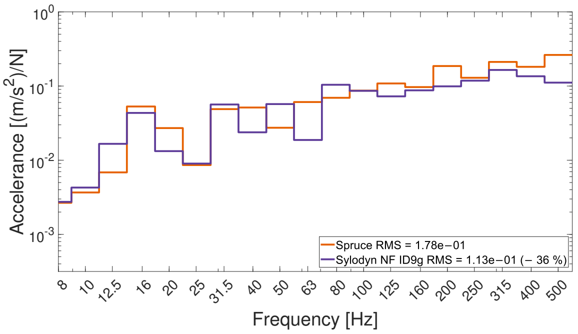

(h) Sylodyn NF ID9g

Figure 10.8: The steady–state dynamic response for partial configurations of ID6 and ID9 in 1/3 octave bands. The value in legend within parentheses indicates the change in RMS–value compared to the reference level. The center frequency of 1/3 octave bands are shown in the horizontal axis.

The configurations ID6a,b and ID9a,b showed reductions or amplifications in accelerance at different 1/3 octave bands over the entire studied frequency interval, i.e., up to 562 Hz.

In ID6c, notable reductions in accelerance were observed continuously between the 1/3 octave bands of 200–315 Hz, and for ID6g between 315–500 Hz. Outside these intervals, ID6c,g showed reductions in accelerance at certain 1/3 octave bands and amplifications in others.

In ID9c, notable reductions in accelerance were observed continuously between the 1/3 octave bands of 125–315 Hz, and for ID9g between 125–500 Hz. Outside these intervals, ID9c,g showed reductions in accelerance at certain 1/3 octave bands and amplifications in others.

It is notable that all configurations of 2 layers showed an amplification in accelerance at the center frequency of 31.5 Hz and significant reductions in accelerance at 40 Hz. It is due to the lowering of the peak frequency in the 40 Hz band to the 1/3 octave band just before, which is the 31.5 Hz band.

10.1.2.3 2 layers summary

Considering the RMS–values, placing Sylodyn NF lamellae in longitudinal direction (ID6 and ID9) showed greater reductions in accelerance than placing them in transverse direction (ID7).

It appeared that significant reductions in accelerance (ID4,5,8) were achieved by combining a full layer in the transverse direction with a full layer in the longitudinal direction. However, there was one combination (ID4) that showed greater reductions in accelerance than configurations with only longitudinal lamellae are exchanged (ID6 and ID9). In contrast, other combinations (ID5 and ID8) showed less reductions in accelerance than configurations with only longitudinal lamellae are exchanged (ID6 and ID9)

On the one hand, placing Sylodyn NF closer to the surface (ID4) resulted in a greater reduction in accelerance than placing it in the center of the panel (ID5). On the other hand, there were configurations (ID6 vs. ID9, as well as ID8 vs. ID5) that showed insignificant differences in accelerance reductions, regardless of placement.

Considering RMS–values of the partial configurations of 2 layers, exchanging spruce lamellae with Sylodyn NF closer to the edges (ID6g and ID9g) showed greater reductions in accelerance compared to placing Sylodyn NF closer to the center (ID6b and ID9b).

Moreover, full layers (ID6 and ID9) appeared to exhibit greater reductions in accelerance compared to their respective partial layers. However, the partial layers also displayed significant reductions in accelerance with lower volume ratios.

Even though the predicted accelerance was shown to be, for example, reduced by using an RMS–value, which is a single–value metric, the accelerance in specific 1/3 octave bands could be either amplified or reduced, respectively, in relation to the equivalent 1/3 octave bands for the reference panel.

10.1.3 3 layers

The 3 layer configurations deemed necessary to illustrate the results can be viewed in Figure 10.9, with corresponding ID:s.

The partial 3 layers configurations deemed necessary to illustrate the results can be seen in Figure 10.10.

For the full list of 3 layer Sylodyn NF configurations, see Appendix C.

It is important to note that these configurations are not directly comparable for the purpose of finding potential trends in the dynamic behavior of the panel. This is due to the fact that they do not have the same number of layers in each direction. However, configurations ID10–12 were still considered as they could provide further insights into the structural behavior of the panel.

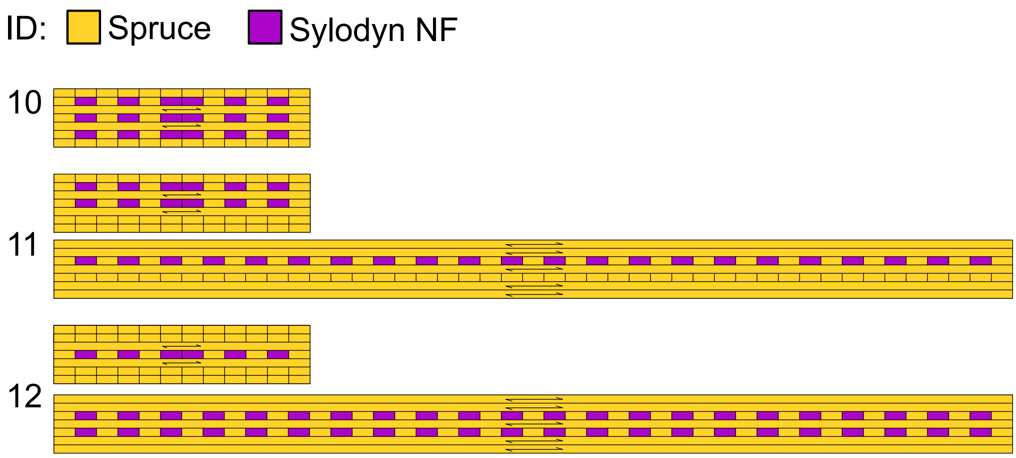

Figure 10.9: Sylodyn NF – the full layers configurations for the 3 layers analysis, with corresponding ID:s. ID10 exchanges lamellae in longitudinal direction and ID11–12 in both transverse and longitudinal direction.

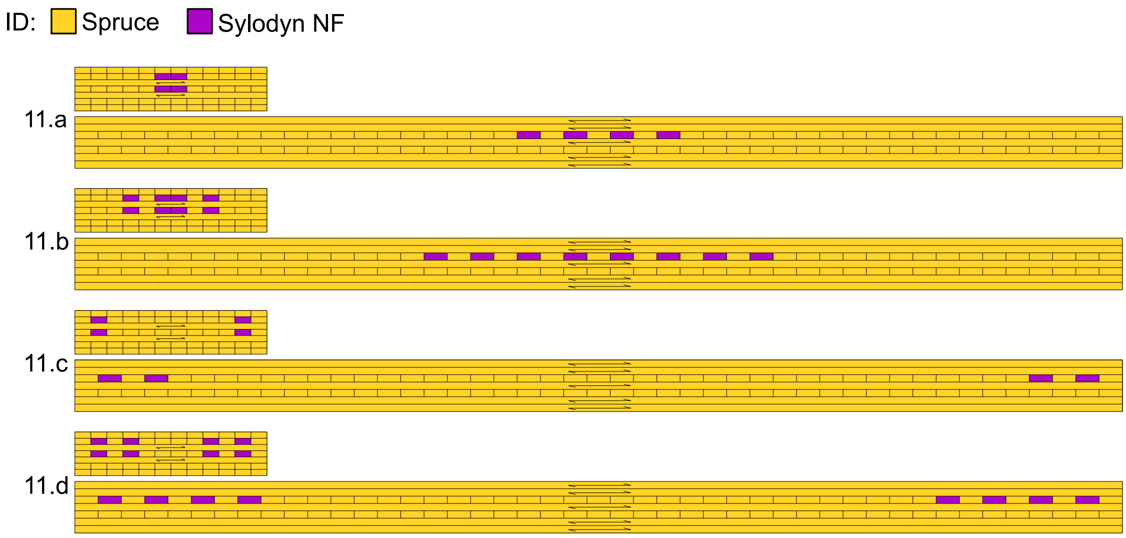

Figure 10.10: Sylodyn NF – the partial layer configurations for the 3 layers analysis, with lamellae in longitudinal– (upper image of each ID:s) and transverse (lower image of each ID:s) direction.

10.1.3.1 Full layer

RMS–value

The effect on accelerance evaluated as RMS–value for ID10–12 can be seen in Table 10.5, where a negative change denotes a reduction in the level of vibration as compared to the reference level obtained by a panel composed entirely of spruce.

Table 10.5: Sylodyn NF – the change in RMS–value, compared to the reference level, and the volume ratio for configurations with ID10–12. Volume ratio indicates the percentage of Sylodyn NF in the panel.

ID	RMS [%]	Volume ratio [%]
10	–45	21
11	–65	21
12	–51	21

The RMS–values of ID10–12 showed significant reductions in accelerance.

Comparing RMS–values, ID12 showed a greater reduction in accelerance compared to ID10.

The RMS–values of ID11 and ID12 indicated significant reductions in accelerance for combinations of full layers in transverse direction with full layers in longitudinal direction. However, ID11 displayed a greater reduction than ID12.

The RMS–values of configurations ID11 and 12 showed greater reductions in accelerance than ID10. It seemed that combining 3 layers in different directions provided greater reductions in accelerance compared to three full layers in longitudinal direction.

1/3 octave band

The effect on accelerance evaluated in 1/3 octave bands for ID10–12 can be seen in Figure 10.11.

The responses of ID10–12 indicated significant reductions in accelerance continuously from the 1/3 octave bands of 63–500 Hz, except band 125 Hz where the reductions in accelerance is insignificant.

Under the 1/3 octave band of 63 Hz, configurations ID10–12 exhibited reductions in accelerance at certain 1/3 octave bands and amplifications in others.

Combinations of Sylodyn NF lamellae in different directions (ID11 and 12) displayed greater reductions in accelerance compared to ID10 at the 1/3 octave bands of 400 Hz and 500 Hz.

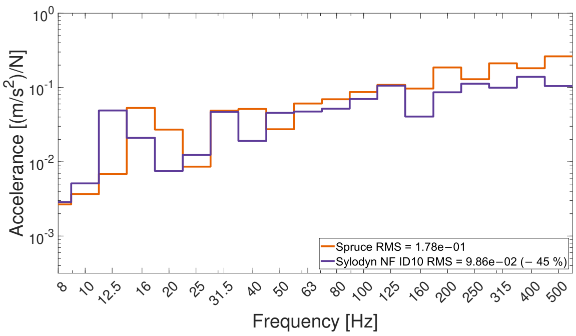

(a) Sylodyn NF ID10

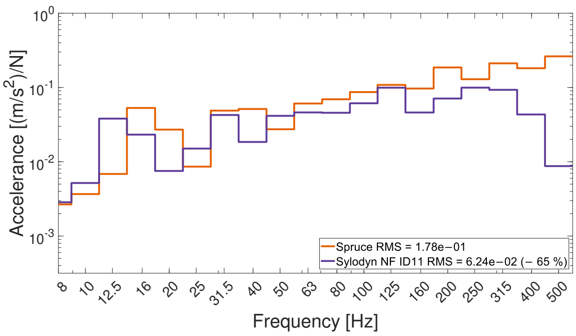

(b) Sylodyn NF ID11

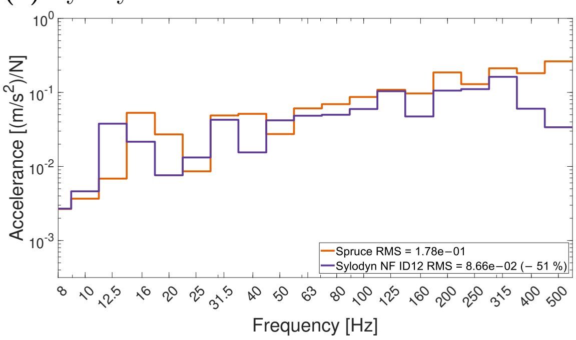

(c) Sylodyn NF ID12

Figure 10.11: Sylodyn NF – the steady–state dynamic response of configuration ID10–12, in 1/3 octave bands. The value in legend within parentheses indicates the change in RMS–value compared to the reference level. The center frequency of 1/3 octave bands are shown in the horizontal axis.

10.1.3.2 Partial layers

RMS–value
The effect on accelerance evaluated as RMS–value for the partial layer configurations of ID11 can be seen in Table 10.6, where a negative change denotes a reduction in the level of vibration as compared to the reference level obtained by a panel composed entirely of spruce.

Table 10.6: Sylodyn NF – the change in RMS–value, compared to the reference level, and the volume ratio for the partial layer configurations of ID11. Volume ratio indicates the percentage of Sylodyn NF in the panel.

ID	RMS [%]	Volume ratio [%]
11a	–29	6
11b	–34	12
11c	–35	6
11d	–46	12

The RMS–values for all partial layer configurations of ID11 demonstrated notable reductions in accelerance. However, the accelerance reductions displayed in ID11c,d were greater that in ID11a,b. It appeared that placing Sylodyn NF lamellae closer to the edges of the panel provided greater reductions in accelerance than placing them closer to the center (in both directions).

1/3 octave band
The effect on accelerance evaluated in 1/3 octave bands for the partial layer configurations of ID11 can be seen in Figure 10.12.

ID11a displayed reductions in accelerance between the 1/3 octave bands of 40–125 Hz. While ID11b showed significant reductions from 63–100 Hz and 315 – 500 Hz. Outside these intervals, ID11a,b showed reductions in accelerance at certain 1/3 octave bands and amplifications in others.

ID11c showed reductions in accelerance between the 1/3 octave band 125–500 Hz except band 160 Hz and 400 Hz where the differences in accelerance were insignificant. Moreover, ID11d showed significant reductions in accelerance from the 1/3 octave band of 63 Hz up to 500 Hz, except band 160 Hz and 250 Hz, where the differences in accelerance were insignificant. Outside these intervals, ID11c,g showed reductions in accelerance at certain 1/3 octave bands and amplifications in others.

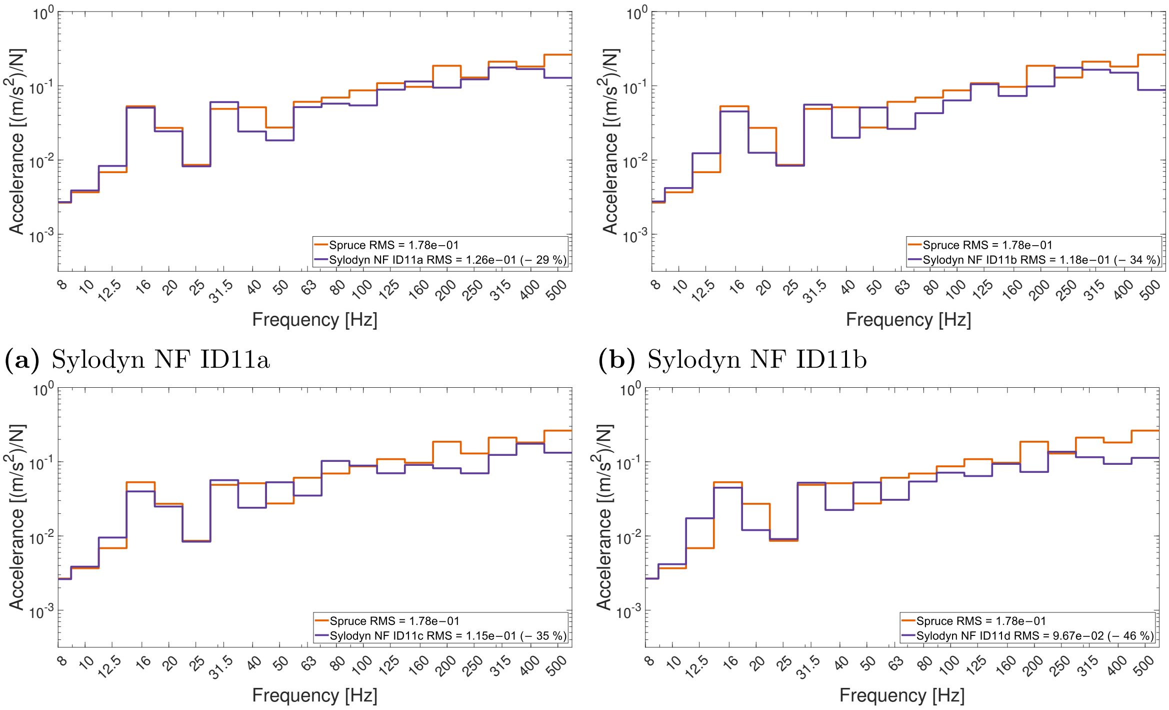

(a) Sylodyn NF ID11a **(b)** Sylodyn NF ID11b

(c) Sylodyn NF ID11c **(d)** Sylodyn NF ID11d

Figure 10.12: The steady–state dynamic response for partial configurations of ID9 in 1/3 octave bands. The value in legend within parentheses indicates the change in RMS–value compared to the reference level. The center frequency of 1/3 octave bands are shown in the horizontal axis.

10.1.3.3 3 layers summary

The most common frequency range with accelerance reductions in three full layer configurations was between the 1/3 octave band 160 and 500 Hz.

Considering the RMS–values, it appeared that combinations of Sylodyn NF layers in different directions provides significant reductions in accelerance. This was valid for both full layer and partial layer configurations (ID11 and ID12).

The reductions in accelerance were greater with Sylodyn NF lamellae placed closer to the edges of the panel (ID11c,d) compared to those placed closer to the center (ID11a,b) in both directions.

Moreover, considering RMS–values, full layer (ID11) appeared to exhibit greater a reduction in accelerance compared to its partial layers. However, the partial layers also displayed significant reductions in accelerance with lower volume ratios.

Even though the predicted accelerance was shown to be, for example, reduced by using an RMS–value, which is a single–value metric, the accelerance in specific 1/3 octave bands could be either amplified or reduced, respectively, in relation to the equivalent 1/3 octave bands for the reference panel.

10.1.4 Large sized panel summary

The impact of exchanging lamellae from spruce to Sylodyn NF in the L–sized panel are consolidated in this section.

- There were configurations which showed that placing Sylodyn NF closer to the surface (ID1,ID4) provided larger reductions in accelerance than placing them closer to the center of the panel (ID3, ID5). However, there were configurations which showed comparisons between ID6 and ID9, as well as ID8 to ID5, showed no significant differences in accelerance reductions, regardless of placement closer to the surfaces or closer to the center of the panel (ID6 compared to ID9, as well as ID5 compared to ID8)

- Placing Sylodyn NF lamellae in the longitudinal direction showed greater reductions in accelerance than placing them in the transverse direction (ID1,3 compared to ID2 and ID6,9 compared to ID7).

- Combinations of Sylodyn NF lamellae in different directions (ID4, ID5, ID8, ID11, and ID12) showed significant reductions in accelerance. However, these combinations provided both larger and less reductions compared to placing the same number of layers solely in the longitudinal direction.

- In partial layers, the reductions in accelerance were greater with Sylodyn NF lamellae placed closer to the edges of the panel (ID1c,g, ID6g, ID9g and ID11c,d) compared to those placed closer to the center (ID1a,b, ID6b, ID9b and ID11a,b). This held true in both directions.

- Considering RMS–values, full layers (ID1,6,9,11) appeared to exhibit greater reductions in accelerance compared to their respective partial layers. Apart from one configuration exchanging Sylodyn NF lamellae in transverse direction (ID2), which showed no difference in accelerance, while its partial configurations displayed reductions in accelerance. Generally, partial layer configurations also displayed significant reductions in accelerance with lower volume ratios compared to their respective full layer.

- Even though the predicted accelerance was shown to be, for example, reduced by using an RMS–value, which is a single–value metric, the accelerance in specific 1/3 octave bands could be either amplified or reduced, respectively, in relation to the equivalent 1/3 octave bands for the reference panel.

10.2 Medium size panel

1 layer

The investigation whether the dimensions and/or lay–ups of the panels influence the results are presented here.

The configurations analyzed can be viewed in Figure 10.13.

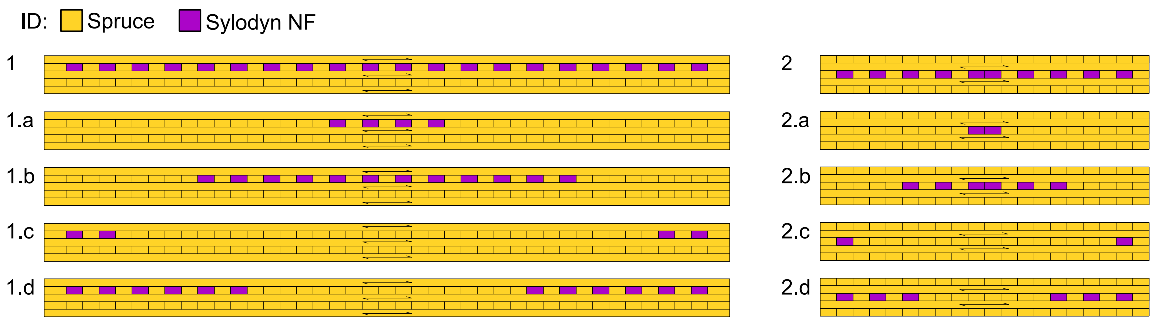

Figure 10.13: Sylodyn NF – Illustration of the analyzed configurations, performed on the M–sized panel.

The effect on accelerance evaluated as RMS–value for these configurations can be seen in Table 10.7, where a negative change denotes a reduction in the level of vibration as compared to the reference level obtained by a panel comprised entirety of spruce.

The effect on accelerance evaluated in 1/3 octave bands for these configurations can be seen in Figure 10.14.

Table 10.7: The change in RMS–value, compared to the reference level, and the volume ratio for configurations visualized in Figure 10.14. Volume ratio indicates the percentage of Sylodyn NF in the panel.

ID	RMS [%]	Volume ratio [%]
1	–20	10
2	–23	10
1a	–7	2
1b	–13	6
1c	–19	2
1d	–24	6
2a	–14	2
2b	–12	6
2c	–20	2
2d	–23	6

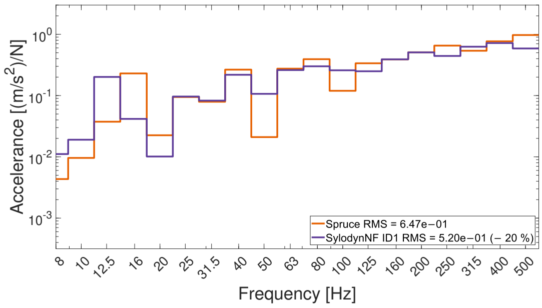

(a) Sylodyn NF M–sized panel ID1

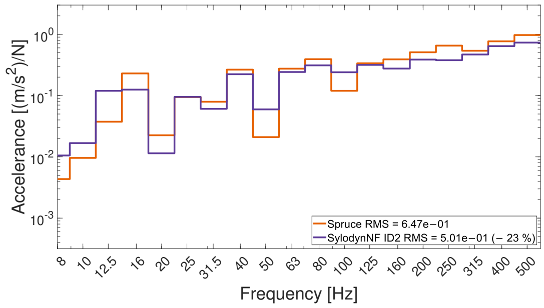

(b) Sylodyn NF M–sized panel ID2

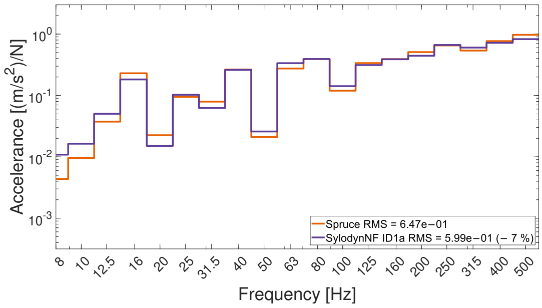

(c) Sylodyn NF M–sized panel ID1a

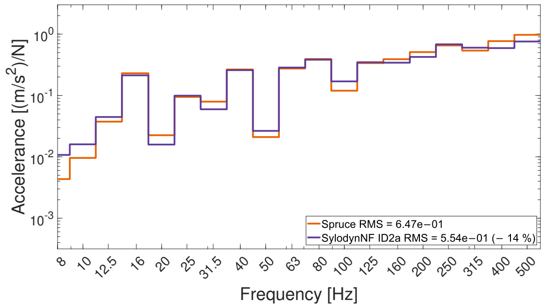

(d) Sylodyn NF M–sized panel ID2a

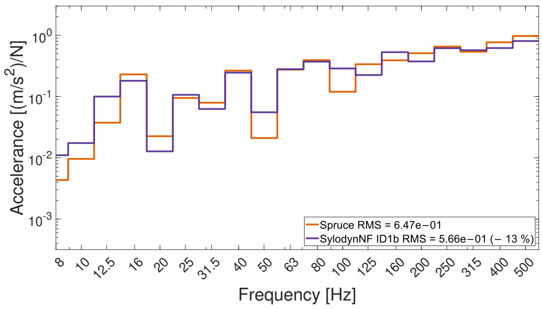

(e) Sylodyn NF M–sized panel ID1b

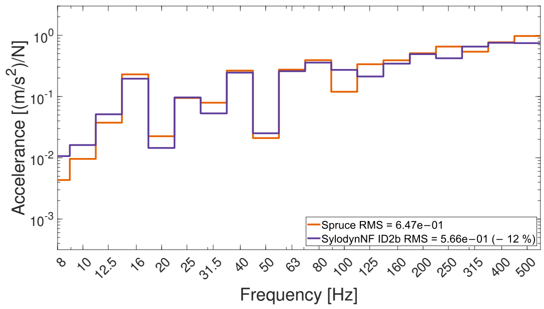

(f) Sylodyn NF M–sized panel ID2b

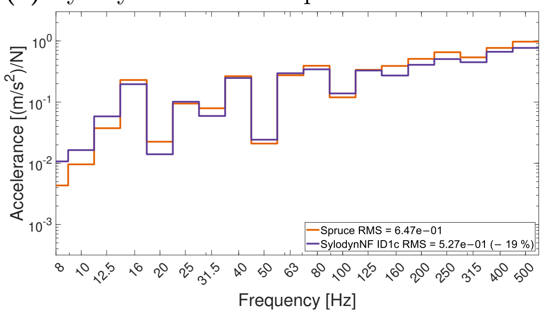

(g) Sylodyn NF M–sized panel ID1c

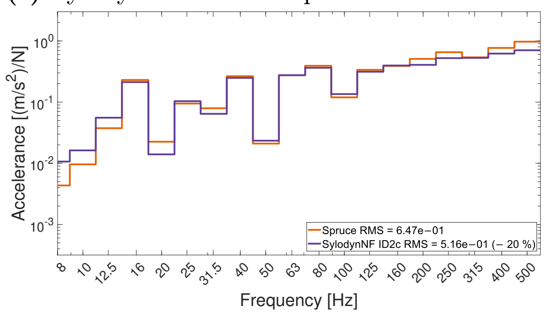

(h) Sylodyn NF M–sized panel ID2c

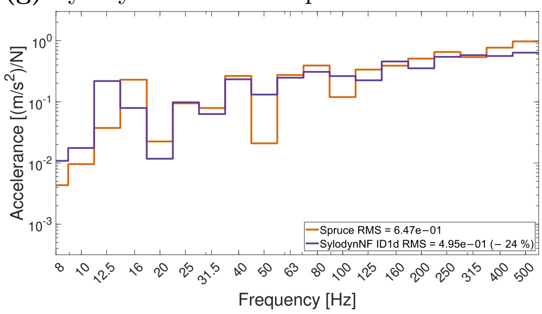

(i) Sylodyn NF M–sized panel ID1d

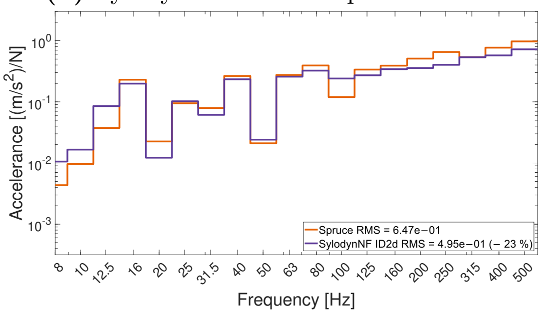

(j) Sylodyn NF M–sized panel ID2d

Figure 10.14: Sylodyn NF – The steady–state dynamic response in 1/3 octave bands for configurations illustrated in Figure 10.13. The value in legend within parentheses indicates the change in RMS–value compared to the reference level. The center frequency of 1/3 octave bands are shown in the horizontal axis.

The RMS–values for the M–sized panel indicated no significant difference in accelerance when comparing full layers of Sylodyn NF in longitudinal direction (ID2) compared to transverse direction (ID1).

The response of ID1 showed reductions or amplifications in accelerance at different 1/3 octave bands over the entire studied frequency interval, i.e., up to 562 Hz.

The response of ID2 showed significant reductions in accelerance continuously between the 1/3 octave bands of 160–500 Hz. Under 125 Hz, ID2 showed reductions in accelerance at certain 1/3 octave bands and amplifications in others.

Considering RMS–values, a greater reduction in accelerance appeared to be achieved by placing Sylodyn NF closer to the edges (ID1c,d and ID2c,d) rather than closer to placing them closer to the center of the panel (ID1a,b and ID2a,b).

The configurations ID1a,b and ID2a,b showed reductions or amplifications in accelerance at different 1/3 octave bands over the entire studied frequency interval, i.e., up to 562 Hz.

The response of ID1c showed significant reductions continuously between the 1/3 octave bands of 160–500 Hz. The response of ID1d and ID2c,d displayed significant reductions continuously between the 1/3 octave bands of 200–250 Hz, and also 400–500 Hz. Outside these intervals, ID1c,d and ID2,d showed reductions in accelerance at certain 1/3 octave bands and amplifications in others.

Considering RMS–values, the partial layers (ID1a–d and ID2a–d) displayed significant reductions in accelerance with lower volume ratios compared to their respective full layers.

Even though the predicted accelerance was shown to be, for example, reduced by using an RMS–value, which is a single–value metric, the accelerance in specific 1/3 octave bands could be either amplified or reduced, respectively, in relation to the equivalent 1/3 octave bands for the reference panel.

It is important to note that the lay–up of the M–sized panel with 5 layers would mean unreasonable placement of Sylodyn NF in the top layer. Therefore, the trend of placing Sylodyn NF closer to surfaces could not be analyzed and verified.

11 Impact of soft elastomer lamellae

In this chapter, the impact of exchanging lamellae from spruce to elastomer Sylodyn NB, is presented. To be clear, it is not precisely Sylodyn NB that has been modeled, but rather a close replicate of a soft elastomer.

The terms "full layer/full layers" will be used in this section. However, the term will not refer to exchanging the actual full layer/layers, but instead every other lamellae. This approach ensured practical relevance.

11.1 Large sized panel

11.1.1 1 layer

The 1 layer configurations deemed necessary to illustrate the results can be viewed in Figure 11.1, with corresponding ID:s.

The partial 1 layer configurations deemed necessary to illustrate the results can be seen in Figure 11.2.

For the full list of 1 layer Sylodyn NB configurations, see Appendix D.

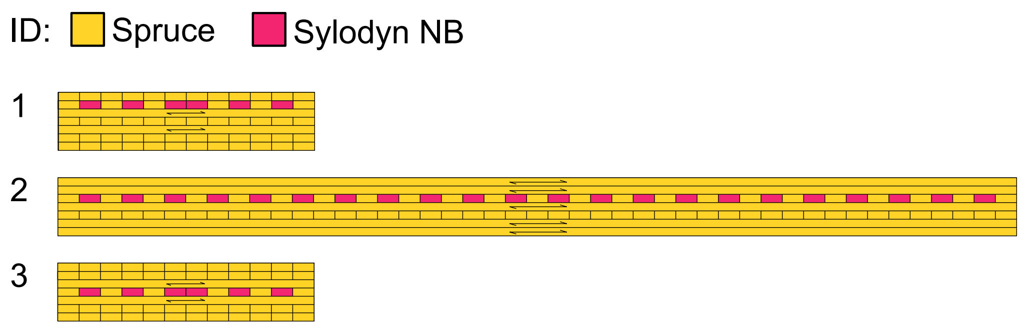

Figure 11.1: Sylodyn NB – the full layer configurations for the 1 layer analysis, with corresponding ID:s. In ID1,3 lamellae in longitudinal direction are exchanged, while in ID2 lamellae in transverse direction are exchanged.

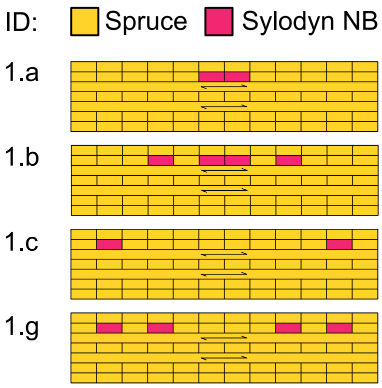

(a) Sylodyn NB – partial layers of ID1, with lamellae in longitudinal direction.

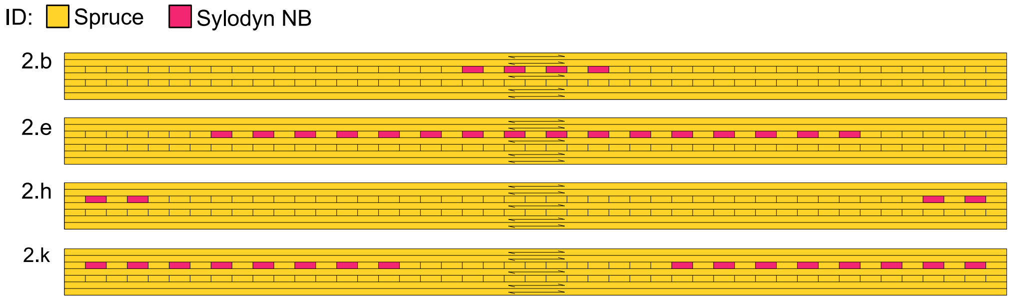

(b) Sylodyn NB – partial layers of ID2, with lamellae in transverse direction.

Figure 11.2: Sylodyn NB – the partial layers configurations for the 1 layer analysis, with corresponding ID:s.

11.1.1.1 Full layer

RMS–value

The effect on accelerance evaluated as RMS–value for ID1–3 can be seen in Table 11.1, where a negative change denotes a reduction in the level of vibration as compared to the reference level obtained by a panel composed entirely of spruce.

Table 11.1: Sylodyn NB – the change in RMS–value, compared to reference level, and the volume ratio for configurations with ID1–3. Volume ratio indicates the percentage of Sylodyn NB in the panel.

ID	RMS [%]	Volume ratio [%]
1	–41	7
2	+8	7
3	–3	7

The RMS–values of ID1 exhibited a notable reduction in accelerance compared the reference level. The RMS–values of ID2 showed an amplification in accelerance while ID3 showed insignificant change in accelerance.

Comparing configuration ID1 to ID3, it appeared that placing Sylodyn NB lamellae closer to the surface (ID1) resulted in a greater reduction in accelerance compared to placing them closer to the center (ID3)

Comparing ID2 to ID1 and ID3, placing Sylodyn NB lamellae in longitudinal direction showed greater reductions in accelerance than placing them in transverse direction.

1/3 octave band

The effect on accelerance evaluated in 1/3 octave bands for ID1–3 can be seen in Figure 11.3.

The response of ID1 showed significant reductions in accelerance between the 1/3 octave band of 200–500 Hz. From the 1/3 octave band of 160 Hz and downwards, ID1 showed reductions in accelerance at certain 1/3 octave bands and amplifications in others.

The response of ID2 showed reductions or amplifications in accelerance at different 1/3 octave bands over the entire studied frequency interval, i.e., up to 562 Hz.

The response of ID3 showed significant reductions in accelerance between the 1/3 octave band of 40–125 Hz. Outside this interval, ID3 showed reductions in accelerance at certain 1/3 octave bands and amplifications in others.

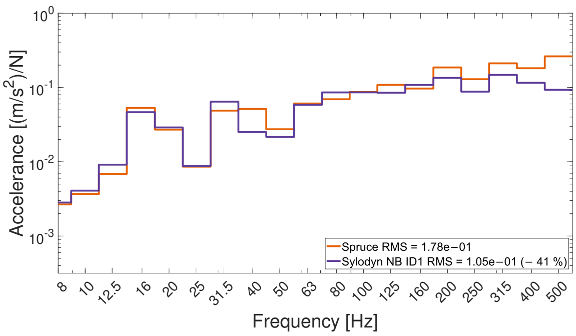

(a) Sylodyn NB ID1

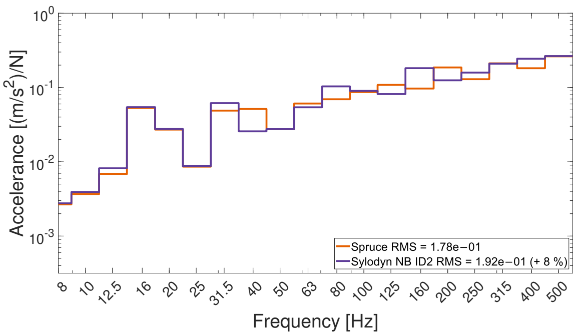

(b) Sylodyn NB ID2

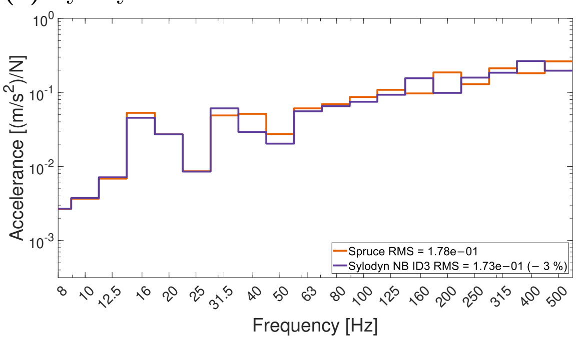

(c) Sylodyn NB ID3

Figure 11.3: Sylodyn NB – the steady–state dynamic response of configuration ID1–3, in 1/3 octave bands. The value in legend within parentheses indicates the change in RMS–value compared to reference level. The center frequency of 1/3 octave bands are shown in the horizontal axis.

It is notable that all configurations of the 1 layer configurations showed amplification in accelerance at the 1/3 octave band of 31.5 Hz and significant reductions at 40 Hz. It is due to the lowering of the peak frequency in the 40 Hz band to the 1/3 octave band just before, which is the 31.5 Hz band.

11.1.1.2 Partial layer

RMS–value

The effect on accelerance evaluated as RMS–value for the partial layer configurations of ID1–2 can be seen in Table 11.2, where a negative change denotes a reduction in the level of vibration as compared to the reference level obtained by a panel composed entirely of spruce.

Table 11.2: Sylodyn NB – the change in RMS–value, compared to reference level, and the volume ratio for the partial layer configurations of ID1–2. Volume ratio indicates the percentage of Sylodyn NB in the panel.

ID	RMS [%]	Volume ratio [%]
1a	–25	2
1b	–25	5
1c	–14	2
1g	–21	5
2b	+1	1
2e	+10	5
2h	–2	1
2k	–2	5

The RMS–values for the partial layer configurations of ID1 exhibited significant reductions in accelerance for ID1a–g. Among them, ID1a showed a greater reduction in accelerance than ID1c. It appeared that, up to certain limits, it is more advantageous to place Sylodyn NB lamellae closer to the center of the panel (ID1a) rather than closer to the edges (ID1c).

Comparing ID1b to ID1g, no significant difference in accelerance was observed between them.

The most partial layer configurations of ID2 showed insignificant change in accelerance except for ID2e, which exhibited an amplification in accelerance.

Comparing the RMS–values for the partial layer configurations of ID1 and ID2, placing Sylodyn NB lamellae in longitudinal direction showed a greater reduction in accelerance than placing them in transverse direction.

1/3 octave band

The effect on accelerance evaluated in 1/3 octave bands for the partial layer configurations of ID1–2 can be seen in Figure 11.4.

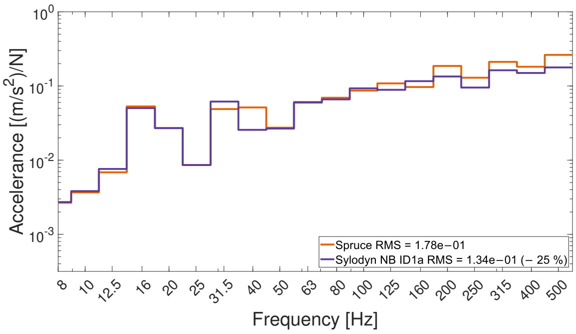

(a) Sylodyn NB ID1a

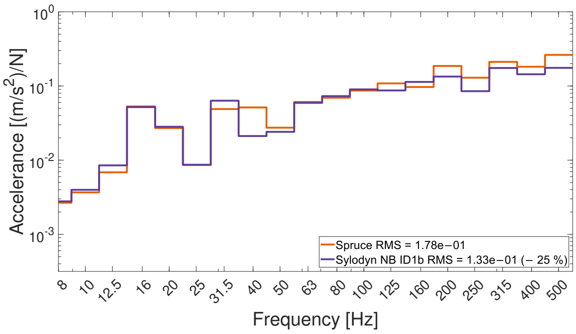

(b) Sylodyn NB ID1b

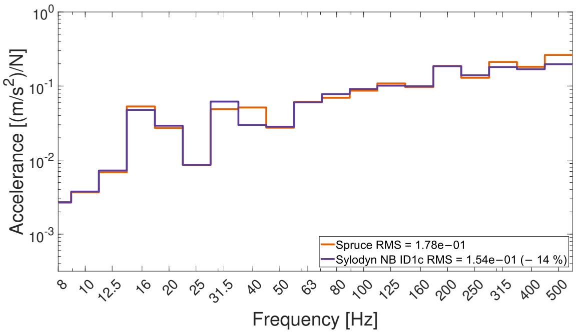

(c) Sylodyn NB ID1c

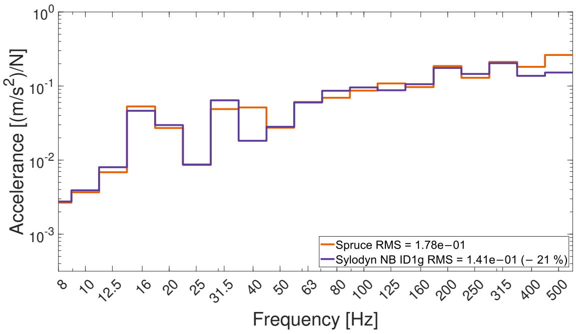

(d) Sylodyn NB ID1g

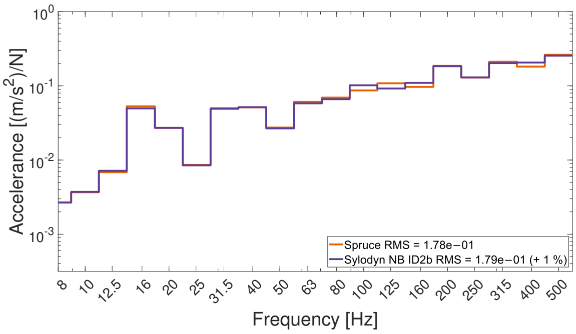

(e) Sylodyn NB ID2b

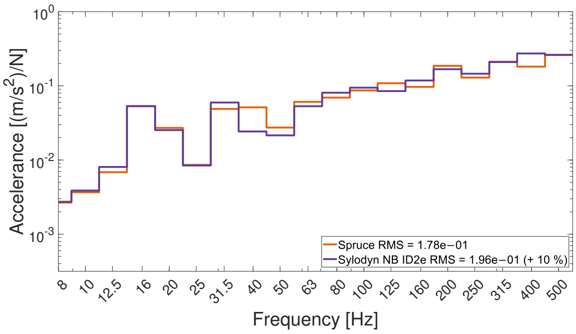

(f) Sylodyn NB ID2e

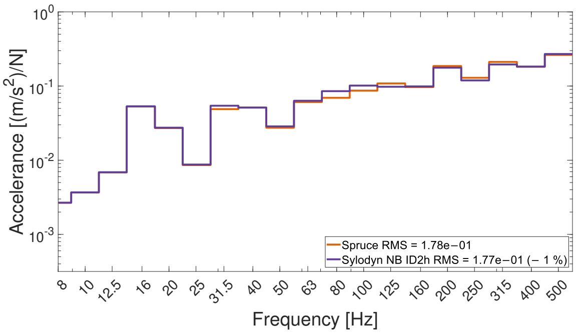

(g) Sylodyn NB ID2h

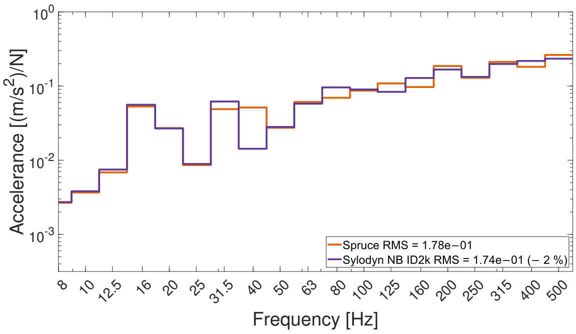

(h) Sylodyn NB ID2k

Figure 11.4: The steady–state dynamic response for partial configurations of ID1–2, in 1/3 octave bands. The value in legend within parentheses indicates the change in RMS–value compared to reference level. The center frequency of 1/3 octave bands are shown in the horizontal axis.

The response of ID1a,b showed significant reductions in accelerance between the 1/3 octave band of 200–500 Hz. From the 1/3 octave band of 160 Hz and downwards, ID1a,b showed reductions in accelerance at certain 1/3 octave bands and amplifications in others.

The response of ID2b–k showed reductions or amplifications in accelerance at different 1/3 octave bands over the entire studied frequency interval, i.e., up to 562 Hz.

The response of ID1c showed significant reductions in accelerance between the 1/3 octave band of 315–500 Hz, and for ID1g between 400–500 Hz. Outside these intervals, ID1c,g showed reductions in accelerance at certain 1/3 octave bands and amplifications in others.

11.1.1.3 1 layer summary

Significant reductions was observed continuously between the 1/3 octave band of 200–500 Hz, (ID1 and ID1a,b).

Considering the RMS–values, placing Sylodyn NB lamellae in longitudinal direction (ID1 and ID3) showed a greater reduction in accelerance than placing them in transverse direction.

Considering the RMS–values, placing Sylodyn NB lamellae closer to the surface (ID1) showed a greater reduction in accelerance compared to placing them closer to the center of the panel (ID3).

Concerning partial layer configurations, exchanging spruce lamellae with Sylodyn NB closer to the center (ID1a,b) showed greater reductions in accelerance compared to placing Sylodyn NB closer to the edges (ID1c,g). This held true in longitudinal direction.

Moreover, considering RMS–values, full layer (ID1) appeared to exhibit a greater reduction in accelerance compared to its respective partial layers (see Table 11.1 and Table 11.2). However, the partial layers also displayed significant reductions in accelerance with lower volume ratios.

Even though the predicted accelerance was shown to be, for example, reduced by using an RMS–value, which is a single–value metric, the accelerance in specific 1/3 octave bands could be either amplified or reduced, respectively, in relation to the equivalent 1/3 octave bands for the reference panel.

11.1.2 2 layers

The 2 layer configurations deemed necessary to illustrate the results can be viewed in Figure 11.5, with corresponding ID:s.

The partial 2 layers configurations deemed necessary to illustrate the results can be seen in Figure 11.6.

For the full list of 2 layer Sylodyn NB configurations, see Appendix D.

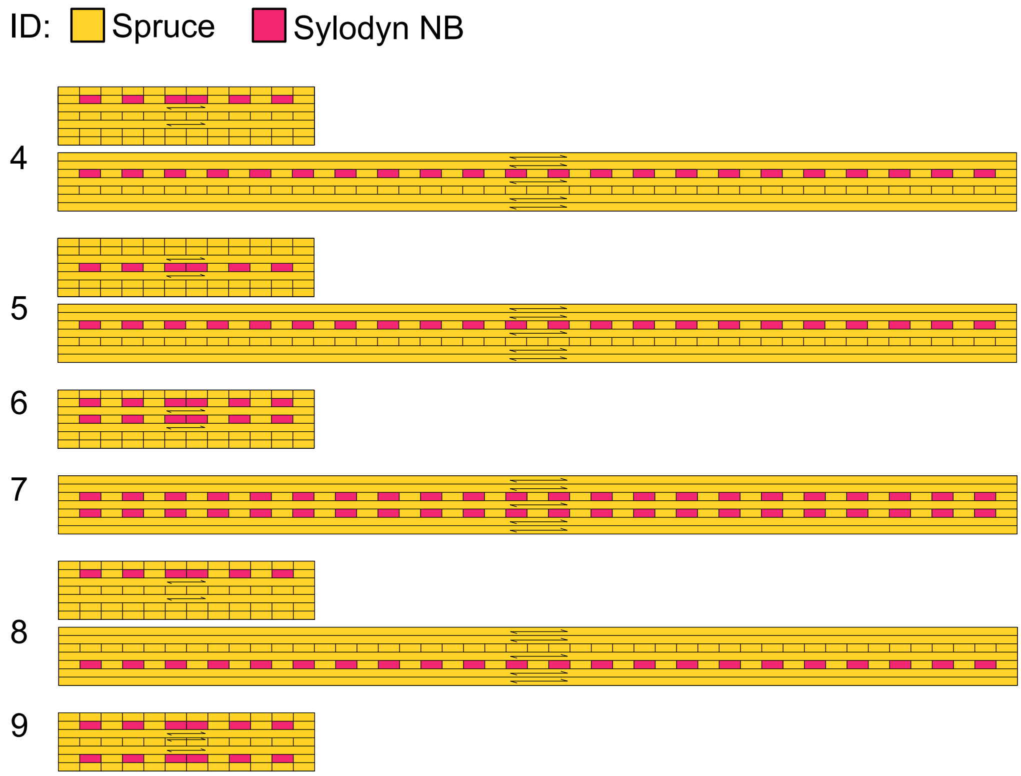

Figure 11.5: Sylodyn NB – the full layers configurations for the 2 layers analysis, with corresponding ID:s. In ID4–5,8 lamellae in both transverse and longitudinal direction are exchanged. In ID6,9 lamellae in longitudinal direction are exchanged, while in ID7 lamellae in transverse direction are exchanged.

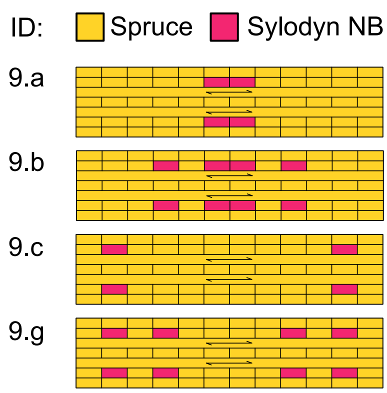

Figure 11.6: Sylodyn NB – partial layers of ID9, with lamellae in longitudinal direction.

11.1.2.1 Full layer

RMS–value
The effect on accelerance evaluated as RMS–value for ID4–9 can be seen in Table 11.3, where a negative change denotes a reduction in the level of vibration as compared to the reference level obtained by a panel composed entirely of spruce.

Table 11.3: Sylodyn NB – the change in RMS–value, compared to reference level, and the volume ratio for configurations with ID4–9. Volume ratio indicates the percentage of Sylodyn NB in the panel.

ID	RMS [%]	Volume ratio [%]
4	–54	14
5	–10	14
6	–37	14
7	+14	14
8	–37	14
9	–43	14

For configurations ID4–6 and ID8–9, the RMS–values showed significant reductions in accelerance. Conversely, ID7 indicated a significant amplification.

Comparing ID7 to ID6 and ID9, placing Sylodyn NB lamellae in longitudinal direction showed greater reductions in accelerance than placing them in transverse direction.

Comparing ID4 to ID5, as well as ID8 to ID5, placing Sylodyn NB lamellae closer to the surface displayed greater reductions in accelerance than placing them closer to the center of the panel.

The RMS–value for ID9 showed a greater reduction in accelerance compared to ID6, which also indicated placing Sylodyn NB lamellae closer to the surface provide a greater reduction in accelerance than placing them closer to the center.

It appeared that the combinations of a full layer in the transverse direction with a full layer in the longitudinal direction provided significant reductions in accelerance (ID4,5, and 8). Additionally, ID4 showed greater reductions in accelerance than ID6 and ID9 (In ID6,9, Sylodyn NF lamellae in longitudinal direction are exchanged). Conversely, ID5 showed a less reductions in accelerance than ID6 and ID9. Moreover ID8 displayed no significant difference in accelerance compared to ID6 and ID9.

1/3 octave band
The effect on accelerance evaluated in 1/3 octave bands for ID4–9 can be seen in Figure 11.7.

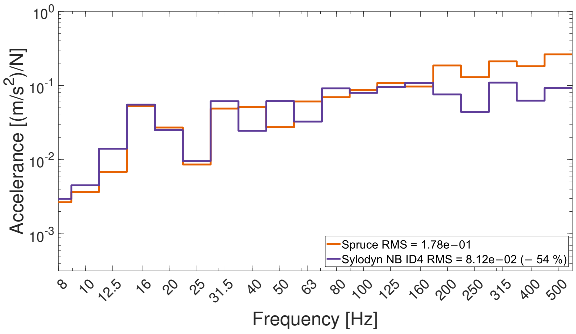

(a) Sylodyn NB ID4

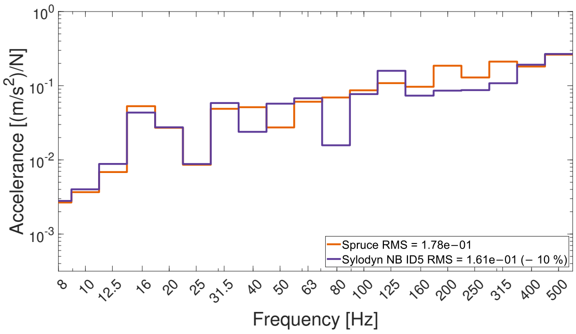

(b) Sylodyn NB ID5

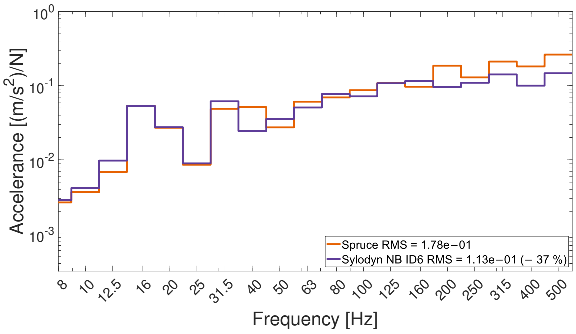

(c) Sylodyn NB ID6

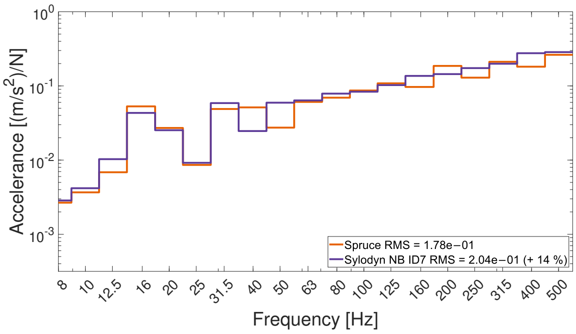

(d) Sylodyn NB ID7

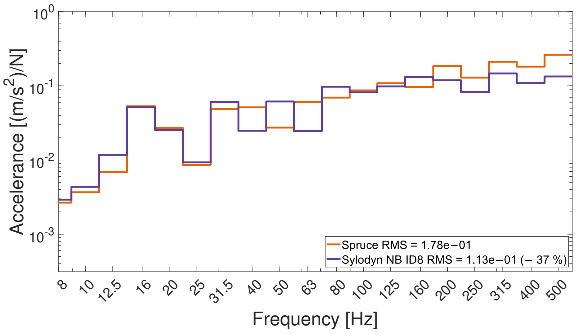

(e) Sylodyn NB ID8

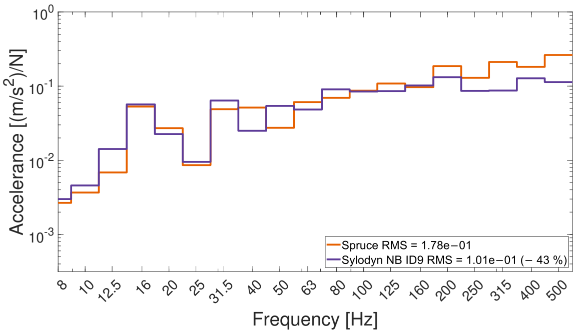

(f) Sylodyn NB ID9

Figure 11.7: Sylodyn NB – the steady–state dynamic response of configuration ID4–9, in 1/3 octave bands. The value in legend within parentheses indicates the change in RMS–value compared to reference level. The center frequency of 1/3 octave bands are shown in the horizontal axis.

The responses of ID4,6,8,9 indicated significant reductions in accelerance between the 1/3 octave band 200 and 500 Hz. Under 200 Hz, response of ID4,6,8,9 showed reductions in accelerance at certain 1/3 octave bands and amplifications in others.

The responses of ID7 exhibited reductions or amplifications in accelerance at different 1/3 octave bands over the entire studied frequency interval, i.e., up to 562 Hz.

The responses of ID5 indicated significant reductions in accelerance between the 1/3 octave band 160–315 Hz. Outside this interval, ID6 showed reductions in accelerance at certain 1/3 octave bands and amplifications in others.

11.1.2.2 Partial layer

RMS–value

The effect on accelerance evaluated as RMS–value for the partial layer configurations of ID9 can be seen in Table 11.4, where a negative change denotes a reduction in the level of vibration as compared to the reference level obtained by a panel composed entirely of spruce.

Table 11.4: Sylodyn NB – the change in RMS–value, compared to reference level, and the volume ratio for the partial layer configurations of ID9. Volume ratio indicates the percentage of Sylodyn NB in the panel.

ID	RMS [%]	Volume ratio [%]
9a	–34	5
9b	–35	10
9c	–8	5
9g	–23	10

The RMS–values for all partial layers configurations of ID9 exhibited significant reductions in accelerance. However, the reductions of ID9c,g were lower than ID9a,b.

Comparing ID9a to ID9c as well as ID9b to ID9g, exchanging spruce lamellae with Sylodyn NB closer to the center showed greater reductions in accelerance than placing Sylodyn NB lamellae closer to the edges of the panel.

1/3 octave band

The effect on accelerance evaluated in 1/3 octave bands for the partial layer configurations of ID9 can be seen in Figure 11.8.

The response of ID9a,b showed significant reductions in accelerance between the 1/3 octave band of 200–500 Hz. From the 1/3 octave band of 160 Hz and downwards, ID9a,b showed reductions in accelerance at certain 1/3 octave bands and amplifications in others.

The response of ID9c,g showed reductions or amplifications in accelerance at different 1/3 octave bands over the entire studied frequency interval, i.e., up to 562 Hz.

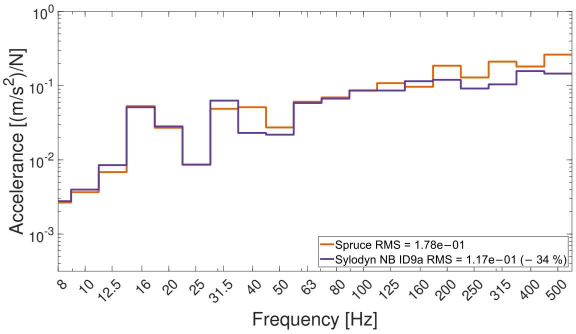

(a) Sylodyn NB ID9a

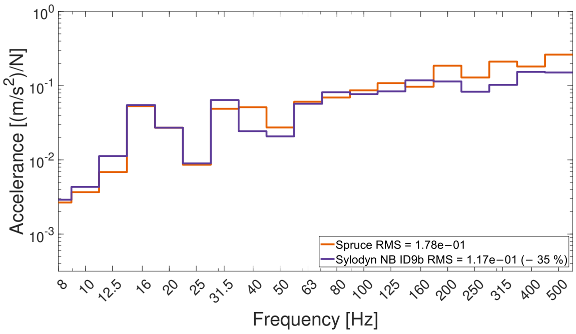

(b) Sylodyn NB ID9b

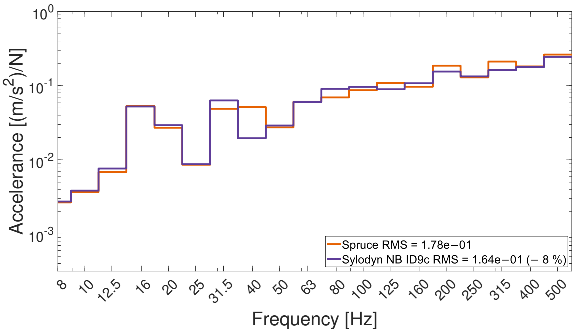

(c) Sylodyn NB ID9c

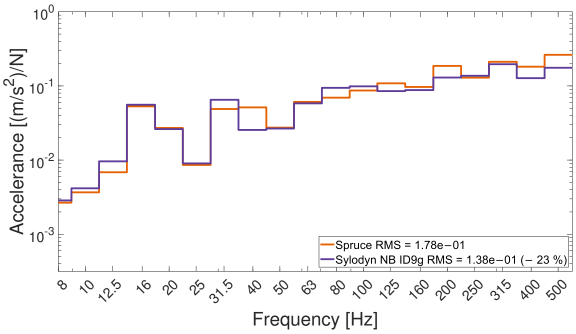

(d) Sylodyn NB ID9g

Figure 11.8: The steady–state dynamic response for partial configurations of 9 in 1/3 octave bands. The value in legend within parentheses indicates the change in RMS–value compared to reference level. The center frequency of 1/3 octave bands are shown in the horizontal axis.

11.1.2.3 2 layers summary

Significant reductions was observed continuously between the 1/3 octave band of 200–500 Hz (ID4, ID6, ID8, ID9 and ID9a,b).

Considering the RMS–values, placing Sylodyn NB lamellae in longitudinal direction (ID6,9) showed greater reductions in accelerance than placing them in transverse direction (ID7).

It appeared that significant reductions in accelerance (ID4, ID5 and ID8) were achieved by combining a full layer in the transverse direction with a full layer in the longitudinal direction.

Considering the RMS–values, placing Sylodyn NB lamellae closer to the surface (ID4, ID8 and ID9) showed greater reductions in accelerance compared to placing them closer to the center of the panel (ID5 and ID6). Moreover, there was one combination (ID4) that showed greater reductions in accelerance than configurations with only longitudinal lamellae are exchanged (ID6 and ID9). Conversely, other combinations (ID5 and ID8) showed either less reductions or no differences in accelerance than configurations with only longitudinal lamellae are exchanged (ID6 and ID9)

Concerning partial layer configurations, exchanging spruce lamellae with Sylodyn NB closer to the center (ID9a,b) showed greater reductions in accelerance compared to placing Sylodyn NB closer to the edges (ID9c,g). This held true in longitudinal direction.

Moreover, considering RMS–values, full layer (ID9) appeared to exhibit a greater reduction in accelerance compared to its partial layers (see Table 11.3 and Table 11.4). However, the partial layers also displayed significant reductions in accelerance with lower volume ratios.

Even though the predicted accelerance was shown to be, for example, reduced by using an RMS–value, which is a single–value metric, the accelerance in specific 1/3 octave bands could be either amplified or reduced, respectively, in relation to the equivalent 1/3 octave bands for the reference panel.

11.1.3 3 layers

The 3 layer configurations deemed necessary to illustrate the results can be viewed in Figure 11.9, with corresponding ID:s.

The partial 2 layers configurations deemed necessary to illustrate the results can be seen in Figure D.5.

For the full list of 3 layer Sylodyn NB configurations, see Appendix D.

It is important to note that these configurations are not directly comparable for the purpose of finding potential trends in the dynamic behavior of the panel. This is due to the fact that they do not have the same number of layers in each direction. However, configurations ID10–12 were still considered as they could provide further insights into the structural behavior of the panel.

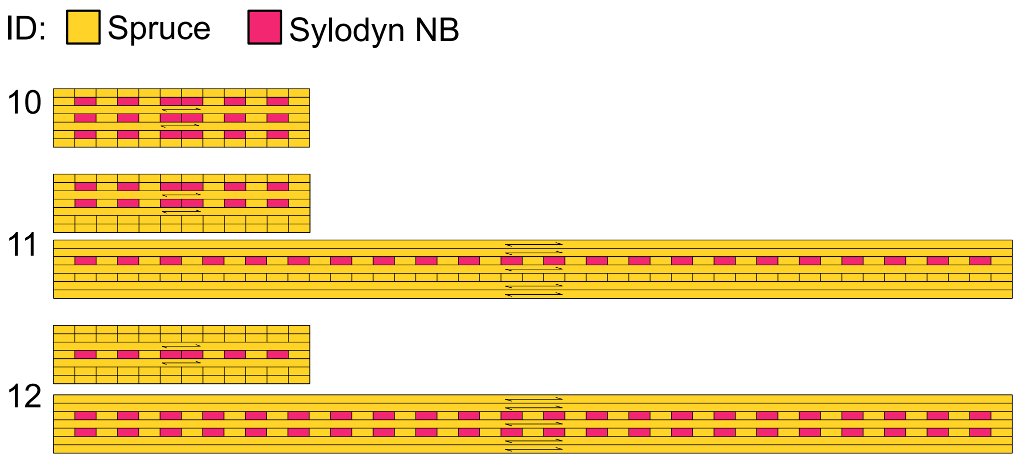

Figure 11.9: Sylodyn NB – the full layers configurations for the 3 layers analysis, with corresponding ID:s. ID10 exchanges lamellae in longitudinal direction and ID11–12 in both transverse and longitudinal direction.

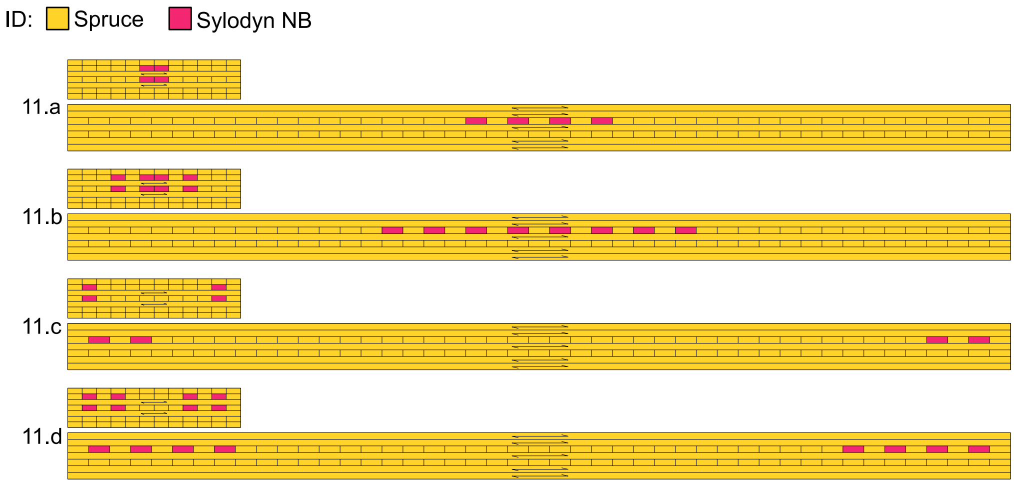

Figure 11.10: Sylodyn NB – the partial layers configurations for the 3 layers analysis, with lamellae in longitudinal (upper image of each ID:s) and transverse (lower image of each ID:s) direction.

11.1.3.1 Full layer

RMS–value

The effect on accelerance evaluated as RMS–value for ID10–12 can be seen in Table 11.5, where a negative change denotes a reduction in the level of vibration as compared to the reference level obtained by a panel composed entirely of spruce.

Table 11.5: Sylodyn NB – the change in RMS–value, compared to reference level, and the volume ratio for configurations with ID10–12. Volume ratio indicates the percentage of Sylodyn NB in the panel.

ID	RMS [%]	Volume ratio [%]
10	–40	21
11	–49	21
12	–6	21

The RMS–values of ID10–ID12 showed reductions in accelerance.

Comparing RMS–values, ID10 showed a greater reduction in accelerance compared to ID12, indicated placing Sylodyn NB lamellae closer to the surface provide a greater reduction in accelerance than placing them closer to the center. It is notable that the configurations ID10 and 12 are not directly comparable.

The RMS–values of ID11 and ID12 indicated significant reductions in accelerance for combinations of full layers in transverse direction with full layers in longitudinal direction. However, ID11 displayed a greater reduction in accelerance than ID12.

1/3 octave band

The effect on accelerance evaluated in 1/3 octave bands for ID10–12 can be seen in Figure 11.11.

The responses of ID10,11 indicated significant reductions continuously from the 1/3 octave band of 160–500 Hz. Under 160 Hz, response of ID10,11 showed reductions in accelerance at certain 1/3 octave bands and amplifications in others.

The responses of ID12 indicated significant reductions continuously from the 1/3 octave band of 160–315 Hz. Outside this interval, response of ID12 showed reductions in accelerance at certain 1/3 octave bands and amplifications in others.

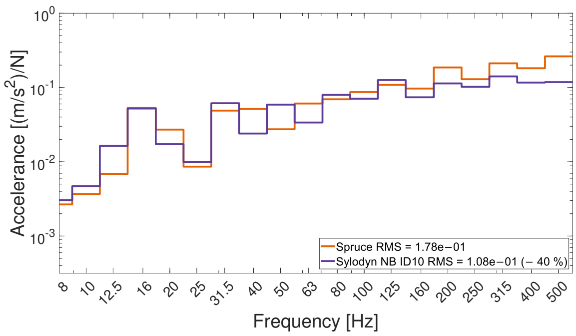

(a) Sylodyn NB ID10

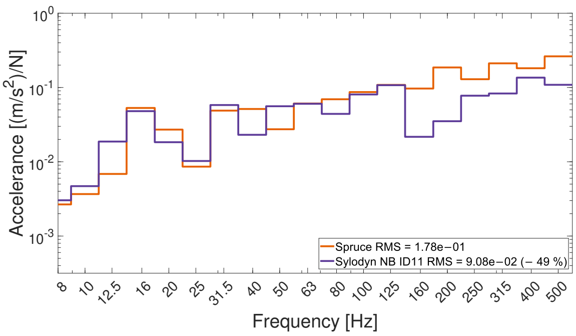

(b) Sylodyn NB ID11

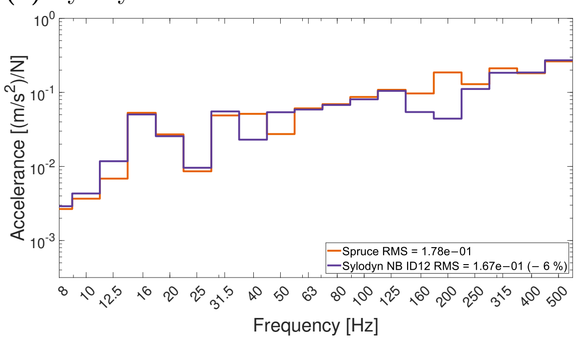

(c) Sylodyn NB ID12

Figure 11.11: Sylodyn NB – the steady–state dynamic response of configuration ID10–12, in 1/3 octave bands. The value in legend within parentheses indicates the change in RMS–value compared to reference level. The center frequency of 1/3 octave bands are shown in the horizontal axis.

11.1.3.2 Partial layer

RMS–value

The effect on accelerance evaluated as RMS–value for the partial layer configurations of ID11 can be seen in Table 11.6, where a negative change denotes a reduction in the level of vibration as compared to the reference level obtained by a panel composed entirely of spruce.

Table 11.6: Sylodyn NB – the change in RMS–value, compared to reference level, and the volume ratio for the partial layer configurations of ID11. Volume ratio indicates the percentage of Sylodyn NB in the panel.

ID	RMS [%]	Volume ratio [%]
11a	–36	6
11b	–33	12
11c	–16	6
11d	–26	12

The RMS–values for all partial layer configurations of ID11 demonstrated notable reductions in accelerance. However, the accelerance reductions in ID11a,b were greater that in ID11c,g. It appeared that placing Sylodyn NB lamellae closer to the center of the panel provided greater reductions in accelerance than placing them closer to the edges (in both directions).

1/3 octave band

The effect on accelerance evaluated in 1/3 octave bands for the partial layer configurations of ID11 can be seen in Figure 11.12.

The response of ID11a displayed significant reductions in accelerance between the 1/3 octave band 200–500 Hz. While ID11b showed significant reductions from 100 – 500 Hz. Outside these intervals, ID11a, b showed reductions in accelerance at certain 1/3 octave bands and amplifications in others.

The configurations ID11c,g showed reductions or amplifications in accelerance at different 1/3 octave bands over the entire studied frequency interval, i.e., up to 562 Hz.

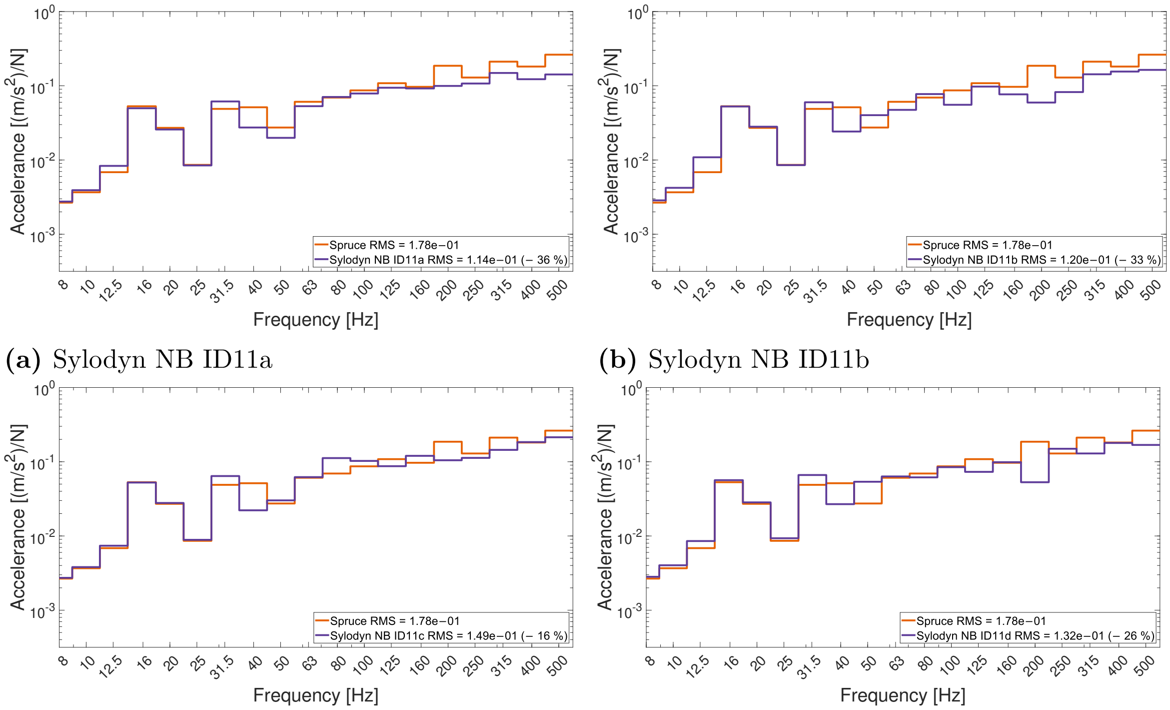

(a) Sylodyn NB ID11a

(b) Sylodyn NB ID11b

(c) Sylodyn NB ID11c

(d) Sylodyn NB ID11d

Figure 11.12: The steady–state dynamic response for partial configurations of ID11 in 1/3 octave bands. The value in legend within parentheses indicates the change in RMS–value compared to reference level. The center frequency of 1/3 octave bands are shown in the horizontal axis.

11.1.3.3 3 layers summary

Significant reductions was observed continuously between the 1/3 octave band of 200–500 Hz (ID10, ID11 and ID11a,b)

Considering the RMS–values, it appeared that combinations of Sylodyn NB layers in different directions provides significant reductions in accelerance. This was valid for both full layer and partial layer configurations (ID11 and ID12).

Considering the RMS–values, placing Sylodyn NB lamellae closer to the surface (ID10) showed greater reductions in accelerance compared to placing them closer to the center of the panel (ID12).

Concerning partial layer configurations, exchanging spruce lamellae with Sylodyn NB closer to the center (ID11a,b) showed greater reductions in accelerance compared to placing Sylodyn NB closer to the edges (ID11c,g). This held true in both longitudinal and transverse directions.

Moreover, considering RMS–values, full layer (ID11) appeared to exhibit a greater reduction in accelerance compared to its partial layers (see Table 11.5 and Table 11.6). However, the partial layers also displayed significant reductions in accelerance with lower volume ratios.

Even though the predicted accelerance was shown to be, for example, reduced by using an RMS–value, which is a single–value metric, the accelerance in specific 1/3 octave bands could be either amplified or reduced, respectively, in relation to the equivalent 1/3 octave bands for the reference panel.

11.1.4 Large sized panel summary

The impact of exchanging lamellae from spruce to Sylodyn NB in the L–sized panel are consolidated in this section.

- Placing Sylodyn NB lamellae in the longitudinal direction showed greater reductions in accelerance than placing them the transverse direction (ID2 compared to ID1, and ID3, as well as ID7 to ID6 and ID9), but only when all lamellae are oriented in the same respective direction.
- Combinations of Sylodyn NB lamellae in different directions (ID4, ID5, ID8, ID11, and ID12) showed significant reductions in accelerance. However, some of these combinations (ID4, ID11 and ID12) provided greater reductions compared to placing the same number of layers solely in the longitudinal direction (ID6, ID9, and ID10), while others (ID5 and ID8) displayed less reductions in accelerance (compared to ID6 and ID9)
- In full layers, greater reductions in accelerance appeared to be achieved by placing Sylodyn NB lamellae closer the surfaces of the panel (ID1, ID4 and ID10), rather than closer to the center (ID3, ID5 and ID12).
- In partial layers, the reductions in accelerance were greater with Sylodyn NB lamellae placed closer to the center of the panel (ID1a,b, ID9a,b and ID11a,b) compared to those placed closer to the edges (ID1c,g, ID9c,g and ID11c,d).
- Considering RMS–values, full layers configurations (ID1,9,11) appeared to exhibit greater reductions in accelerance compared to their respective partial layers configurations. Apart from one configuration exchanging Sylodyn NB lamellae in transverse direction (ID2), which showed amplification in accelerance. Generally, partial layers configurations displayed significant reductions in accelerance with lower volume ratios compared to their respective full layers configurations.
- Notably, significant reductions was observed continuously between the 1/3 octave band of 200–500 Hz, in many configurations such as ID1, ID4, ID6, ID8–11, ID1a,b, ID9a,b and ID11a,b.
- Even though the predicted accelerance was shown to be, for example, reduced by using an RMS–value, which is a single–value metric, the accelerance in specific 1/3 octave bands could be either amplified or reduced, respectively, in relation to the equivalent 1/3 octave bands for the reference panel.

11.2 Medium size panel

1 layer

The investigation whether the dimensions and/or lay–ups of the panels influence the results are presented here.

The configurations analyzed can be viewed in Figure 11.13.

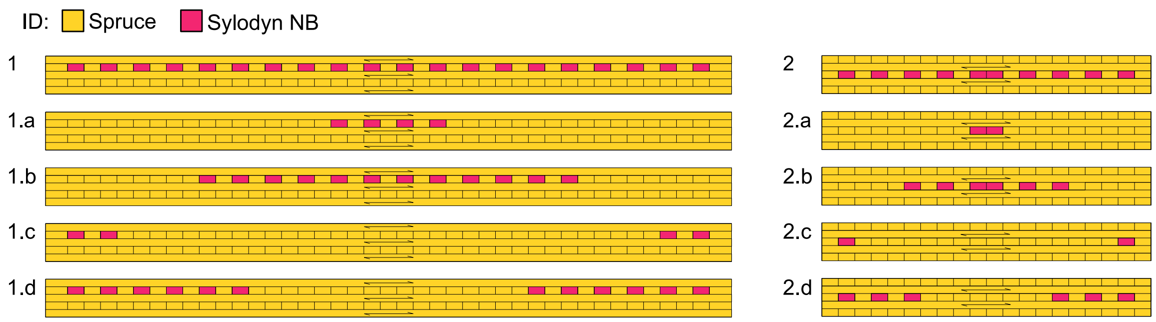

Figure 11.13: Sylodyn NB – Illustration of the analyzed configuration, performed on the M–sized panel.

The effect on accelerance evaluated as RMS–value for these configurations can be seen in Table 11.7, where a negative change denotes a reduction in the level of vibration as compared to the reference level obtained by a panel comprised entirety of spruce.

The effect on accelerance evaluated in 1/3 octave bands for these configurations can be seen in Figure 11.14.

Table 11.7: The change in RMS–value, compared to reference level, and the volume ratio for configurations visualized in Figure 11.13. Volume ratio indicates the percentage of Sylodyn NB in the panel.

ID	RMS [%]	Volume ratio [%]
1	–13	10
2	–2	10
1a	–5	2
1b	–9	6
1c	–12	2
1d	–15	6
2a	–8	2
2b	–8	6
2c	–11	2
2d	–10	6

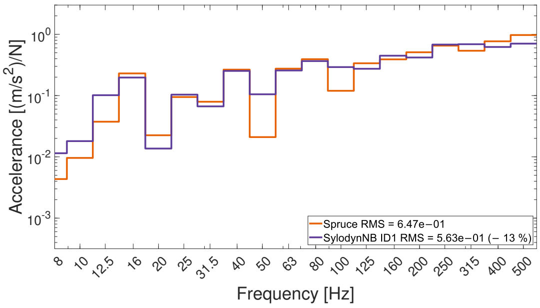

(a) Sylodyn NB M–sized panel ID1

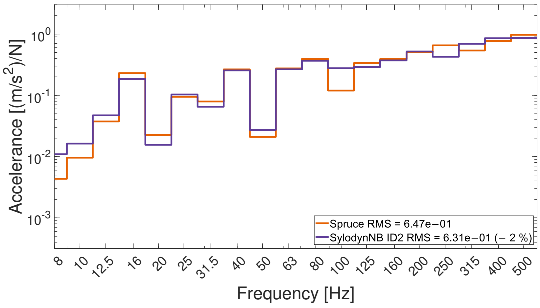

(b) Sylodyn NB M–sized panel ID2

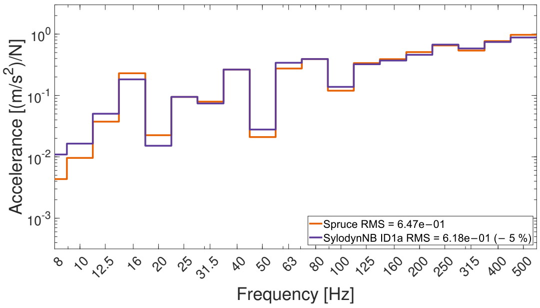

(c) Sylodyn NB M–sized panel ID1a

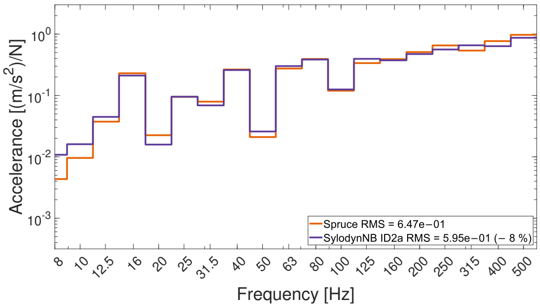

(d) Sylodyn NB M–sized panel ID2a

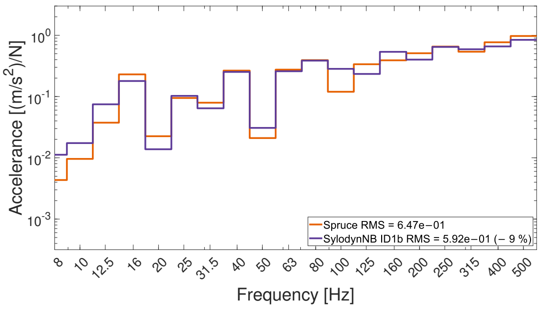

(e) Sylodyn NB M–sized panel ID1b

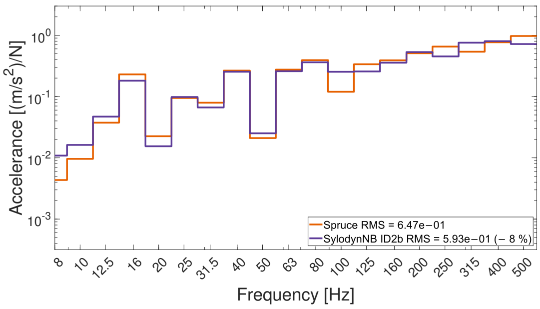

(f) Sylodyn NB M–sized panel ID2b

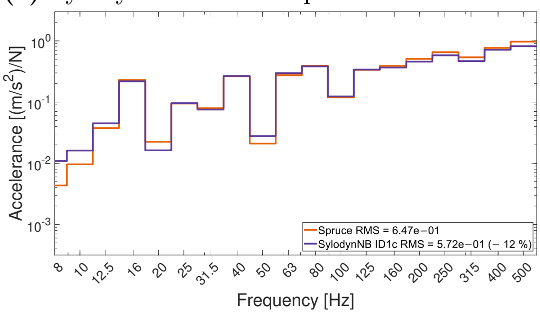

(g) Sylodyn NB M–sized panel ID1c

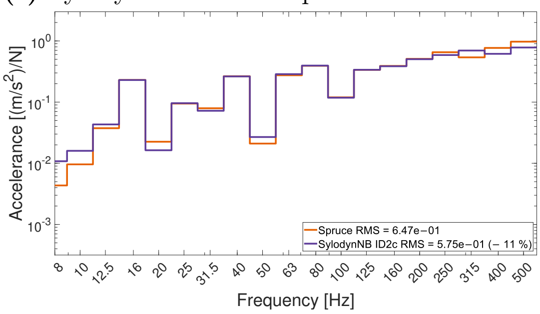

(h) Sylodyn NB M–sized panel ID2c

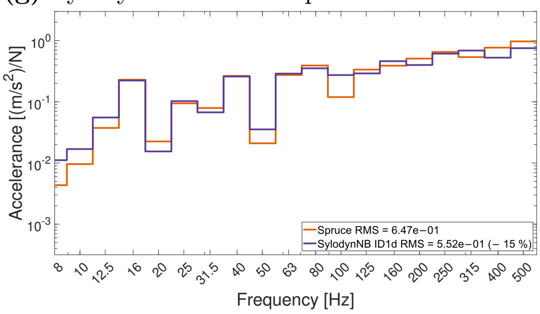

(i) Sylodyn NB M–sized panel ID1d

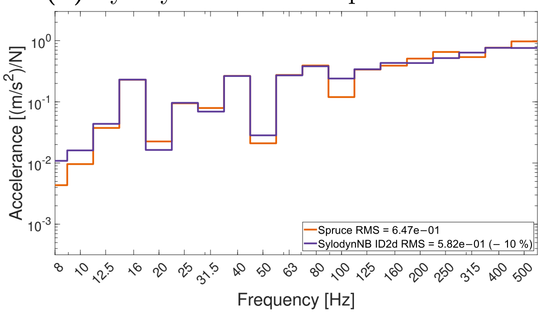

(j) Sylodyn NB M–sized panel ID2d

Figure 11.14: Sylodyn NB – the steady–state dynamic response in 1/3 octave bands for configurations illustrated in Figure 11.13. The value in legend within parentheses indicates the change in RMS–value compared to reference level. The center frequency of 1/3 octave bands are shown in the horizontal axis.

RMS–values showed that placing Sylodyn NB lamellae in transverse direction (ID1) indicated a greater reduction in accelerance compared to placing them in longitudinal direction (ID2).

The responses of configurations in M-sized panel showed reductions or amplifications in accelerance at different 1/3 octave bands over the entire studied frequency interval, i.e., up to 562 Hz.

Considering RMS–values of partial layer configurations, no significant in accelerance was observed between placing Sylodyn NB closer to the center of the panel (ID1a,b and ID2a,b) and placing them closer to the edges of the panel (ID1c,d and ID2c,d).

Considering RMS–values, the partial layers (ID1a–d and ID2a–d) displayed significant reductions in accelerance with lower volume ratios compared to their respective full layers.

Even though the predicted accelerance was shown to be, for example, reduced by using an RMS–value, which is a single–value metric, the accelerance in specific 1/3 octave bands could be either amplified or reduced, respectively, in relation to the equivalent 1/3 octave bands for the reference panel.

It is important to note that the lay–up of the M–sized panel with 5 layers would mean unreasonable placement of Sylodyn NB in the top layer. Therefore, the trend of placing Sylodyn NB closer to surfaces could not be analyzed and verified.

12 Discussion

In this section, a discussion of the process of determining material properties, the numerical modeling and results are presented.

12.1 Material properties

To obtain data for the sensitivity analysis in Section 5.2, a literature study was conducted. This raises questions whether the number of sources studied were sufficient and reliable, and whether the chosen interval (for the sensitivity analysis) was adequate. However, this was considered sufficient and reliable as the interval was mainly obtained from the European standard SS–EN 338:2016 [8].

Challenges emerged during the process of determining the rolling shear modulus (G_{RT}) for the sensitivity analysis interval. These were not listed in the European standard SS–EN 338:2016 [8]. However, in [16] several experiments were conducted where a ratio between G_{LT}/G_{RT} and G_{RL}/G_{RT} have been found to approximately 14. This ratio was used to determine the rolling shear modulus for the interval in the sensitivity analysis. This approach could raise uncertainties, depending on the accuracy of the experiments.

The 16 experiments conducted in [4] were used for the calibrations of spruce properties in Section 5.3. Uncertainties could arise depending on the accuracy of these experiments. For instance, replicating a free–free boundary condition is impossible in practice. However, with the use of elastic ropes to suspend the CLT panels, a close replication was found. In addition, it could be interesting to include further experiments with different dimensions and include more modes to determine whether it has any effects on the results. Especially since the panels in the studies were of different dimensions and covers considerably more modes compared to the experiments.

In Section 5.3, parameter calibrations for spruce were performed. An adjustment was made to the parameter G_{LR}, aligning its value to the calibrated value for G_{LT}. This was due to the difficulty in determining tangential and radial orientation in practical applications. It could have been interesting to retain the original value for G_{LR} to determine if it affects the results. Alternately, averaging G_{LR} and G_{LT} which accounts for variations in annual ring orientation of the lamellae.

In this dissertation, the conventional concrete strength C25/30 was used. It could be interesting to perform the analyzes using concrete of different strengths, for example C30/C37, to determine if it has any effects on the results. However, the results should indicate the same trends, as these trends are affected by the mass and stiffness relation between the materials spruce to concrete, which would remain the same.

For Sylodyn NF and NB properties, there exist a couple of uncertainties because many material properties are depended on the shape factor (loaded area/area of perimeter). For example, the load deflection curve in the data sheets were determined by a certain load on a certain load factor (q=3). Many other properties were also determined with this shape factor as references, such as dynamic Young modulus as well as the loss factor. Meaning if a different shape factor is used, the properties of Sylodyn NF and NB obtained would be affected. This was the case in this dissertation, however close replications of the material Sylodyn NF and NB were obtained.

12.2 Numerical modeling

In this dissertation, two finite element models were used: Layered model and Lamellae model. These models introduce several aspects worth elaborating further. For instance, the partitions forming the layers and lamellae generates tie–constraints vertically between the layers and horizontally between the lamellae. This is sort of contrary to the general manufacturing process of CLT panels, as lamellae are usually not glued horizontally between lamellae. However, as these panels are glued under pressure, glue slips in between these lamellae. Therefore, these models were deemed appropriate. Moreover, the calibrations conducted in Section 5.3 do, to some extent, account for this, as they were based on data from real CLT panels.

The materials were modulated as homogeneous and with the same material orientation. Consequently, each lamella has the same material properties in each direction. Still, each layers oriented perpendicular to the next. In reality, the material properties of timber are heterogeneous and could differ in directions, even from one lamellae to another. However, the calibrations conducted in Section 5.3 do, to some extent, account for this, as they were based on data from real CLT panels.

The boundary conditions have significant impacts on the dynamic response of CLT panels. Free–free BC was utilized in this dissertation, which removes any interference on the material behavior from the BC. Other boundary conditions, such as simply supported or 4 line supports, could be interesting to analyze to obtain more practical results. In addition, modulating the connecting walls to include the increased stiffness could be interesting. However, this would result in a very specific model which was not the intent for this dissertation.

The load case in this dissertation consisted of a point load of 1 N placed in one of the corners of the CLT panel, with a measurement point in the opposite corner. This ensured the excitement of all modes within the frequency range. It could be interesting to analyze other load cases, such as footfalls, to determine if it affects the results. However, this would again result in a very specific load case which was not the intent for this dissertation.

Moreover, no definite verification was conducted to determine whether the material effects of concrete and empty space/air were actually captured in the modal truncation. It would be advantageous to perform some analyzes considering a full steady–state dynamic response, and compare this to the truncated one. For instance, the modal damping parameter was obtained from a experiment conducted on panels compromised of solely spruce. This parameter would be impacted when alternating material in the panels.

Furthermore, there were an uncertainty regarding the chosen frequency range of interest. This uncertainty arises from the predetermined range of 0–562 Hz, used for all analyzes when evaluating the impact of different lamellae materials. It could be interesting to instead compare the number of peaks, or even specific peaks of interest, to determine if it affects the results.

12.3 Lamellae material – concrete

Greater reduction in accelerance was achieved when exchanging spruce lamellae to concrete closer to the edges. This was valid for different panel dimensions and lay–ups. However, it is not of certain that this would apply to CLT panels in general, highlighting the necessity of further works. For the L–sized panel, greater reduction in accelerance was found when exchanging layers closer to the center of the panel rather than the surface. Note that the potential trend of exchanging material from the surface inwards for the 7 layered L–sized panel is not possible to replicate for the M–sized panel, as it only consists of 5 layers.

The relation between the stiffness and mass significantly impacts the natural frequencies of structures, and thereby also CLT panels. For a SDOF, this relation can be determined by Equation 3.2. When this ratio increases, the natural frequencies appear at higher frequencies than before, resulting in lowered RMS–values as less peaks would be included in the frequency interval of interest. When exchanging spruce lamellae to concrete lamellae closer to the edges, this ratio perhaps increased – resulting in lowered RMS–values compared to the reference level. However, the studies conducted in this dissertation involves MDOF, which includes stiffness and mass matrices. Therefore, a higher complexity than addressing the ratio in Equation 3.2 exists. Moreover, the damping of each material significantly affects the change of magnitude for each peak within the frequency range, which affects the accelerance of the panels, which further highlights the complexity of the studies.

No significant difference in accelerance were indicated when comparing exchanging lamellae to concrete either longitudinally or transversely, towards the center of the panels. This was valid for different panel dimensions and lay–ups. However, in the L–sized panel, significant difference in accelerance was showcased in the outer areas of the panel, both towards the surface and edges. A possible explanation for this result is that the relation between stiffness and mass does not vary significantly when exchanging spruce lamellae to concrete lamellae towards the center of the panels.

Interestingly, the majority of the configurations showcased significant amplifications in accelerance for the 1/3 octave band of 12.5 Hz. This could be the result of using 1/3 octave bands, where a peak in response of reference level might be just above the 1/3 octave band of the center frequency 12.5 Hz. Consequently, when exchanging spruce with the heavier concrete, this peak is moved from the adjacent 1/3 octave band of 16 Hz to the 12.5 Hz one.

Noteworthy, in the L–sized panel, majority of the configurations displayed continuous reduction in accelerance from the 1/3 octave band of 63 Hz up to 562 Hz.

12.4 Lamellae material – air cavities

No significant differences in accelerance were indicated between the two studied modeling methods of air cavities. This was valid for different panel dimensions and lay–ups.

For the majority of the studied configurations, exchanging spruce lamellae to empty space lamellae closer to the surface resulted in either less amplification or greater reduction in accelerance compared to exchanging spruce lamellae to empty space lamellae closer to the center. However, for a certain configuration, the results indicated insignificant difference in accelerance. Note that the potential trend of exchanging material from the surface inwards for the 7 layered L–sized panel is not possible to replicate for the M–sized panel, as it only consists of 5 layers. Moreover, it is not of certain that this would apply to CLT panels in general, highlighting the necessity of further works.

This finding is especially interesting when addressing the relation between stiffness and mass, previously mentioned in Section 12.3. Concrete inherent higher stiffness and mass compared to timber and was found to reduce accelerance, in the L–sized panel, particularly when exchanging material in the middle layer and closer to the edges. On the contrary, empty space inherent less stiffness and mass compared to timber, meaning a result indicating it to showcase either less amplification in accelerance or greater reduction in accelerance towards the surface of the panel would make sense. However, the effects on the change of magnitude for each peak do also significantly impact the dynamic behavior, which further highlights the complexity of the studies.

Furthermore, no significant amplifications in accelerance were showcased when exchanging spruce lamellae to empty space lamellae in the longitudinal direction. This was valid for different panel dimensions and lay–ups. In L–sized panel, exchanging spruce lamellae to empty space lamellae resulted in up to 21% material reduction without significantly affecting the accelerance.

Moreover, in the L–sized panel, significant amplifications in accelerance were showcased when exchanging spruce lamellae to empty space lamellae in the transverse direction. However, some partial configurations exchanging lamellae in transverse direction exhibited no significant differences in accelerance. In the M–sized panel, exchanging spruce lamellae to empty space lamellae in transverse direction indicated greater reduction in accelerance than exchanging spruce lamellae to empty space lamellae in longitudinal direction.

12.5 Lamellae material – elastomer

The results from the impact of stiff and soft elastomer lamellae in Chapters 10 and 11, showed reductions in accelerance at certain 1/3 octave bands and amplifications in others. However, significant reductions in accelerance were observed over different coherent 1/3 octave bands. This behavior demonstrates possibilities on reducing accelerance at different specific frequency intervals.

As described in Section 12.3, the relation between the stiffness and mass has a significant impact on the dynamic behavior of structures. Sylodyn NF is heavier than spruce and Sylodyn NB is lighter. Moreover, spruce is stiffer than both these types of Sylodyn. When exchanging lamellae material with Sylodyn, the ratio between the stiffness and mass can increase or decrease. This affects the number of peaks that are included within the same studied frequency range, i.e. up to 562 Hz. Increasing this relation results in the number of peaks decreases, which in turn reduce the RMS–value of the same frequency range. Conversely, decreasing this relation includes peaks, which in turn raise the RMS–value.

Moreover, the damping of Sylodyn, which is frequency–dependent, increases at higher frequencies. This might be the reason for why exchanging spruce lamellae to Sylodyn indicated significant reductions at higher frequencies.

Additionally, the combinations of Sylodyn in longitudinal and transverse directions indicated significant reductions in accelerance. In the L–sized panel, exchanging spruce lamellae to Sylodyn in longitudinal direction provided greater reductions in accelerance compared to in transverse direction. However, considering RMS–values, combinations of Sylodyn lamellae in different directions showed greater reductions in accelerance for certain configuration and less reductions for other configurations, compared to only placing Sylodyn NF in longitudinal direction.

12.5.1 Stiff elastomer

The results of Sylodyn NF showed reductions in accelerance at certain 1/3 octave bands and amplifications in others. However, there were certain configurations which showed significant reduction in accelerance over coherent 1/3 octave bands. For example, in L–sized panel, ID1 and ID1c showed significant reductions in accelerance between 200–500 Hz, ID9 between 100–500Hz, ID4 and ID6g between 315–500 Hz, ID6c between 200–315Hz, ID10–12 between 160–500Hz.

Some results were observed in both L–sized and M–sized panels. However, there were results that exhibited in the L–sized panel but could not be verified in the M–sized panel.

The results that appeared in both panels are presented below:

- Considering RMS–values, full layers appeared to exhibit greater reductions in accelerance compared to their respective partial layers. However, partial layers also displayed significant reductions in accelerance with lower volume ratios.

- Considering RMS–values, greater reductions in accelerance seemed to be achieved by placing Sylodyn closer to the edges rather than the center. This is valid for both directions.

The results that could not be verified in both panels is as follows:

- In L–sized panel, placing Sylodyn NF lamellae in the longitudinal direction showed greater reductions in accelerance compared to the transverse direction. However, in the M–sized panel, there were no significant differences in RMS–values between both directions.
- In L–sized panel, when comparing RMS–values, it is unclear if placing Sylodyn NF lamellae towards the surfaces or towards the center of the panel could provide greater reductions in accelerance. Certain configurations showed exchanging spruce lamellae to Sylodyn NF closer to the surface provided greater reduction in accelerance, while other showed insignificant difference in accelerance between the directions.
- Panels with other lay–ups with more layers could be analyzed to verify these above mentioned observations.

12.5.2 Soft elastomer

The results of Sylodyn NB showed reductions in accelerance at certain 1/3 octave bands and amplifications in others. However, there were certain configurations, which showed significant reduction in accelerance over coherent 1/3 octave bands.

Some results were observed in both L–sized and M–sized panels. However, there were results that exhibited in the L–sized panel but could not be verified in the M–sized panel.

The result that was valid for both panels are presented below:

- Considering RMS–values, full layers appeared to exhibit greater reductions in accelerance compared to their respective partial layers. However, partial layers also displayed significant reductions in accelerance with lower volume ratios.

The results that exhibited in the L–sized panel but could not be verified in the M–sized panel are presented below:

- In the L–sized panel, there were certain configurations, which showed significant reductions in accelerance over coherent 1/3 octave bands. For example ID1,4,6,8–11, ID1a,b, ID9a,b and ID11a,b showed continuous reductions in accelerance between 200–500 Hz. The responses of configurations in M–sized panel showed reductions or amplifications in accelerance at different 1/3 octave bands over the entire studied frequency interval, i.e., up to 562 Hz.

- In the L–sized panel, when comparing RMS–values, placing Sylodyn NB lamellae closer the surfaces of the panel provided grater reductions in accelerance than placing them closer to the center. Due to the lay–up of the M–sized panel with 5 layers and replacing spruce lamellae in the top layer is not reasonable, this trend could not be analyzed and verified.

- Considering RMS–values of the L–sized panel, greater reductions in accelerance seemed to be achieved by placing Sylodyn NB lamellae in longitudinal direction rather than placing them in transverse direction. The responses of configurations having Sylodyn NB lamellae placed in longitudinal direction displayed continuous reductions in accelerance between the 1/3 octave band of 200–500 Hz.
  Conversely, in the M–sized panel, RMS–values of ID1 (Sylodyn NB lamellae in transverse direction were exchanged) showed a greater reduction in accelerance than ID2 (Sylodyn NB lamellae in longitudinal direction were exchanged). The responses of these configurations in M–sized panel showed reductions or amplifications in accelerance at different 1/3 octave bands over the entire studied frequency interval, i.e., up to 562 Hz.

- For partial configurations, considering RMS–values of the L–sized panel, greater reductions in accelerance seemed to be achieved by placing Sylodyn NB lamellae closer to the center rather than placing them closer to the edges of the panel. The responses of configurations having Sylodyn NB lamellae placed closer to the center also displayed continuous reduction in accelerance between the 1/3 octave band of 200–500 Hz.
  Conversely, RMS–values of ID1 partial layer configurations (Sylodyn NB lamellae in transverse direction were exchanged) in the M–sized panel, showed that placing Sylodyn NB lamellae closer to the edges of the panel provides greater reduction in accelerance. Additionally, the RMS–values of ID2 partial layer configurations (Sylodyn NB lamellae in longitudinal direction were exchanged) in the M–sized panel, showed no significant difference in accelerance reduction between these placements. The responses of all configurations in M–sized panel showed reductions or amplifications in accelerance at different 1/3 octave bands over the entire studied frequency interval, i.e., up to 562 Hz.

13 Concluding Remarks

In this chapter, the key results, main conclusions as well as suggestions for further work are presented.

13.1 Key results

The following key results were observed in the large sized panel (9 m in length):

- Replace 2% of the spruce lamellae to concrete to achieve approximately 60% reduction in the level of vibration.
- Remove approximately 20% of the spruce lamellae without amplifying the vibration response.
- Replace 2% of the spruce lamellae to stiff elastomer to achieve approximately 20% reduction in the level of vibration.
- Replace 2% of the spruce lamellae to soft elastomer to achieve approximately 25% reduction in the level of vibration.

13.2 Main conclusions

The results from the numerical parametric studies indicate the following conclusions:

- Significant reductions in the level of vibration can be achieved by replacing spruce lamellae with concrete, particularly when the concrete is located in lamellae closest to the outermost parts of CLT panels, along both the longitudinal and transverse directions.
- For the 7 layered large sized panel (9 m in length), greater reduction in accelerance was found when exchanging layers closer to the center of the panel rather than the surface. This was not possible to validate in the medium sized panel (5 m in length), as it only consists of 5 layers.
- Air cavities in CLT panels can be modeled as an empty space because modeling air as an acoustic medium in comparison to as an empty space indicated no significant difference in vibration level.
- Potential to remove spruce lamellae in CLT panels giving up to 20% material reduction without significantly affecting the vibration level.

- Removing spruce lamellae in longitudinal direction did not indicate any significant amplifications in vibration level of CLT panels. In the large sized panel (9 m in length), removing spruce lamellae in transverse direction showed significant amplifications in vibration level. However, in the medium sized panel (5 m in length), removing spruce lamellae in transverse direction displayed no amplifications in vibration level.

- Exchanging spruce lamellae to elastomer demonstrated reductions in vibration level at certain frequency intervals and amplifications in others. However, there were certain configurations, which showed significant reduction in vibration level over continuous frequency intervals. It demonstrates potential to place elastomer lamellae in a way that is favorable for specific frequency intervals.

- Full layers configurations of elastomer lamellae appeared to exhibit greater reductions in vibration level compared to their respective partial layers configurations. However, partial layers configurations also displayed significant reductions in vibration level with lower amount of elastomer lamellae.

- Coherent 1/3 octave bands where stiff elastomer lamellae showed reductions in vibration level, depended on the location of stiff elastomer lamellae, but commonly between 315–500 Hz.

- Coherent 1/3 octave bands where soft elastomer lamellae showed reductions in vibration level, depended on the location of soft elastomer lamellae, but commonly between 200–500 Hz in large sized panel (9 m in length). However, the configurations in medium sized panel (5 m in length) did not show any clear coherent 1/3 octave bands where soft elastomer showed reductions in vibration level.

- Significant reductions in the level of vibration can be achieved by replacing spruce lamellae with stiff elastomer, particularly when the stiff elastomer is located in lamellae closest to the outermost parts of CLT panels, along both the longitudinal and transverse directions.

13.3 Further work

Suggestions for further work are presented as follows:

- Study the impact of different lamellae material under different boundary conditions, such as four line supports and simply supported, and load cases, for example, footfall vibrations and step–sound.
- Study the effects on the sound radiation from the panels by averaging the velocity response of the surface of the panels.
- In the large sized panel (9 m in length), combinations of elastomer lamellae in both longitudinal and transverse direction showed greater reductions in vibration level for certain configurations and less reductions for other configurations, compared to only placing elastomer in longitudinal direction. Therefore, it would be interesting to study the effects of combining elastomer in different directions further.
- Study the impact of different lamellae materials in panels with other dimensions and number of layers compared to the studied panels in this dissertation. Some trends were found in the large sized panel (9 m in length) but could not be verified in the medium sized panel (5 m in length).
- Conduct experiments on CLT panels and study greater numbers of natural frequencies. It will provide better basis for calibrations of mechanical properties of spruce.

Bibliography

[1] Reinhard Brandner. "Production and Technology of Cross Laminated Timber (CLT): A state-of-the-art Report". In: *Graz* (May 2013).

[2] Peter Persson, Ola Flodén, Henrik Danielsson, Andrew Peplow and Lars Vabbersgaard Andersen. "Improved low-frequency performance of cross-laminated timber floor panels by informed material selection". In: *Applied Acoustics* 179 (2021), p. 108017. DOI: https://doi.org/10.1016/j.apacoust.2021.108017.

[3] Fredrik Ljunggren, Christian Simmons and Klas Hagberg. "Correlation between sound insulation and occupants' perception – Proposal of alternative single number rating of impact sound". In: *Applied Acoustics* 85 (2014), pp. 57–68. DOI: https://doi.org/10.1016/j.apacoust.2014.04.003.

[4] Fredrik Ljunggren. "Innovative solutions to improved sound insulation of CLT floors". In: *Developments in the Built Environment* 13 (2023), p. 100117. DOI: https://doi.org/10.1016/j.dibe.2022.100117.

[5] L. Barham, G. A. T. Duller, I. Candy, C. Scott, C. R. Cartwright, J. R. Peterson, C. Kabukcu, M. S. Chapot, F. Melia, V. Rots, N. George, N. Taipale, P. Gethin and P. Nkombwe. "Evidence for the earliest structural use of wood at least 476,000 years ago". In: *Nature* 622.3458 (2023), p. 14. DOI: https://doi.org/10.1038/s41586-023-06557-9.

[6] Swedish Wood. *Properties of softwood - Swedish Wood — swedishwood.com*. https://www.swedishwood.com/wood-facts/about-wood/from-log-to-plank/properties-of-softwood/. [Accessed 24-01-2024].

[7] Marie Johansson. *Design of timber structures*. Edition 3:2022. Vol. 1. Swedish Forest Industries Federation - Swedish Wood. Chap. 2. ISBN: 978-91-985212-5-2.

[8] *SS-EN 338:2016 - Structural timber - Strength classes*. Standard. Swedish Institute for Standards sis, 2016. URL: https://www.sis.se/en/produkter/wood-technology/wood-sawlogs-and-sawn-timber/ssen3382016/.

[9] Swedish Wood. *The CLT Handbook*. May 2019. ISBN: 978-91-983214-4-3.

[10] Cristóbal Tapia, Marian Claus and Simon Aicher. "A finger-joint based edge connection for the weak direction of CLT plates". In: *Construction and Building Materials* 340 (2022), p. 127645. DOI: https://doi.org/10.1016/j.conbuildmat.2022.127645.

[11] Anil K. Chopra. *Dynamics of Structures: Theory and applications to earthquake engineering*. Pearson, 2017. ISBN: 9780134555126.

[12] Hans Petter Wallin, Ulf Carlsson, Mats Åbom, Hans Bodén, Ragnar Glav and Robert Hildebrand. *Sound and vibration*. 2nd ed. KTH Aeronautical and Vehicle engineering. ISBN: 9789174155532.

[13] Johannes Jonasson, Peter Persson and Henrik Danielsson. “Mitigating footfall-induced vibrations in cross-laminated timber floor-panels by using beech or birch”. In: *Journal of Building Engineering* 86 (2024), p. 108751. DOI: `https://doi.org/10.1016/j.jobe.2024.108751`.

[14] Peter Persson, Ola Flodén, Henrik Danielsson, Andrew Peplow and Lars Vabbersgaard Andersen. “Improved low-frequency performance of cross-laminated timber floor panels by informed material selection”. In: *Applied Acoustics* 179 (2021), p. 108017. DOI: `https://doi.org/10.1016/j.apacoust.2021.108017`.

[15] O. Flodén, K. Persson and G. Sandberg. “A multi-level model correlation approach for low-frequency vibration transmission in wood structures”. In: *Engineering Structures* 157 (2018), pp. 27–41. DOI: `https://doi.org/10.1016/j.engstruct.2017.11.062`.

[16] T. Ehrhart and R. Brandner. “Rolling shear: Test configurations and properties of some European soft- and hardwood species”. In: *Engineering Structures* 172 (2018), pp. 554–572. DOI: `https://doi.org/10.1016/j.engstruct.2018.05.118`.

[17] *SS-EN 1992-1-1:2005 - Eurocode 2: Design of concrete structures – Part 1-1: General rules and rules for buildings*. Standard. Swedish Institute for Standards sis, 2008. URL: `https://www.sis.se/produkter/byggnadsmaterial-och-byggnader/byggnadsindustrin/tekniska-aspekter/ssen1992112005a120142/`.

[18] *SS-EN 1991-1-1 - Eurocode 1: Actions on structures - Part 1-1: General actions - Densities, self-weight, imposed loads for buildings*. Standard. Swedish Institute for Standards sis, 2009. URL: `https://www.sis.se/produkter/byggnadsmaterial-och-byggnader/byggnadsindustrin/tekniska-aspekter/ssen199111/`.

[19] O. Flodén, J. Negreira, K. Persson and G. Sandberg. “The effect of modelling acoustic media in cavities of lightweight buildings on the transmission of structural vibrations”. In: *Engineering Structures* 83 (2015), pp. 7–16. DOI: `https://doi.org/10.1016/j.engstruct.2014.10.037`.

[20] Dassault Systèmes. “Abaqus 2016”. In: *Analysis User’s Guide* (2016).

[21] Getzner Werkstoffe GmbH. *Sylodyn*. Accessed: 2024-05-18. URL: `https://www.getzner.com/en/products/sylodyn`.

[22] Juan Negreira, Per-Erik Austrell, Ola Flodén and Delphine Bard. “Characterisation of an Elastomer for Noise and Vibration Insulation in Lightweight Timber Buildings”. In: *Building Acoustics* 21.4 (2014), pp. 251–276. DOI: `10.1260/1351-010X.21.4.251`.

[23] Christian Berner AB. *Sylodyn - Vibrationsdämpning inom bygg*. Accessed: 2024-05-18. URL: `https://www.christianberner.se/produkter/vibrationsteknik/vibrationsdampning-inom-bygg/sylodyn/`.

[24] Getzner Werkstoffe GmbH. *Data Sheet Sylodyn NE*. 2022.

[25] Getzner Werkstoffe GmbH. *Data Sheet Sylodyn NF*. 2022.

[26] Getzner Werkstoffe GmbH. *Data Sheet Sylodyn NB*. 2022.

[27] Getzner Werkstoffe GmbH. *Sylodyn Detailed Data Sheet*. 2022.

[28] *SS-EN 1995-1-1:2004 - Eurocode 5: Design of timber structures - Part 1-1: General - Common rules and rules for buildings*. Standard. Swedish Institute for Standards sis, 2004. URL: https://www.sis.se/produkter/byggnadsmaterial-och-byggnader/byggnadsindustrin/tekniska-aspekter/ssen1995112004/.

[29] Boverket. *BFS 2015:6, EKS 10*. 2015.

Appendix A

Concrete configurations in large sized panel

For the steady–state dynamic response data of all configurations in Appendix A, readers are refereed to the Division of Structural Mechanics at Lund University.

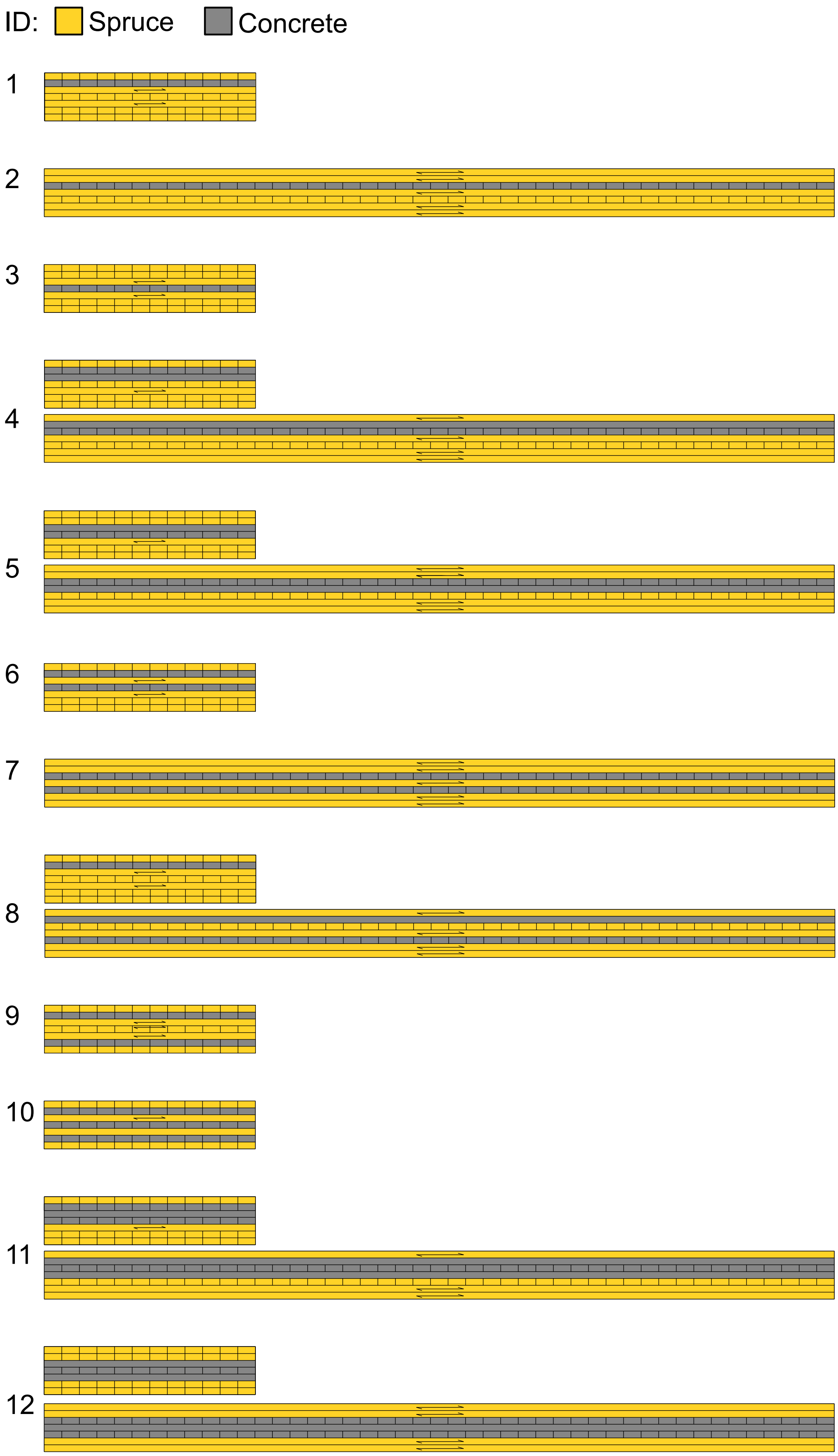

Figure A.1: Concrete - the full layer configurations ID1-12, with lamellae in both longitudinal and transverse direction.

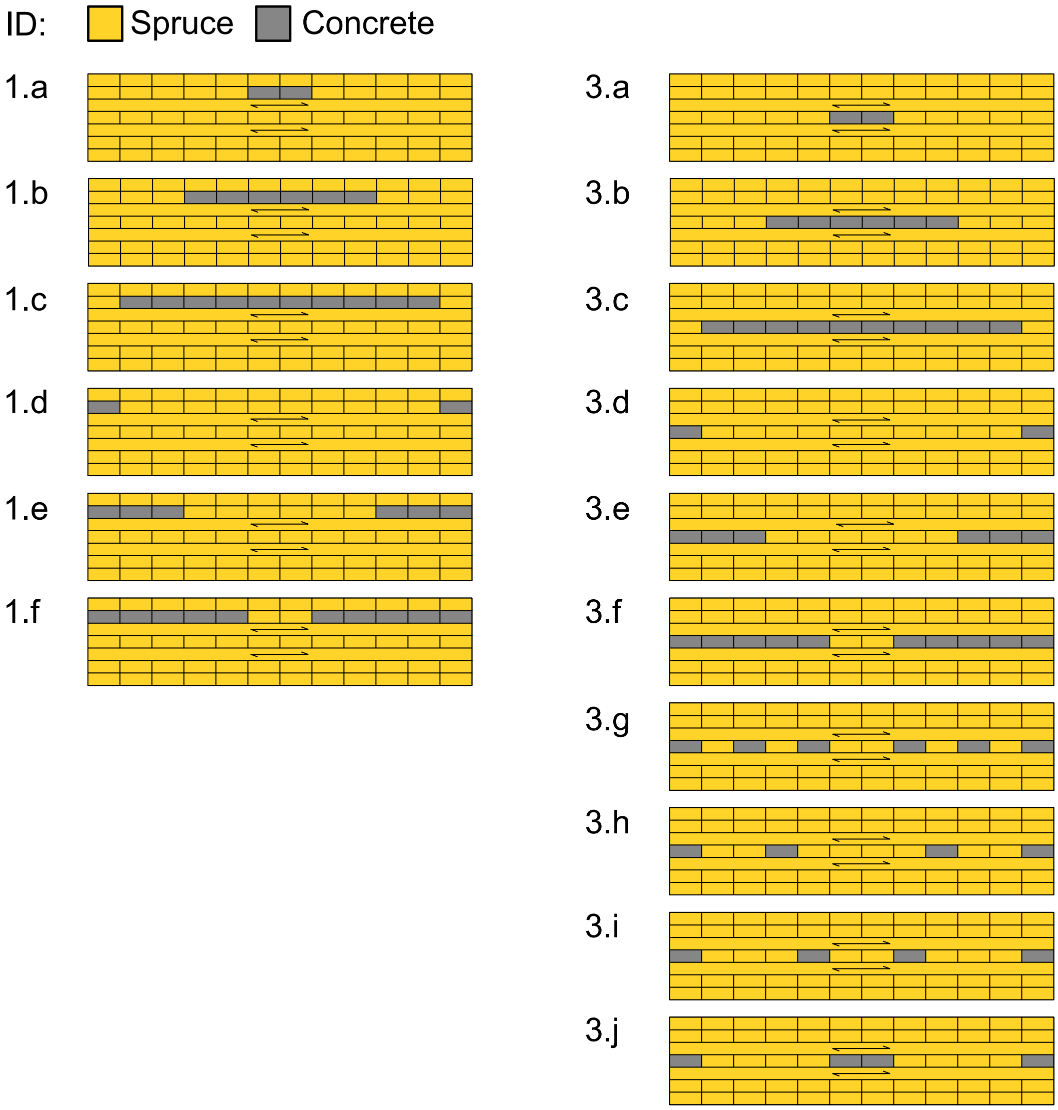

Figure A.2: Concrete - partial layer of ID1 and ID3, with lamellae in longitudinal direction.

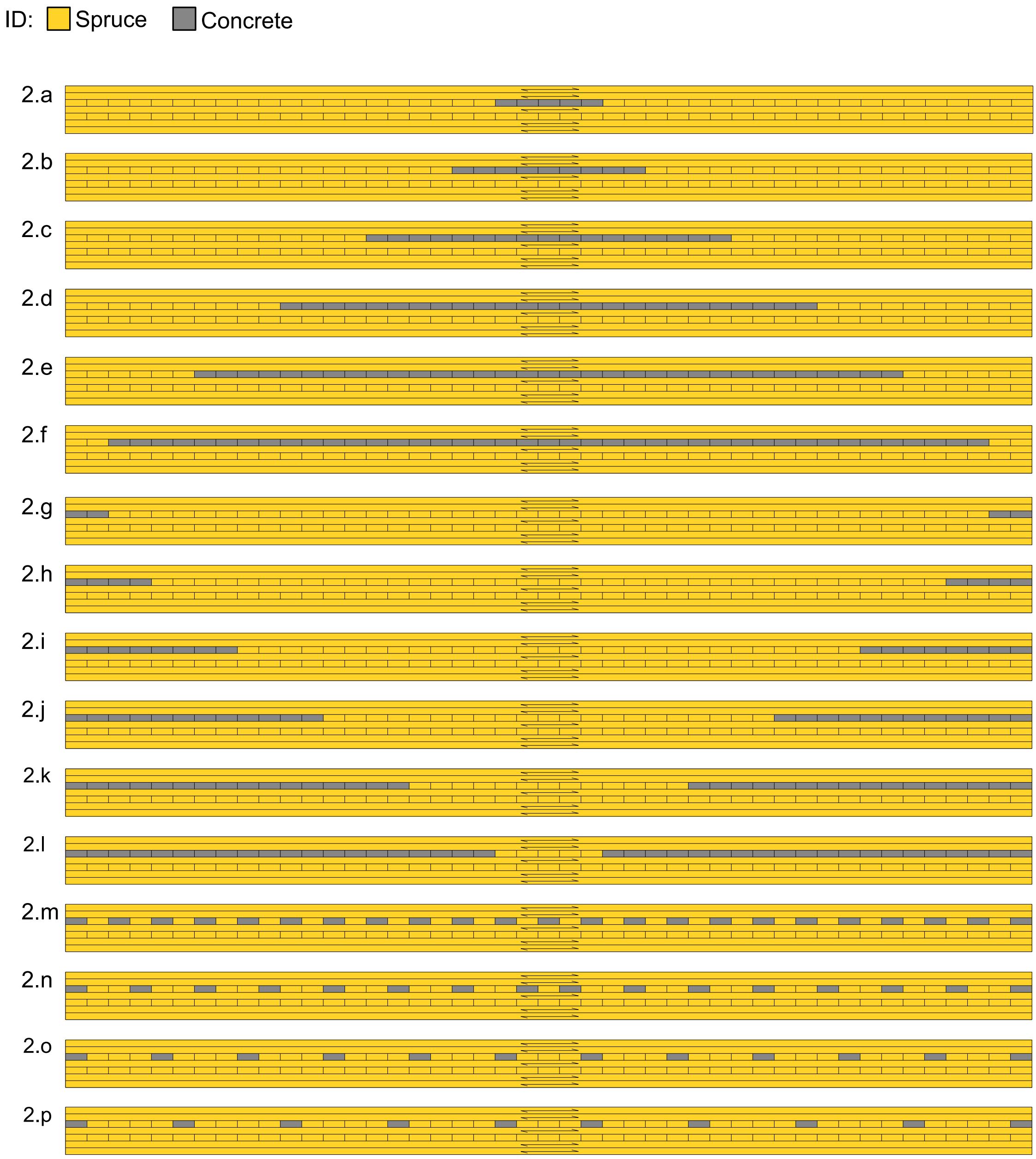

Figure A.3: Concrete - partial layer of ID2, with lamellae in transverse direction.

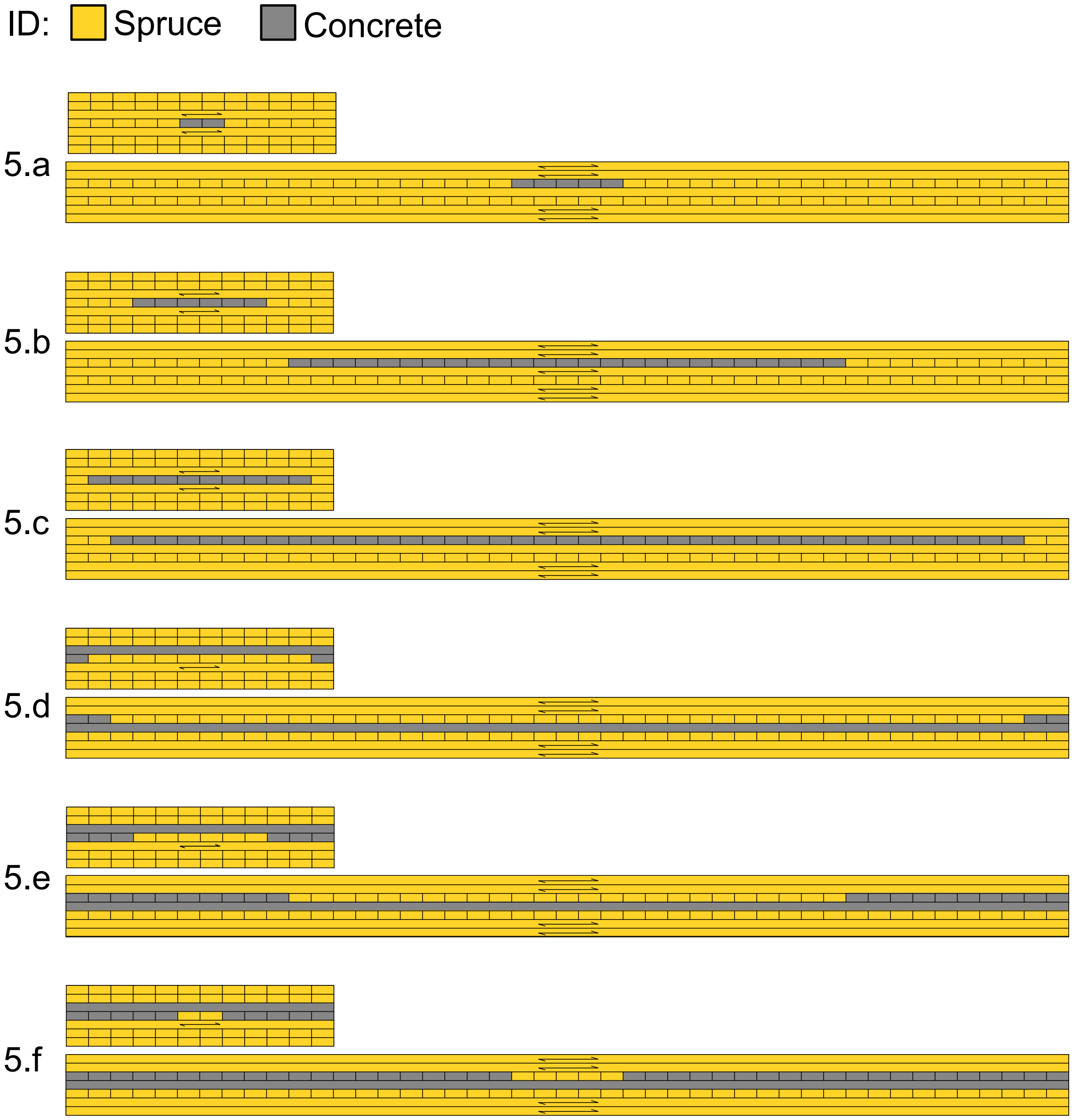

Figure A.4: Concrete - partial layer of ID5, with lamellae in both longitudinal and transverse direction.

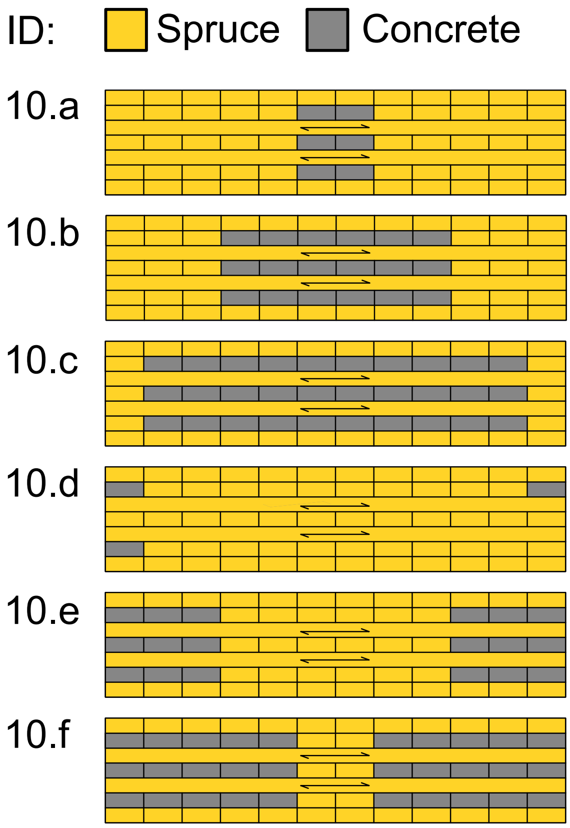

Figure A.5: Concrete - partial layer of ID10, with lamellae in longitudinal direction.

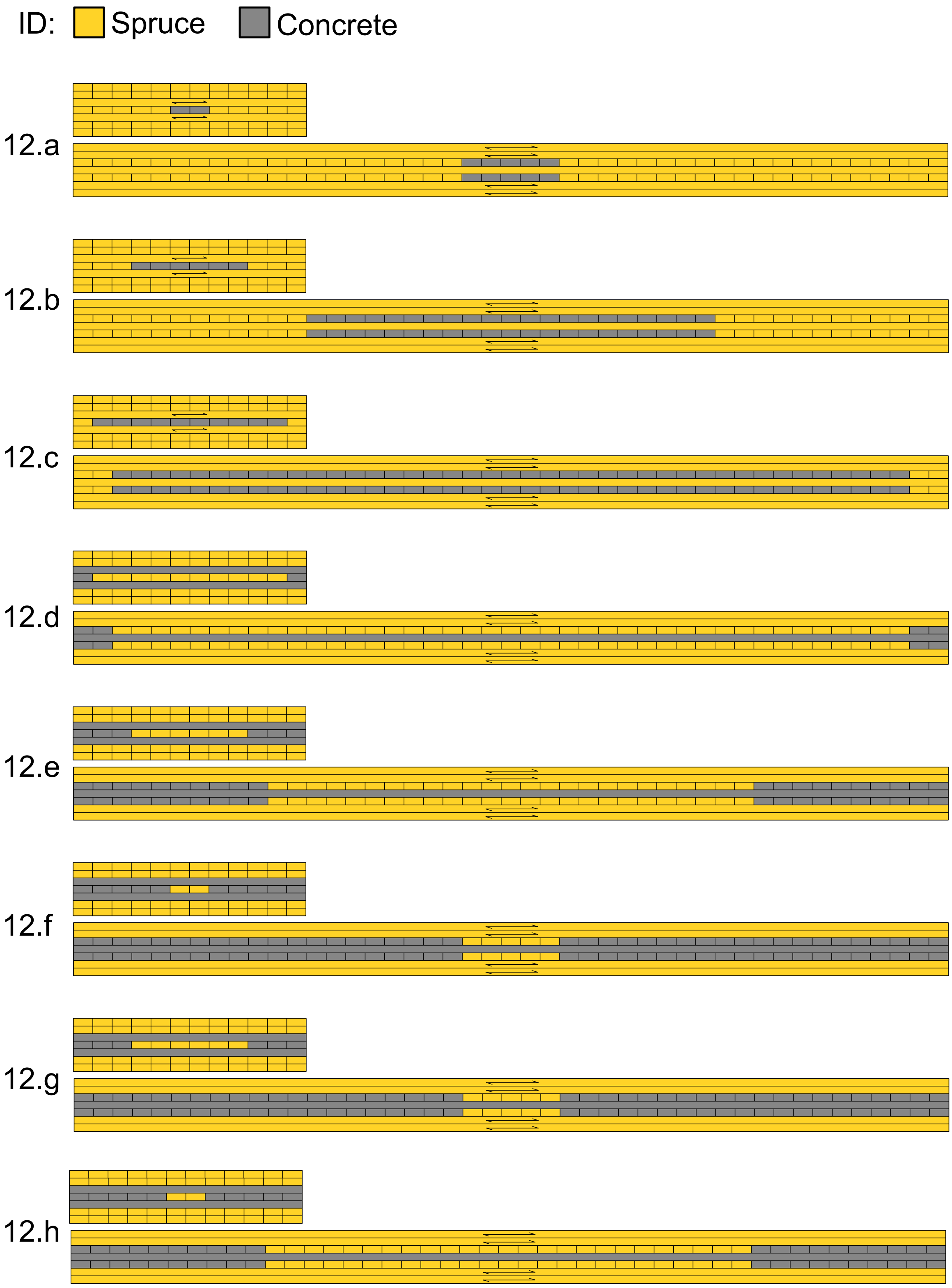

Figure A.6: Concrete - partial layer of ID12, with lamellae in both longitudinal and transverse direction.

Appendix B

Air cavity configurations in large sized panel

For the steady–state dynamic response data of all configurations in Appendix B, readers are refereed to the Division of Structural Mechanics at Lund University.

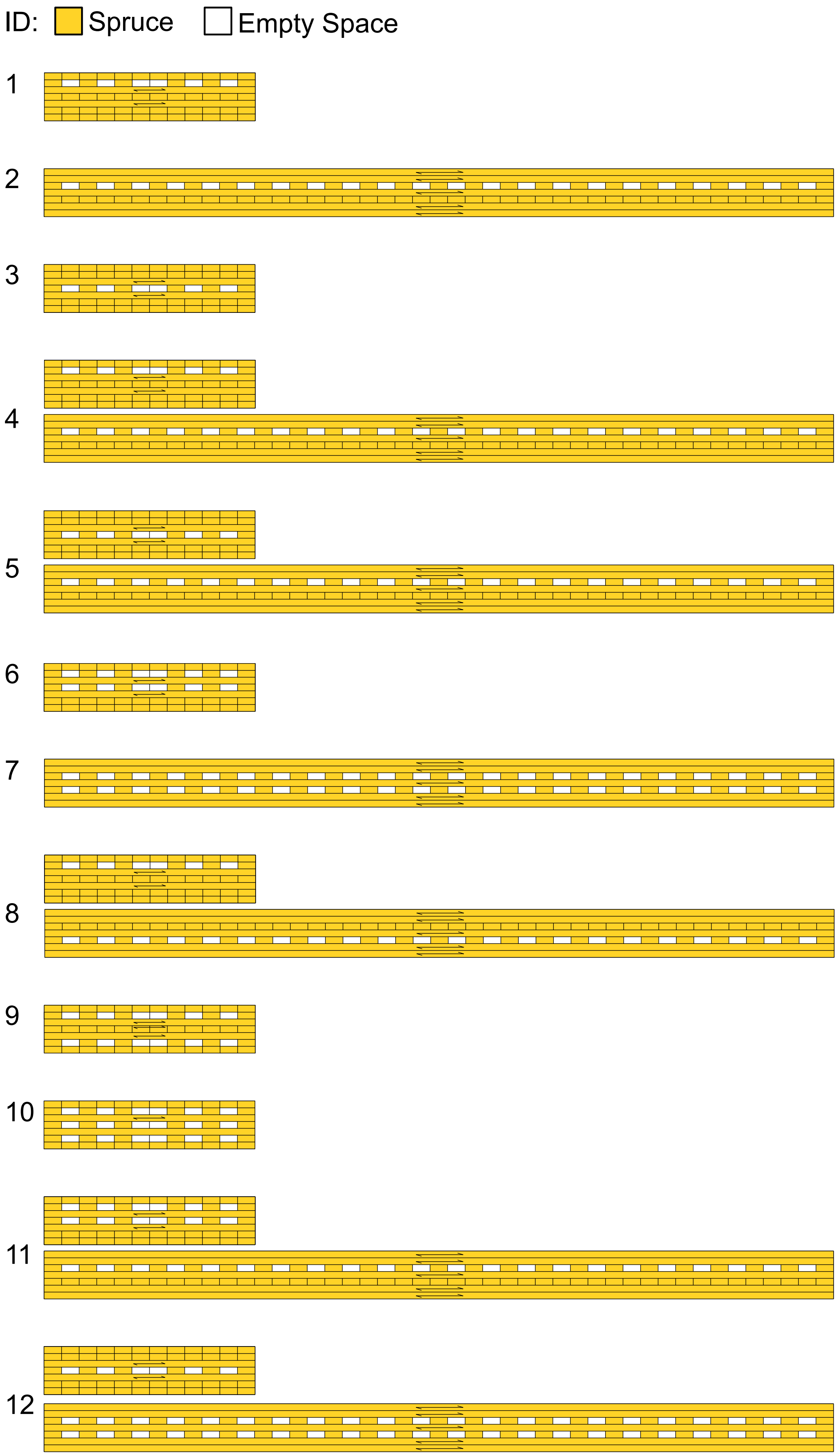

Figure B.1: Empty space - the full layer configurations ID1-12, with lamellae in both longitudinal and transverse direction.

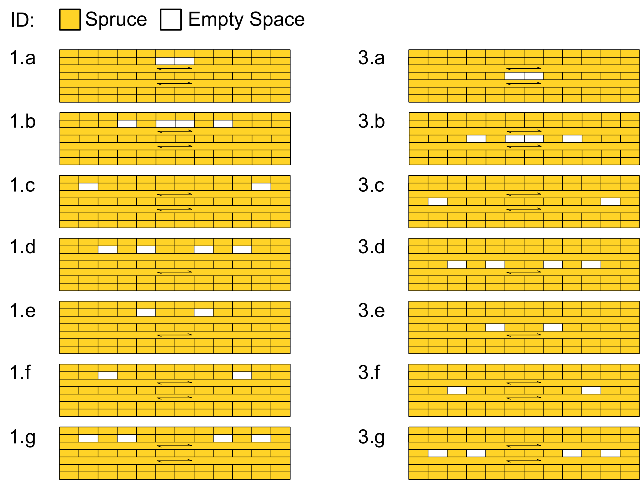

Figure B.2: Empty space - partial layer of ID1 and ID3, with lamellae in longitudinal direction.

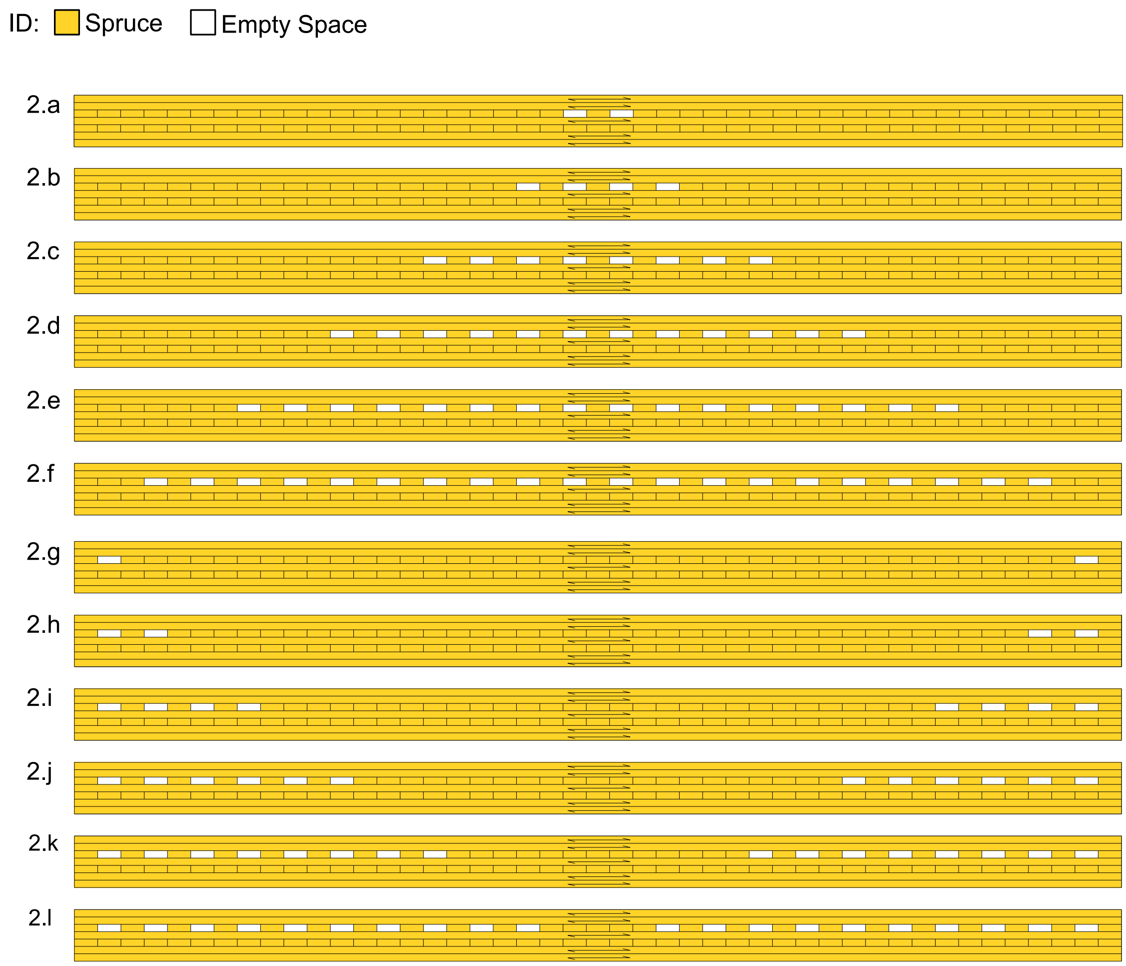

Figure B.3: Empty space - partial layer of ID2, with lamellae in transverse direction.

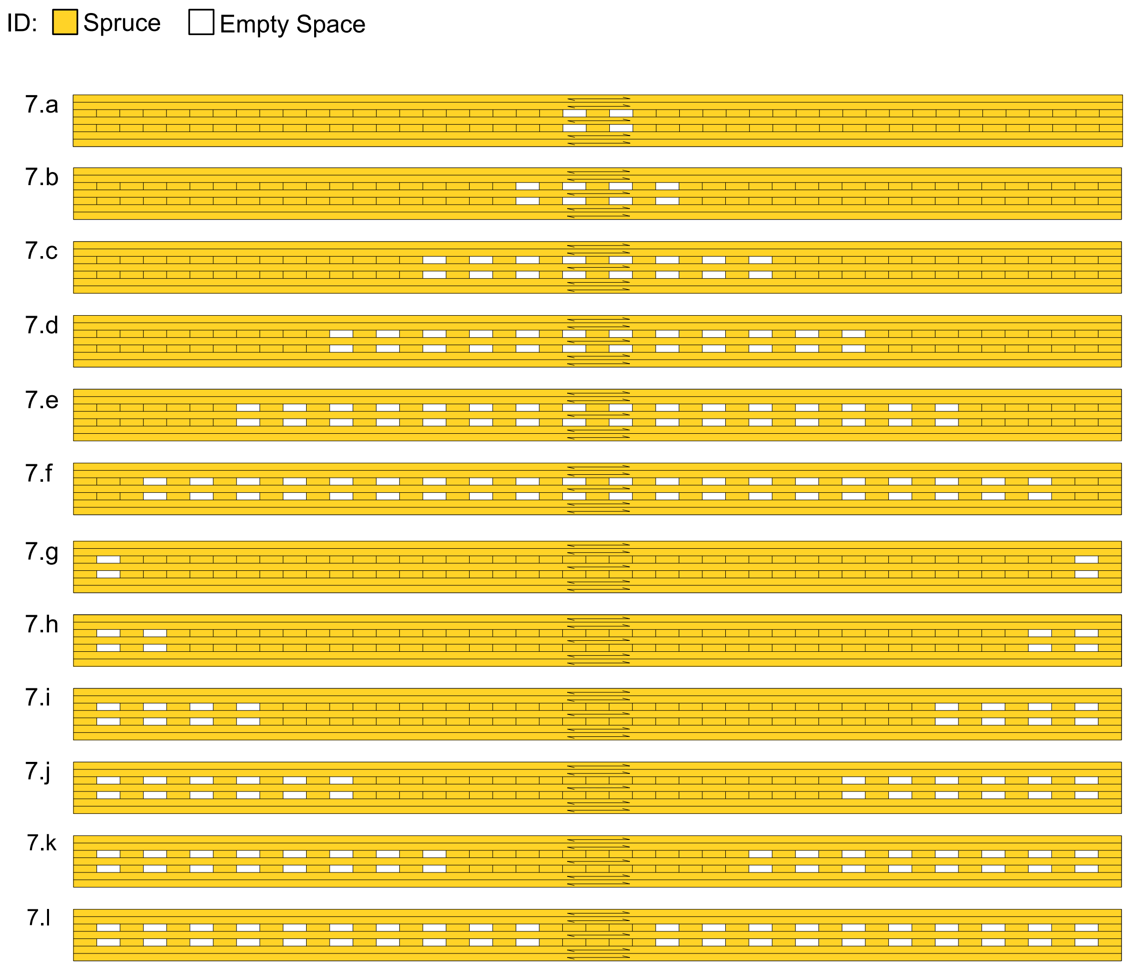

Figure B.4: Empty space - partial layer of ID7, with lamellae in transverse direction.

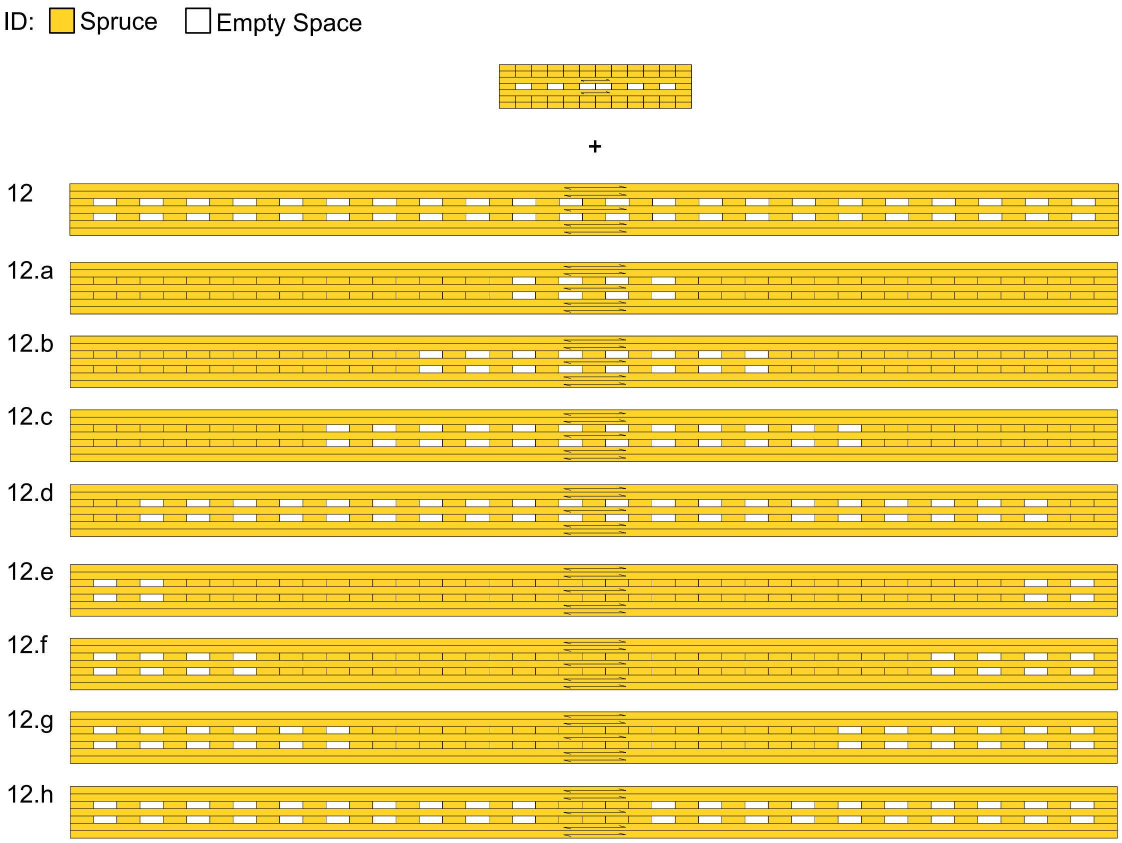

Figure B.5: Empty space - partial layer of ID12, with lamellae in both longitudinal and transverse direction.

Appendix C

Sylodyn NF configurations in large sized panel

For the steady–state dynamic response data of all configurations in Appendix C, readers are refereed to the Division of Structural Mechanics at Lund University.

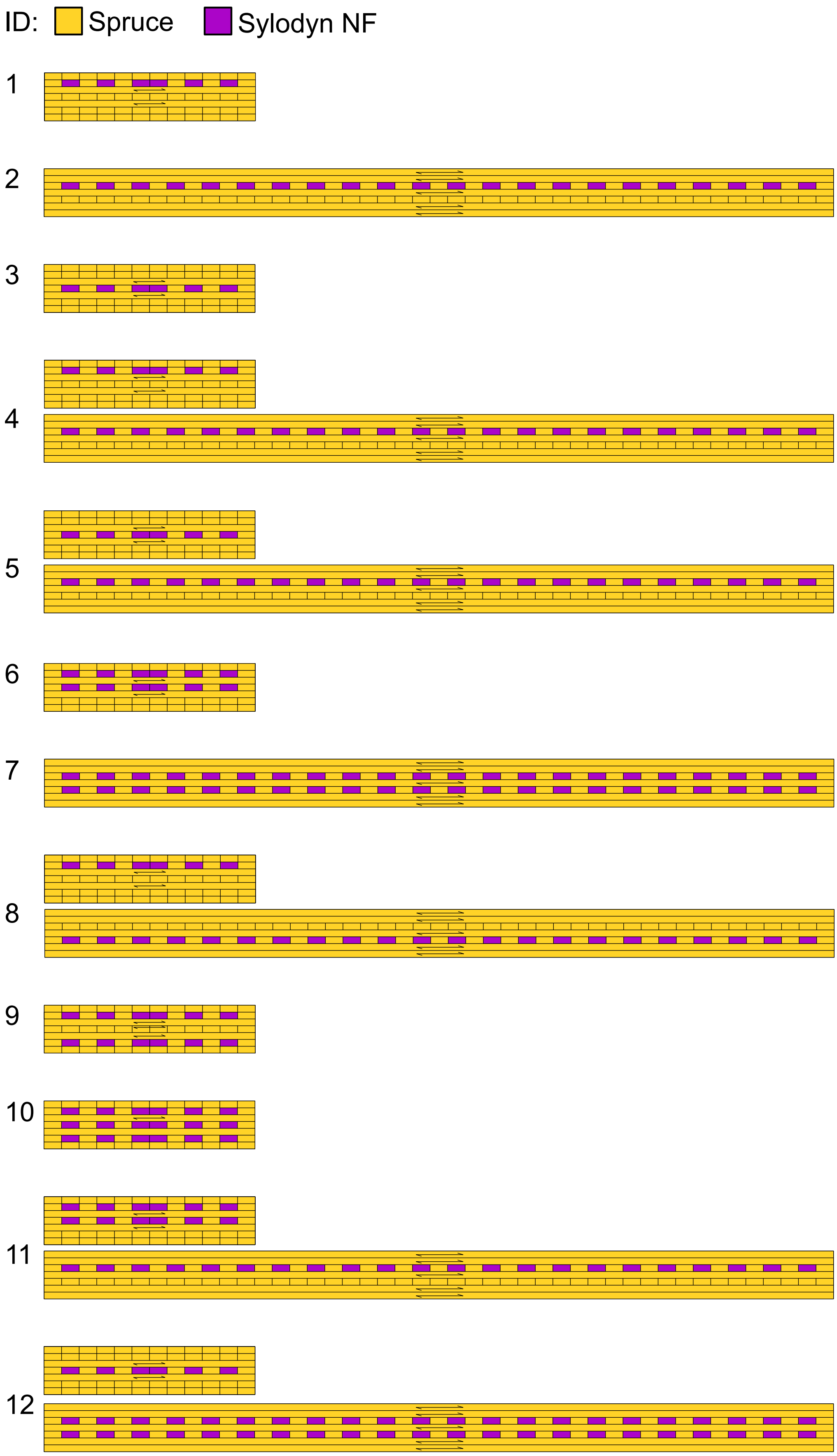

Figure C.1: Sylodyn NF - the full layer configurations ID1-12, with lamellae in both longitudinal and transverse direction.

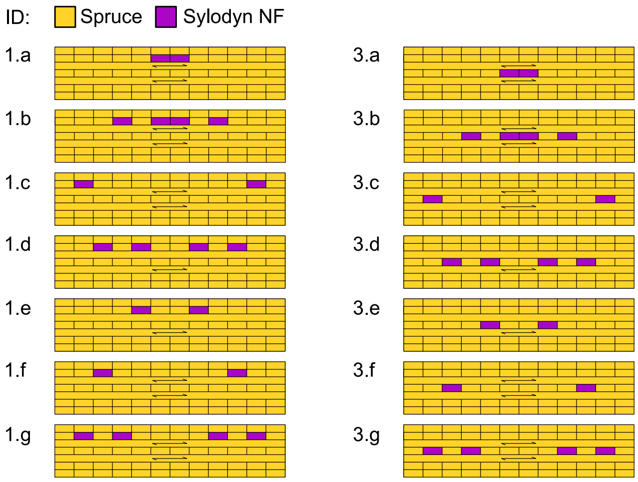

Figure C.2: Sylodyn NF - partial layer of ID1 and ID3, with lamellae in longitudinal direction.

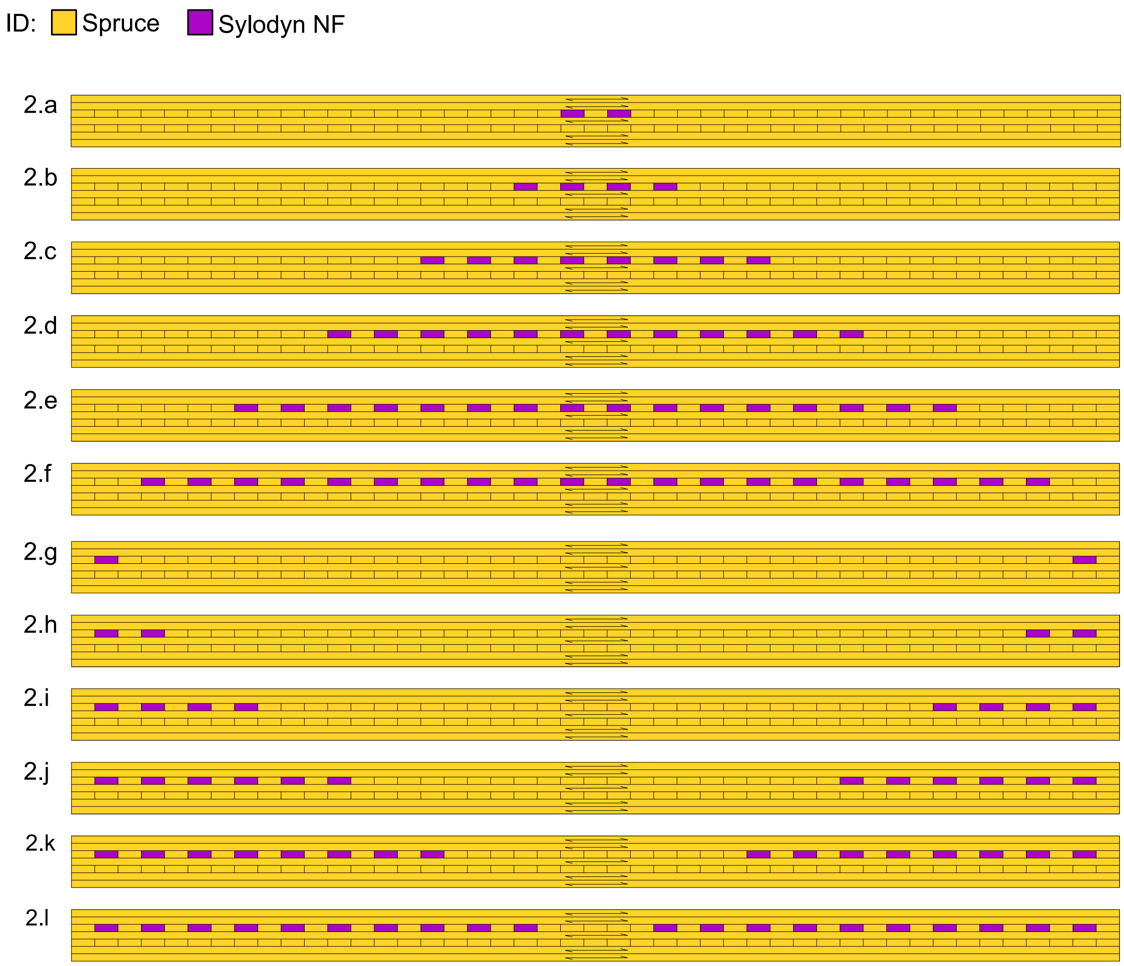

Figure C.3: Sylodyn NF - partial layer of ID2, with lamellae in transverse direction.

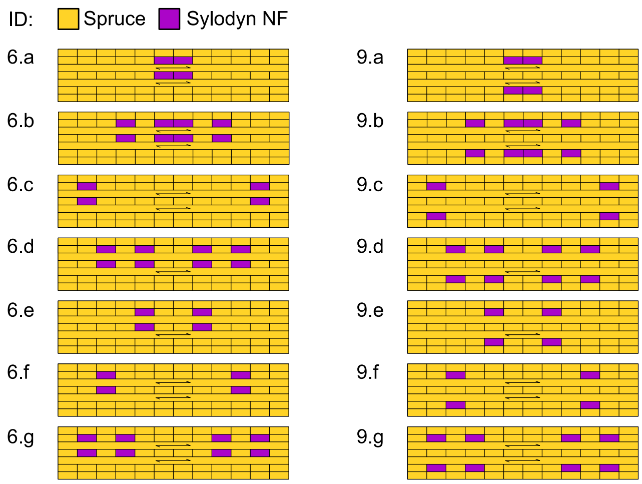

Figure C.4: Sylodyn NF - partial layer of ID6 and ID9, with lamellae in longitudinal direction.

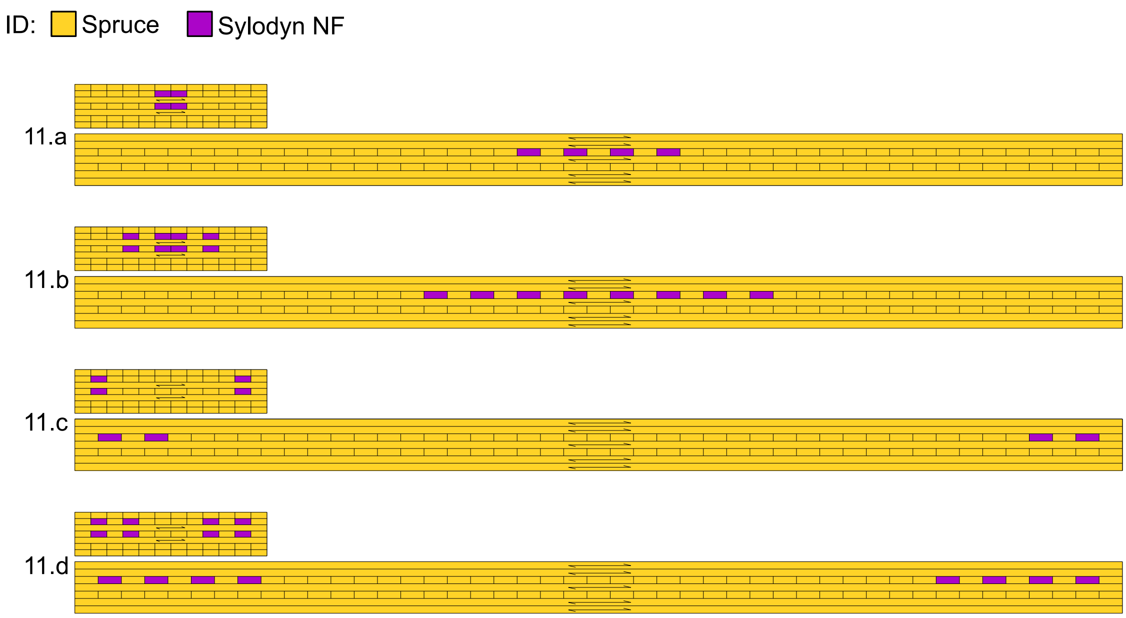

Figure C.5: Sylodyn NF - partial layer of ID11, with lamellae in both longitudinal and transverse direction.

Appendix D

Sylodyn NB configurations in large sized panel

For the steady–state dynamic response data of all configurations in Appendix D, readers are refereed to the Division of Structural Mechanics at Lund University.

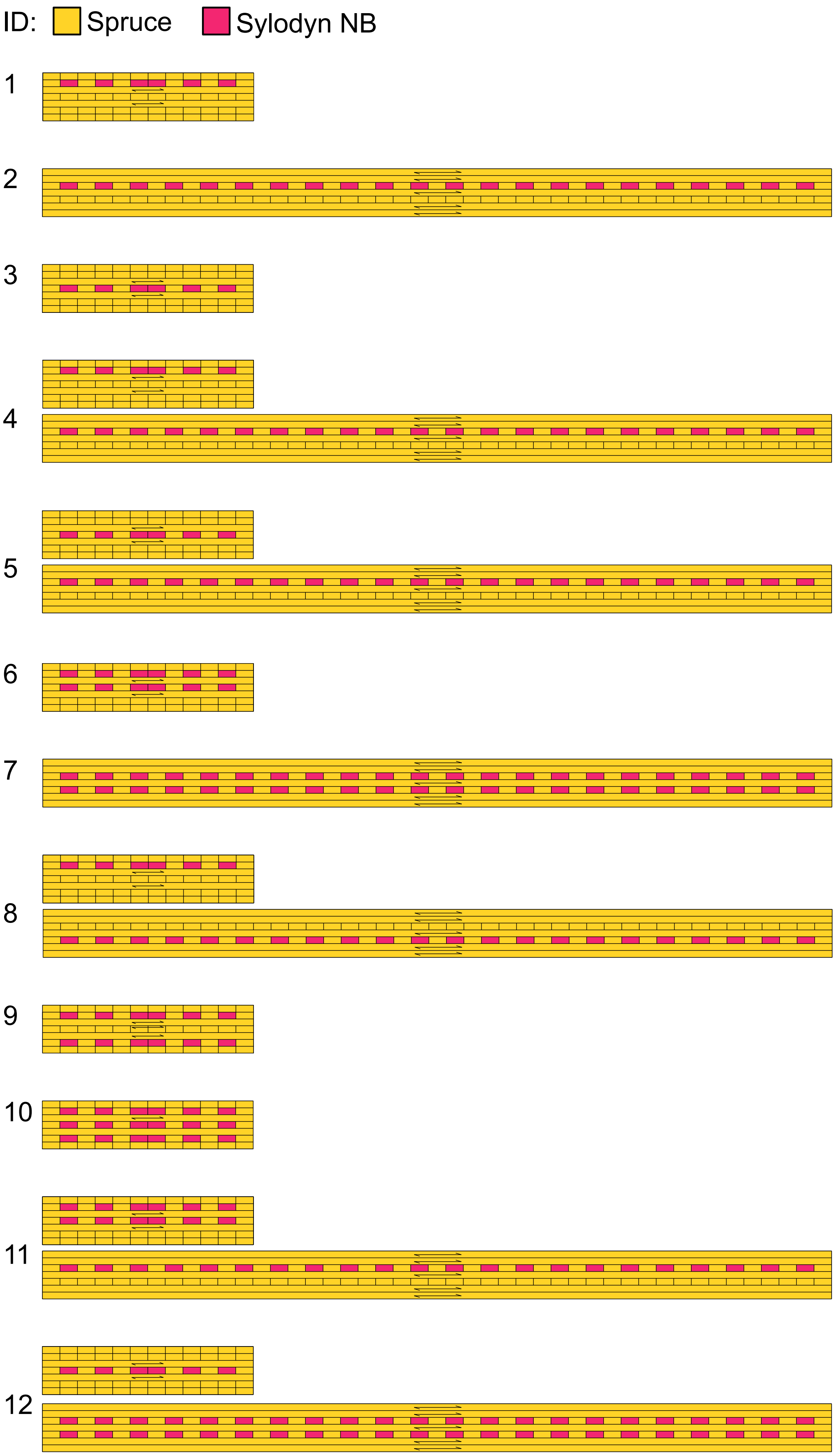

Figure D.1: Sylodyn NB - the full layer configurations ID1-12, with lamellae in both longitudinal and transverse direction.

Figure D.2: Sylodyn NB - partial layer of ID1 and ID3, with lamellae in longitudinal direction.

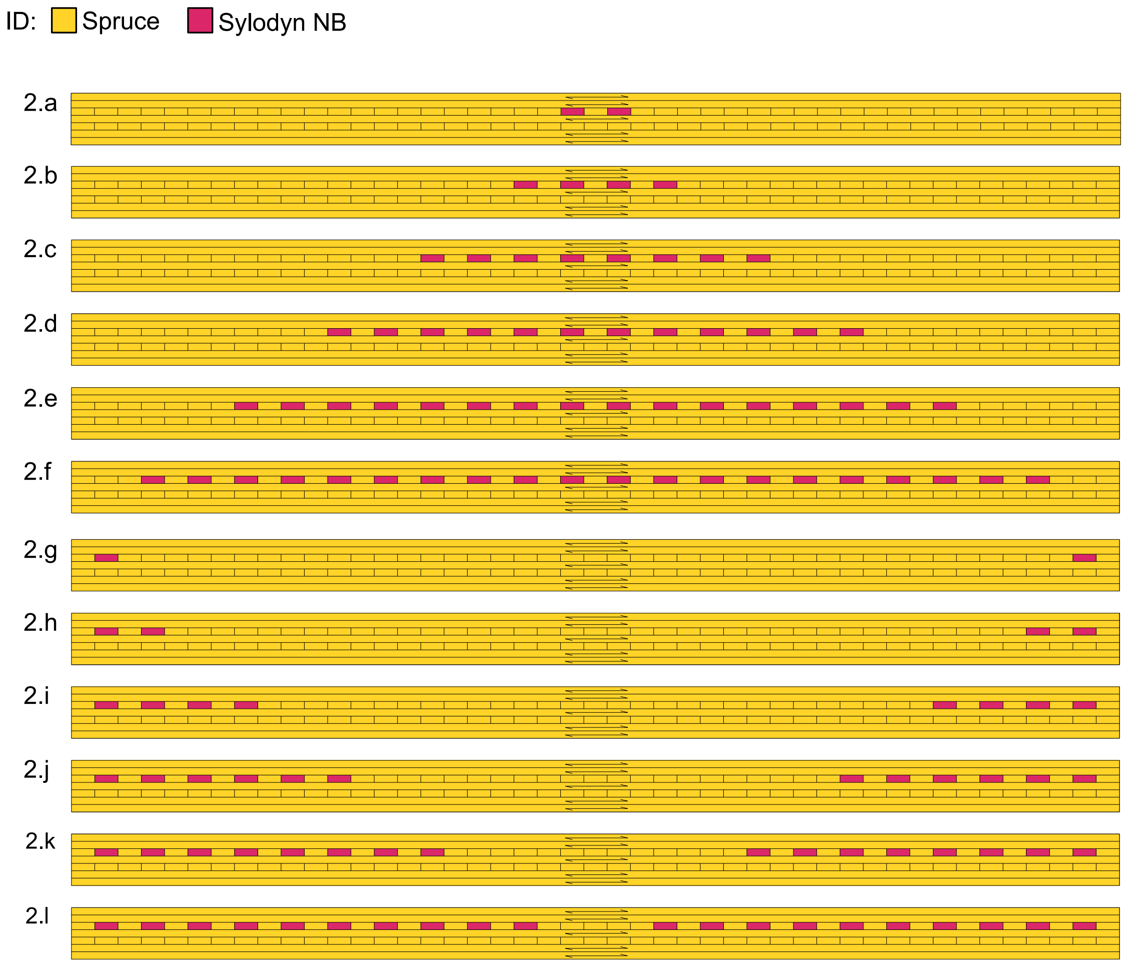

Figure D.3: Sylodyn NB - partial layer of ID2, with lamellae in transverse direction.

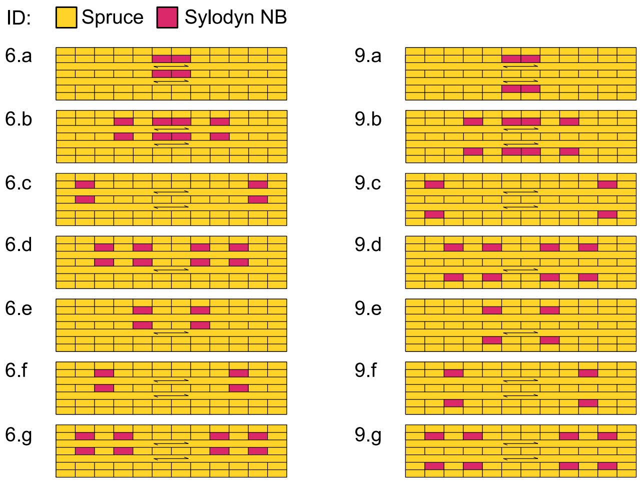

Figure D.4: Sylodyn NB - partial layer of ID6 and ID9, with lamellae in longitudinal direction.

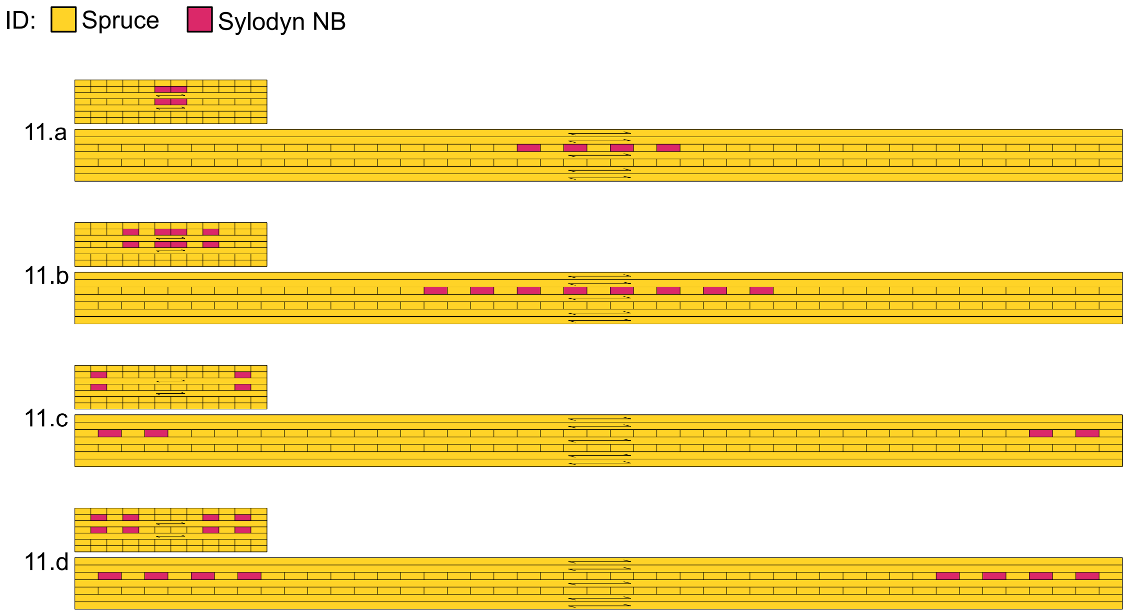

Figure D.5: Sylodyn NB - partial layer of ID11, with lamellae in both longitudinal and transverse direction.